RADIOCARBON, Vol 47, Nr 1, 2005, p 11–19

REASSESSING HUMAN SETTLEMENT ON THE SOUTH COAST OF SAN MIGUEL ISLAND, CALIFORNIA: THE USE OF ^{14}C DATING AS A RECONNAISSANCE TOOL

Todd J Braje[1,2] • Jon M Erlandson[1,3] • Torben C Rick[4]

ABSTRACT. California's San Miguel Island contains over 600 archaeological sites, some occupied as early as 12,000 yr ago and most located along the island's north coast. Archaeologists have long believed the south coast to have been marginal or largely uninhabited. Burial of some landforms by sand dunes deposited after historical overgrazing, the lack of systematic survey, and a dearth of radiocarbon dating have also contributed to an underestimation of the intensity of human land use along the south coast of San Miguel Island. Our recent reconnaissance and dating of shell middens on the island's south coast indicate more intensive occupation than previously thought, with numerous south coast sites spanning at least the past 9000 yr, and demonstrate the utility of combining systematic archaeological reconnaissance and radiometrics in reconstructions of human settlement and historical ecology in coastal environments.

INTRODUCTION

San Miguel Island, the westernmost of California's Northern Channel Islands (Figure 1), contains hundreds of archaeological sites and a nearly continuous record of human occupation spanning at least the past 11,000 to 12,000 calendar years. Along with over a dozen shell middens dating between about 10,500 and 8000 BP (Erlandson et al. 1996; Erlandson and Moss 1996), a stratified occupational record spanning virtually the entire Holocene has been assembled from sites located on the northeast and northwest coasts of the island. Archaeological studies of these well-preserved shell middens—including extensive radiocarbon dating, detailed faunal and technological analyses, and changes in average shellfish size measurements—can help elucidate the human history of the island, the historical ecology of the region, and the changing nature of human impacts on local marine and terrestrial environments (see Erlandson et al. 2004, forthcoming; Rick and Erlandson 2003).

Archaeological studies have been conducted on San Miguel since the late 1800s, and the island was intensively surveyed for archaeological sites during the 1960s, 1970s, and 1980s (Glassow 1980; Greenwood 1978, 1982; Rozaire 1978). Until recently, however, archaeological investigations had been conducted almost exclusively along the island's north coast, where numerous large, multicomponent shell middens have been the focus of research. In contrast, relatively little is known about the human use of the south coast, long considered to have been sparsely populated (e.g. Kennett, forthcoming; Rogers 1929:266).

After recent summaries of the historical ecology of the island (Erlandson et al. 2004, forthcoming; Rick and Erlandson 2003), it became clear that we needed to better understand the antiquity and nature of the human use of south coast land and seascapes, and to compare such patterns to what we know from the much better documented north coast. During the last 2 yr, therefore, we have revisited many of the known archaeological sites along the south coast, recorded numerous previously undocumented sites, and initiated a program of systematic ground reconnaissance and ^{14}C dating to document the chronology and nature of human settlement in the area. In this paper, we summarize the results of recent reconnaissance and dating efforts along San Miguel Island's south coast, where we have found a much longer and more extensive record of human occupation than previously recognized, including archaeological sites that span much of the Holocene. Our work illustrates the potential and importance of using ^{14}C dating as a survey tool in reconstructing the human occupational history in coastal and other erosional environments (see Erlandson and Moss 1999).

[1]Department of Anthropology, University of Oregon, Eugene, Oregon 97403-1218, USA.
[2]Corresponding author. Email: tbraje@uoregon.edu.
[3]Email: jerland@uoregon.edu.
[4]Department of Anthropology, Southern Methodist University, Dallas, Texas 75275-0336, USA. Email: trick@smu.edu.

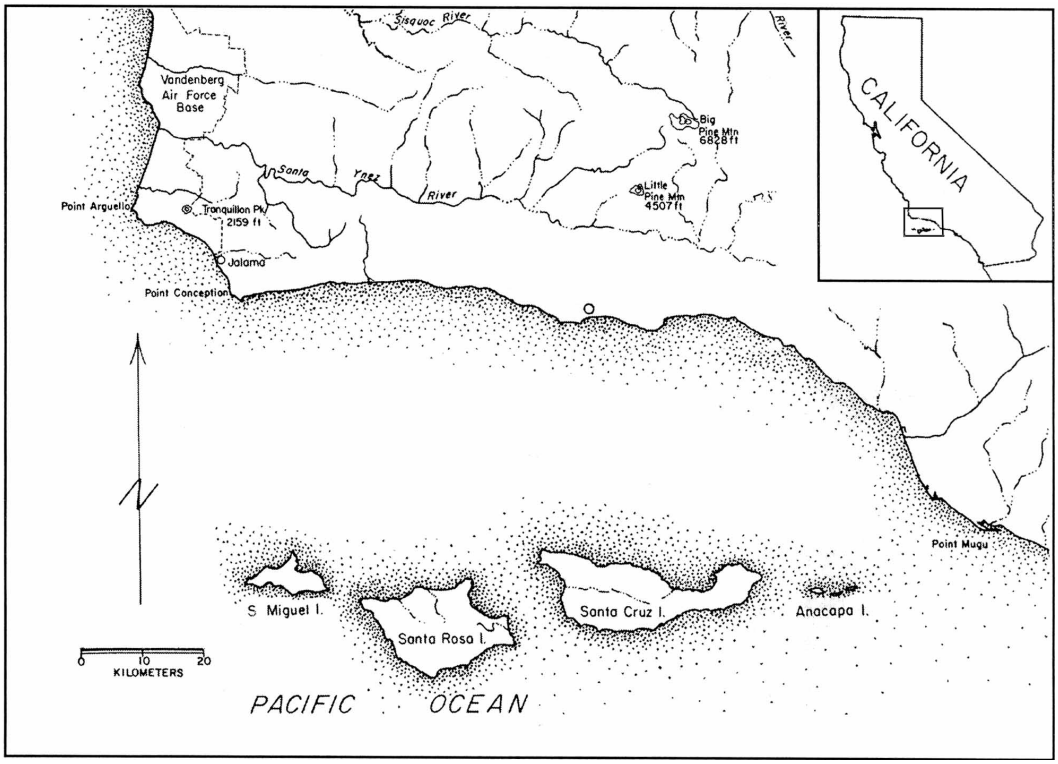

Figure 1 Location of San Miguel Island and the Santa Barbara Channel area

Environmental and Cultural Background

San Miguel is located about 40 km off the Santa Barbara coast. A maximum of about 17 km long and 8 km wide, it encompasses an area of approximately 37 km^2. The island landscape is dominated by tablelands, raised marine terraces, rolling hills, and shifting dune fields deposited and redeposited by strong northwesterly winds that blow almost continuously off the North Pacific. Two small peaks, Green Mountain and San Miguel Hill, rise from the central mass of the island, reaching elevations of 249 m and 253 m, respectively. The coastline consists of 43 km of rocky shoreline interspersed with sandy beaches. Although the endemic terrestrial flora and fauna are depauperate, the island is surrounded by extensive kelp forests and other marine habitats that support diverse and highly productive populations of marine fishes, shellfish, sea mammals, and sea birds.

San Miguel has a Mediterranean climate with relatively mild temperatures (11.9 to 15.5 °C) throughout the year. The island's climate is heavily influenced by an upwelling of cool oceanic currents, powerful winds, and heavy coastal fog. Rainfall averages just 35.5 cm/yr, falling mostly between January and March, and perennial freshwater sources are limited in number, size, and quality. The island contains only 3 substantial drainages, none of which are located on the south coast (see Kennett 1998), but several springs of marginal quality have been mapped in the area.

The Northern Channel Islands have been separated from the California mainland throughout the Quaternary, although they coalesced into a single landmass (Santarosae) during the last glacial (Jugger and Johnson 1980; Orr 1968). Once thought to have been colonized by humans relatively recently, we now know that the Northern Channel Islands were first settled at least 12,000 to 13,000

calendar years ago (Erlandson et al. 1996; Johnson et al. 2000). San Miguel is one of four Northern Channel Islands occupied historically by the Chumash Indians, and archaeological evidence suggests that the larger Santa Barbara Channel region was occupied by the Chumash and their ancestors for millennia—possibly throughout the Holocene. By about AD 1000, the coastal Chumash had developed a complex and sophisticated maritime society, organized in a number of relatively large villages and towns led by hereditary chiefs, with extensive craft-specialization and regional trade networks facilitated by the production and use of a shell bead currency (see Arnold 1992, 2000; King 1990). First contacted by Europeans in AD 1542–3, when 3 Spanish ships commanded by Juan Rodriguez Cabrillo wintered on San Miguel, the Island Chumash may have been impacted early by Old World diseases (Erlandson and Bartoy 1995; Erlandson et al. 2001). Nonetheless, historical accounts suggest that they were thriving when the Spanish first settled Alta California in AD 1769. By about AD 1822, however, the last of the Island Chumash had been removed to Spanish missions or towns on the mainland.

Starting in the mid-1850s, overgrazing by sheep and other livestock introduced by American ranchers resulted in severe vegetation stripping, dune destabilization, and soil erosion (Johnson 1980; Rick and Erlandson 2003), rendering San Miguel Island into a "sand waste." During the mid-1900s, the island was also used as a bombing range by the US military. With the removal of livestock, the cessation of bombing, and careful management by the US Navy and National Park Service, the island's vegetation is now undergoing a dramatic recovery. Preliminary observations suggest that the hydrology of the island (dune aquifers) may also be recovering and that freshwater sources may have been more abundant and reliable prior to European contact.

The "Marginal" South Coast

Our understanding of San Miguel Island archaeology has been hindered by the differential intensity of archaeological investigations on the north and south shores of the island. Conclusions concerning the limited nature of human occupation along the south coast were formed early and have changed little over the past 75 yr. Investigation by antiquarians in the late 1800s and early 1900s focused on the excavation of numerous cemeteries, nearly all of which were located along the north coast of the island (e.g. Heye 1921: Plate II). D B Rogers (1929) of the Santa Barbara Museum of Natural History conducted the first reasonably thorough shoreline survey in the 1920s, systematically walking the perimeter of the entire island. As Figure 2 shows, he recorded extensive aggregations of archaeological sites on the north coast, but he found little evidence of occupation on the south coast. Rogers (1929:266) concluded that the "southern shore of the island had, broadly speaking, been unpopular with the Indians as a residential site."

From 1963 to 1966, an intensive survey of the island by archaeologists from the Los Angeles County Museum of Natural History was directed by Rozaire and Kritzman. Of the 542 sites recorded, only about 60 were located along the south coast (Rozaire 1978). Subsequent survey work has been conducted by Greenwood (1978, 1982), Glassow (1980), Kennett (1998), and ourselves (e.g. Erlandson 2001; Rick and Erlandson 2004), bringing the total number of recorded sites to 608. Of these, only 67 (11%) are located along the south coast. Our recent work, however, like Glassow's 1980 survey, demonstrates that large numbers of archaeological sites remain undocumented and unrecorded on the south coast of San Miguel Island.

Investigations over the past 30 yr have also yielded over 200 ^{14}C dates from island archaeological sites. Until recently, however, only 1 south coast site had been dated, a deeply buried "red abalone" midden near Crook Point that Glassow (1980) dated to about 6000 yr ago. The dearth of dated sites has seriously hindered our ability to understand the antiquity and chronology of human settlement, subsistence, and demography along the south coast.

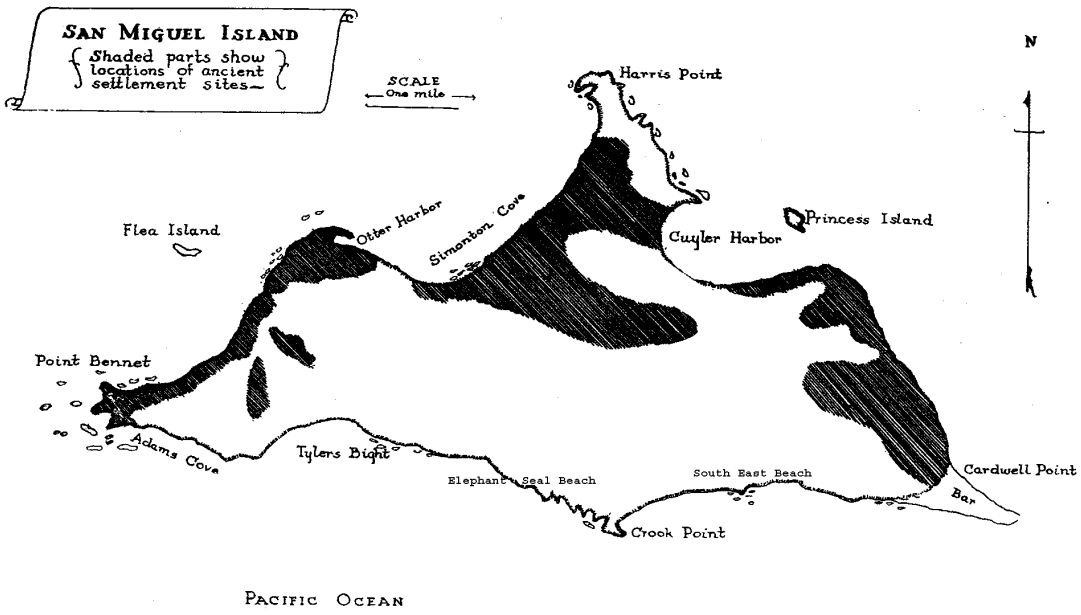

Figure 2 Rogers' (1929) map of the distribution of archaeological sites on San Miguel Island

The view that the south coast of San Miguel Island was not heavily used contrasts with the occupational record for extensive and permanent settlement of the southern coastlines of Santa Rosa and Santa Cruz islands, which included at least 5 relatively large historic Chumash villages (see Kennett, forthcoming). Moreover, the south coast of San Miguel offers several major advantages to people on both the land and the sea. First, it is relatively sheltered from the strong northwesterly winds and ocean swells that sweep the island most of the year. Several sources of freshwater have also been identified, including springs in the Crook Point area and intermittent streams or seeps much more widely available. Finally, the south coast also contains extensive rocky intertidal, kelp forest, and shallow rocky reef habitats that support an abundance of marine resources.

Some hints of the possibility of extensive and intensive human settlement along the southern boundary of San Miguel Island have emerged over the years. For instance, site records prepared by Kritzman, Rozaire, and Greenwood refer to several locations containing human burials. The presence of burials and associated midden deposits suggests a degree of sedentism that seems more consistent with village occupations than with relatively brief or specialized logistical use of the area. In 1980, Glassow identified 22 previously unrecorded archaeological sites in a systematic survey of 2 quarter-mile-wide transects that ran north-south across sections of the south coast east of Crook Point. If the total number (15) of south coast sites recorded for these 2 transects is representative of the entire south coast, as many as 255 sites may be present along the 14 km of coastline from Cardwell Point to Point Bennett.

METHODS

For more than a decade, University of Oregon archaeologists have been engaged in an intensive study of the archaeology and historical ecology of San Miguel Island, work that has also assisted the National Park Service in managing and interpreting the cultural and natural resources of the island. In 2000 and 2001, as part of a search for early sites on San Miguel, Erlandson visited and dated shell

middens associated with 2 small rockshelters overlooking the southwest coast and conducted a preliminary reconnaissance of some south coast springs.

From 2002 to 2004, as part of a project to assess the condition of eroding and endangered sites on San Miguel and Santa Rosa islands, we visited scores of recorded sites located in various areas on San Miguel Island and collected numerous ^{14}C samples to help develop a chronology of island site occupation, environmental changes, and human demography (Rick and Erlandson 2004). We selected several discrete study areas of the island for relatively intensive site assessment work, including the Crook Point, Tyler Bight, and Point Bennett areas along the southern shoreline. Prior to the 2002–4 field work, we conducted background research on the nature of known south coast sites, including the compilation of information on their location, size, structure, and contents, as recorded by various archaeologists during visits over the past 40 yr.

For our current work, we defined the south coast area as extending from Point Bennett on the west to Cardwell Point on the east, and including all land located between the ocean and the rim of the steep southern escarpment, which varies from about 80 to 170 m in elevation. Following our background research, we used pedestrian survey techniques to relocate the known sites selected for condition assessments, mapped their locations using Global Positioning System technology, documented the current condition of the sites, and, wherever possible, collected organic samples from erosional exposures for ^{14}C dating. In the process of relocating known sites in our survey areas, we also found numerous Native American shell middens that had not been documented. Many of the previously recorded sites had also badly eroded in the roughly 20-yr period since they were recorded, suggesting this area is relatively dynamic.

RESULTS AND DISCUSSION

In relocating several south coast sites chosen for assessment, we found at least 22 shell middens that had not been recorded. The previously recorded and newly discovered sites ranged from small rock shelters to large open sites and appear to encompass a range of site types from short-term camps or shellfish processing locations, to seasonal encampments, to villages with substantial midden deposits and human burials.

One of our south coast survey areas was near the southwest end of the island, from Adams Cove to Tyler Bight. Here, high on the bluffs overlooking the southwest coast, the badly eroded remnants of 3 shell middens (CA-SMI-575, -577, and -578) were evaluated. In this windswept region, where a vast area has been largely denuded of soil, we found isolated soil islands containing shell midden deposits of low to moderate density. Well-preserved shells from these middens were recently dated to about 8800, 8700, and 1160 cal BP (Table 1). In response to erosion caused by seals and sea lions hauling out on CA-SMI-602 at Adams Cove, Walker et al. (2000) also investigated this sizeable shell midden, dating it between about AD 1500 and 1800. Over the years, a number of human burials have eroded out of this site and Walker et al. (2000) tentatively identified the remains of a house floor. More recent examination of CA-SMI-602 by Erlandson and Rick identified at least 8 large house depressions, confirming that a substantial Chumash village existed along the southwest coast during Protohistoric and early Historic times (Rick 2004). Another large site (CA-SMI-520) near the west end of Tyler Bight contains multiple occupational components, including discrete shell middens dated to about 5860 and 3300 yr. We also dated shell middens located in 2 small rock shelters (CA-SMI-516 and -573) situated high on the escarpment overlooking Tyler Bight—one to Protohistoric times, the other to about 2400 yr ago.

Table 1 Radiocarbon dates from the south coast of San Miguel Island, California.

Site# [a] SMI-	Material[b]	Lab #	Provenience	Uncorrected ^{14}C age	$^{13}C/^{12}C$ adjusted	Age range (cal BP, 1 σ)	Approximate location
188	Mc	Beta-180767	Base of midden (25 cm bs)	6050 ± 90	6400 ± 90	6725–6490	Crook Point
190	Hr	Beta-180768	Upper 10 cm in 30 cm midden	1670 ± 60	2110 ± 60	1515–1345	Crook Point
192	Hr	Beta-180769	10 cm surface midden	1380 ± 60	1810 ± 60	1235–1055	Crook Point
232	Hr	Beta-180770	East gully wall, near base	1370 ± 60	1810 ± 60	1230–1060	South East Beach
232	Mc	OS-44639	Unit 1, Column sample	N/A	1910 ± 30	1280–1200	South East Beach
516	Hc	Beta-145312	Cave mouth, 35–40 above bedrock	430 ± 60	860 ± 60	320–250	Elephant Seal Beach
516	Hc	Beta-145313	Cave mouth, 70 cm above bedrock	520 ± 90	950 ± 90	470–280	Elephant Seal Beach
520	Mc	OS-37736	Surface	N/A	3630 ± 25	3330–3220	Tyler Bight
520	Hr	Beta-171805	Surface	5250 ± 80	5680 ± 80	5920–5720	Tyler Bight
557*	Hr	UCR-1831	Exposure, 5 m	5525 ± 130	5955 ± 130	6280–5960	South East Beach
557	Hr	OS-44640	Bulk Sample 1	N/A	6310 ± 35	6400–6565	South East Beach
573	Cr	Beta-145316	2–3 cm bs in overhang	2520 ± 90	2950 ± 90	2610–2320	Tyler Bight
575	Mc	OS-42695	Soil island SE of Pt. Bennett trail	N/A	1830 ± 25	1220–1120	Tyler Bight
577	Mc	OS-42737	SE most intact soil island	N/A	8540 ± 35	8910–8760	Tyler Bight
578	Mc	OS-42738	Site adjacent to eagle nest	N/A	8500 ± 40	8870–8700	Tyler Bight
602*	Mc	Beta-098743	Unit 2, 39 cm	460 ± 60	900 ± 60	400–260	Adams Cove
602*	Mc	Beta-098744	Unit 5, 48 cm	650 ± 60	1100 ± 60	530–450	Adams Cove
602*	Mc	Beta-114533	Unit 2, 10 cm/Stratum A	310 ± 60	730 ± 60	270–80	Adams Cove
602*	Mc	Beta-098742	Unit 5, 10 cm	650 ± 70	1100 ± 70	530–440	Adams Cove
608	Mc	OS-44638	Unit 1 Bulk sample	N/A	9200 ± 50	9800–9440	Elephant Seal Beach
608	Mc	Beta-180771	Gully wall, SE site area	8020 ± 80	8430 ± 80	8900–8575	Elephant Seal Beach
JPt1	Mc	OS-43079	Dune paleosol	N/A	1680 ± 30	1040–950	Tyler Bight
SC2	Hr	Beta-183156	Gully wall, NW site area	5650 ± 60	6090 ± 60	6340–6210	Elephant Seal Beach
SC22	L	Beta-190678	Surface	4670 ± 50	5080 ± 50	5280–5040	Crook Point area
SC64	Cr	Beta-195745	Southern loci, E gully wall	6240 ± 80	6670 ± 80	7020–6800	Crook Point area

[a] * Denotes sites dated by previous researchers.

[b] Mc = *Mytilus californianus*; Hr = *H. rufescens*; Hc = *H. cracherodii*; Cr = *Cryptochiton stelleri;* L = *Lottia gigantea.*

A second focus of our reconnaissance and dating program was located near Crook Point on the south-central coast. Here, several sites had been described that reportedly contained burials. In relocating 11 previously recorded sites in this area, we traversed a series of arroyo complexes in the Crook Point area and discovered at least 13 unrecorded shell middens, many of them buried sites exposed only in gully walls. These buried shell lenses varied in depth and composition, but consisted mostly of California mussel (*Mytilus californianus*) and abalone (*Haliotis* spp.). What is most surprising is not the density or composition of the deposits but that shell lenses were found in every arroyo and were highly visible from the gully walls. Many of these unrecorded shell middens were rapidly eroding, spreading the deposits up to 100 m or more from their likely places of origin.

Unlike the north coast, at least some of the sites we have found—including several of the most substantial shell middens—are not located adjacent to the modern shoreline. Instead, they are located along the northern margin of the coastal plain, near the base of the steep escarpment that separates the south coast from the tablelands of the island's interior. These locations offer greater protection from the northwesterly winds and better access to freshwater sources. In addition to the 5 ^{14}C dates obtained by Glassow (1980) and Walker et al. (2000) for 2 south coast sites, we have added another 20 dates from 15 sites. Although there are several gaps in the sequence, we now have dates ranging from over 9400 cal BP to Protohistoric and Historic times (about AD 1540 to 1820). Three sites have been dated to the Early Holocene, six to the Middle Holocene, and eight to the Late Holocene.

Our recent research suggests that human use of San Miguel's south coast by the Chumash and their ancestors was more extensive than previously thought and began more than 3000 yr earlier than previously documented. One reason that few sites have been recorded in the area may be that portions of the coastal plain were blanketed historically by dune sand deposited after historical overgrazing destabilized the island's extensive dune fields (see Erlandson et al., forthcoming). Our recent work shows that thick layers of sand cover some portions of the south coast and that numerous shell middens have been identified eroding from paleosols exposed in gullies that are cutting through this sand overburden. Thus, other sites may only have been exposed by the recent downcutting, headward erosion, and expansion of the numerous gully complexes that dissect the coastal plain along the south coast. Also contributing to the limited number of recorded sites, however, is the longstanding historical perception that the south coast was less heavily occupied, which has resulted in more cursory reconnaissance efforts by archaeologists, almost no systematic excavations of south coast sites, and only limited ^{14}C dating.

CONCLUSIONS

The north coast of San Miguel Island was probably the primary focus of settlement by the Chumash and their ancestors. Our recent research suggests, however, that the south coast of the island was more intensively settled than previously recognized and that such settlement began at least 9000 yr ago. Lingering preconceptions about the marginality of the south coast are contradicted by the number and variety of site types present in the area, the antiquity of human settlement, and the productivity of its intertidal, kelp forest, and other habitats. Unfortunately, these preconceptions have limited the amount of systematic survey, excavation, and ^{14}C dating done along the south coast, contributing to the marginalization of that area by archaeologists. We believe the presence of several springs, the shelter provided from the strong northwesterly winds and swells, and the productivity of nearshore resources all indicate the south coast to have been considerably more attractive to coastal foragers than previously believed.

Ironically, although erosion has exposed many of the newly identified sites, such erosion also threatens their continued existence. Virtually all the south coast sites we have examined are in danger of being lost to rapid coastal erosion, slope wash and gullying, or the effects of seals or sea lions hauling out on them. Protected for decades under sheets of sand stripped off windward north coast landforms and deposited on the lee side of the island, the exposure and rapid erosion of many south coast sites now requires a timely response to survey the expanding gully systems, sample the identified archaeological deposits, and secure material for ^{14}C dating and other analyses. We now are conducting such survey, sampling, dating, and analyses to help understand the history of the human use of the south coast, the historical ecology of its unique ecosystems, and the impacts that humans have had on them.

Around the world we are rapidly losing valuable archaeological, historical, and ecological data sets to erosion and other destructive processes at an alarming rate. As one response to such problems in coastal areas, Erlandson and Moss (1999) advocated the systematic collection and dating of organic samples during survey projects to help facilitate site management, prioritize sites for further research, and aid in a variety of regional research projects. They demonstrated, for instance, how ^{14}C dating of numerous sites can help identify and explain changes in local environments as well as human settlement, demography, and social organization within a region through time (see also Erlandson et al. 2001). By applying such methods to the archaeological record of the south coast of San Miguel Island, we have also demonstrated their effectiveness in rapidly illuminating the long history of human settlement in a poorly known area.

ACKNOWLEDGMENTS

Our research was supported by Channel Islands National Park (Grant #CA8120-00-007), the Western National Parks Association, the US Navy, the National Science Foundation, the Foundation for Exploration and Research on Cultural Origins, and the University of Oregon. We thank Ann Huston, Georganna Hawley, Kelly Minas, Bob DeLong (NMFS), Steve Schwartz, and Ian Williams for their time and support. We are also grateful to Doug Kennett, the editors, and an anonymous reviewer for their comments and assistance in the final revisions and production of this paper.

REFERENCES

Arnold JE. 1992. Complex hunter-gatherer-fishers of prehistoric California: chiefs, specialists, and maritime adaptations of the Channel Islands. *American Antiquity* 57(1):60–84.

Arnold JE. 2000. The origins of hierarchy and the nature of hierarchical structures in prehistoric California. In: *Hierarchies in Action: Cui Bono?* Carbondale, California: Center for Archaeological Investigations. p 221–40.

Erlandson JM. 2001. The search for early shell middens on San Miguel Island, California. Unpublished report submitted to The Foundation for the Exploration and Research on Cultural Origins and Channel Islands National Park.

Erlandson JM, Bartoy K. 1995. Cabrillo, the Chumash, and Old World diseases. *Journal of California and Great Basin Anthropology* 17(2):153–73.

Erlandson JM, Kennett DJ, Ingram BL, Guthrie DA, Morris DP, Tveskov MA, West GJ, Walker PL. 1996. An archaeological and paleontological chronology for Daisy Cave (CA-SMI-261), San Miguel Island, California. *Radiocarbon* 38(2):355–73.

Erlandson JM, Moss ML. 1996. The Pleistocene-Holocene transition along the Pacific Coast of North America. In: Straus L, Eriksen B, Erlandson J, Yesner D, editors. *Humans at the End of the Ice Age: The Archaeology of the Pleistocene-Holocene Transition*. New York: Plenum. p 277–302.

Erlandson JM, Moss ML. 1999. The systematic use of radiocarbon dating in archaeological surveys in coastal and other erosional environments. *American Antiquity* 64(3):431–43.

Erlandson JM, Rick TC, Kennett DJ, Walker PL. 2001. Dates, demography, and disease: cultural contacts and possible evidence for Old World epidemics among the Island Chumash. *Pacific Coast Archaeological Society Quarterly* 37(3):11–26.

Erlandson JM, Rick TC, Vellanoweth RL. 2004. Human impacts on ancient environments: a case study from California's Northern Channel Islands. In: Fitzpatrick

SM, editor. *Voyages of Discovery: The Archaeology of Islands*. Westport, Connecticut: Praeger. p 51–83.

Erlandson JM, Rick TC, Estes JA, Graham MH, Braje TJ, Vellanoweth RL. Forthcoming. Sea otters, shellfish, and humans: a 10,000-year record from San Miguel Island, California. In: Garcelon D, editor. *Proceedings of the Sixth California Islands Conference*.

Glassow MA. 1980. Recent developments in the archaeology of the Channel Islands. In: Power DM, editor. *Proceedings of a Multidisciplinary Symposium*. Santa Barbara: Santa Barbara Museum of Natural History. p 79–99.

Greenwood RS. 1978. Archaeological survey and investigation: Channel Islands National Monument, California. Volumes I and II [manuscript on file]. Santa Barbara: Department of Anthropology, University of California, Santa Barbara.

Greenwood RS. 1982. Archaeological survey on San Miguel Island Channel Islands National Monument California. Volumes I and II [report on file at the Central Coast Information Center]. Santa Barbara: Department of Anthropology, University of California, Santa Barbara.

Heye G. 1921. Certain artifacts from San Miguel Island, California. *Indian Notes and Monographs* 7(4):1–211. New York: Museum of the American Indian, Heye Foundation.

Johnson DL. 1980. Episodic vegetation stripping, soil erosion, and landscape modification in prehistoric and recent historic time, San Miguel Island, California. In: Power DM, editor. *The California Islands: Proceedings of a Multidisciplinary Symposium*. Santa Barbara: Santa Barbara Museum of Natural History. p 103–21.

Johnson JR, Stafford Jr TW, Ajie HO, Morris DP. 2000. Arlington Springs revisited. In: Browne D, Mitchell K, Chaney H, editors. *Proceedings of the Fifth California Channel Islands Symposium*. Santa Barbara: Santa Barbara Museum of Natural History. p 628–32

Juger A, Johnson DL. 1980. Was there a Quaternary land bridge to the Northern Channel Islands? In: Power DM, editor. *The California Islands Symposium: Proceedings of a Multidisciplinary Symposium*. Santa Barbara: Santa Barbara Museum of Natural History. p 33–9.

Kennett DJ. 1998. Behavioral ecology and the evolution of hunter-gatherer societies on the Northern Channel Islands, California [PhD dissertation]. Santa Barbara: University of California, Santa Barbara.

Kennett DJ. Forthcoming. *The Island Chumash: Behavioral Ecology of a Maritime Society.* Berkeley: University of California Press. 310 p.

King CD. 1990. *Evolution of Chumash Society: A Comparative Study of Artifacts Used for Social System Maintenance in the Santa Barbara Channel Region Before AD 1804*. New York: Garland Publishing.

Orr PC. 1968. *Prehistory of Santa Rosa Island*. Santa Barbara: Santa Barbara Museum of Natural History.

Rick TC. 2004. Daily activities, community dynamics, and historical ecology on California's Northern Channel Islands [PhD dissertation]. Eugene: University of Oregon.

Rick TC, Erlandson JM. 2003. Archaeology, ancient human impacts on the environment, and cultural resource management on Channel Islands National Park, California. *CRM: The Journal of Heritage Stewardship* 1(1):86–9.

Rick TC, Erlandson JM. 2004. Archaeological site assessments on San Miguel and Santa Rosa Islands, Channel Islands National Park, California. Department of Anthropology, University of Oregon. Report submitted to Channel Islands National Park.

Rogers DB. 1929. *Prehistoric Man on the Santa Barbara Coast*. Santa Barbara: Santa Barbara Museum of Natural History.

Rozaire CE. 1978. *Archaeological Investigations on San Miguel Island, California*. Los Angeles: Los Angeles County Museum of Natural History.

Walker PL, Kennett DJ, Jones TL, DeLong R. 2000. Archaeological investigations at the Point Bennett Pinniped Rookery on San Miguel Island. In: Browne D, Mitchell K, Chaney H, editors. *Proceedings of the Fifth California Channel Islands Symposium*. Santa Barbara Museum of Natural History. p 628–32.

RADIOCARBON, Vol 47, Nr 1, 2005, p 115–134

RADIOCARBON DATING OF MODERN PEAT PROFILES: PRE- AND POST-BOMB ^{14}C VARIATIONS IN THE CONSTRUCTION OF AGE-DEPTH MODELS

Tomasz Goslar[1,2] • W O van der Knaap[3] • Sheila Hicks[4] • Maja Andrič[5,6] • Justyna Czernik[2] • Ewa Goslar[2] • Satu Räsänen[4] • Heidi Hyötylä[4]

ABSTRACT. We present studies of 9 modern (up to 400-yr-old) peat sections from Slovenia, Switzerland, Austria, Italy, and Finland. Precise radiocarbon dating of modern samples is possible due to the large bomb peak of atmospheric ^{14}C concentration in 1963 and the following rapid decline in the ^{14}C level. All the analyzed ^{14}C profiles appeared concordant with the shape of the bomb peak of atmospheric ^{14}C concentration, integrated over some time interval with a length specific to the peat section. In the peat layers covered by the bomb peak, calendar ages of individual peat samples could be determined almost immediately, with an accuracy of 2–3 yr. In the pre-bomb sections, the calendar ages of individual dated samples are determined in the form of multi-modal probability distributions of about 300 yr wide (about AD 1650–1950). However, simultaneous use of the post-bomb and pre-bomb ^{14}C dates, and lithological information, enabled the rejection of most modes of probability distributions in the pre-bomb section. In effect, precise age-depth models of the post-bomb sections have been extended back in time, into the "wiggly" part of the ^{14}C calibration curve.

Our study has demonstrated that where annual resolution is concerned, tissues of *Sphagnum* are the only representative material for ^{14}C dating, although even samples of pure *Sphagnum* collected from a very thin slice of the peat section contain tissues grown in different years, so they integrate the atmospheric ^{14}C signal over a period of time. This time period (0.5–8 yr, depending on the site) seems to correlate with the peat accumulation rate, but it also depends on how the sampled peat sections were handled. When constructing age-depth models, for some peat sections we used the strategy of multi-stage ^{14}C dating. This led to a drastic reduction in the uncertainty of the age-depth models, by dating only a few additional samples in the profile.

Our study is the first in which peat sections from the late pre-bomb time (AD 1900–1960) have been precisely dated at a high temporal resolution. In this time interval, ^{14}C ages of all the samples dated were younger than those derived from the atmospheric calibration curve, apparently due to the effect of integration. Evidently, the determination of calendar ages based on ^{14}C dating of single peat samples from that interval may be affected by a serious error if the possibility of integration is ignored.

INTRODUCTION

Recent scientific work has demonstrated the capability of peat mires to store information of past environments with a high temporal resolution (Goodsite et al. 2001). Peat sections have served as archives of heavy metal pollutants of the atmosphere (Shotyk et al. 1998; Benoit et al. 1998) and yielded records of both climate and atmospheric CO_2 content (Martínez-Cortizas et al. 1999; White et al. 1994). Recently, the global importance of peatlands as a carbon sink has been documented (Smith et al. 2004). In every case, a precise age control was required and achieved by using either the ^{210}Pb or the ^{14}C method.

Because of past variations in atmospheric ^{14}C content, individual ^{14}C dates do not usually allow a precise determination of calendar age. The situation is much better if a series of ^{14}C dates is available and additional information about the time intervals between dated samples is known. Then, one may try to use the wiggle-matching technique, which was successfully applied in some old peat sections where thick sections of almost constant accumulation rate were documented (Kilian et al. 1995, 2000; Blaauw 2003).

Here, we deal with 9 peat profiles from Slovenia, Switzerland, Austria, Italy, and Finland (Figure 1), investigated in the framework of a project called PINE (Predicting Impacts on Natural Ecotones).

[1]Faculty of Physics, A. Mickiewicz University, Umultowska 85, 61-614 Poznań, Poland. Email: goslar@radiocarbon.pl.
[2]Poznań Radiocarbon Laboratory, Rubież 46, 61-612 Poznań, Poland.
[3]Institute of Plant Sciences, University of Bern, Altenbergrain 21, 3013 Bern, Switzerland.
[4]Institute of Geosciences, P.O. Box 3000, 90014 University of Oulu, Finland.
[5]Slovenian Forestry Institute, Večna pot 2, 1000 Ljubljana, Slovenia.
[6]Institute of Archaeology, Slovenian Academy of Sciences and Arts, Novi trg 2, PB 306, 1001 Ljubljana, Slovenia.

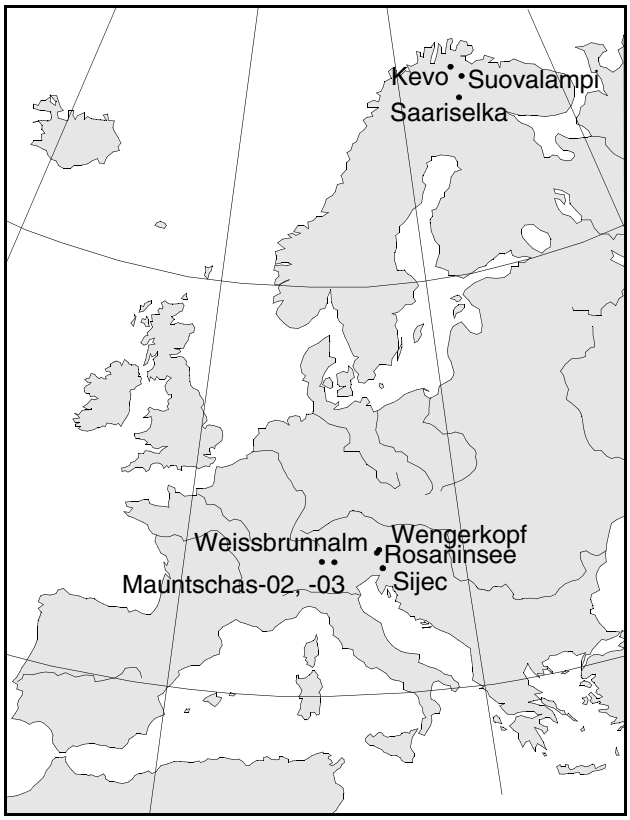

Figure 1 Locations of the studied peat sections

This project requires pollen accumulation rates (grains cm^{-2} yr^{-1}) to be calculated at high temporal resolution for the last 300 yr, then compared with the tree-ring records. The project therefore requires a precise and robust age-depth chronology. The pollen calculations will be discussed in future publications. The present paper is concerned with the problems of ^{14}C dating and the determination of age-depth models for the peat sections studied.

Age determination by ^{14}C dating individual modern (post-1950 AD) samples is possible due to the large bomb peak of atmospheric ^{14}C concentration in 1963 and the following rapid decline in the ^{14}C level (Nydal and Lövseth 1983). Accurate calibration of older ^{14}C dates, from AD 1650 to 1950, is more problematic because of large wiggles in the ^{14}C calibration curve (Stuiver et al. 1998). Moreover, because the peat accumulation rate in young sections of peat mires changes with depth, the wiggle-matching technique is not applicable.

In the present study, we treated jointly the series of dates encompassing both the pre-bomb and post-bomb periods, which enabled us to derive precise age-depth models even in the critical period of the wiggly calibration curve (about AD 1650–1950).

MATERIAL AND METHODS

At each of the sites studied (Figure 1), the material was collected in the form of a peat monolith. In order to obtain high-resolution records, samples for ^{14}C dating were taken from within 3–5-mm-thick slices, and within vertical columns of about 2 × 2 cm wide. From most of the sections sampled, pure *Sphagnum* was selected for ^{14}C dating.

Although peat is generally regarded as a reliable material for ^{14}C dating, Kilian (1995) found that ^{14}C dates of bulk material are sometimes affected by the reservoir effect. The same appears to be true when the samples are not completely cleaned of rootlets (e.g. of *Ericaceae*) or fungal remains (Kilian et al. 2000; Speranza et al. 2000). Therefore, when accurate ^{14}C dating of peat is desired, the use of only aboveground plant material is recommended (Blaauw 2003).

Sphagnum is used because it forms the bulk of most peat deposits; it is a moss and therefore does not have roots, so its growth is upward from the apex only. This means that there is little possibility for this plant to derive carbon from the underlying older peat. Other types of plant material were used for ^{14}C dating, in only a few cases where *Sphagnum* was not available.

As the amount of pure *Sphagnum* available in each sample was small, only the accelerator mass spectrometry (AMS) technique was applicable in ^{14}C dating. Most samples were dated in the Poznań Radiocarbon Laboratory. The samples for ^{14}C dating were treated chemically according to the standard AAA (acid-alkali-acid) procedure (e.g. de Jong 1981). After chemical pretreatment, the samples were combusted in sealed quartz tubes (with CuO and Ag), and the CO_2 produced was purified and graphitized by reduction with H_2, using Fe powder as a catalyst. The details of the laboratory procedure are described by Czernik and Goslar (2001). The graphite targets were then loaded into the AMS spectrometer, which enabled measurements of $^{14}C/^{12}C$ and $^{13}C/^{12}C$ ratios (Goslar et al. 2004). A few samples from one of the peat sections were dated earlier in the ^{14}C laboratory in Utrecht (Hicks et al. 2004), and these earlier results were included in the present study.

All the ^{14}C dates used in this paper are shown in Table 1 and Figure 2a. The younger parts of the peat sections reveal modern ^{14}C ages (>100 pMC), reflecting the bomb peak of atmospheric ^{14}C. Most of the dates in the older parts fall within the interval 0–200 ^{14}C BP, representing the wiggly part of the ^{14}C calibration curve between AD 1650 and 1950.

Joint Calibration of ^{14}C Dates in the Pre-Bomb and Post-Bomb Periods

In previous studies using the bomb peak for ^{14}C dating, ^{14}C concentrations in dated samples were expressed as pMC (percent modern carbon) and compared with the ^{14}C levels ($\Delta^{14}C$) recorded in the past in atmospheric air (Goodsite et al. 2001; Jungner et al. 1995). However, concentrations of ^{14}C measured in peat samples dated today are not directly comparable with those in the atmospheric $\Delta^{14}C$ records, which were determined in particular years in the past, i.e. several years or decades ago. In each case, the records of atmospheric $\Delta^{14}C$ have to be corrected for radioactive decay back to the measurement year.

Therefore, we decided to express the decay-corrected bomb atmospheric ^{14}C data in terms of ^{14}C age (negative in this case) in order to compare them directly with ^{14}C ages measured in the dated peat samples. In this approach, the ^{14}C data in the post-bomb period are treated in exactly the same manner as classic calibration of "normal" (i.e. pre-bomb) ^{14}C dates. In the approach of joint calibration, the uniform sets of (positive and negative) ^{14}C ages measured along the peat section are calibrated using the ^{14}C calibration curve, which extends into the post-bomb period.

In order to construct the extended "calibration curve" (Figure 2b), we used the Washington single-year tree-ring data for the period AD 1600–1950 (Stuiver and Braziunas 1993), supplemented by the $\Delta^{14}C$ biweekly data from Nordkapp (Nydal and Lövseth 1996) in 1963–1997 and Schauinsland (Levin et al. 1997) in 1977–1996. For each year, the biweekly data were averaged over the growing season only. In the transition period 1950–1963, we used the compilation made by Goodsite et al. (2001), while the data after 1997 were obtained by extrapolation of the Nordkapp record using an exponential function.

Table 1 Results of radiocarbon dating of the peat sections studied, expressed as conventional ^{14}C age and as content with respect to the modern standard (pMC = percent modern carbon).

Depth (mm)	Material dated	Lab nr[a]	^{14}C BP	pMC	Year AD[b]
Kevo (collected 1997. lat 69°45′N, long 27°00′E)					
20	*Betula nana* leaf	UtC-8183	−1067 ± 56	114.2 ± 0.8	1994.9
40	*Betula nana* leaf	UtC-8184	−1518 ± 33	120.8 ± 0.5	1992
51	*Betula nana* leaf	UtC-9195	−1185 ± 42	115.9 ± 0.6	1990.1
52	*Betula nana* leaf	UtC-8134	−1857 ± 32	126.0 ± 0.5	1989.9
52.5	*Sphagnum*	Poz-4403	−1404 ± 24	119.1 ± 0.3	1989.8
70	*Betula nana* leaf	UtC-8135	−1391 ± 122	118.9 ± 1.8	1986.4
90	*Betula nana* leaf	UtC-8136	−2145 ± 43	130.6 ± 0.7	1981.6
100	*Betula nana* leaf	UtC-8158	−2236 ± 36	132.1 ± 0.6	1979
142	*Sphagnum*	Poz-2375	−3825 ± 20	161.0 ± 0.4	1966
182	*Sphagnum*	Poz-2376	75 ± 25	99.1 ± 0.3	1945.8
227	*Sphagnum*	Poz-2377	75 ± 25	99.1 ± 0.3	1909
262	*Sphagnum*	Poz-3680	120 ± 30	98.5 ± 0.4	1870
560	Peat	Poz-2378	2475 ± 30	73.5 ± 0.3	
550	*Sphagnum*	Poz-2951	90 ± 25	98.9 ± 0.3	1819.6
600	*Sphagnum*	Poz-2952	190 ± 25	97.7 ± 0.3	1750
Suovalampi (collected 1997. lat 69°36′N, long 28°51′E)					
20	*Sphagnum*	Poz-2391	−1282 ± 22	117.3 ± 0.3	1990
40	*Sphagnum*	Poz-2392	−2068 ± 22	129.4 ± 0.4	1982
60	*Sphagnum*	Poz-2393	−2470 ± 22	136.0 ± 0.4	1979
80	*Sphagnum*	Poz-2395	−2519 ± 31	136.8 ± 0.5	1976
105	*Sphagnum*	Poz-2396	−3216 ± 28	149.2 ± 0.5	1963
115	*Sphagnum*	Poz-3679	55 ± 25	99.3 ± 0.3	1948
140	*Sphagnum*	Poz-2397	130 ± 35	98.4 ± 0.4	1862
180	*Sphagnum*	Poz-2398	195 ± 30	97.6 ± 0.4	1792
220	*Sphagnum*	Poz-2399	680 ± 30	91.9 ± 0.3	1707
220	*Sphagnum*	Poz-2724	845 ± 30	90.0 ± 0.3	1707
280	*Sphagnum*	Poz-2401	355 ± 30	95.7 ± 0.4	1550
Saariselkä (collected 2002. lat 68°25′N, long 27°26′E)					
30	*Sphagnum* leaves	Poz-1823	−851 ± 25	111.2 ± 0.3	1996.1
50	*Sphagnum* leaves	Poz-1829	−1414 ± 25	119.2 ± 0.4	1987.8
70	*Sphagnum* leaves	Poz-1825	−3367 ± 25	152.1 ± 0.5	1972.4
90	*Sphagnum* leaves	Poz-1827	40 ± 35	99.5 ± 0.4	1950.5
120	*Sphagnum* leaves	Poz-1826	20 ± 35	99.8 ± 0.4	1892.3
140	*Sphagnum* leaves	Poz-1824	−17 ± 103	100.2 ± 1.3	1852.3
150	*Sphagnum* leaves	Poz-2388	75 ± 25	99.1 ± 0.3	1833
165	*Sphagnum* leaves	Poz-1831	−68 ± 33	100.9 ± 0.4	1789.3
168	*Sphagnum* leaves	Poz-2389	0 ± 25	100.0 ± 0.3	1791.4
190	Fine (<0.18 mm) fraction of peat	Poz-1834	75 ± 30	99.1 ± 0.4	1728.3
220	Fine (<0.18 mm) fraction of peat	Poz-1830	220 ± 30	97.3 ± 0.4	
250	*Carex*, *Eriophorum*	Poz-3678	475 ± 30	94.3 ± 0.4	
260	Fine (<0.18 mm) fraction of peat	Poz-1833	670 ± 30	92.0 ± 0.3	
320	Fine (<0.18 mm) fraction of peat	Poz-1822	1055 ± 30	87.7 ± 0.3	
1045	Peat	Poz-1835	6340 ± 40	45.4 ± 0.2	

Table 1 Results of radiocarbon dating of the peat sections studied, expressed as conventional ^{14}C age and as content with respect to the modern standard (pMC = percent modern carbon). *(Continued)*

Depth (mm)	Material dated	Lab nr[a]	^{14}C BP	pMC	Year AD[b]
Wengerkopf (collected 2002. lat 13°52′E, long 47°10′N)					
115	*Sphagnum*	Poz-1842	–860 ± 26	111.3 ± 0.4	1996
213	*Sphagnum*	Poz-1840	–1236 ± 29	116.6 ± 0.4	1991
260	*Sphagnum*	Poz-951	–1333 ± 25	118.1 ± 0.4	1988.1
275	*Sphagnum*	Poz-1839	–1305 ± 26	117.6 ± 0.4	1987.1
290	*Sphagnum*	Poz-3599	–1575 ± 34	121.7 ± 0.5	1986.1
320	*Sphagnum*	Poz-1838	–1702 ± 27	123.6 ± 0.4	1982.1
354	*Sphagnum*	Poz-1813	–3325 ± 40	151.3 ± 0.8	1972.7
380	*Sphagnum*	Poz-1099	–4423 ± 20	173.4 ± 0.4	1965.8
386	*Sphagnum*	Poz-3600	–4441 ± 27	173.8 ± 0.6	1964.2
406	*Sphagnum*	Poz-1819	–1663 ± 28	123.0 ± 0.4	1959.2
430	*Sphagnum*	Poz-1814	2 ± 29	100.0 ± 0.4	1952.4
458	*Sphagnum*	Poz-1820	95 ± 50	98.8 ± 0.6	1942
500	*Sphagnum*	Poz-952	100 ± 30	98.8 ± 0.4	1924.9
515	*Sphagnum*	Poz-1821	120 ± 30	98.5 ± 0.4	1919.5
549	*Sphagnum*	Poz-1837	100 ± 30	98.8 ± 0.4	1906.8
585	*Sphagnum*	Poz-956	60 ± 30	99.3 ± 0.4	1881.5
615	Fine (<0.2 mm) fraction of peat	Poz-947	90 ± 30	98.9 ± 0.4	1831.5
665	Fine (<0.2 mm) fraction of peat	Poz-3409	85 ± 30	98.9 ± 0.4	1708.4
690	*Sphagnum*	Poz-3944	310 ± 30	96.2 ± 0.4	1630
715	Fine (<0.2 mm) fraction of peat	Poz-3581	470 ± 30	94.3 ± 0.4	
Weissbrunnalm-01 (collected 2002. lat 46°28′N, long 10°49′E)					
110	*Sphagnum*	Poz-1100	–2477 ± 23	136.1 ± 0.4	1977
160	*Sphagnum*	Poz-949	–4116 ± 21	166.9 ± 0.4	1968.1
210	*Sphagnum*	Poz-953	–1693 ± 27	123.5 ± 0.4	1959.2
230	Fine (<0.2 mm) fraction of peat	Poz-955	–288 ± 26	103.7 ± 0.3	1954.5
275	*Potentilla* seeds	Poz-3737	110 ± 30	98.6 ± 0.4	1938
Rosaninsee (collected 2002. lat 13°46′E, long 46°57′N)					
90	*Sphagnum*	Poz-2434	–1036 ± 21	113.8 ± 0.3	1993
170	*Sphagnum*	Poz-2435	–1681 ± 20	123.3 ± 0.3	1985
250	*Sphagnum*	Poz-1849	–2279 ± 26	132.8 ± 0.4	1978.1
300	*Sphagnum*	Poz-1850	–2982 ± 25	145.0 ± 0.5	1973.3
335	*Sphagnum*	Poz-2498	–4156 ± 20	167.8 ± 0.4	1966.9
366	Fine (<0.2 mm) fraction of peat	Poz-2499	–275 ± 27	103.5 ± 0.3	1954
366	Seeds and spores	Poz-3763	155 ± 30	98.1 ± 0.4	1954
400	Mosses	Poz-3761	195 ± 30	97.6 ± 0.4	1931
Mauntschas-02 (collected 2002. lat 46°29′N, long 9°51′E)					
60	*Sphagnum*	Poz-2949	–940 ± 23	112.4 ± 0.3	1995.2
115	*Sphagnum*	Poz-2414	–1427 ± 21	119.4 ± 0.3	1987.7
177	*Sphagnum*	Poz-2415	–2747 ± 20	140.8 ± 0.4	1972.2
207	*Sphagnum*	Poz-2950	–2969 ± 29	144.7 ± 0.5	1963.6
215	*Sphagnum*	Poz-3597	–1478 ± 46	120.2 ± 0.7	1961.2
238	*Sphagnum*	Poz-2416	10 ± 25	99.9 ± 0.3	1954.3
278	*Sphagnum*	Poz-2417	75 ± 25	99.1 ± 0.3	1944.1
320	*Sphagnum*	Poz-2418	95 ± 25	98.8 ± 0.3	1934.9
370	*Sphagnum* + moss	Poz-2420	150 ± 25	98.2 ± 0.3	1922.9
430	*Sphagnum*	Poz-2421	95 ± 25	98.8 ± 0.3	1908
495	*Sphagnum* + moss	Poz-2422	80 ± 25	99.0 ± 0.3	1883.1

Table 1 Results of radiocarbon dating of the peat sections studied, expressed as conventional ^{14}C age and as content with respect to the modern standard (pMC = percent modern carbon). *(Continued)*

Depth (mm)	Material dated	Lab nr[a]	^{14}C BP	pMC	Year AD[b]
518	*Sphagnum* + *Calluna* branches	Poz-2424	105 ± 25	98.7 ± 0.3	1860.4
550	*Sphagnum*	Poz-2951	90 ± 25	98.9 ± 0.3	1819.6
600	*Sphagnum*	Poz-2952	190 ± 25	97.7 ± 0.3	1750
Šijec (collected 2002. lat 46°20′N, long 14°00′E)					
50	*Sphagnum*	Poz-1527	–789 ± 28	110.3 ± 0.4	1999
100	*Sphagnum*	Poz-1530	–918 ± 29	112.1 ± 0.4	1996.1
150	*Sphagnum*	Poz-1525	–1073 ± 26	114.3 ± 0.4	1992.8
200	*Sphagnum*	Poz-1531	–1318 ± 29	117.8 ± 0.4	1988
250	*Sphagnum*	Poz-1524	–1854 ± 27	126.0 ± 0.4	1981.8
300	*Sphagnum*	Poz-1532	–2844 ± 27	142.5 ± 0.5	1974.5
350	*Sphagnum*	Poz-1526	–4435 ± 23	173.7 ± 0.5	1966.9
400	*Sphagnum*	Poz-1533	–1393 ± 30	118.9 ± 0.4	1957.3
450	*Sphagnum*	Poz-2746	80 ± 25	99.0 ± 0.3	1933.6
475	*Sphagnum*	Poz-3629	65 ± 30	99.2 ± 0.4	1918.5
500	*Sphagnum*	Poz-2747	0 ± 30	100.0 ± 0.4	1901.7
550	*Sphagnum*	Poz-1523	90 ± 30	98.9 ± 0.4	1864.3
585	*Sphagnum*	Poz-2748	105 ± 25	98.7 ± 0.3	1835.7
620	*Sphagnum*	Poz-3630	620 ± 50	92.6 ± 0.6	
650	Organic sediment	Poz-1529	595 ± 30	92.9 ± 0.3	
Mauntschas-03 (collected 2003. lat 46°29′N, long 9°51′E)					
110	*Sphagnum*	Poz-3998	–1247 ± 24	116.8 ± 0.4	1988
170	*Sphagnum*	Poz-5181	–3280 ± 26	150.4 ± 0.5	1973
220	*Sphagnum*	Poz-3999	–4607 ± 24	177.4 ± 0.5	1963
272	*Sphagnum*	Poz-5445	110 ± 35	98.6 ± 0.4	1949
320	*Sphagnum*	Poz-4055	135 ± 30	98.3 ± 0.4	1936
420	*Sphagnum*	Poz-4000	130 ± 25	98.4 ± 0.3	1905
520	*Sphagnum*	Poz-4001	120 ± 25	98.5 ± 0.3	1870
550	*Sphagnum*	Poz-5179	80 ± 30	99.0 ± 0.4	1858
680	*Sphagnum*	Poz-5484	235 ± 30	97.1 ± 0.4	1795.5
720	*Sphagnum*	Poz-4002	225 ± 30	97.2 ± 0.3	1762.5
770	*Sphagnum*	Poz-5180	200 ± 30	97.6 ± 0.4	1638
820	*Sphagnum*	Poz-4004	450 ± 30	94.6 ± 0.3	1450
920	*Sphagnum*	Poz-3762	865 ± 30	89.8 ± 0.3	1180

[a]Most samples were dated in the Poznań Radiocarbon Laboratory (code Poz-). The laboratory numbers with the code UtC- are samples dated in the AMS ^{14}C laboratory in Utrecht (Hicks et al. 2004).

[b]The calendar ages of peat samples are derived from the age-depth models described in the text.

Relevant for the calibration of ^{14}C dates is whether the dated organisms derived their carbon in equilibrium with the atmosphere. This problem is evident in marine environments where the marine ^{14}C calibration curve has to be applied, which takes into account a site-specific reservoir age. The problem of reservoir age does not seem to be applicable for peat. Nevertheless, Jungner et al. (1995) in their studies of modern peat sections did show a bomb peak in peat distinctly smaller than in the atmosphere, and they concluded that the ^{14}C content in the air near a peatbog surface was seriously affected by ^{14}C-depleted CO_2 produced by the decomposition of older plant tissues, and emanating from the underlying layers. Goodsite et al. (2001), on the other hand, found that the ^{14}C peaks in 2 peat profiles from Denmark and Greenland were as large as in the atmosphere, suggesting absence of ^{14}C depletion in those profiles.

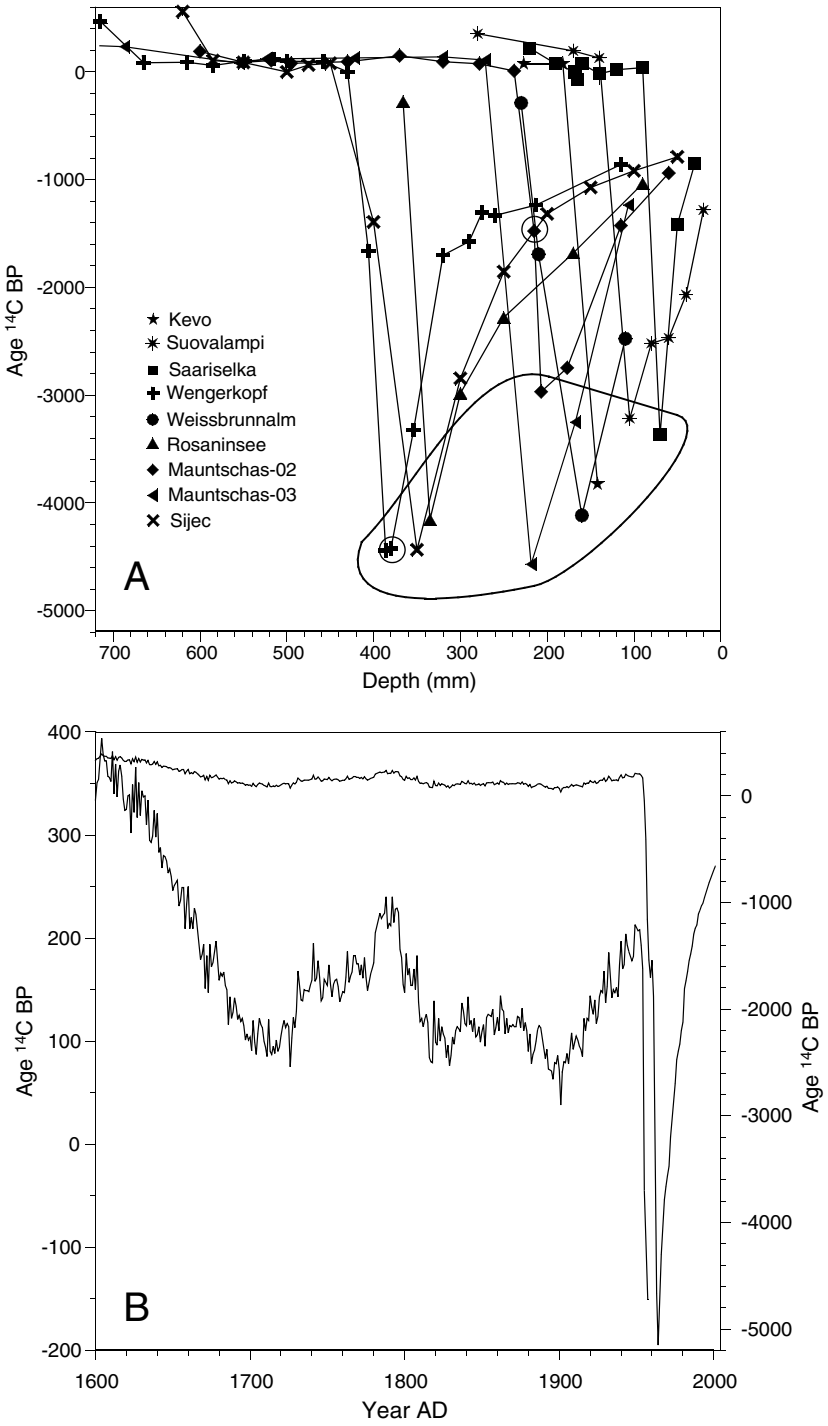

Figure 2 a) ^{14}C dates of samples from the peat sections studied plotted as a function of depth. Negative ^{14}C ages correspond to samples with a ^{14}C concentration higher than in the standard of the modern biosphere (due to the atomic bomb effect). The points representing the maximum ^{14}C values measured in each peat section are enclosed with a band. The 2 dates from levels sampled intentionally to meet the absolute ^{14}C maxima are circled. b) The single-year ^{14}C calibration curve extended onto the post-bomb period. Note that the curve is shown on 2 different vertical scales.

In this study, we note that the ^{14}C maxima in all the peat profiles are smaller than the atmospheric bomb peak (Figure 2), and we observe a correlation between the maximum ^{14}C measured in a peat section and the peat accumulation rate (expressed as the depth at which the ^{14}C maximum occurs). This correlation is significant ($r^2 = 0.43$, $df = 8$) at a level of 0.05, implying a relationship between the 2 variables.

One potential reason for that correlation could be that the maximum ^{14}C levels in the peat profiles were just missed because of limited sampling resolution. Indeed, the chance of sampling at the maximum decreases with decreasing sampling resolution, which in turn might be related to the peat accumulation rate. However, the height of the ^{14}C maximum and the sampling resolution are not directly correlative.

Another mechanism could be that both the maximum ^{14}C level recorded in the peat section and the peat accumulation rate were controlled by the same factor, e.g. the length of the vegetation period. Indeed, most of the peat sections with a slow accumulation rate occur in northern Finland, where the growing season is shorter than that in central Europe. However, the shorter vegetation season means higher seasonal averages of ^{14}C in peat, which is the opposite of the observed relationship.

The ultimate reason for the correlation described above is that the samples dated encompassed several years, so that the bomb ^{14}C maxima were flattened simply by integration. We must stress that the samples analyzed came from very thin layers (2–5 mm), which would scarcely correspond to more than 1 yr based on the mean peat accumulation rate between the mid-1960s and today. Nevertheless, it seems possible that the dead *Sphagnum* fragments in the peat are mixed due to compression of peat layers, and tissues grown in different years may be found at the same level. Such a mixing would result in the situation where the specific levels analyzed from the peat sections contain a mixture of ^{14}C assimilated over a number of years. In other words, we must agree that the ^{14}C concentration in peat from a specific level reflects the atmospheric record integrated over some period of time. An additional integration of ^{14}C concentration would also be caused by CO_2 or CH_4 produced by decomposition of older plant tissues, and emanating from the underlying peat, taken up by overlying peat layers.

Site-Specific Integration Time of Atmospheric ^{14}C in Peat

We assume that the integration of the atmospheric ^{14}C record in peat might be expressed by a Gaussian curve with a site-specific width (expressed as integration time τ). Therefore, the longer the integration time is, the more flattened the bomb ^{14}C maximum in peat would be expected (see Figure 3).

The integration time τ in a particular peat section can be quantified using the information on the height of the ^{14}C maximum and the sampling resolution (Figure 3). For example, the maximum ^{14}C measured in Mauntschas-02 (at 207 mm) is distinctly lower than the atmospheric peak (which corresponds to −5150 ^{14}C BP). If there would be no integration, this would imply that the sampling has missed the absolute peak of atmospheric ^{14}C and the sample at 207 mm would correspond to AD 1973. This, however, is unlikely as the underlying sample (at 215 mm) has a lower ^{14}C content of atmospheric ^{14}C, whereas a higher content corresponding to around AD 1967 would be expected. This contradiction disappears when we assume that in the peat section the atmospheric ^{14}C record is integrated, with an integration time as long as 8 yr.

Another situation is represented in the Šijec peat section. Here, the maximum ^{14}C is also lower than the atmospheric peak. If no integration took place, the maximum sample (350 mm) would originate from AD 1966, which is possible since the underlying sample with lower ^{14}C content would represent AD 1960 (400 mm), the year when the atmospheric ^{14}C concentration was indeed lower.

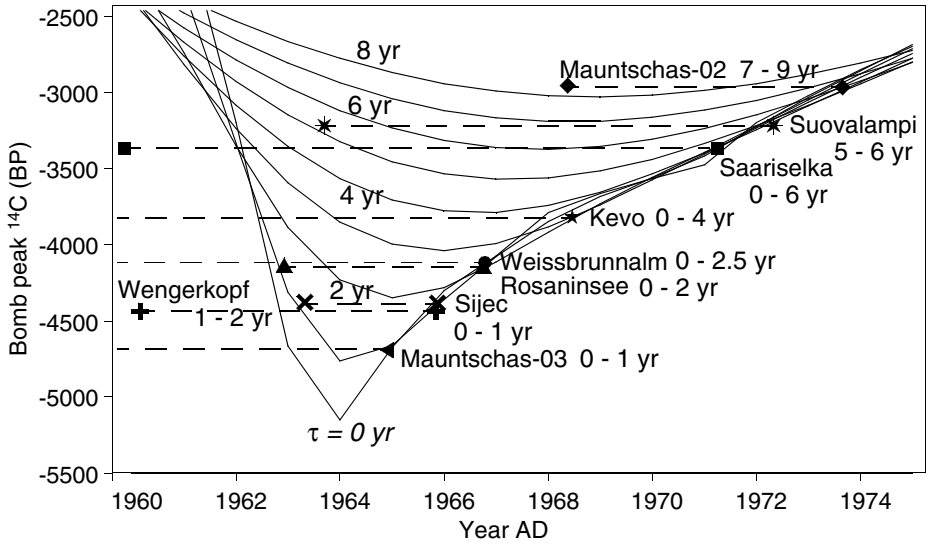

Figure 3 Illustration of the assessment of the integration time τ. The smooth lines represent "theoretical" profiles of ^{14}C age, obtained for different values of integration time. The maximum ^{14}C values measured in particular profiles are represented by horizontal segments. The lengths of the segments correspond to the time intervals between adjacent samples in particular peat profiles.

As shown in Figure 3, the integration time is longer (3–6 yr) in the northern sites (Suovalampi, Kevo, Saariselkä) and shorter in the Alps (0.7–2 yr), which is clearly correlative with the slower peat accumulation rate in the north. An exception is Mauntschas-02, where the integration time is long (8 yr) despite a relatively high accumulation rate.

Surprised by the large integration time in Mauntschas-02, we sampled the twin peat section Mauntschas-03 (taken a few tens of meters away from the -02 section). Although the accumulation rate was the same (Figure 2a), the ^{14}C peak in Mauntschas-03 appeared much higher and the integration time much shorter than in Mauntschas-02. One reason for this difference could be that before we started our work on Mauntschas-02, the section had been sampled by other researchers for a variety of studies, and it may be that the section was not handled carefully with regard to the peat stratigraphy. We sampled Mauntschas-02 by cutting a sub-section from one edge of the section over the full length and 4×4 cm in surface area with a sharp knife; samples for AMS ^{14}C dating were taken from this sub-section. Mauntschas-03 was treated very carefully with regard to the peat stratigraphy, both in the field and in the laboratory as follows. A sub-section about 10×10 cm in surface area was sawed from the larger peat section in the frozen condition. The samples for AMS ^{14}C dating were taken from the cleaned surface below a saw cut, away from the original outer surface of the section.

The case of the Mauntschas site leads us to believe that the difference in the length of the estimated ^{14}C integration time between Mauntschas-02 and -03 may have resulted from differences in handling the peat sections. The estimated short ^{14}C integration time in Mauntschas-03 (<1 yr) suggests that the peat layers in the mire are not vertically mixed. We infer that the same was the case at the location Mauntschas-02 before the section was collected, because the 2 sections comprise very similar peat types. We think that the initial sampling of Mauntschas-02 and the position of the dated sub-section at the edge of the section have caused distortion of the peat layers, which resulted in the inclusion of material from several consecutive years in the dated samples, and therefore a long ^{14}C integration time (8 yr).

Age-Depth Models of the Peat Sections

In constructing the age-depth models, we applied the specially developed computer program PozCal. Using a standard algorithm for calibration of ^{14}C ages (e.g. Michczyńska et al. 1990; Bronk Ramsey 2003), PozCal calculates probability distributions of calendar age for individual samples in the peat section via a comparison with the "extended" calibration curve integrated over the site-specific calibration time τ. These distributions are displayed with vertical positions proportional to sample depths (Figure 4a–e). On each plot, the age-depth model is directly represented by a curve passing through (or close to) the maxima of the probability distributions.

When deriving the age-depth curve, one should be aware of some additional facts. First, abrupt lithological boundaries (transitions in the peat stratigraphy) at certain levels in the peat sections studied indicate abrupt changes in peat accumulation rate. Second, the degree of preservation/humification of the peat strongly suggests that between these abrupt boundaries, peat growth was rather regular, without inversions and with a gradual decrease of the peat accumulation rate down the section, because of plant decomposition and compaction increasing with depth. Therefore, monotonic and smooth age-depth curves were expected, except at lithological boundaries where abrupt changes in their slopes were possible. However, these transitions in lithology could be expressed only qualitatively and are displayed at the right-hand side of the plots in Figure 4.

In the post-bomb parts of the majority of the peat sections, the probability maxima are thin and clearly placed along smooth lines, unequivocally tracing the age-depth curves. The only exception is Kevo, where the ages of the samples at 20, 40, and 51 mm appear too old with respect to those suggested by the samples at 52, 70, and 90 mm. In all probability, this is related to the fact that the anomalous dates (represented in Figure 4 by white silhouettes) were obtained on dwarf-birch leaves. Such leaves, unlike *Sphagnum* stems, may undergo redeposition, so it is probable that these leaves were actually older than the peat at the same depths. This interpretation seems to be confirmed by the date of the *Sphagnum* sample at 52.5 mm (gray silhouette in Figure 4a), which lies perfectly on the smooth age-depth curve.

It is worth noting that the age-depth curves traced by the probability maxima (Figure 4) bend at just the levels of the lithological boundaries. This is especially clear in Wengerkopf at 320 mm (Figure 4b), Mauntschas-02 at ~170 mm (Figure 4d), Šijec at ~400 mm (Figure 4d), Rosaninsee at ~330 mm (Figure 4c), and Saariselkä at ~35 mm (Figure 4b).

In the pre-bomb sections, the probability distributions for individual samples are multi-modal and about 300 yr wide. However, the simultaneous use of post-bomb and pre-bomb dates enables the rejection of most maxima of the probability distributions in the pre-bomb section. Considering the example of Mauntschas-02 (Figure 4d), passing the age-depth curve through the older maxima at 430–278 mm would mean either an inversion in the peat or an abrupt major increase in the peat accumulation rate down the peat section, which is in disagreement with the degree of peat preservation and the lithology. Therefore, the most probable age-depth curve is that passing around AD 1900 at 495 mm. An alternative model has the age-depth curve passing at about AD 1800 at 518 mm.

The Strategy of Multi-Stage ^{14}C Dating

In Mauntschas-02, a discrimination between the 2 age-depth models shown (Figure 4d) would be possible after dating one additional sample between 550 and 518 mm. It is worth noting that the selection of the level to be dated for such discrimination was not possible before the dates at 600, 550, and 518 mm were available. On the other hand, the dates at 495 and 320 mm provide no additional information to that given by the other dates. This example shows that the selection of samples for ^{14}C dating should be made in stages—the sampling depths at each stage being dependent on the results obtained in the previous stage.

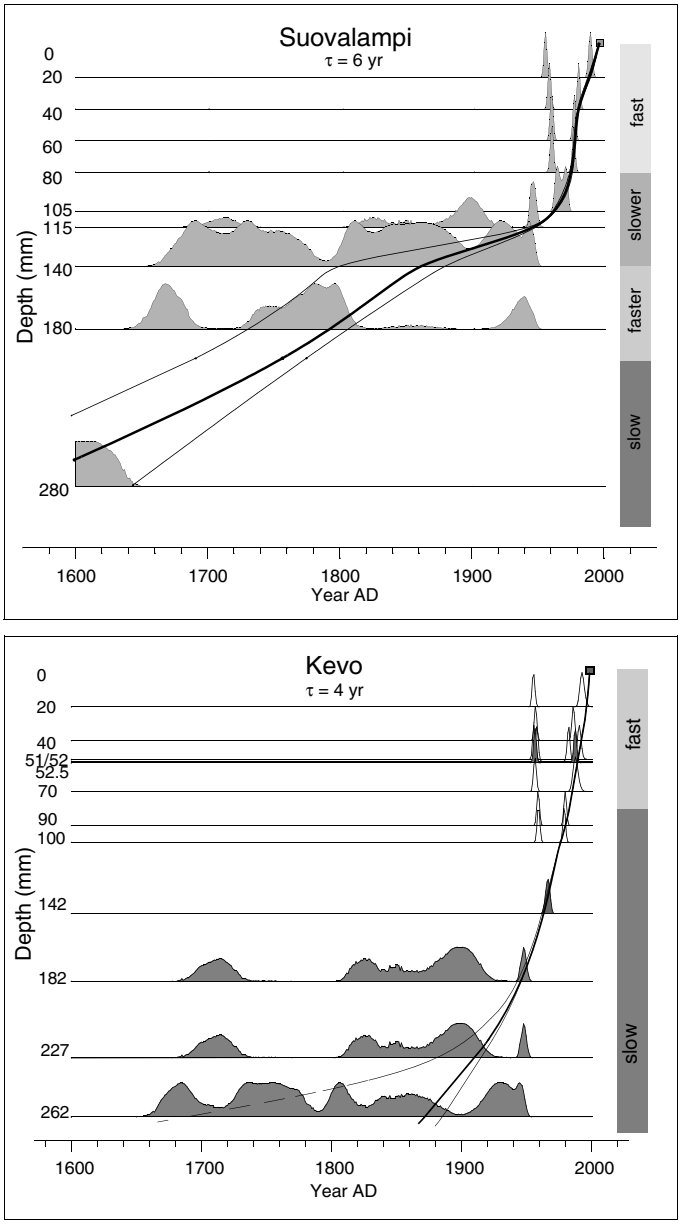

Figure 4 a–d) Diagrams illustrating the construction of the age-depth models. For each peat section, the probability distributions of calibrated ^{14}C ages of individual samples are shown with gray silhouettes and displayed at vertical positions proportional to sample depths. White silhouettes correspond to samples of dwarf-birch leaves (Kevo) or samples with clearly outlying ^{14}C ages (Saariselkä). The rectangles in the upper-right corners represent the year of collection of the peat sections (depth = 0). The left-pointing arrows at the lower-left corners represent peat samples with calendar ages beyond the range of the diagram. The smooth lines passing through the maxima of probability distributions represent the most probable age-depth curves; the 2 dashed lines drawn beside represent the uncertainties of the age-depth models. The gray bars at the right-hand side illustrate changes of peat accumulation rate, derived from the lithology. e) Illustration of the evolution of the age-depth models of Mauntschas-03, after 3 stages of ^{14}C dating. The meaning of all diagram components is the same as in parts a–d. (Figures 4b–e are on the following pages.)

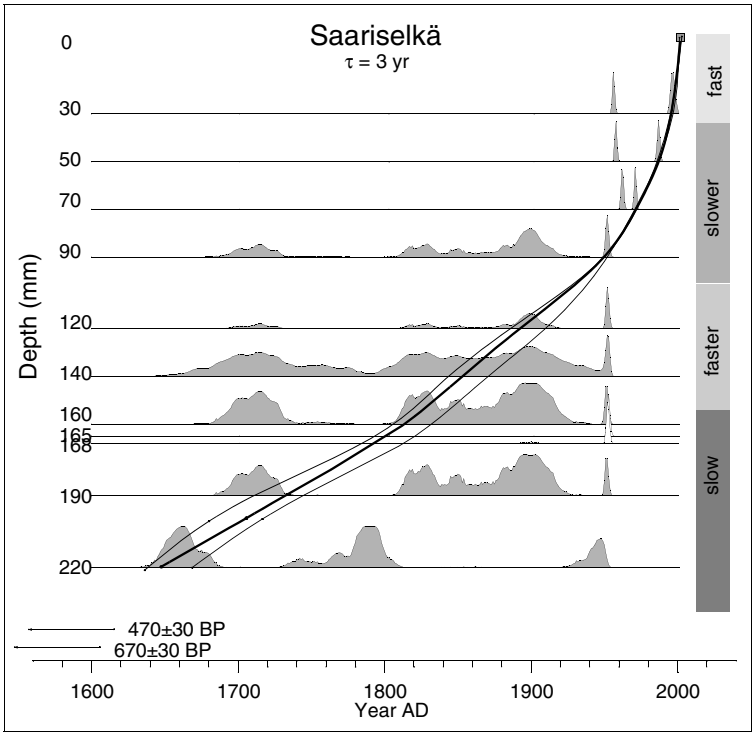

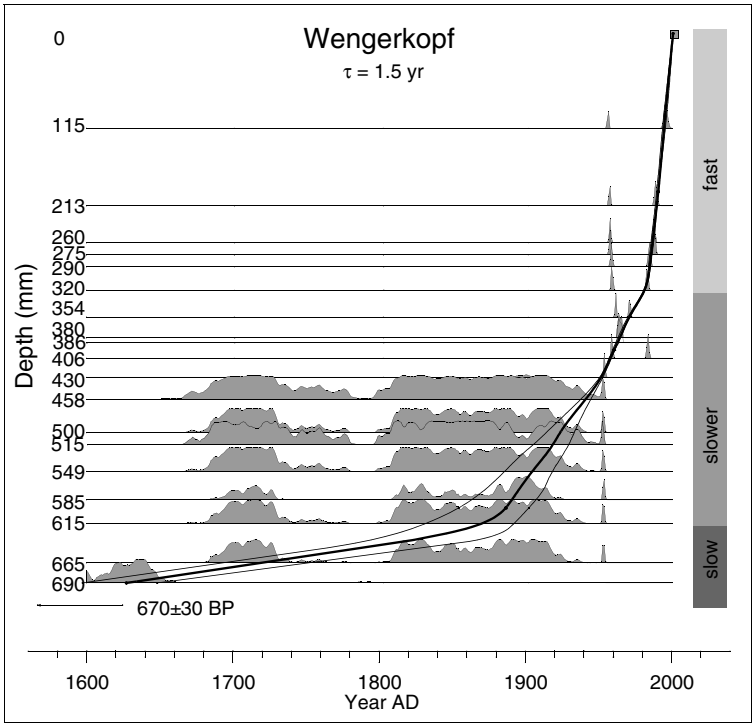

Figure 4b See Figure 4a for description

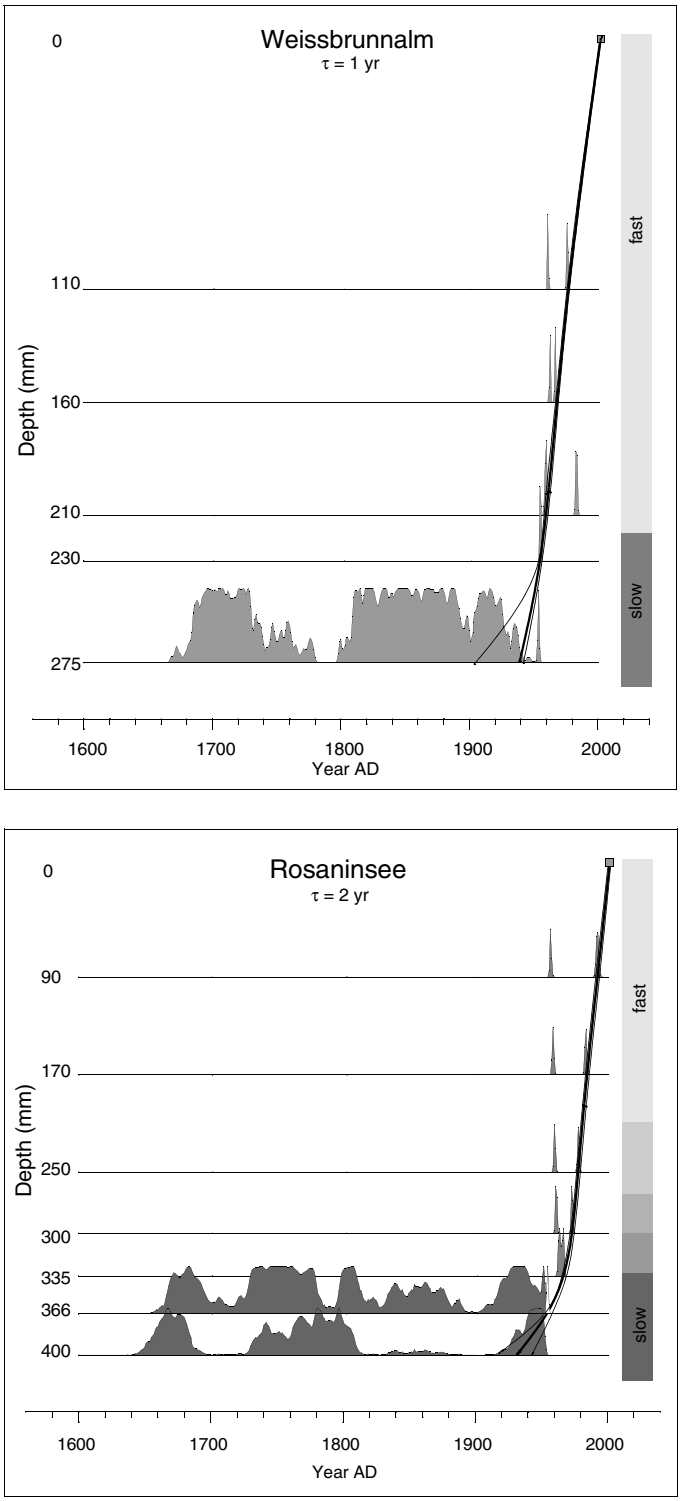

Figure 4c See Figure 4a for description

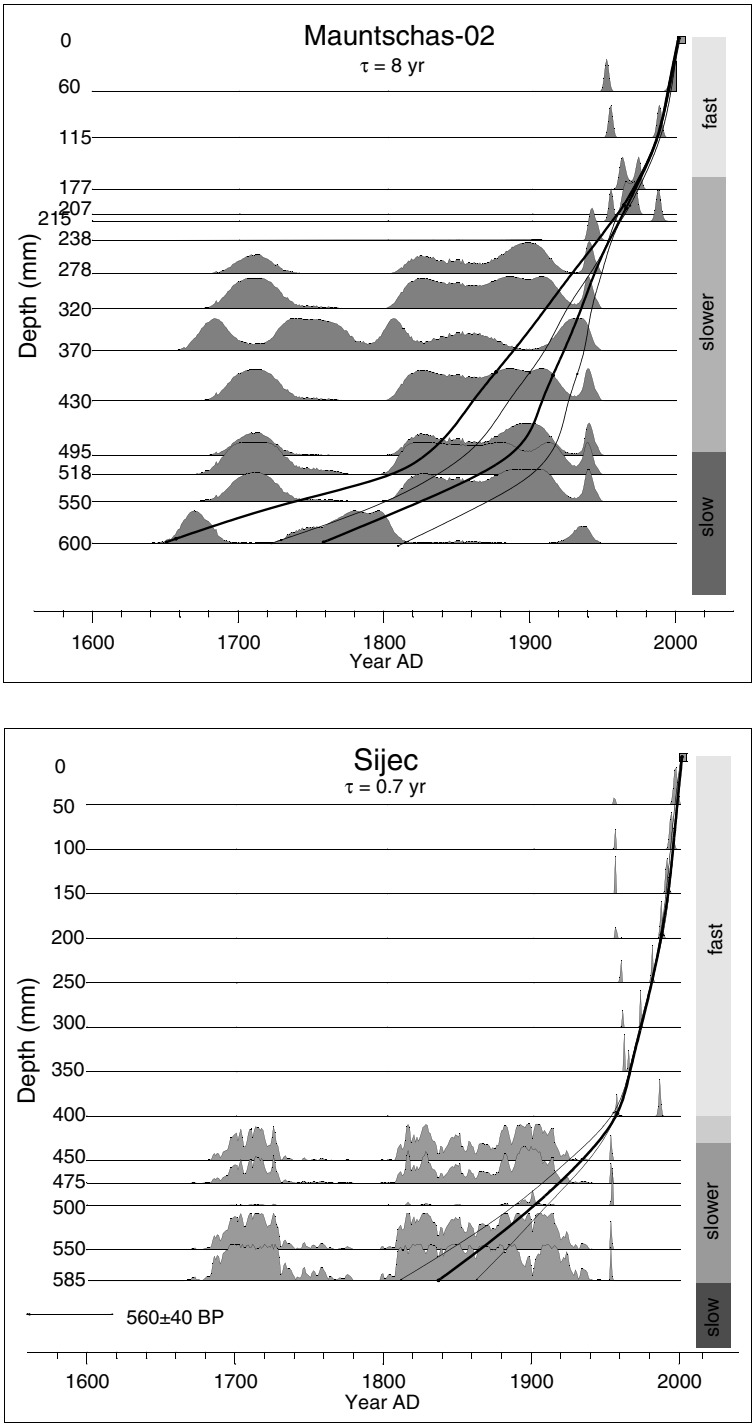

Figure 4d See Figure 4a for description

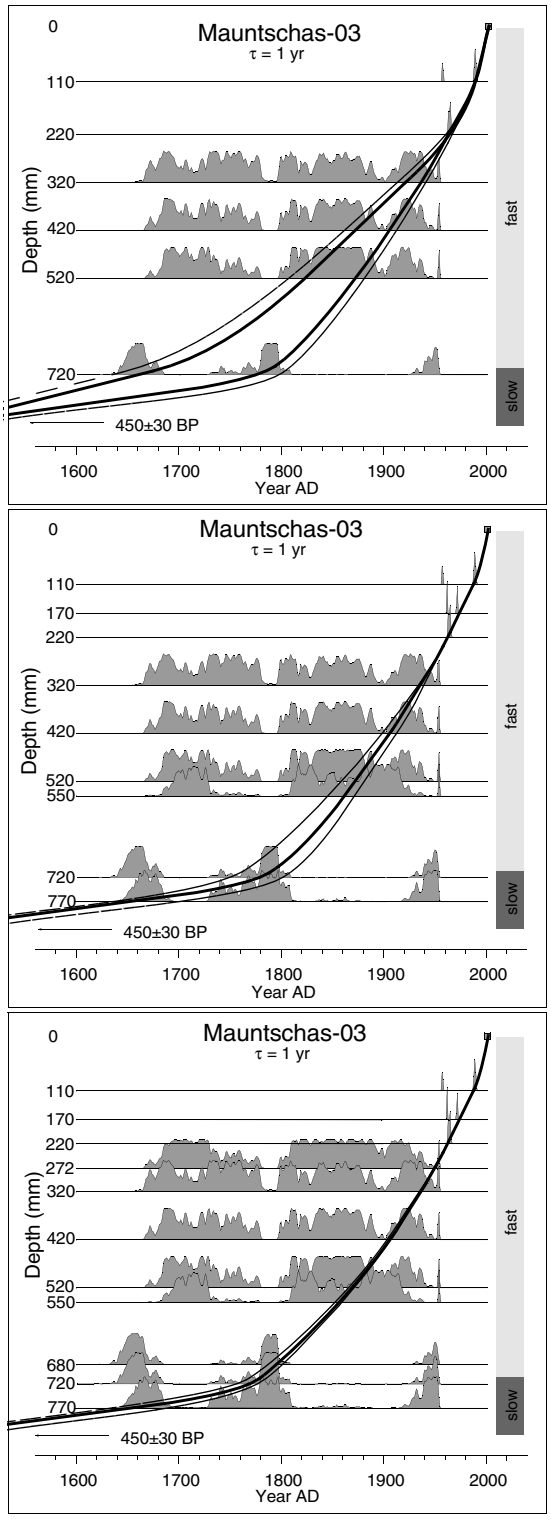

Figure 4e See Figure 4a for description

The strategy of multi-stage ^{14}C dating, with selection of samples for the next stage depending on the results already obtained, was applied to Mauntschas-03. Seven samples dated in the first stage (Figure 4e, top) allowed us to estimate the level of the bomb peak (at 220 mm) and to approximate the depth corresponding to the beginning of the wiggly part of the ^{14}C calibration curve age (about AD 1650; 820–720 mm). However, 2 different age-depth models were possible, with calendar ages at 720 mm differing by as much as 150 yr. Two additional ^{14}C dates (at 550 mm and 770 mm) allowed the "older" model to be rejected, and reduced the uncertainty of the calendar age at 720 mm to about ±30 yr (Figure 4e, center). A further reduction of this uncertainty (to about ±15 yr) was brought about by the ^{14}C date at 680 mm (Figure 4e, bottom).

It is noteworthy that in the pre-bomb period, both age-depth models for Mauntschas-03 show a change of accumulation rate around 720 mm, which is in close agreement with the lithology (Figure 4e). Abrupt increases in peat accumulation rates above ~140 mm in Suovalampi (Figure 4a), 620 mm in Wengerkopf (Figure 4b), 500 mm in Mauntschas-02 (Figure 4d), and ~100 mm in Saariselkä also agree with the lithological changes. The agreement of accumulation rate changes shown by the age-depth models with those suggested by the lithological boundaries supports the reliability of the age-depth models.

An integration with $\tau = 0.7$–8 yr affects the ^{14}C concentration in peat mainly in periods of rapid atmospheric ^{14}C changes, but very little in the pre-bomb period with its slow atmospheric ^{14}C changes. In fact, it has only a minor effect on the age-depth models of the peat sections studied (Figure 5), causing a slight shift towards older ages before and shortly after the atmospheric ^{14}C peak, and a shift towards younger ages in the later period. It is symptomatic that the check ^{14}C sample from Mauntschas-02 (Figure 2a), taken from the depth ascribed to AD 1963 by an age-depth model without integration, actually appeared older (not younger) than AD 1963. This demonstrates that neglecting integration would produce an erroneous age-depth model for Mauntschas-02. On the other hand, neglecting integration in the Wengerkopf profile would have no visible influence on the model (cf. the result of the check sample in Figure 2a), which is reasonable because the inferred integration time in that section is very short.

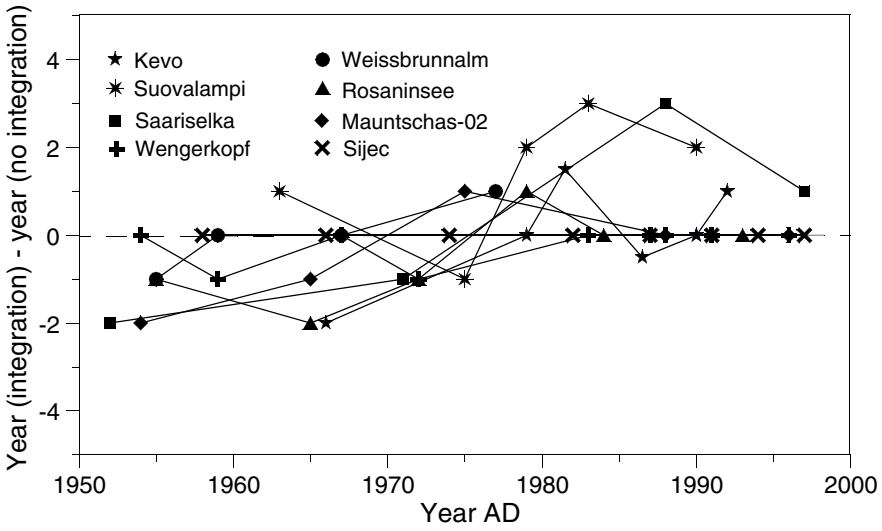

Figure 5 Differences between calendar ages of samples from the studied peat sections and derived from 2 scenarios of the age-depth models (with and without integration).

^{14}C Dates of Peat Sections Compared to Atmospheric Calibration Data

Having established robust chronologies for the peat sections, we are able to plot the ^{14}C ages of the dated samples versus calendar age and compare them directly with the atmospheric ^{14}C records (Figure 6). The effect of ^{14}C integration within the peat sections is illustrated by the fact that around AD 1963, all the peat ^{14}C data points lie below the atmospheric ^{14}C curve, while after AD 1970 they are all placed above the atmospheric curve.

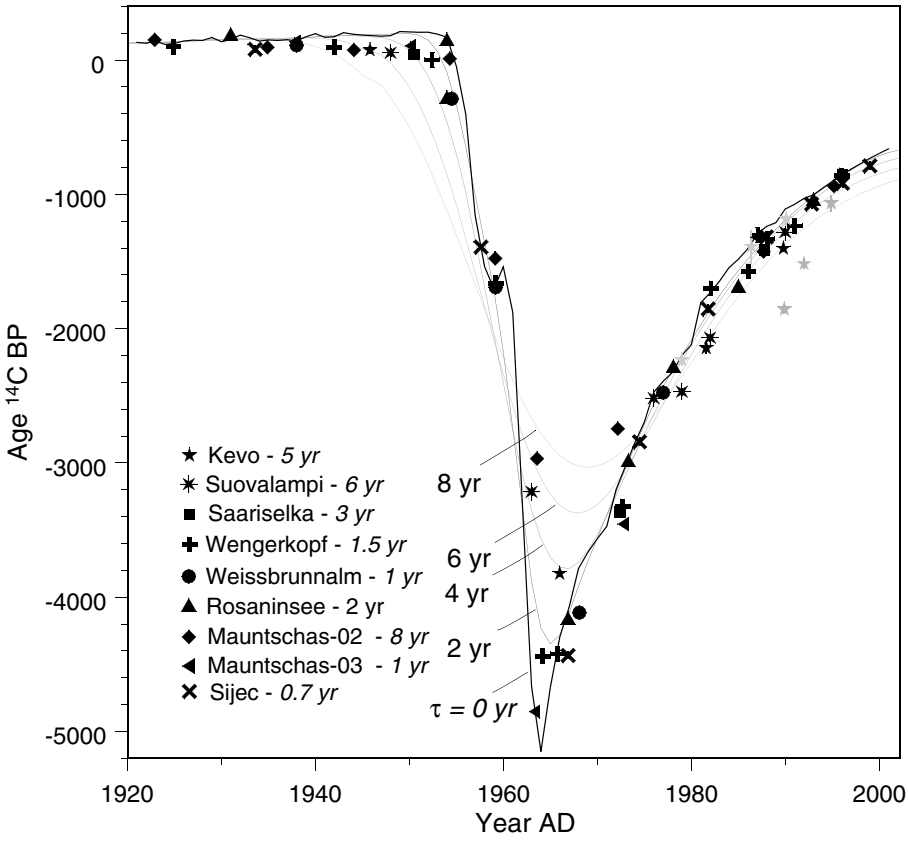

Figure 6 ^{14}C dates of samples from the peat sections studied are plotted against calendar ages derived from the age-depth models in the time interval AD 1920–2000. The smooth lines show the "theoretical" ^{14}C profiles in peat, calculated for different values of the integration time τ. The ^{14}C dates obtained on dwarf-birch leaves (Kevo) are marked with light gray symbols.

One might suspect that the location of the peat data-points above the atmospheric curve in Figure 6 is an artifact of the integration time used in the age-depth models, and therefore does not confirm the existence of integration. Indeed, slight modifications of the age-depth curves after AD 1970 would provide a perfect match of the peat ^{14}C dates with the atmospheric curve.

However, integration is verified by the ^{14}C dates in the interval AD 1930–1955 as follows. The situation is similar to that after AD 1970, in that all the ^{14}C data points in the period AD 1930–1955 (Figure 6) lie above the atmospheric ^{14}C curve. However, unlike the situation after AD 1970, matching these points with the atmospheric curve would require *large* distortions of *all* age-depth models, which is unlikely as these models are robust in the period before AD 1920. It is symptomatic that, although most ^{14}C dates between AD 1600 and 1930 fit the atmospheric curve quite well (Figure 7), all the dates between 1930 and 1955 are younger than the atmospheric ones.

The period just preceding the bomb-induced increase of ^{14}C in the atmosphere appears to be especially problematical in the ^{14}C dating of sediments where some dispersion of the ^{14}C signal occurs. In fact, this is the only period where peat layers of "originally natural" ^{14}C concentration (which varied at a rate slower than 20‰ per 100 yr) are in touch with layers with ^{14}C concentrations higher by hundreds of per mil. So, even slight contamination with carbon from overlying layers may totally corrupt the ^{14}C dating in the late pre-bomb section.

Goodsite et al. (2001) noted that below the ^{14}C bomb peak, the Danish and Greenland peat sections with elevated ^{14}C levels were abnormally thick in comparison with the peat growth rate deduced from the thickness of the post-bomb sections. Therefore, the age-depth models of the Goodsite peat sections assume extremely high peat accumulation rates in the period AD 1950–1960, a feature in clear disagreement with indications given by the ^{210}Pb data.

A similar effect is observed in the peat sections studied here. However, large sets of ^{14}C dates in the pre-bomb peat layers make the age-depth models prior to AD 1960 very robust and leave no space for large variations in peat accumulation rates. Therefore, we are sure that this is the effect of ^{14}C integration, and we strongly believe that the thick layers of elevated ^{14}C levels in the Goodsite et al. (2001) peat sections reflect the same mechanism and have nothing to do with an increase in peat accumulation rate. It must be noted that this conclusion could not be drawn on the basis of Goodsite et al. data alone, because ^{14}C dates in the pre-bomb period were lacking and their age-depth models for that time interval could not be well anchored.

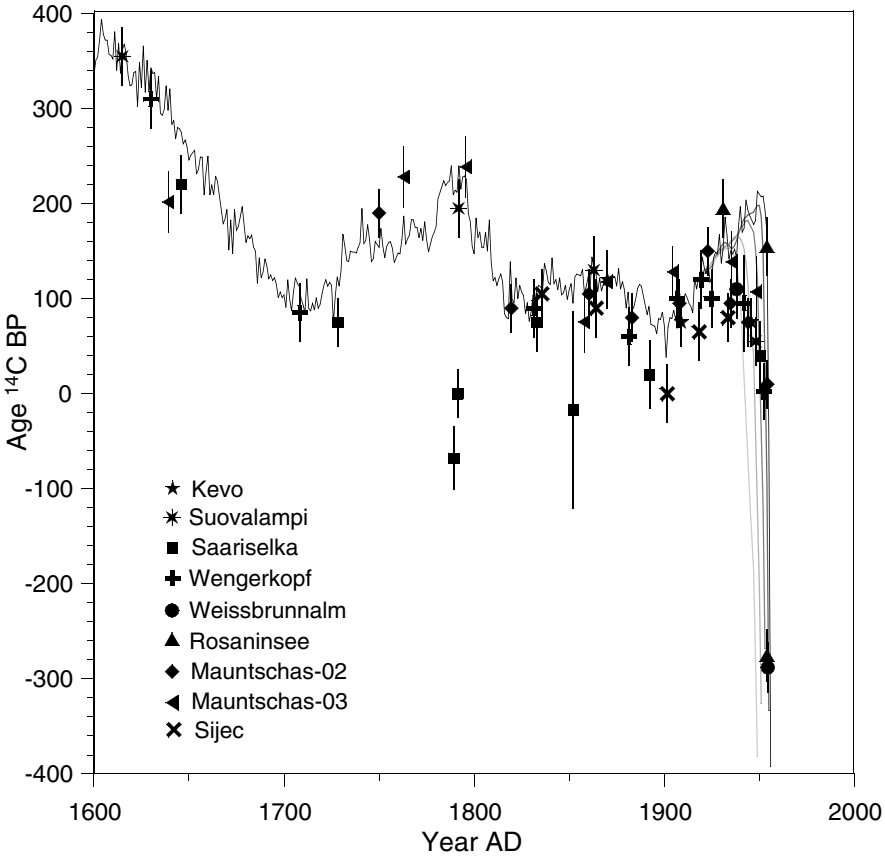

Figure 7 ^{14}C dates of samples from the peat sections studied plotted against calendar ages derived from the age-depth models. The dates from the post-bomb period are beyond the range of this graph.

CONCLUSIONS

This study is the first where modern peat profiles were ^{14}C dated at a high resolution in both the pre-bomb and post-bomb periods. Joint treatment of the series of dates from both periods enabled us to derive precise age-depth models for all the profiles analyzed. In the parts of the peat sections covered by the bomb peak, calendar ages of individual peat samples could be determined almost immediately, with an accuracy of 2–3 yr. In the pre-bomb sections, the construction of unequivocal age-depth relationships was more difficult, as the calendar ages of individual samples have the form of multi-modal probability distributions of about 300 yr wide (about AD 1650–1950). However, the simultaneous use of the post-bomb and pre-bomb ^{14}C dates, and lithological information on abrupt changes in peat accumulation rates, enabled the rejection of most modes of probability distributions in the pre-bomb section. Our results refute the concluding statement of the recent paper on age-depth modeling (Telford et al. 2004) that "uncertainties may always be high during radiocarbon plateaux."

Despite the fact that the samples for ^{14}C dating were carefully selected (pure *Sphagnum* in the majority of cases), we note some integration of the atmospheric ^{14}C record in the dated peat sections. The most probable reason for this integration is that below the surface of a peat mire, the dead *Sphagnum* fragments are mixed, so that tissues grown in different years may be found at the same level. The degree of integration, expressed in form of integration time τ, seems correlative with the peat growth rate, but it also depends on the manner of handling the peat sections to be sampled. The case of the 2 peat sections from the Mauntschas site clearly shows that careless handling affects the time resolution of the peat section and produces a large increase in the integration time.

The strategy of multi-stage ^{14}C dating, with the selection of samples for the next stage depending on the results obtained previously, enables a significant reduction in the uncertainty of the age-depth model, by dating only a few additional samples in a peat section. This strategy allows pinpointing a ^{14}C date at the bomb peak maximum, which is crucial for determining the ^{14}C integration time.

Our study is the first in which peat sections from the late pre-bomb period (AD 1900–1960) have been precisely dated at a high temporal resolution. This study demonstrates that during this time interval, ^{14}C ages of all the samples dated were younger than those derived from the atmospheric calibration curve, which strongly supports the concept of integration. Evidently, the determination of calendar ages based on ^{14}C dating of single samples from that interval may be affected by a serious error if the possibility of integration is ignored.

ACKNOWLEDGMENTS

The authors are grateful to Dr K van der Borg (University of Utrecht) for sharing ^{14}C dates of the Kevo peat section obtained in his laboratory. This paper is a contribution to the EU project PINE (Predicting Impacts on Natural Ecotones, Contract nr EVK2-CT-2002-00136)

REFERENCES

Benoit JM, Fitzgerald WF, Damman AWH. 1998. The biogeochemistry of an ombrotrophic bog: evaluation of use as an archive of atmospheric mercury deposition. *Environmental Research* 78(A):118–33.

Blaauw M. 2003. An investigation of Holocene Sun-climate relationships using numerical C-14 wiggle-match dating of peat deposits [PhD dissertation]. Amsterdam: University of Amsterdam.

Bronk Ramsey C. 2001. Development of the radiocarbon program OxCal. *Radiocarbon* 43(2A):355–63.

Czernik J, Goslar T. 2001. Preparation of graphite targets in the Gliwice Radiocarbon Laboratory for AMS ^{14}C dating. *Radiocarbon* 43(2A):283–91.

de Jong AFM. 1981. Natural ^{14}C variations [PhD dissertation]. Gröningen: University of Gröningen.

Goslar T, Czernik J, Goslar E. Forthcoming. Low-energy ^{14}C AMS in Poznań Radiocarbon Laboratory, Poland. *Nuclear Instruments and Methods in Physics*

Research B.

Goodsite ME, Rom W, Heinemeier J, Lange T, Ooi S, Appleby PG, Shotyk W, van der Knaap WO, Lohse Ch, Hansen TS. 2001. High-resolution AMS ^{14}C dating of post-bomb peat archives of atmospheric pollutants. *Radiocarbon* 43(2B):495–515.

Hicks S, Goslar T, van der Borg K. 2004. A near annual record of recent tree line dynamics from northern Finland. *Acta Palaeobotanica* 223–224C:5–11.

Jungner H, Sonninen E, Possnert G, Tolonen K. 1995. Use of bomb-produced ^{14}C to evaluate the amount of CO_2 emanating from two peat bogs in Finland. *Radiocarbon* 37(3):567–73.

Kilian MR, van der Plicht J, van Geel B. 1995. Dating raised bogs: new aspects of AMS ^{14}C wiggle matching, a reservoir effect and climatic change. *Quaternary Science Reviews* 14:959–66.

Kilian MR, van Geel B, van der Plicht J. 2000. ^{14}C AMS wiggle matching of raised bog deposits and models of peat accumulation. *Quaternary Science Reviews* 19: 1011–33.

Levin I, Kromer B, Schoch-Fischer H, Bruns M, Münnich KO. 1997. $^{14}CO_2$ records from two sites in central Schauinsland & Vermunt. URL: <http://cdiac.esd.ornl.gov/ftp/trends/co2/cent.htm>.

Martínez-Cortizas A, Pontevedra-Pombal X, García-Rodeja E, Nóvoa-Muñoz JC, Shotyk W. 1999. Mercury in a Spanish peat bog: archive of climate change and atmospheric metal deposition. *Science* 284:939–42.

Michczyńska DJ, Pazdur MF, Walanus A. 1990. Bayesian approach to probabilistic calibration of radiocarbon ages. *PACT* 29:69–79.

Nydal R, Lövseth K. 1983. Tracing bomb ^{14}C in the atmosphere, 1962–1980. *Journal of Geophysical Research* 88:3621–42.

Nydal R, Lövseth K. 1996. Carbon-14 measurements in atmospheric CO_2 from Northern and Southern Hemisphere sites, 1962–1993. URL: <http://cdiac.esd.ornl.gov/epubs/ndp/ndp057/ndp057.htm>.

Shotyk W, Weiss D, Appleby PG, Cheburkin AK, Frei R, Gloor M, Kramers JD, Reese S, van der Knaap WO. 1998. History of atmospheric lead deposition since 12,370 ^{14}C yr BP recorded in a peat bog profile, Jura Mountains, Switzerland. *Science* 281:1635–40.

Smith LC, MacDonald GM, Velichko AA, Beilman DW, Borisova OK, Frey KE, Kremenetski KV, Sheng Y. 2004. Siberian peatlands a net carbon sink and global methane source since the early Holocene. *Science* 303:353–6.

Speranza A, van der Plicht J, van Geel B. 2000. Improving the time control of the Subboreal/Subatlantic transition in a Czech peat sequence by ^{14}C wiggle-matching. *Quaternary Science Reviews* 19:1589–604.

Stuiver M, Braziunas T. 1993. Sun, ocean, climate and atmospheric $^{14}CO_2$: an evaluation of causal and spectral relationships. *The Holocene* 3:289–305.

Stuiver M, Reimer PJ, Bard E, Beck JW, Burr GS, Hughen KA, Kromer B, McCormac G, van der Plicht J, Spurk M. 1998. IntCal98 radiocarbon age calibration, 24,000–0 cal BP. *Radiocarbon* 40(3):1041–83.

Telford RJ, Heegaard E, Birks HJB. 2004. All age-depth models are wrong: but how badly? *Quaternary Science Reviews* 23:1–5.

White JWC, Ciaia P, Figge RA, Kenny R, Markgraf V. 1994. A high-resolution record of atmospheric CO_2 content from carbon isotopes in peat. *Nature* 367:153–6.

RADIOCARBON, Vol 47, Nr 1, 2005, p 135–145

CHRONOLOGIES FOR RECENT PEAT DEPOSITS USING WIGGLE-MATCHED RADIOCARBON AGES: PROBLEMS WITH OLD CARBON CONTAMINATION

Dan J Charman

School of Geography, University of Plymouth, Plymouth, Devon PL4 8AA, United Kingdom.
Corresponding author. Email:dcharman@plymouth.ac.uk.

Mark H Garnett

NERC Radiocarbon Laboratory, Scottish Enterprise Technology Park, Rankine Avenue, East Kilbride, Glasgow G75 0QF, United Kingdom.

ABSTRACT. Dating sediments which have accumulated over the last few hundred years is critical to the calibration of longer-term paleoclimate records with instrumental climate data. We attempted to use wiggle-matched radiocarbon ages to date 2 peat profiles from northern England which have high-resolution records of paleomoisture variability over the last ~300 yr. A total of 65 ^{14}C accelerator mass spectrometry (AMS) measurements were made on 33 macrofossil samples. A number of the age estimates were older than expected and some of the oldest ages occurred in the upper parts of the sequence, which had been dated to the late 19th and early 20th century using other techniques. We suggest that the older ^{14}C ages are the result of contamination by industrial pollution. Based on counts of spheroidal carbonaceous particles (SCPs), the potential aging effect for SCP carbon was calculated and shown to be appreciable for samples from the early 20th century. Ages corrected for this effect were still too old in some cases, which could be a result of fossil CO_2 fixation, non-SCP particulate carbon, contamination due to imperfect cleaning of samples, or the "reservoir effect" from fixation of fossil carbon emanating from deeper peat layers. Wiggle matches based on the overall shape of the depth-^{14}C relationship and the ^{14}C minima in the calibration curve could still be identified. These were tested against other age estimates (^{210}Pb, pollen, and SCPs) to provide new age-depth models for the profiles. New approaches are needed to measure the impact of industrially derived carbon on recent sediment ages to provide more secure chronologies over the last few hundred years.

INTRODUCTION

There is a growing interest in documenting environmental and climatic changes over recent time periods, especially the last few hundred years. This period is important for several reasons. First, it is the time in which instrumental data overlap paleoenvironmental data, and thus there is an opportunity to test and calibrate paleo-records against instrumentally measured time series. Second, it is a period in which human impacts on climate and environment have been most intense and have accelerated most rapidly. A key issue in establishing paleoenvironmental records which can be matched securely with instrumental data is to develop chronologies that are sufficiently accurate and precise over the last few hundred years. In annually resolved records such as tree rings, the problem does not arise, but in non-annually resolved records such as lake sediments and peat, this is still a major limitation.

In peats, a number of possible techniques for dating are available. Short-lived radioisotopes (^{210}Pb, ^{241}Am, ^{137}Cs) are the most commonly used (Appleby et al. 1997), but this approach has shown variable results in some situations and often needs to be cross-checked with other chronological markers (Oldfield et al. 1995). Stable isotopes of lead have also been used successfully, especially to provide age markers in the 20th century (Martínez-Cortizas et al. 1999). Other useful age markers are spheroidal carbonaceous particles (SCPs; Yang et al. 2001), historical tephras (Schoning et al. 2005), and pollen markers (Barber et al. 1998). Used together, these techniques can provide a high-quality chronology for the last 100–150 yr. However, the quality of chronologies tends to decline for the early 20th and late 19th century, and dating is reliant on only a few markers before AD 1850. In addition, radiocarbon dating of single samples is of limited value for sediments from between AD 1650 and 1950 because of the plateau in the relationship between ^{14}C activity and calendar age over this period. One approach to extend peat chronologies back to around AD 1600, as well as to provide a cross-check on other techniques from AD 1850–1950, is to apply wiggle matching to a

series of ^{14}C ages. This technique has been used with success in older peats (Kilian et al. 2000; Kilian et al. 1995; Mauquoy et al. 2002; Speranza et al. 2000), but has been attempted rather infrequently for more recent peats (Clymo et al. 1990; Gedye 1998).

In this paper, we report the results from an attempt at using wiggle-matched ^{14}C ages on 2 short peat profiles from northern England. In particular, we explore the problems associated with obtaining accurate assessments of ^{14}C age from such profiles in the light of results which suggest significant contamination from older carbon.

METHODS AND DATING RATIONALE

Two profiles were sampled from Butterburn Flow (55°5′N 2°30′W), a large raised mire in northern England, using a large volume sampler (Wardenaar 1987). The cores (BFA and BFB) were taken from the central dome of the northern section (intersection of the transects in Hendon et al. 2001) from separate *Sphagnum magellanicum* lawns approximately 10 m apart. The profiles were the subject of an investigation into the relationships between high-resolution paleohydrological reconstructions, land use, and climate (Hendon and Charman 2004; Charman et al. 2004). These records probably span the last 300–400 yr of peat accumulation. Although short-lived radioisotopes (^{210}Pb, ^{241}Am), pollen, and SCP markers have provided estimated chronologies for the period AD 1800 to present, the accuracy of the dating declined in the earlier part of the record and there were no estimated ages from before AD 1800. The aim of the analyses reported here was to establish a wiggle-matched ^{14}C chronology to provide a cross-check with age estimates in the 19th and early 20th century, as well as to extend the chronology back in time.

Samples from 0.5-cm-thick slices of the monoliths were washed through a 125-µm mesh using distilled water. The residue was examined under a dissecting microscope (10× to 50×) in sterile petri dishes, and subsamples of *Sphagnum* leaves and stems were picked and placed in a separate petri dish of distilled water. Where sufficient quantities of *Sphagnum* were not available, leaves of *Erica tetralix* and *Calluna vulgaris* were picked either to supplement *Sphagnum* remains or to provide additional replicate samples. Visible roots and other extraneous organic material were removed using fine forceps, and the subsamples were washed through distilled water again. Samples were sent to the ^{14}C laboratory in distilled water in polypropylene vials. In the ^{14}C laboratory, the samples were subjected to a standard pretreatment (acid wash), dried, and homogenized. The total carbon in the pretreated sample was recovered as CO_2 by heating (900 °C) with CuO in a sealed quartz tube. The gas was converted to graphite by Fe/Zn reduction and analyzed for ^{14}C by the University of Arizona NSF-AMS facility. To achieve higher ^{14}C precision, samples with sufficient CO_2 were split into sub-samples after CO_2 production and up to 3 replicate graphite targets were prepared and analyzed for ^{14}C.

RESULTS AND DISCUSSION

Radiocarbon Ages

Adequate material for the preparation of 3 replicate graphite targets was available from 12 of the samples and 7 of the samples had adequate material for 2 replicate targets. A single age was obtained for the remaining samples (Table 1). Replicates from each level had overlapping error terms at 2 σ, except 1 replicate from BFB 36–36.5 cm depth (AA-49801) which we rejected from further analysis.

Table 1 Sample characteristics and results of ^{14}C analyses. Key to sample composition: A = *Sphagnum* leaves and stems, B = *Erica tetralix* and *Calluna vulgaris* leaves.

Publication code	Identifier	Mid-point (cm)	Replicate	Composition	^{14}C age (yr BP)	±1 σ (yr)	$\delta^{13}C_{PDB}$ (‰)
BFA							
AA-49754	BFA 17.5–18.0 cm	17.75	1	A	304	58	–25.5
AA-49755			2	A	181	46	
AA-49756			3	A	326	49	
AA-49757	BFA 20.0–20.5 cm	20.25	1	A	146	44	–25.5[a]
AA-49758			2	A	150	46	
AA-49759			3	A	76	47	
AA-49760	BFA 21.5–22.0 cm	21.75	1	A	457	51	–25.6
AA-49761			2	A	487	45	
AA-49762			3	A	470	49	
AA-49763	BFA 24.5–25.0 cm	24.75	1	A	346	66	–26.5
AA-49764			2	A	264	43	
AA-49765			3	A	135	55	
AA-49766	BFA 29.0–29.5 cm	29.25	1	A	414	41	–25.2
AA-49767			2	A	313	39	
AA-49804	BFA 33.0–33.5 cm	33.25	1	A	447	38	–25.5[a]
AA-49768	BFA 34.5–35.0 cm	34.75	1	A, B	262	40	–26.0[a]
AA-49769			2	A, B	138	38	
AA-49770			3	A, B	195	40	
AA-49771	BFA 37.0–37.5 cm	37.25	1	A, B	225	44	–28.8
AA-49772			2	A, B	320	53	
AA-49773			3	A, B	154	42	
AA-49805	BFA 38.0–38.5 cm	38.25	1	A, B	186	39	–26.7
AA-49774	BFA 39.5–40 cm	39.75	1	A, B	253	40	–26.8[a]
AA-49775			2	A, B	315	39	
AA-39729	BFA 41.0–41.5 cm	41.25	1	A	324	42	–26.0[a]
AA-49776	BFA 44.5–45.0 cm	44.75	1	A	379	70	–27.0
AA-49777			2	A	384	43	
AA-49778	BFA 46.0–46.5 cm	46.25	1	A	450	40	–27.4
AA-49779			2	A	334	38	
AA-49780	BFA 47.0–47.5 cm	47.25	1	A	332	39	–26.9
AA-49781			2	A	269	39	
AA-49782			3	A	359	42	
AA-49783	BFA 49.0–49.5 cm	49.25	1	A	428	30	–26.8
AA-49784			2	A	379	41	
AA-49785			3	A	389	30	
AA-39730	BFA 52.0–52.5 cm	52.25	1	A	333	46	–26.2
AA-39731	BFA 66.5–67.0 cm	66.75	1	A	300	140	–26.0[a]
BFB							
AA-49806	BFB 18.0–18.5 cm	18.25	1	A	1272	41	–26.7
AA-49807	BFB 20.5–21.0 cm	20.75	1	A	870	46	–26.6
AA-49786	BFB 21.5–22.0 cm	21.75	1	A	784	31	–26.7
AA-49787			2	A	818	43	
AA-49788	BFB 23.5–24.0 cm	23.75	1	A	487	32	–27.0
AA-49789			2	A	502	44	
AA-49790	BFB 26.5–27.0 cm	26.75	1	A	318	30	–26.8
AA-49791			2	A	301	39	
AA-49792			3	A	517	31	

Table 1 Sample characteristics and results of ^{14}C analyses. Key to sample composition: A = *Sphagnum* leaves and stems, B = *Erica tetralix* and *Calluna vulgaris* leaves. *(Continued)*

Publication code	Identifier	Mid-point (cm)	Replicate	Composition	^{14}C age (yr BP)	±1 σ (yr)	$\delta^{13}C_{PDB}$ (‰)
AA-49793	BFB 28.5–29.0 cm	28.75	1	A	343	30	–27.5
AA-49794			2	A	326	44	
AA-49795			3	A	413	30	
AA-49808	BFB 29.5–30.0 cm	29.75	1	A	559	41	–26.8
AA-49809	BFB 31.0–31.5 cm	31.25	1	A	552	44	–27.1
AA-49796	BFB 31.5–32.0 cm	31.75	1	A	551	31	–26.8
AA-49797			2	A	558	43	
AA-39732	BFB 32.5–33.0 cm	32.75	1	A	213	52	–26.0
AA-49798	BFB 34.0–34.5 cm	34.25	1	A	296	29	–26.7
AA-49799			2	A	527	49	
AA-49800			3	A	308	29	
AA-49801	BFB 36.0–36.5 cm	36.25	1	A, B	891	47	–26.6
AA-49802			2	A, B	239	40	
AA-49803			3	A, B	295	29	
AA-49810	BFB 36.5–37.0 cm	36.75	1	A	541	47	–26.3[a]
AA-49811	BFB 36.5–37.0 cm		2	A, B	420	43	–26.3[a]
AA-39733	BFB 37.5–38.0 cm	37.75	1	A	315	54	–26.5
AA-49812	BFB 39.5–40.0 cm	39.75	1	A	485	66	–26.3[a]
AA-39734	BFB 43.0–43.5 cm	43.25	1	A	377	44	–26.1

[a]Estimated $\delta^{13}C$ value due to insufficient sample material for an independent measurement.

The replicate age estimates were combined to produce single values using OxCal 3.5 (Bronk Ramsey 2000). The ages range from 126 ± 26 BP to 473 ± 28 BP for BFA and from 213 ± 52 BP to 1272 ± 41 BP for BFB. These ages compare with an expected range of 79 BP to 365 BP in IntCal98 for the period cal AD 1505 to cal AD 1945 (Stuiver et al. 1998). Many of the ages are clearly much older than expected. In particular, some of the oldest ages occur at the top of the profiles, especially at the top of core BFB where the ages above 24 cm depth are all >490 yr, at least 300 yr older than expected. There are a number of possible reasons for these older ages, including a reservoir effect (Kilian et al. 1995) and contamination during the preparation process (although quality assurance standards processed concurrently with the samples suggested contamination at this stage had not occurred). However, the fact that the most recent peats show a greater deviation from the expected ages points to a factor that has changed over time.

The Influence of Industrial Emissions

One possible explanation for the apparently older ages obtained for the more recent peats is that they have been affected by inputs of older carbon from industrial emissions. These inputs would include the fixation of carbon in CO_2 derived from coal burning as well as the fall-out of particulates. The latter would include SCPs, which we have already established are present in the cores (Hendon and Charman 2004). While these may have been removed by washing during the preparation process, it is well known that these particles have a strong affinity for *Sphagnum* leaves, even being retained within the pores on the cells (Punning and Alliksaar 1997). Therefore, we made estimates of the potential influence of contamination by SCPs on the peat ages (Table 2) using the following mass balance equation applied to the counts of SCP particles made previously (Hendon and Charman 2004):

$$Au = (Mt \times At - Mc \times Ac) / (Mt - Mc)$$

where Au = activity of sample corrected for contamination, Mt = carbon mass in total sample, At = measured activity of total sample, Mc = carbon mass of SCP contaminant, and Ac = activity of SCP contaminant.

Table 2 Estimated sample ages from combining replicates and the possible influence of SCP carbon on ages. The column "SCP effect" is the total aging effect of SCPs in the sample (see text for details).

Material ID code	Mid-point (cm)	^{14}C age (yr BP)	^{14}C age 1 σ (yr)	Sample carbon (mg)	SCP mass (mg)	SCP effect (yr)	Adjusted age (yr BP)
BFA							
BFA 17.5–18.0 cm	17.75	264	29	4.706	0.01562	27	237
BFA 20.0–20.5 cm	20.25	126	26	2.727	0.01562	46	80
BFA 21.5–22.0 cm	21.75	473	28	2.995	0.01562	42	431
BFA 24.5–25.0 cm	24.75	243	30	2.567	0.01562	49	194
BFA 29.0–29.5 cm	29.25	361	28	1.647	0.00731	36	325
BFA 33.0–33.5 cm	33.25	447	38	0.556	0.00121	17	430
BFA 34.5–35.0 cm	34.75	197	23	2.176	0.00121	4	193
BFA 37.0–37.5 cm	37.25	221	26	8.112	0.00000	N/A	221
BFA 38.0–38.5 cm	38.25	186	39	1.797	0.00000	N/A	186
BFA 39.5–40.0 cm	39.75	285	28	2.348	0.00000	N/A	285
BFA 41.0–41.5 cm	41.25	324	42	0.695	0.00000	N/A	324
BFA 44.5–45.0 cm	44.75	383	37	2.225	0.00000	N/A	383
BFA 46.0–46.5 cm	46.25	390	28	3.369	0.00000	N/A	390
BFA 47.0–47.5 cm	47.25	318	23	3.679	0.00000	N/A	318
BFA 49.0–49.5 cm	49.25	402	19	4.316	0.00000	N/A	402
BFA 52.0–52.5 cm	52.25	333	46	1.754	0.00000	N/A	333
BFA 66.5–67.0 cm	66.75	300	140	0.348	0.00000	N/A	300
BFB							
BFB 18.0–18.5 cm	18.25	1272	41	1.481	0.12378	701	571
BFB 20.5–21.0 cm	20.75	870	46	1.658	0.05332	263	607
BFB 21.5–22.0 cm	21.75	796	25	1.995	0.03468	141	655
BFB 23.5–24.0 cm	23.75	492	26	1.834	0.00993	44	448
BFB 26.5–27.0 cm	26.75	390	19	6.845	0.00993	12	378
BFB 28.5–29.0 cm	28.75	368	19	3.834	0.00993	21	347
BFB 29.5–30.0 cm	29.75	559	41	1.112	0.00993	72	487
BFB 31.0–31.5 cm	31.25	552	44	1.572	0.00993	51	502
BFB 31.5–32.0 cm	31.75	552	25	2.096	0.00993	38	513
BFB 32.5–33.0 cm	32.75	213	52	1.428	0.00993	56	157
BFB 34.0–34.5 cm	34.25	337	19	3.957	0.00993	20	317
BFB 36.0–36.5 cm	36.25	276	23	3.118	0.00192	5	271
BFB 36.5–37.0 cm	36.75	476	32	0.497	0.00192	31	445
BFB 37.5–38.0 cm	37.75	315	54	0.738	0.00192	21	294
BFB 39.5–40.0 cm	39.75	485	66	0.749	0.00192	21	464
BFB 43.0–43.5 cm	43.25	377	44	1.257	0.00000	N/A	377

In addition, we have assumed the following:

1. The concentration of SCPs in the samples counted for pollen/SCP is the same as that in the samples prepared for dating;
2. The mean mass of an SCP is 4.2×10^{-9} g (Rose 2001);
3. The *Sphagnum* samples retain all the SCPs present in the original sample after processing;
4. The SCPs are 100% dead carbon.

The potential influence of SCPs on ^{14}C age is relatively small for most of the profiles, except in the top part of BFB where including the effects of SCPs results in an adjustment of up to 700 yr for the topmost sample (Table 2). However, the ages of these upper samples and the ages for samples with relatively low or zero counts of SCPs are still too old by several hundred years when compared with likely age ranges from IntCal98 (Figure 1). This suggests that either the estimate of the level of contamination from industrial sources is too low or that there is an additional source of older carbon.

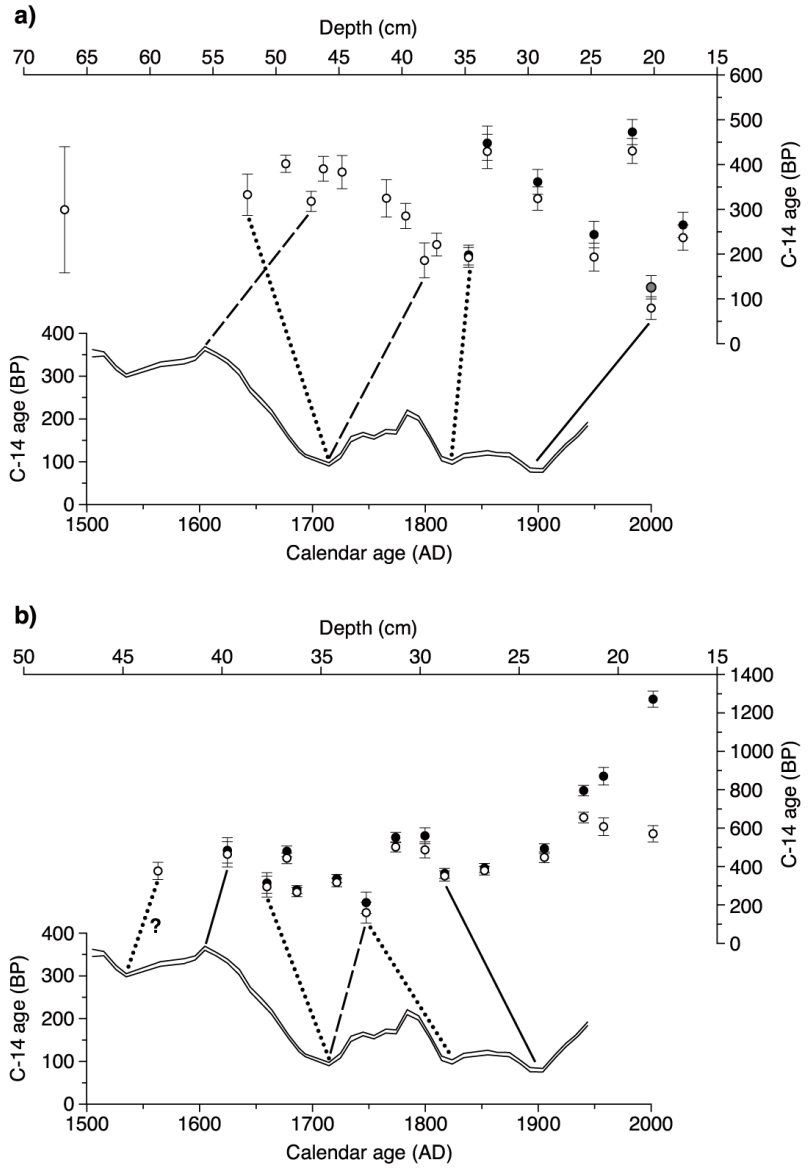

Figure 1 Possible wiggle matches of a) core BFA and b) core BFB with the IntCal98 calibration curve (Stuiver et al. 1998), shown below each peat profile. Closed symbols show original ^{14}C age estimates and open symbols show adjusted ages after taking into account the possible effect of SCP contamination. Dashed lines represent wiggle match 1 and dotted lines represent wiggle match 2. Solid lines represent both wiggle match 1 and 2. Error bars are ±1 σ.

Additional sources of older carbon in the samples could include non-SCP particulate carbon or the fixation of CO_2 containing older carbon. The latter process may be less likely than the former because CO_2 is a well-mixed gas in the atmosphere. However, Levin and Hesshaimer (2000) have shown that fossil fuel-derived CO_2 frequently depletes the atmospheric $^{14}CO_2$ signal at their Heidelberg site by up to 5 pMC, which, had it occurred in early 20th century samples, would age them by about 400 yr. Also, ^{13}C analyses of urban and rural grasses by Lichtfouse et al. (2003) suggested that fossil fuel-derived carbon can contribute even more to urban plant tissues, with up to 29.1% of plant tissue carbon being fossil fuel-derived. Our study site is relatively close to the areas that were some of the largest industrial sources of CO_2 in the late 19th and early 20th century (Manchester/Leeds/Sheffield ~150 km to the south and the Tyne-Tees areas 70–100 km to the east) and, although overall rates of fossil fuel CO_2 emissions were lower then, it is conceivable that there was significant local depletion of atmospheric $^{14}CO_2$ at this time. The $\delta^{13}C$ values do not help in determining the source of carbon (Table 1), as there is no relationship between $\delta^{13}C$ and the calculated amount of SCP contamination. The $\delta^{13}C$ of SCPs is likely to be similar to that of peat, as it is derived from coal and oil and therefore primarily of plant origin.

Other Influences on ^{14}C Ages

There have been few other attempts to use wiggle-matched ages over this time period, but those that have been carried out also show an offset between measured ages and those expected. The data of Clymo et al. (1990) and Gedye (1998) both show offsets of ~125 yr on samples covering this period. Clymo et al. (1990) do not discuss the offset, but Gedye (1998) attributes it to the reservoir effect, which was proposed by Kilian et al. (1995). This suggestion arose from dating older late-Holocene peat, which showed systematic offsets of ~100–150 yr. The exact mechanisms behind this reservoir effect are unclear, but the main suggestion is that fungi attached to the roots of higher plants fix older C in methane derived from deeper peat. Others have suggested that CO_2 derived from decay of older peat is fixed by *Sphagnum* and higher plants, which may derive up to 20% of their carbon from this source (Jungner et al. 1995). However, measurement of ^{14}C in growing *Sphagnum* has shown activity levels apparently unaffected by this process (Nilsson et al. 2001). In addition, Blaauw (2003) and Blaauw et al. (2004) found that this systematic offset was not present in their late-Holocene samples and attributed this to more intensive cleaning and careful selection of aboveground plant remains only. In particular, thorough cleaning is thought to be important to remove fungal contamination. Although we paid careful attention to cleaning, we may have not removed every single fine root, and since our samples were treated only in distilled water during preparation rather than in KOH (cf. Blaauw 2003), they may not have been cleaned of all the adhering fine organic material.

Wiggle Matching Corrected ^{14}C Ages

Despite the fact that ages of recent peats may be affected by several possible sources of contamination from older carbon, it may still be possible to use the shape of the relationship between ^{14}C age and depth to provide wiggle-match age estimates. Figure 1 shows 2 possible wiggle matches for BFA and BFB. Although many ages are significantly older than expected, the youngest ages may be more reliable than the older ages, where peaks in activity are hard to identify. Low points in ^{14}C activity are present at 2 main points in BFA and at 3 main points in BFB. However, the distortion in the curve from the old carbon contamination makes it difficult to know whether the lower minimum value in each profile relates to the ^{14}C minimum at AD 1825 or AD 1715. We can test these alternative interpretations by comparison with other chronological markers (Figure 2).

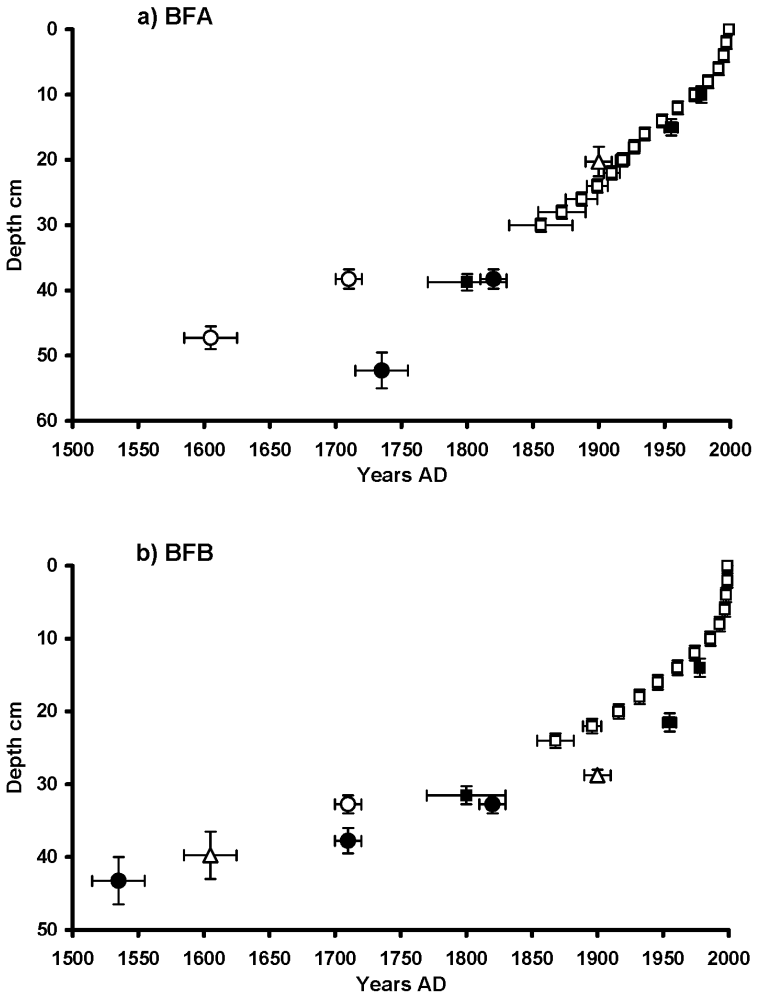

Figure 2 Comparison between age estimates based on ^{14}C wiggle matching, ^{210}Pb, SCP, and pollen markers for a) core BFA and b) core BFB. Open squares = ^{210}Pb ages; closed squares = pollen and SCP ages; open circles = wiggle match 1; closed circles = wiggle match 2; triangles = both wiggle match 1 and 2. Age error bars are 1 σ for ^{14}C age estimates and ^{210}Pb. SCPs and pollen age errors are given according to Rose et al. (1995) and Barber et al. (1998), respectively. Error bars on the depth scale refer to uncertainty arising from sample thickness and distance between sample depths.

For BFA, the age estimates based on the second interpretation of the ^{14}C age-depth relationship are strongly supported by the other age markers. The minimum value at 20.0–20.5 cm overlaps with the 2-σ age ranges of the ^{210}Pb age estimates. The minimum at 38.0–38.5 cm is supported by the pollen marker at AD 1800 (the rise in pine pollen; see Figure 3 and Hendon and Charman 2004). The suggested age at 52.0–52.5 cm—associated with the shoulder of the peak in ^{14}C activity—has no supporting marker but is in line with the extrapolated curve from ^{210}Pb, pollen, and SCP markers. In the case of BFA then, the ages from the wiggle-matched ^{14}C ages agree well with the other age markers, which also have a high degree of internal consistency.

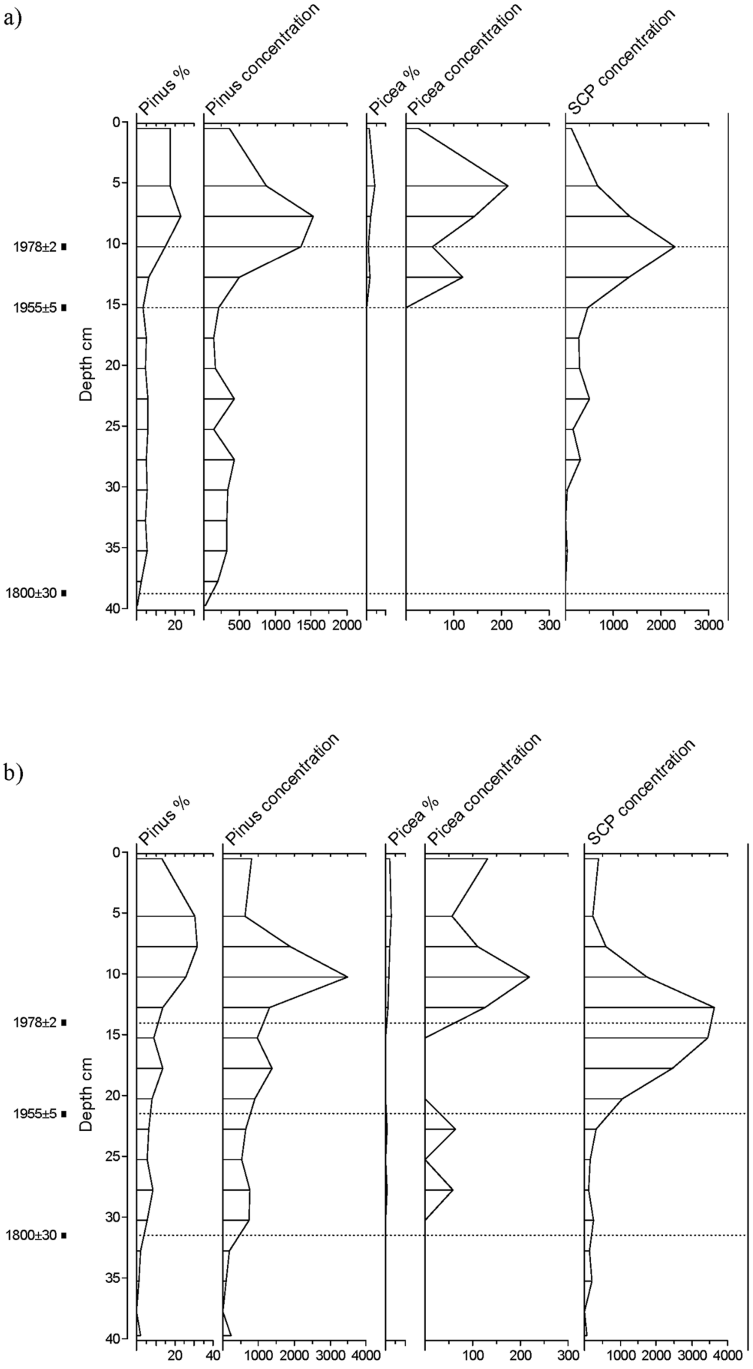

Figure 3 Age estimates based on changes in pine pollen and SCPs for a) core BFA and b) core BFB. The AD 1800 age estimate is based on the initial rise in pine pollen. The 2 SCP markers are based on the rapid increase in SCPs during the 1950s and the peak in SCPs from the late 1970s (Rose et al. 1995). The secondary pine rise reflects the expansion of forest plantations after the 1950s. Pollen % curves expressed as % total land pollen; concentrations expressed as number cm^{-3}.

In BFB, there was a disagreement between the ages derived previously from ^{210}Pb and the age estimates based on SCPs (Figures 2b and 3). The wiggle-matched ^{14}C minimum at 28.5–29.0 cm is much younger than an extrapolation of the ^{210}Pb chronology for an equivalent depth. The minimum at 32.5–33.0 cm is close to the AD 1800 pine pollen rise, which has an estimated error of ±30 yr (Barber et al. 1998). Therefore, it seems unlikely that this minimum represents the AD 1715 minimum in the calibration curve, but is more likely to be AD 1825. The older age estimates based on wiggle matching are not supported by other age estimates. In this case, the new age estimates from wiggle-matched ^{14}C ages shed light on the previously unresolved disagreement between ^{210}Pb and SCP/pollen age estimates. Up until now, we had rejected the age estimates based on SCPs, suspecting some downward movement of SCPs within the profile. However, the wiggle-matched ^{14}C age estimates are more in line with the SCP and pollen ages than they are with the ^{210}Pb. Given that ^{210}Pb chronologies generally require cross-validation with other techniques (Oldfield et al. 1995), the new results suggest that the ^{210}Pb chronology should be rejected in favor of one based on a combination of the SCP, pollen, and wiggle-matched ^{14}C estimates.

CONCLUSIONS

Wiggle matching ^{14}C ages for the period AD 1600–1950 is an attractive approach to cross-check chronologies based on ^{210}Pb, SCPs, and pollen markers, as well as to extend the chronology over a period that is impossible to date accurately using fewer ^{14}C ages. However, we have shown that the approach is not without problems and that ages older than expected may be obtained. Contamination with SCPs seems to be the most likely cause of the largest aging effects in late 19th- and early 20th-century samples, probably augmented by other industrial carbon contamination. This effect is likely to be particularly acute in regions close to industrial sources, such as northern England. The previously reported "reservoir effect" may also be present in the samples analyzed here, although we have no direct evidence for this. Careful cleaning of samples as recommended by Blaauw (2003) may solve the problem of older carbon contamination to some extent, but other approaches designed to assess the influence of industrial carbon directly are also needed. Differential temperature combustion of samples is one possible approach to separating carbon fixed by plants from industrial particulate carbon.

ACKNOWLEDGMENTS

D J C acknowledges allocation 862.0500 from the NERC Radiocarbon Laboratory Steering Committee for funding the ^{14}C analyses.

REFERENCES

Appleby PG, Shotyk W, Fankhauser A. 1997. Lead-210 age dating of peat cores in the Jura Mountains, Switzerland. *Water Air and Soil Pollution* 100:223–31.

Barber K, Dumayne-Peaty L, Hughes P, Mauquoy D, Scaife R. 1998. Replicability and variability of the recent macrofossil and proxy-climate record from raised bogs: field stratigraphy and macrofossil data from Bolton Fell Moss and Walton Moss, Cumbria, England. *Journal of Quaternary Science* 13:515–28.

Blaauw M. 2003. An investigation of Holocene sun-climate relationships using numerical C-14 wiggle-match dating of peat deposits [PhD dissertation]. Amsterdam: University of Amsterdam.

Blaauw M, van der Plicht J, van Geel B. 2004. Radiocarbon dating of bulk peat samples from raised bogs: non-existence of a previously reported "reservoir effect"? *Quaternary Science Reviews* 23:1537–42.

Bronk Ramsey C. 2000. OxCal Program v3.5. Oxford: University of Oxford Radiocarbon Accelerator Unit. URL: http://www.rlaha.ox.ac.uk/orau/oxcal.html.

Charman DJ, Brown AD, Hendon D, Kimmel A, Karofeld E. 2004. Testing the relationship between Holocene peatland palaeoclimate reconstructions and instrumental data. *Quaternary Science Reviews* 23: 137–43.

Clymo RS, Oldfield F, Appleby PG, Pearson GW, Ratnesar P, Richardson N. 1990. The record of atmospheric deposition on a rainwater-dependent peatland. *Philo-*

sophical Transactions of The Royal Society of London Series B: Biological Sciences 327:331–8.

Gedye SJ. 1998. Mass balance in recent peats [PhD dissertation]. Liverpool: University of Liverpool.

Hendon D, Charman DJ. 2004. High-resolution peatland water table changes for the past 200 years: the influence of climate and implications for management. *Holocene* 14:125–34.

Hendon D, Charman DJ, Kent M. 2001. Comparisons of the palaeohydrological record derived from testate amoebae analysis from peatlands in northern England: within-site variability, between-site comparability and palaeoclimatic implications. *Holocene* 11:127–48.

Jungner H, Sonninen E, Possnert G, Tolonen K. 1995. Use of bomb-produced C-14 to evaluate the amount of CO_2 emanating from two peat bogs in Finland. *Radiocarbon* 37(2):567–73.

Kilian MR, van Geel B, van der Plicht J. 2000. C-14 AMS wiggle matching of raised bog deposits and models of peat accumulation. *Quaternary Science Reviews* 19:1011–33.

Kilian MR, van der Plicht J, van Geel B. 1995. Dating raised bogs: new aspects of AMS C-14 wiggle matching, a reservoir effect and climatic change. *Quaternary Science Reviews* 14:959–66.

Levin I, Hesshaimer V. 2000. Radiocarbon—a unique tracer of global carbon cycle dynamics. *Radiocarbon* 42(1):69–80.

Lichtfouse E, Lichtfouse M, Jaffrezic A. 2003. Delta C-13 values of grasses as a novel indicator of pollution by fossil fuel-derived greenhouse gas CO_2 in urban areas. *Environmental Science and Technology* 37:87–9.

Martínez-Cortizas A, Pontevedra-Pombal X, García-Rodeja E, Nóvoa-Muñoz JC, Shotyk W. 1999. Mercury in a Spanish peat bog: archive of climate change and atmospheric metal deposition. *Science* 284:939–42.

Mauquoy D, van Geel B, Blaauw M, van der Plicht J. 2002. Evidence from northwest European bogs shows "Little Ice Age" climatic changes driven by variations in solar activity. *Holocene* 12:1–6.

Nilsson M, Klarqvist M, Bohlin E, Possnert G. 2001. Variation in C-14 age of macrofossils and different fractions of minute peat samples dated by AMS. *Holocene* 11:579–86.

Oldfield F, Richardson N, Appleby PG. 1995. Radiometric dating (Pb-210, Cs-137, Am-241) of recent ombrotrophic peat accumulation and evidence for changes in mass-balance. *Holocene* 5:141–8.

Punning JM, Alliksaar T. 1997. The trapping of fly-ash particles in the surface layers of *Sphagnum*-dominated peat. *Water Air and Soil Pollution* 94:59–69.

Rose NL, Harlock S, Appleby PG, Battarbee RW. 1995. Dating of recent lake sediments in the United Kingdom and Ireland using spheroidal carbonaceous particle (SCP) concentration profiles. *Holocene* 5:328–35.

Rose N. 2001. Fly ash particles. In: Last WM, Smol JP, editors. *Tracking Environmental Change Using Lake Sediments. Volume 2: Physical and Geochemical Methods.* Dordrecht: Kluwer Academic. p 319–49.

Schoning K, Charman DJ, Wastegård S. 2005. Reconstructed water tables from two ombrotrophic mires in eastern central Sweden compared with instrumental meteorological data. *The Holocene* 15(1):111–8.

Speranza A, van der Plicht J, van Geel B. 2000. Improving the time control of the Subboreal/Subatlantic transition in a Czech peat sequence by C-14 wiggle-matching. *Quaternary Science Reviews* 19:1589–1604.

Stuiver M, Reimer PJ, Bard E, Beck JW, Burr GS, Hughen KA, Kromer B, McCormac G, van der Plicht J, Spurk M. 1998. IntCal98 radiocarbon age calibration 24,000–0 cal BP. *Radiocarbon* 40(3):1041–83.

Wardenaar ECP. 1987. A new hand tool for cutting peat profiles. *Canadian Journal of Botany* 65:1772–3.

Yang HD, Rose NL, Battarbee RW. 2001. Dating of recent catchment peats using spheroidal carbonaceous particle (SCP) concentration profiles with particular reference to Lochnagar, Scotland. *Holocene* 11:593–7.

RADIOCARBON, Vol 47, Nr 1, 2005, p 147–158

THE STRATIGRAPHIC SEQUENCE AT YALÂ (YEMEN): A STATISTICAL EVALUATION

Andrea Manzo

University of Naples "L'Orientale." Email: andreamanzo@virgilio.it.

INTRODUCTION

The South Arabian chronology has been problematic for a long time and this is also a true *vexata quaestio* for the ancient history of South Arabia. Three different chronologies have been suggested for the first literate phase of South Arabian cultures, which may date to the 11th century BC, the late 8th century BC, or the 5th century BC (see de Maigret 1996:157–63; de Maigret and Robin 1989: 276–8; Pirenne 1988; Robin 1997; Figure 1). At the site of Yalâ, potsherds with incised South Arabian inscriptions have been recovered in a stratum dating at least to the 8th century BC, if not earlier, and offer evidence of the existence of South Arabian culture at that time (de Maigret and Robin 1989:288–9).

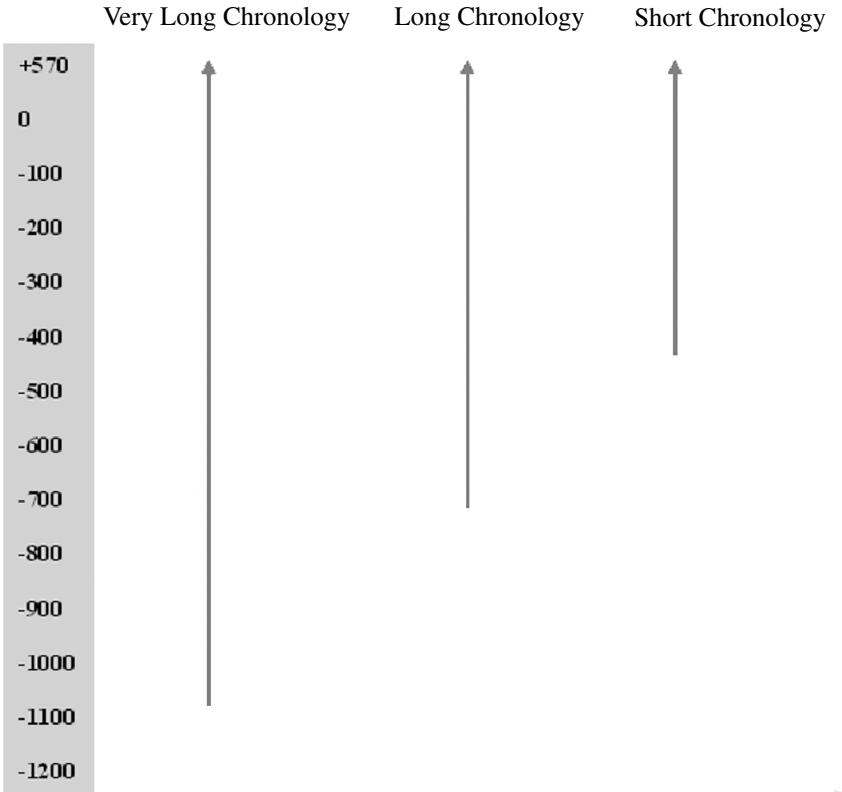

Figure 1 Alternative chronologies for the beginning of the literate phase of South Arabian cultures

RESULTS

The site of Yalâ—excavated in 1987 by the Italian Archaeological Expedition to Yemen of the Instituto Italiano per il Medio ed Estremo Oriente (IsMEO), led by Alessandro de Maigret—is 30 km southwest of Ma'rib, the capital of the Sabean kingdom (de Maigret and Robin 1989:278; de Mai-

gret 1996:163; Figure 2). In an upper sector of the site, an elite Sabean domestic structure (House A) was excavated (de Maigret and Robin 1989:280; de Maigret 1996:163). The walls were well preserved up to a height of 5 m, and the remains of a collapsed first floor were recovered in the room fill (de Maigret and Robin 1989:282; de Maigret 1996:166). Three stratigraphic test-pits were excavated in the rooms under the living-floor of the house, exposing the remains of at least 3 phases of use (phases B, C, and D) under the strata linked to the latest structure (phase A) (de Maigret and Robin 1989:284; de Maigret 1996:170–1).

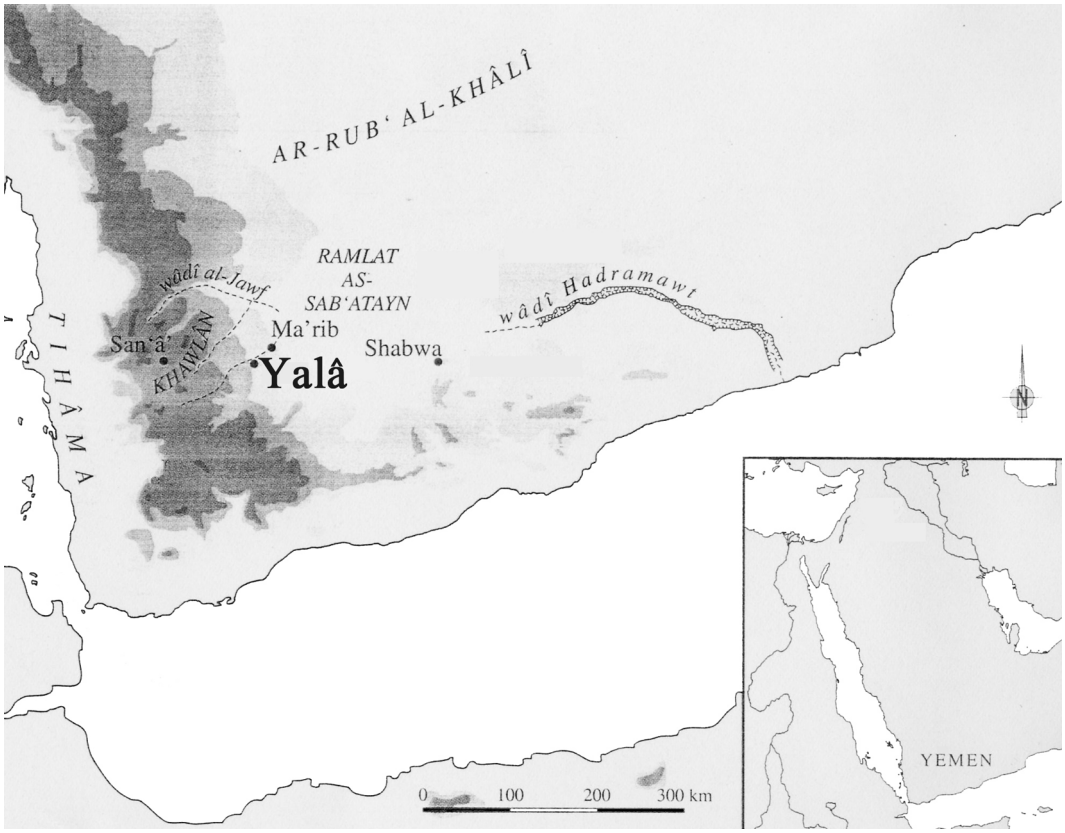

Figure 2 Location of Yalâ in Yemen (modified from *Yemen au pays de la Reine de Saba*. Paris: Institut de Monde Arabe. 1997. p 23).

The first phase of use of the area (Phase D) is represented by a sequence of occupation layers ~1 m thick that overlapped the natural fluvial gravel; artifacts were found in these layers but without any traces of structures. The second phase of use (Phase C) is characterized by several occupation layers ~1 m thick, with traces of a stone wall. The third phase (Phase B) is characterized by several occupation layers ~1.5 m thick associated with stone structures. The latest occupation phase corresponds to the collapse of the upper floor and to the living-floor of the basement of the House A, the occupation of which ended with a fire (de Maigret and Robin 1989:284–5, Figure 3, Plate 9a–b, Plate 10a–b).

Five charcoal samples were collected for radiocarbon dating (de Maigret and Robin 1989:286–7, Figure 3; de Maigret 1996:171–2): two from the collapse stratum marking the last phase of use of

House A, two from a destruction level marking the end of the use of the structures of phase C and the beginning of phase B, and one from a destruction level at the beginning of phase C. The dates are as follows (de Maigret and Robin 1989:287, note 45, 290):

Phase A (end of the phase)

1 (R 1945a): 2600 ± 50 BP
2 (R 1949a): 2570 ± 60 BP

Phase B (beginning of the phase)

3 (R 1948a): 2750 ± 75 BP
4 (R 1946a): 2840 ± 70 BP

Phase C (beginning of the phase)

5 (R 1947a): 2980 ± 65 BP

On the basis of the calibrated ^{14}C dates, the charcoal from House A, and its subsequent abandonment, dates to 850–650 BC and 825–585 BC. The charcoal at the beginning of phase B dates to 1100–795 BC and 1240–830 BC, and the charcoal at the beginning of phase C dates to 1395–920 BC (de Maigret and Robin 1989:287; de Maigret 1996:171–2). If the latest values of calibrated dates and an average period of use of 50 yr for wood are considered, 535 BC and 600 BC are the dates for the end of the last phase of House A, 745 BC for the end of phase B, and 870 BC for the end of phase C (de Maigret and Robin 1989:287–8; de Maigret 1996:172). Thus, phase B, associated with sherds inscribed in South Arabian script (de Maigret and Robin 1989:288), dates to 870–750 BC. Dates for the beginning of phase C and the underlying phase D, characterized by a Sabean-type pottery (de Maigret and Robin 1989:286; de Maigret 1996:171; de Maigret 1997:51), could not be given precisely.

The importance of the new data from Yalâ has been correctly pointed out by epigraphers trying to date the earliest appearance of the South Arabian script (see Garbini 1995:279–80). Nevertheless, for the sequence of Yalâ and the data from other South Arabian sites, a problem exists in the ^{14}C dates associated with the inscribed sherds due to uncertainties and inconsistencies of the ^{14}C dates, which apparently were considered too old by the excavator who accepted only the more recent calibrated intervals plus an additional period of 50 yr as an average time of wood usage in the buildings (see Garbini 1995:280, note 16; see also p 288, note 41).

Given the importance of the Yalâ sequence for South Arabian archaeology, re-calibration of the ^{14}C dates was done using an updated calibration curve (Stuiver et al. 1998). Moreover, as the Yalâ samples came from a well-established stratigraphic sequence, the OxCal v3.9 program (Bronk Ramsey 2003) was used to evaluate the sequence and its boundaries, mainly focusing on the appearance of inscribed sherds in the sequence. The OxCal v3.9 program allowed the integrated analysis of groups of ^{14}C dates and the inclusion of contextual information, such as stratigraphic and cultural elements, into the calibration and evaluation process by means of Bayesian statistics (Bronk Ramsey 1995, 2000; Buck et al. 1992).

The results of the simple re-calibration of these dates (Stuiver et al. 1998) are as follows:

R 1947a **2980 ± 65 BP**

68.2% probability (1 σ)
1370 BC (2.2%) 1350 BC
1320 BC (64.5%) 1110 BC
1100 BC (1.5%) 1080 BC
95.4% probability (2 σ)
1390 BC (95.4%) 1000 BC
99.7% probability (3 σ)
1450 BC (99.7%) 900 BC

R 1946a **2840 ± 70 BP**

68.2% probability (1 σ)
1130 BC (68.2%) 900 BC
95.4% probability (2 σ)
1220 BC (95.4%) 830 BC
99.7% probability (3 σ)
1400 BC (99.7%) 800 BC

R 1948a **2750 ± 75 BP**

68.2% probability (1 σ)
1000 BC (68.2%) 820 BC
95.4% probability (2 σ)
1130 BC (95.4%) 790 BC
99.7% probability (3 σ)
1300 BC (99.7%) 750 BC

R 1945a **2600 ± 50 BP**

68.2% probability (1 σ)
830 BC (58.8%) 760 BC
680 BC (5.0%) 660 BC
610 BC (4.4%) 590 BC
95.4% probability (2 σ)
900 BC (1.8%) 870 BC
840 BC (61.4%) 750 BC
720 BC (32.2%) 540 BC
99.7% probability (3 σ)
910 BC (99.7%) 480 BC

R 1949a **2570 ± 60 BP**

68.2% probability (1 σ)
810 BC (27.7%) 750 BC
690 BC (8.4%) 660 BC
650 BC (32.1%) 540 BC
95.4% probability (2 σ)
840 BC (92.7%) 510 BC
470 BC (2.7%) 410 BC
99.7% probability (3 σ)
900 BC (99.7%) 400 BC

If we plot these results, we have the sequence shown below.

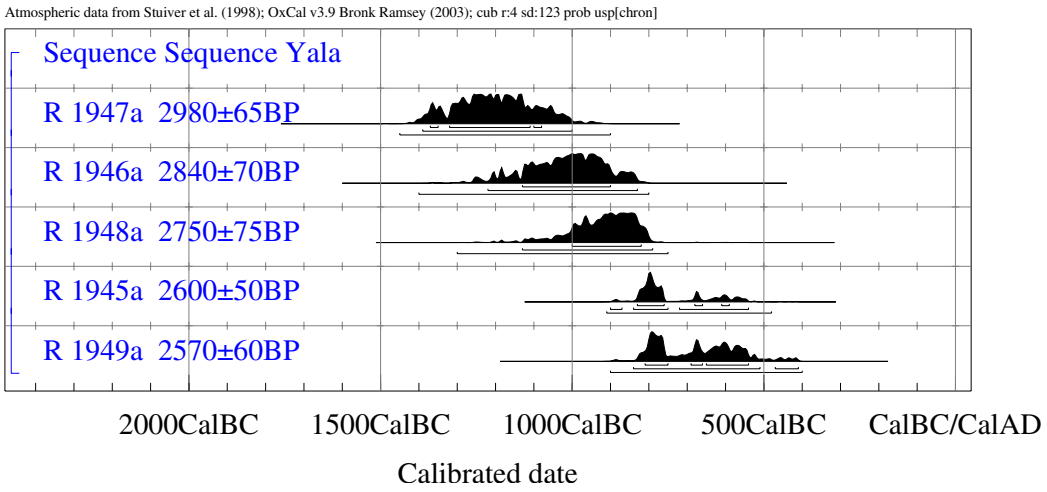

Figure 3 Atmospheric data from Stuiver et al. (1998), OxCal v3.9 Bronk Ramsey (2003)

The stratigraphic relationships of the contexts of the collected samples allows one to evaluate the coherence of the sequence and to derive more narrow dates:

Sampled R 1947a **2980 ± 65 BP**

68.2% probability (1 σ)
1260 BC (68.2%) 1040 BC
95.4% probability (2 σ)
1380 BC (95.4%) 990 BC
99.7% probability (3 σ)
1410 BC (99.7%) 920 BC

Agreement 98.2%

Sampled R 1946a **2840 ± 70 BP**

68.2% probability (1 σ)
1030 BC (63.3%) 890 BC
880 BC (4.9%) 850 BC
95.4% probability (2 σ)
1110 BC (95.4%) 820 BC
99.7% probability (3 σ)
1210 BC (99.7%) 800 BC

Agreement 107.5%

Sampled R 1948a **2750 ± 75 BP**

68.2% probability (1 σ)
990 BC (68.2%) 840 BC
95.4% probability (2 σ)
1050 BC (95.4%) 800 BC

99.7% probability (3 σ)
1130 BC (99.7%) 790 BC

Agreement 104.8%

Sampled R 1945a **2600 ± 50 BP**

68.2% probability (1 σ)
820 BC (68.2%) 760 BC
95.4% probability (2 σ)
840 BC (78.8%) 750 BC
710 BC (16.6%) 540 BC
99.7% probability (3 σ)
910 BC (99.7%) 520 BC

Agreement 121%

Sampled R 1949a **2570 ± 60 BP**

68.2% probability (1 σ)
830 BC (64.9%) 750 BC
690 BC (3.3%) 660 BC
95.4% probability (2 σ)
840 BC (95.4%) 550 BC
99.7% probability (3 σ)
900 BC (99.7%) 410 BC

Agreement 124.3%
Overall agreement 125.6%

It is worth noting that the agreement of each date in the framework of the sequence is always higher than 98%. As a consequence, the overall agreement is very high, having a value higher than 100%. This seems to confirm the coherence of the dates with the stratigraphic context in which the samples were collected.

If the function boundary of the OxCal v3.9 program is used to obtain the end and beginning of the sequence as well as the beginning of the phases, the following results are obtained:

Sampled Beginning C

68.2% probability (1 σ)
1410 BC (68.2%) 1060 BC
95.4% probability (2 σ)
1700 BC (95.4%) 1000 BC
99.7% probability (3 σ)
... (99.7%) 953 BC

Sampled Beginning B

68.2% probability (1 σ)
1410 BC (68.2%) 930 BC
95.4% probability (2 σ)
1250 BC (95.4%) 850 BC
99.7% probability (3 σ)
1400 BC (99.7%) 800 BC

Sampled Beginning A

68.2% probability (1 σ)
900 BC (68.2%) 780 BC
95.4% probability (2 σ)
1000 BC (95.4%) 670 BC
99.7% probability (3 σ)
1100 BC (99.7%) 550 BC

Sampled End A

68.2% probability (1 σ)
810 BC (68.2%) 570 BC
95.4% probability (2 σ)
830 BC (95.4%) 340 BC
99.7% probability (3 σ)
850 BC (99.7%) ...

These results can be plotted as follows:

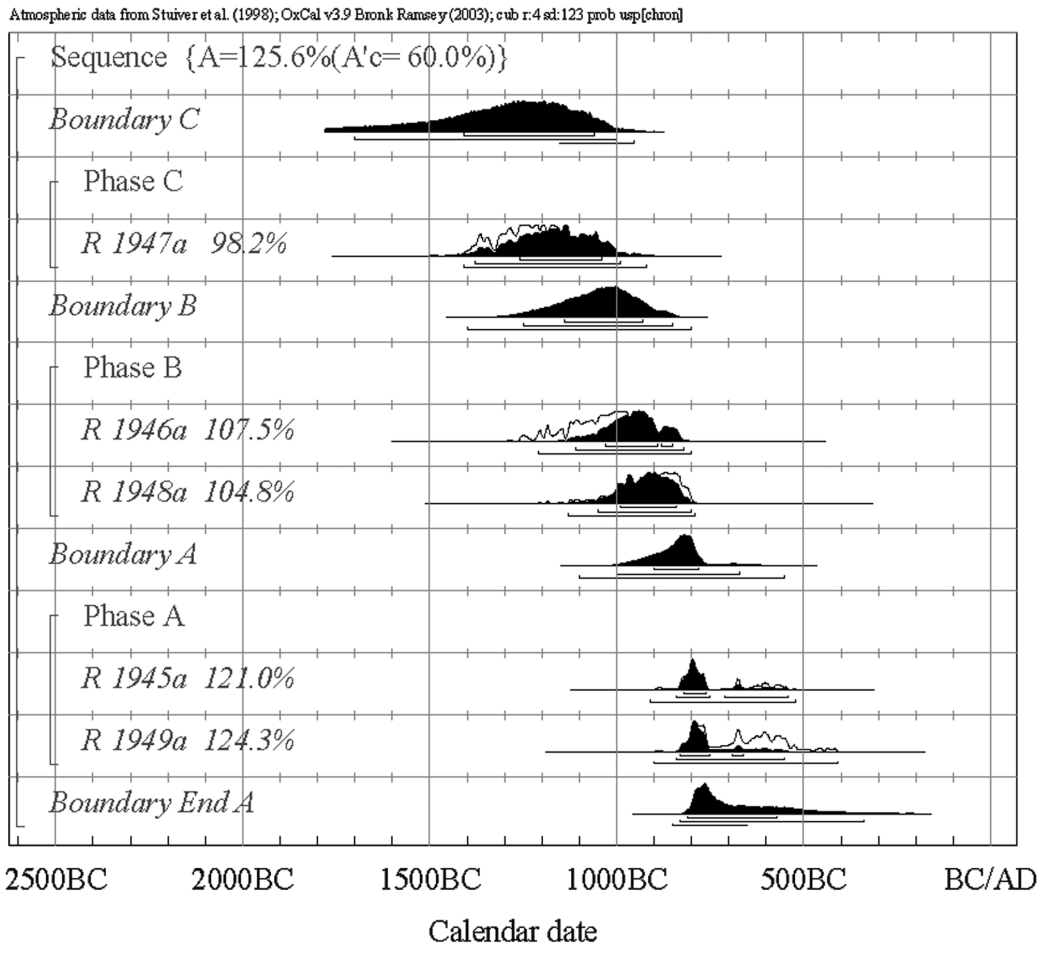

Figure 4 Results of the Yalâ sequence using OxCal v 3.9

The beginning of sequence C is as follows:

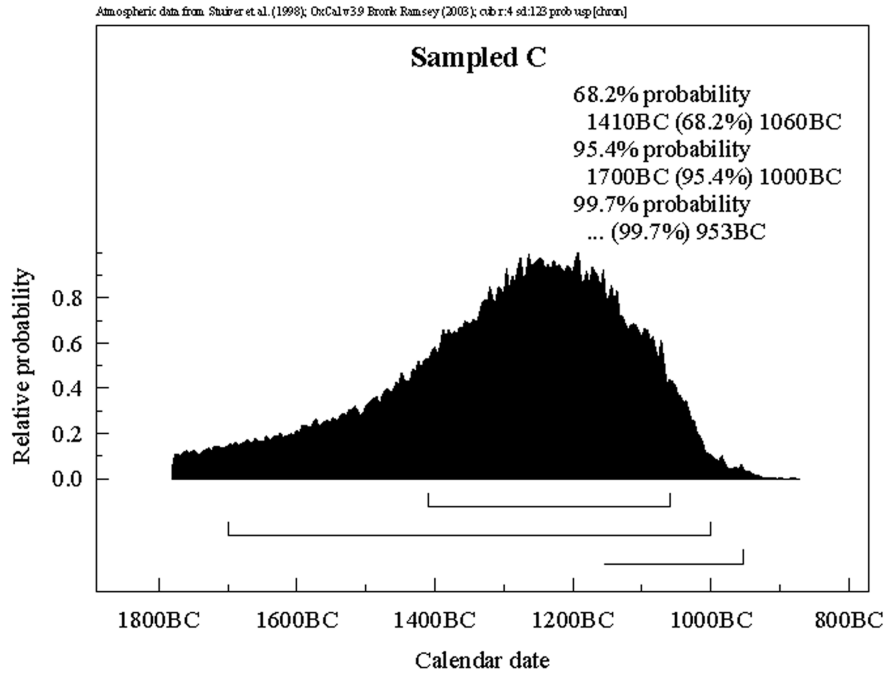

Figure 5 Results for the beginning of sequence C

The beginning of phase B, which contains the inscribed sherds, is as follows:

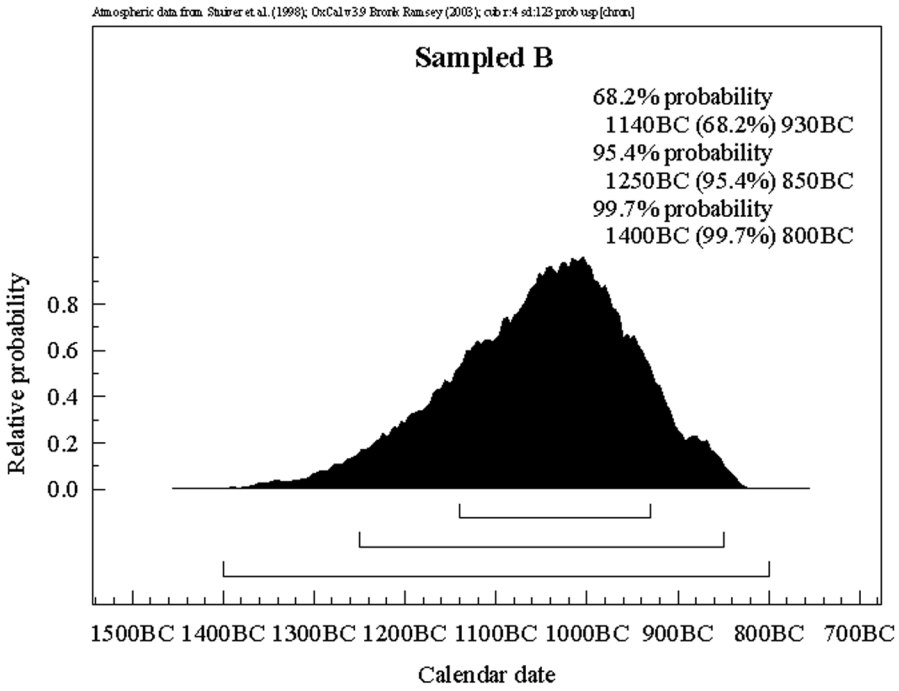

Figure 6 Results for the beginning of phase B

The beginning of phase A, the phase of use of House A, is as follows:

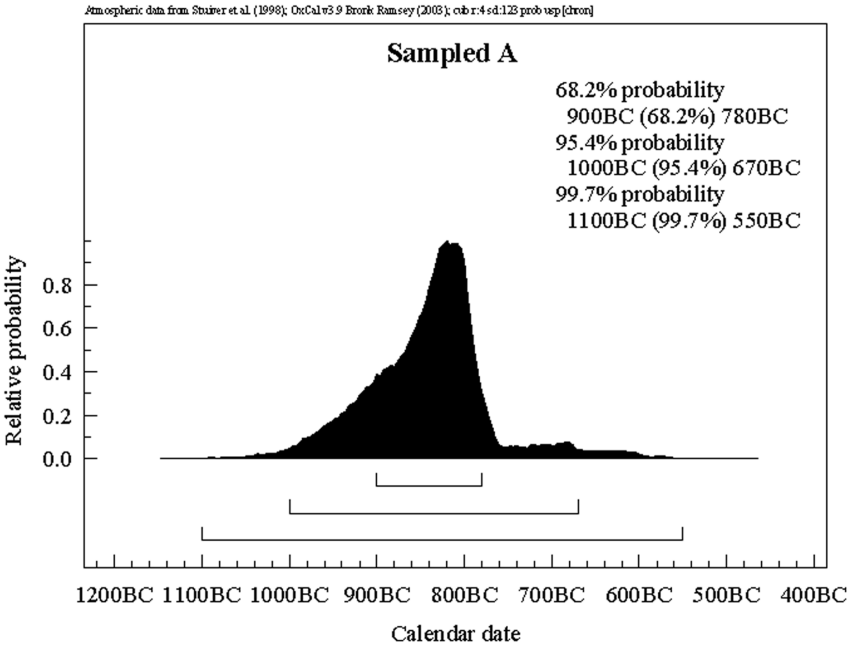

Figure 7 Results for the beginning of phase A

The end of phase A and the sequence is as follows:

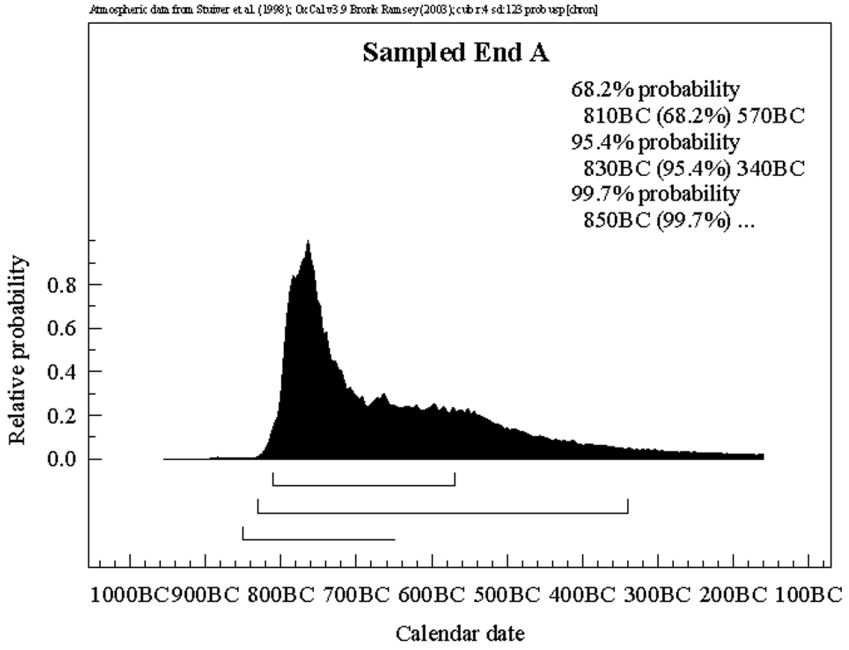

Figure 8 Results for the end of phase A

DISCUSSION

As previously noted, 5 samples were collected in the strata associated with the beginning of phase C (R 1947a), the beginning of phase B (R 1948a, R 1946a), and the end of phase A (R 1945a, R 1949a). Considering the peak of calculated distributions for the boundaries (1 σ), the results suggest a length of 130–270 yr for phase C, 150–240 yr for phase B, and 90–210 yr for phase A. Thus, phases B and C seem longer than A. Given the previously discussed stratigraphic information, this is fully justifiable since phases C and B were characterized by several occupation layers each. On the other hand, phase A corresponds only to the last use of House A.

Regarding the absolute chronology of the phases, since the error in the ^{14}C dates is quite large and the number of determinations is small, it is difficult to define clear boundaries. Nevertheless, considering all of the limitations of the analysis, interesting data are provided on the crucial problem of the origins of the Sabean culture and the date of the earliest South Arabian inscriptions. It is worth noting that in the analysis of the different possible chronologies, reference was made to the extreme higher values obtained from the calibration, and not to the most probable age/interval for the archaeological sequence, in order to outline the shortest possible chronology of the phases.

Moreover, it has correctly been pointed out (de Maigret and Robin 1989:287) that the ^{14}C dates refer to the time of death of the trees and not to the moment when the use of the wood ended, and thus the burned wood used as samples for the ^{14}C dates could have been felled many years before it was burned (de Maigret and Robin 1989:287). Nevertheless, if the charcoal samples come from construction wood, the 50-yr-long period used by de Maigret and Robin (1989:287) might be too brief. Therefore, it was increased to 100 yr, but only for the samples of wood apparently associated with collapsed structures, such as those from the last stratum of phase A and those from the destruction stratum at the end of phase C to the beginning of phase B. This was not done for the sample from the stratum at the beginning of phase C to the end of phase D because it came from a layer apparently without any trace of structures, but in this case an average 50-yr period of wood usage was considered.

As a consequence, the beginning of phase C can be dated before 903 BC, which is also a *terminus ante quem* for the end of the underlying phase D. The beginning of phase B (i.e. the literate phase) can be dated between 1300 and 700 BC. The beginning of phase A (i.e. the phase of use of House A) can be dated between 1000 and 450 BC, and the end of phase A is after 750 BC. All of these limits are calculated using the maximum probability (3 σ, i.e. 99.7% probability). If we consider the lower possible dates among the ranges with the maximum of probabilities, phase D can be dated before 903 BC, phase C between 903 and 700 BC, phase B between 700 and 450 BC, and phase A after 450 BC. The occupation of House A would have ended sometime after 750 BC.

Nevertheless, these suggested dates should be accepted with caution. By only taking the lower possible dates with a slightly lower degree of probability (2 σ, i.e. 95.4% probability), phase D is before 950 BC, phase C between 950 and 750 BC, phase B between 750 and 570 BC, and phase A between 570 and 240 BC.

Thus, these dates suggest that the use of the Sabean script is dated to at least the end of the 8th century BC (3 σ, i.e. 99.7% probability), or possibly the mid-8th century BC (2 σ, i.e. 95.4% probability). Moreover, the first use of the excavated area at Yalâ can be dated before the end of the 10th century BC (3 σ, i.e. 99.7% probability), or possibly even before the mid-10th century BC (2 σ, i.e. 95.4% probability). It is worth noting that at that time, the pottery already showed typical Sabean characteristics, which demonstrated that people associated with Sabean material culture were

present in eastern Hawlân from the beginning of the 10th century BC. In general, these dates are consistent with the evaluations of de Maigret and just a bit later (de Maigret and Robin 1989:286–9, see also Garbini, 286–7; Robin 1997:62).

Nevertheless, one cannot exclude the likeliness that the precise dates for the beginning of the archaeological phases at Yalâ are earlier than these dates. If the earliest possible dates for each phase are used, the chronology is higher: phase D can be dated before 1360 BC, phase C between 1360 and 1300 BC, phase B between 1300 and 1000 BC, and phase A after 1000 BC. The occupation of House A would have ended sometime after 750 BC. Using the higher possible dates with a slightly lower degree of probability (2 σ, i.e. 95.4% probability), phase D can be dated before 1650 BC, phase C between 1650 and 1150 BC, phase B between 1150 and 900 BC, and phase A after 900 BC. The occupation of House A would have ended sometime after 730 BC.

According to our last chronology, the Sabean script was used in the last centuries of the 2nd millennium BC and a Sabean ceramic tradition was already established in first half of the 2nd millennium BC. Of course, this hypothetical chronological reconstruction cannot support the old "very long chronology," as was elaborated by Eduard Glaser and Friz Hommel (see Hommel 1927), but it seems consistent with that suggested by von Wissmann (1982), which is now widely accepted (de Maigret 1997:51; Robin 1997:63). According to this chronology, a long, but still not clearly determined, period of use of South Arabian script can be hypothesized before the evidence of monumental inscriptions, which also suggests a precocious rise of South Arabian hierarchic society (see Bron 1997:56). Thus, the literate phase could have begun at least in the 12th century BC.

Given the statistical evaluation of the ^{14}C dates from Yalâ, the importance of the stratigraphic sequence of this site for South Arabian archaeology is clear. In both the lowest and highest chronologies that can be proposed, after evaluating the sequence by Bayesian statistics, the results of this study confirm that this well-dated sequence cannot support a "short" or "low" chronology, such as the one proposed by J Pirenne (de Maigret and Robin 1989:288–91). The new chronology also demonstrates the appearance of the South Arabian script in the early 1st millennium BC, or even in the last centuries of the 2nd millennium BC (see also de Maigret 1997:51; Robin 1997:63). Moreover, these dates seem to point to the appearance of a South Arabian ceramic tradition at least in the last centuries of the 2nd millennium BC, or even in the mid-2nd millennium BC—earlier than generally thought. This last hypothesis suggests a possible solution for the chronological gap between the end of the South Arabian Bronze Age in the first half of the 2nd millennium BC and the beginning of Sabean culture (de Maigret 1996:151–2; de Maigret 1997:52).

ACKNOWLEDGMENTS

I wish to thank Prof de Maigret, University of Naples "L'Orientale" for his suggestions and comments on this paper, and Prof K A Bard, Boston University, for her suggestions and for editing the text. My study of the sequence of ^{14}C dates of Yalâ began in 2002, when I used it as a case study in a seminar on relative and absolute chronology for undergraduate students in the Laboratory of African Archaeology of the University of Naples "L'Orientale."

REFERENCES

Bron F. 1997. Naissance et destin de l'alphabet sudarabique. In: *Yémen au Pays de la Reine de Sabâ*. Paris: Institut de Monde Arabe. p 55–7.

Bronk Ramsey C. 1995. Radiocarbon calibration and analysis of stratigraphy: the OxCal program. *Radiocarbon* 37(2):425–30.

Bronk Ramsey C. 2000. Comment on "The use of Bayesian statistics for ^{14}C dates of chronologically ordered samples: a critical analysis." *Radiocarbon* 42(2):199–202.

Bronk Ramsey C. 2003. OxCal 3.9 Program. The Manual. URL: <http://www.rlaha.ox.ac.uk/OxCal3/Manual/oxcal.htm.>

Buck CE, Litton CD, Smith AFM. 1992. Calibration of radiocarbon results pertaining to related archaeological events. *Journal of Archaeological Science* 19:497–512.

de Maigret A. 1996. *Arabia Felix. Un Viaggio Nell'Archeologia dello Yemen*. Milan: Rusconi.

de Maigret A. 1997. L'aube de l'histoire dans le Yémen intérieur. In: *Yémen au Pays de la Reine de Sabâ.* Paris: Institut de Monde Arabe. p 50–2.

de Maigret A, Robin C. 1989. Les fouilles italiennes de Yalâ (Yémen du Nord): nouvelles données sur la chronologie de l'Arabie du sud préislamique. *Comptes Rendus de l'Académie des Inscriptions et Belles Lettres*. April–June. p 255–91.

Garbini G. 1995. Sulla più antica scrittura sudarabica. *Rivista degli Studi Orientali* 69:275–94.

Hommel F. 1927. Geschichte Südarabiens im Umriß. In: Nielsen D, editor. *Handbuch der Altarabischen Altertumskunde*. Copenhagen: Nyt Nordisk Forlag. p 57–108.

Pirenne J. 1988. The chronology of ancient South Arabia—diversity of opinion. In: Daum W, editor. *Yemen: 3000 Years of Art and Civilization in Arabia Felix*. Innsbruck, and Frankfurt/Main: Penguin-Verlag and Umschau-Verlag. p 116–22.

Robin C. 1997. La chronologie et ses problèmes. In: *Yémen au Pays de la Reine de Sabâ.* Paris: Institut de Monde Arabe. p 60–2.

Stuiver M, Reimer PJ, Bard E, Beck JW, Burr GS, Hughen KA, Kromer B, McCormac G, van der Plicht J, Spurk M. 1998. IntCal98 radiocarbon age calibration, 24,000–0 cal BP. *Radiocarbon* 40(3):1041–83.

von Wissmann H. 1982. *Die Geschichte von Sabâ, II. Das Großreich der Sebäer bis zu seinen Ende im frühen 4. Jh. v. Chr.* Wien: Österreichische Akademie der Wissenschaften Phil.-Hist. Klasse, Sitzungsberichte. p 402.

RADIOCARBON, Vol 47, Nr 1, 2005, p 159–175

RADIOCARBON DATES FROM SOIL PROFILES IN THE TEOTIHUACÁN VALLEY, MEXICO: INDICATORS OF GEOMORPHOLOGICAL PROCESSES

Emily McClung de Tapia[1] • Irma Domínguez Rubio[2] • Jorge Gama Castro[3] • Elizabeth Solleiro[3] • Sergey Sedov[3]

ABSTRACT. Radiocarbon dates largely obtained from bulk soil samples in 24 soil profiles in the Teotihuacán Valley, Mexico, are reported insofar as they represent a first step towards developing a sequence of soil formation, erosion, vegetation change, and human impact during the Holocene. Limitations of ^{14}C dating in the area are considered, particularly the absence of charcoal in sediments and poor preservation of pollen. A broad temporal scheme is proposed to guide future research in which 4 periods are defined: ~5000–2000 BP (relative stability with short, intermittent episodes of erosion); ~2000–1500 BP (erosion-sedimentation, deforestation, and intensive agriculture); ~1500–1000 BP (relative stability, depopulation, and partial recovery of the landscape); and ~1000–500 BP (erosion-sedimentation, deforestation, and intensive agriculture).

INTRODUCTION

Between 1992 and 1999, 24 soil profiles were excavated in the Teotihuacán Valley, State of Mexico (Figure 1), in order to study the formation of soils, erosion, and human impact associated with prehispanic settlement, resource extraction, and production in the region. The region, located approximately 50 km NE of Mexico City, is best known for the archaeological site of Teotihuacán, the earliest city of its size and density in the Americas, occupied between approximately AD 1–650. Although the prehispanic urban center of Teotihuacán represents a significant focus for our research, our initial goal was to establish a broad outline of the sequence of landscape transformation throughout the Holocene, based on the analysis of sediments and associated plant remains, including macrobotanical remains, pollen, and phytoliths (McClung de Tapia et al. 2003).

In the Teotihuacán Valley, only very limited paleoenvironmental research had been undertaken prior to our investigation, including geological surveys reported by Mooser (1968) and Barba (1995), a palynological study by Kovar (1970), and an analysis of Aztec and Colonial period landscape change in the Texcoco region, which included a portion of the southern extreme of the Teotihuacán Valley (Cordova 1997). Only Cordova's research incorporated radiocarbon determinations of organic materials recovered from profiles. Consequently, our analysis represents the first stage of an attempt to develop a sequence of regional landscape dynamics in the area during the Holocene.

Paleoenvironmental studies of lake sediments reported from other sectors of the Basin of Mexico indicate relatively dry conditions during the Late Glacial continuing into the Early Holocene (Lozano-García and Ortega-Guerrero 1998; Caballero et al. 1999). Palynological studies of cores from lakes Texcoco and Chalco (Lozano-García et al. 1993; Lozano García and Ortega-Guerrero 1998) S and E of the Teotihuacán Valley, respectively, and Lake Tecocomulco in the NE (Caballero et al. 1999), consistently reveal evidence for human impact during the Middle-Late Holocene that obscures possible indicators of episodes of climatic-induced vegetation change or other evidence for climatic variability that could have affected human settlements in prehispanic times.

[1]Laboratorio de Paleoetnobotánica y Paleoambiente, Instituto de Investigaciones Antropológicas, Universidad Nacional Autónoma de México. Corresponding author. Email: mcclung@servidor.unam.mx.
[2]Deceased. Departamento del Hombre y su Medio Ambiente, Universidad Autónoma Metropolitana-Xochimilco.
[3]Departamento de Edafología, Instituto de Geología, Universidad Nacional Autónoma de México.

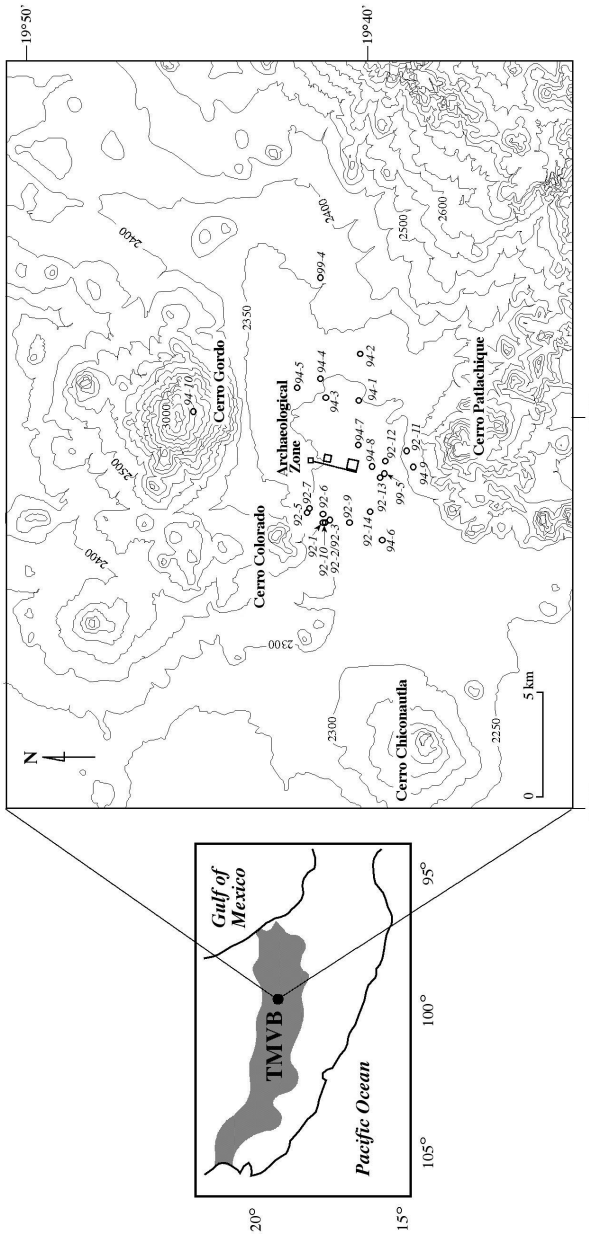

Figure 1 Location of soil profiles in the Teotihuacán Valley, in the W-E Trans-Mexican Volcanic Belt that stretches across central Mexico.

METHODOLOGY

Initially, a N-SE transect between Cerro Colorado and Cerro Patlachique was studied, followed by additional profiles in the alluvial plain S and E of the ancient city and on Cerro Gordo to the N. An attempt was made to locate soil profiles at or beyond the margins of the ancient city in order to evaluate soil variability and its relationship to human occupation. However, buried remains of prehispanic structures were encountered occasionally.

^{14}C dates on bulk sediment were obtained from the upper 5 cm of selected horizons in order to relate formation processes and erosive sequences in different sectors of the valley and to contribute to an understanding of vegetation change over time as indicated by grass phytoliths recovered from dated horizons. Unfortunately, pollen is poorly preserved in the region and in situ pollen materials were insufficient for dating. Both pollen and phytoliths were also subject to redeposition in the alluvial plain. All samples were pretreated by Beta Analytic, Inc, Miami, Florida, USA. Pretreatment consisted of the removal of any apparent roots, followed by mechanical dispersion in hot acid (HCL) to eliminate carbonates. Samples were subsequently rinsed repeatedly until neutralized, then dried and subjected to combustion in an enclosed system. Conventional dates were obtained by benzene synthesis and counting at the Beta Analytic facility. Accelerator mass spectrometry (AMS) measurements based on sample carbon reduced to graphite (processed by Beta Analytic) were undertaken at Lawrence Livermore National Laboratory. The results represent the total organic content of the analyzed material and ^{14}C determinations are interpreted to reflect mean residence time (MRT) of organic carbon in the soil (SOM) unless otherwise indicated. Visible in situ charcoal was absent from all strata, with the unique exception of a fragment of maize stem (*Zea mays* L.) recovered from profile 92-14. The charcoal, dated by AMS (Beta-60633), was soaked in hot alkalai to remove humic acids, followed by rinsing to neutrality, then an acid wash as described above, and another rinsing to neutrality.

The following types of layers were dated: Ah horizons of well-developed buried paleosols with normal A-B-C horizon sequences and primarily in situ humus formation; sedimentary sequences consisting of several superimposed A and AC horizons, both of which contain in situ organic material; and C horizons with sufficient organic carbon. Sometimes, humus-enriched B horizons were sampled because, during field survey, they were first described as A horizons, and relabeled after laboratory results were available.

Because of the relatively large number of dates (79) and their potential significance for establishing stratigraphic relations, this report is organized by zones and associated profiles. Two principal zones are recognized—uplands and the alluvial plain—within which the location of each profile is briefly described, followed by dates and a brief reference to the other horizons. In addition, when profiles are located within the urban area of Teotihuacán, references are included to the 1:2000 map sheets of the Teotihuacán map (Millon et al. 1973); otherwise, profiles are situated with respect to the 1:50,000 Texcoco map (E14B21, INEGI 1983). All samples were submitted to Beta Analytic by Emily McClung de Tapia. ^{14}C determinations are reported as conventional ^{14}C yr before AD 1950, with standard errors as provided by the laboratory. Because we feel that calibrations BC/AD do not contribute significantly to the interpretation of the data, these are only included in Table 1, where specific ^{14}C dates obtained from sediments are compared to associated cultural remains. Calibrations were calculated using CALIB rev 4.3 (Stuiver and Reimer 1993). $\delta^{13}C$ values are not considered in detail at this time since additional research is underway in the region to establish their significance, particularly in chronological terms.

Table 1 Horizons or archaeological strata with associated cultural evidence. Calibrations were calculated in Calib rev 4.3 (Stuiver and Reimer 1993).

Profile/Depth	Horizon	Zone	Lab # (Beta-)	^{14}C determination	Cal BC/AD	Cultural context
92-1 (60–72 cm)	$2A_1$	Upland	68355	5520 ± 110	cal BC 4580–4050	Sediment underlying Teotihuacán structure
92-2 (44–54 cm)	2A	Upland	68332	3600 ± 80	cal BC 2200–1740	Sediment underlying Teotihuacán burial
92-14 (1.10–1.17 cm)	2B	Alluvial plain	60633	490 ± 60 (AMS)	cal AD 1320–1490	Carbonized maize stalk
92-13 (61–167 cm)	n.d.	Alluvial plain	68358	2690 ± 70	cal BC 1000–790	Sediment underlying foundation of Teotihuacán structure
99-5 (95–120 cm)	B_2	Alluvial plain	142228	2890 ± 50	cal BC 1260–920	Classic Teotihuacán ceramics
99-5 (120–133 cm)	C	Alluvial plain	142229	3370 ± 60	cal BC 1870–1520	Classic Teotihuacán ceramics
99-5 (133–158 cm)	$2A_{11}$	Alluvial plain	142230	2990 ± 80	cal BC 1430–980	Classic Teotihuacán ceramics
99-5 (158–171 cm)	$2A_{12}$	Alluvial plain	142231	3110 ± 80	cal BC 1520–1130	Classic Teotihuacán ceramics
99-4 (N86–110cm)	$2A_{11}$	Alluvial plain	142223	2890 ± 60	cal BC 1290–900	Predominantly Mazapan-phase ceramics (Aztec ceramics in upper strata)

RESULTS

Zone 1. Uplands

1. Cerro Colorado. Defensa Nacional (37a Zona Militar)

The profiles described were located on the southeastern flank of Cerro Colorado, at the northwestern limit of the Archaeological Zone of Teotihuacán, San Juan Teotihuacán, State of Mexico. All samples consist of bulk sediment from the upper 5 cm of selected horizons. Descriptions of associated archaeological contexts are as yet unpublished, with the exception of 22:N1W6 (Cid 1998).

92-1. Located next to the visible remains of Structure 22 (19°41′25″N, 98°52′17″W), at an elevation of 2350 m (Teotihuacán map, square NIW6, Millon et al. 1973:70). The dated horizon consists of a buried soil underlying a Classic period Teotihuacán structure (predominantly Tlamimilolpa-phase ceramics, Cid 1998:319). The polycyclic profile is represented by 3 superimposed soils that vary in morphology and age.

	Ap (0–30 cm) C (30–60 A cm) $2A_{11}$ (30–60 B cm)	
Beta-68355	$2A_{12}$ (60–72 cm) underlying structure 22	5520 ± 110
	3C (>72 cm)	

92-2. Located 50 m south of a road (19°41′24.6″N, 98°52′15″W), at an elevation of 2282 m, at the SW corner of Structure 16 (NIW5, Millon et al. 1973:71). The dated horizon consists of a buried soil underlying a Classic period multiple burial. The polycyclic profile is represented by 2 soils. The lim-

ited development and depth of horizon 2A suggests that it formed during a short cycle of landscape stability.

	Ao (0–4 cm)	
	A (4–44 cm)	
Beta-68332	2A (44–54 cm) underlying Classic period multiple burial	3600 ± 80
	2C (>54 cm)	

92-3. Located 50 m W of Structure 22, NIW6, (19°41′24.6″N, 98°52′15″W), on the southeastern flank of Cerro Colorado, at an elevation of 2282 m (NIW6, Millon et al. 1973:70). The origin, morphology, and properties of this profile are similar to 92-2. Beta-68357 from the underlying horizon (>52 cm) provided insufficient carbon for dating.

	A (0–19/32 cm)	
Beta-68356	2A (32–52 cm)	2850 ± 70
	2C (>52 cm)	

92-5. Represents the wall of a *zanja* (ditch), 10 m E of Structure 13 (19°41′56″N, 98°51′56″W), on the southeastern flank of Cerro Colorado, at an elevation of 2306 m (N4W5, Millon et al. 1973: 26). This polycyclic profile is highly stratified, and comprised of 4 poorly developed soils derived from colluvium-alluvium. The dated horizons correspond to the second soil below the surface. Beta-68334 (3C, 64–94 cm) and Beta-68335 (4C, >94 cm) provided insufficient carbon for dating.

	AC (0–14 cm)	
Beta-68333	$2AC_1$ (14–30 cm)	2360 ± 100
	$2AC_2$ (30–40 cm)	
Beta-60626	2C (40–64 cm)	2020 ± 80
	3C (64–90 cm)	
	4C (>94 cm)	

92-6. Wall of a *jaguey* (seasonal water deposit) (19°41′30.6″N, 98°52′04″W), at 2285 m (north face of a leveled mound designated as Site 12:N1W5, Millon et al. 1973:71). Dated horizons A_1, A_2, and A_3 represent a single pedological cycle of considerable depth, although poorly developed, overlying a 2C horizon formed in situ from tuff.

Beta-68342	A_1 (0–28 cm)	101.3 ± 0.9% Modern
Beta-68343	A_2 (28–47 cm)	970 ± 80
Beta-68344	A_3 (47–69 cm)	1690 ± 60
	C (69–81 cm)	
Beta-68345	2C (81–101 cm)	2120 ± 70
	Tuff (>101 cm)	

92-7. Located on a *terraza* (terrace) 40 m W of Structure 19 (19°41′59″N, 98°52′02″W), at an elevation of 2315 m (N4W6, Millon et al. 1973:25). The Ap horizon developed from modern sediment overlying the buried 2C horizon formed by weathering of the underlying tuff. Based on Mielich (1991) and Quantin (1992), Hidalgo (1996:46) refers to the succession of pyroclastic deposits (tuff, or *tepetate* as it is referred to locally) evident in the foothills and alluvial plain of the western slope of the Sierra Nevada, forming the following series: T_1<8000 BP, T_{2a}<13,000 BP, T_{2b}<21,000 BP, T_3<21,000–35,000/40,000 BP. According to Peña and Zebrowski (1992:18), an additional series of unknown origin (T_i) underlies Holocene deposits in the Teotihuacán region. The basalt flow west of Otumba is dated to the same period as the T_{2a} series. They also report a date of 7390 for volcanic ash

(sample P39-4) in the Texcoco region, south of the Patlachique range (Peña and Zebrowski 1992: 11). No additional information (laboratory identification and number, specific material analyzed, confidence interval, etc.) is provided, although horizon descriptions are available. The same authors (1992:19) refer to a date of 7950 from humus corresponding to a buried soil in the alluvial plain of Texcoco (2250 m), again with no additional provenience information with respect to the sample or the laboratory result. It has not been possible to trace this information, but the dates obtained from Beta-68347 and Beta-68348 suggest that the T_i series in the eastern sector of the Teotihuacán Valley may be approximately contemporaneous with T_1 south of the Patlachique Range.

Beta-68346	Ap (0–25 cm) A (25–68 cm) C (68–90 cm)	300 ± 60
Beta-68347	2C (90–110 cm)	7200 ± 110
Beta-68348	Tuff (>110 cm)	7900 ± 160

92-10. Located 20 m SE of structure 12-S, 15 m W of Structure 13 (19°41′31.8″N, 98°52′13.8″W), at an elevation of 2288 m (N2W6, Millon et al. 1973:53). The profile is polycyclic, morphologically similar to 92-6. Beta-68352 (Tuff, >69 cm) provided insufficient carbon for dating.

	Ap (0–6 cm)	
Beta-68351	AC (6–34 cm)	920 ± 80
Beta-68330	2A (34–56 cm)	2150 ± 80
Beta-60628	2A (34–56 cm)	2160 ± 90
Beta-68331	2A (34–56 cm)	2760 ± 60 AMS
(CAMS-10441)	$\delta^{13}C = -16.4$	
	2C (56–69 cm)	
	Tuff >69	

2. Sierra de Patlachique

92-11. Located in Baranquilla del Aguila, 800 m S of the railroad (19°39′30.6″N, 98°50′26.4″W), at 2304 m. A polycyclic profile comprised of a poorly developed soil on tuff is represented, overlain by a thin colluvial stratum in which the modern Ah horizon has developed. Beta-68338 from the 4Bt (>66 cm) horizon contained insufficient carbon for conventional dating.

Beta-68336	Ap (0–26 cm)	380 ± 70
Beta-60629	2AB (36–48 cm)	2370 ± 70
Beta-68326	2AB (36–48 cm)	3850 ± 90
Beta-68327	2AB (36–48 cm)	4120 ± 60 AMS
(CAMS-10439)	$\delta^{13}C = -16.0$	
Beta-68337	3Bt (36/48–66 cm)	4790 ± 130
	4Bt (>66 cm)	

94-9. Located close to La Concepción, 800 m S of the railroad (19°39′19.6″N, 98°50′48.9″W), at 2315 m. This polycyclic profile is comprised of 4 soils considerably altered by intensive erosion.

	Ap (0–27 cm) A (27–36 cm)	
Beta-73332	2AB (36–92 cm)	390 ± 60
Beta-73333	2B (92–146 cm)	2410 ± 80
Beta-73334	3AB (146–200 cm)	2850 ± 80
Beta-73335	4B (200–230 cm)	3440 ± 70

3. Cerro Gordo

94-10. Located 50 m N of an access road to a microwave station, 500 m beyond Barranca Honda (19°44′47″N, 98°49′20.3″W), at 2930 m. A Holocene Ah horizon, which developed over older, clay-illuvial Luvisol horizons of Late Pleistocene origin, is evident.

	Ap (0–34 cm)	
Beta-73336	2Ah (34–50 cm)	5250 ± 70
Beta-73337	3Bt (50–90 cm)	18,740 ± 150
Beta-73338	4Bt (90–143 cm)	22,670 ± 290

Zone 2. Alluvial Plain

This zone represents a NE (Otumba)-SW (San Juan Teotihuacán) gradient that includes the Aztec town of Otumba to the NE and the Teotihuacán Archaeological Zone in the central valley, as well as the upper drainage basin of the San Juan River. The soils in this zone are derived from lacustrine and fluvial sediments.

92-9. Located approximately 50 m south of a road, 200 m W of the parish church of San Juan Teotihuacán (19°40′55.2″N, 98°52′21″W), at an elevation of 2267 m (S1W5, Millon et al. 1973:88). The area is characterized by a high water table that was originally fed by springs prior to the proliferation of artesian wells north of the town of San Juan Teotihuacán. It represents an anthropic profile comprised of a single, apparently well-developed soil with an abnormal chronostratigraphic sequence in the upper part. Dates are unreliable with respect to geomorphic processes and soil formation because layers contain redeposited humus resulting from ancient (and historic) land use practices. This area was cultivated since prehispanic times up to approximately 50 yr ago utilizing a technique similar to the *chinampas* of the southeastern Basin of Mexico (but based on drained fields instead of constructed parcels [McClung de Tapia 2000]) in which sediments were continually dredged from adjacent canals and placed on the surface to be planted in order to increase fertility. Furthermore, recent archaeological research in the immediate area W of the parish church in San Juan Teotihuacán indicated buried Aztec structures at a depth of 3.5–4.0 m below the present surface (Cabrera-Castro 2002).

	Ap (0–18 cm)	
Beta-68353	2Ah (18–40 cm)	1970 ± 70
	2AE (40–60 cm)	
Beta-60627	2BC (60–80 cm)	1380 ± 80
	3B (80–103 cm)	
	3BC (103–143 cm)	
Beta-68354	3C (143–150 cm)	2650 ± 70

92-12. Tlajinga 1 is located approximately 200 m NW of the railroad (19°40′3.2″N, 98°51′2.4″W), at an elevation of 2278 m, in the deep soil agricultural area at the southern margin of the ancient city of Teotihuacán (S3E1, Millon et al. 1973:115). This profile shows moderate development overlying a layer of tuff. Beta-68350 from the tuff (>93 cm) contained insufficient carbon for dating.

	A (0–15 cm)	
Beta-68349	AB (15–30 cm)	470 ± 70
	B_1 (30–43 cm)	
Beta-60630	B_2 (43–93cm)	1460 ± 80
	C (>93 cm)	

92-13. Tlajinga 2 represents the remains of a Classic period apartment compound not visible on the surface, located 100 m W of 92-12 (19°40′4.8″N, 98°51′8.4″W), at an elevation of 2279 m (S3E1, Millon et al. 1973:115). The ^{14}C determination was obtained from soil immediately underlying foundations of a Classic period Teotihuacán structure. No laboratory analyses were carried out for the dated horizon.

	Ap (0–38 cm)	
	2C (38–61 cm)	
	61–167 cm (prehispanic structure)	
Beta-68358	3AC (167–221 cm, below prehispanic structure)	2690 ± 70

92-14. Located 350 m E of the road from San Lorenzo Tlalmimilolpa to San Juan Teotihuacán, approximately 1 km S of San Juan Teotihuacán (19°40′25.2″N, 98°52′1.2″W), at 2267 m (S2W4, unsurveyed zone between S2W5 and S2W3, Millon et al. 1973:102–3). The area is an important agricultural zone situated in the deep soil plain. The polycyclic profile is comprised of 3 soils manifesting different degrees of evolution: 0–86 cm (poorly developed), 86–212 cm and 212 to >291 cm (well developed). Beta-68341 (3C >291 cm) contained insufficient carbon for dating. Charcoal from the 2B horizon (86–132 cm) was identified by E McClung de Tapia as a maize stem fragment, confirmed by the $\delta^{13}C$ value (–10.0).

Beta-68339	Ap (0–34 cm)	113.6 ± 0.9% Modern
Beta-68328	2Ah (34–47 cm)	670 ± 70
Beta-68329	2Ah (34–47 cm)	1080 ± 60 AMS
(CAMS-10440)	$\delta^{13}C = -20.0$	
Beta-60631	2Ah (34–47 cm)	2040 ± 80
	2AB (47–86 cm)	
Beta-60633	2B (86–132 cm). Charcoal between 1.10–1.17 m,	490 ± 60 AMS
(CAMS-10415)	$\delta^{13}C = -10.0$	
Beta-60632	2B (86–132 cm)	2290 ± 90
	3Ah(132–154 cm)	
Beta-68340	3Bt1 (154–212 cm)	2130 ± 70
	3Bt2 (212–266 cm)	
	3BtC (266–291 cm)	
	3C (>291 cm)	

94-6. Located 1.5 km W of the road between San Lorenzo Tlalmimilolpa and San Juan Teotihuacán, 500 m S of Río San Lorenzo (19°40′8.5″N, 98°52′49.8″W), at 2260 m (W of S4W5 outside of survey zone, Millon et al. 1973:122). This highly stratified profile is comprised of 4 poorly developed soils of alluvial origin. Depths vary from 120 cm (surface) to 46, 24, and 30 cm. The depths of the three earliest suggest short periods of landscape stability.

	Ap (0–8 cm)	
Beta-73322	Ap/AC (8–32/54 cm)	107.8 ± 0.9% Modern
Beta-73323	C_1 (32/54–62 cm)	2990 ± 90
Beta-73324	C_2 (62–90cm)	3300 ± 120
Beta-73325	C_3 (90–120 cm)	3280 ± 110
Beta-73326	2C (120–166 cm)	3760 ± 110
Beta-73327	3C (166–190 cm)	3640 ± 80
Beta-73328	$4C_1$ (190–220 cm)	4070 ± 160

94-1. Located 100 m N of Capultitlan, 1.5 km N of the road leading from the federal highway to Oxtoticpac (19°40′42″N, 98°49′04″W), at 2298 m. This polycyclic profile is comprised of 3 poorly developed soils of alluvial origin. The dynamics of formation are similar to profile 94-6. The $3C_3$ horizon may be approximately contemporaneous with the T_{2a} series in the western piedmont of the Sierra Nevada (Hidalgo 1996:46; Peña and Zebrowski 1992:14).

Beta-73304	Ap (0–21 cm)	570 ± 70
Beta-73305	2AC (21–55 cm)	3640 ± 70
Beta-73306	$3C_1$ (55–66 cm)	4680 ± 210
	$3C_2$ (66–86 cm)	
Beta-73307	$3C_3$ (86–114 cm),	11,670 ± 60 AMS
(CAMS-14618)	$\delta^{13}C = -18.4$	

94-3. Located in Santa María Coatlan, 500 m N of a road from the highway to Deportivo Teotihuacán (19°41′32.7″N, 98°48′59″W), at 2298 m. This polycyclic profile is similar to profile 94-1, although stratification is more apparent, in addition to evidence for hydric erosion.

	Ap (0–29 cm)	
Beta-73312	AC (29–63/73 cm)	1070 ± 70
	$2C_1$ (63–73)	
	$2C_2$ (>73 cm)	

94-7. Located in San Sebastian Xolalpan, 250 m E of the main water tank, at the exit to the federal highway to Tulancingo (19°40′42.2″N, 98°50′15.1″W), at 2284 m (S2E1, Millon et al. 1973:106). The profile consists of a partially eroded alluvial soil overlying a highly contrasting flat layer of sand.

	Ap (0–20 cm)	
Beta-73329	Ap/AC (20–40 cm)	1220 ± 70
	2C (40–75cm)	

94-8. Located S of San Sebastián Xolalpan, 50 m N of the federal highway (19°40′22″N, 98°50′50″W), at 2278 m (S2E1, Millon et al. 1973:106). This polycyclic profile is comprised of 2 soils: the surface is of alluvial origin, poorly developed, with a depth of 37 cm, while the underlying soil shows moderate development.

	Ap (0–25 cm)	
	AC (25–37 cm)	
Beta-73330	C (37–56 cm)	1200 ± 80
Beta-73331	2A (56–100 cm)	1590 ± 70
	2Bw (100–170 cm)	
	2C (>170 cm)	

99-5. Tlajinga 3 is located 500 m S of Río San Lorenzo (19°39′57″N, 98°50′41″W), at 2288 m (S3W1, Millon et al. 1973:114). This polycyclic profile is comprised of 2 moderately developed soils of alluvial origin: the first to a depth of 133 cm, the second to approximately 260 cm. It is situated adjacent to prehispanic agricultural fields with evidence for floodwater irrigation (Nichols 1988; Nichols et al. 1991; Nichols and Frederick 1993). Ceramics associated with the $2A_{11}$ horizon indicate Classic Teotihuacán period occupation (predominantly Tlamimilolpa-phase ceramics, Pérez 2003). No ceramics were recovered from the underlying $2A_{12}$ horizon.

A (0–35 cm)
B_1 (35–95 cm)

Beta-142228	B_2 (95–120 cm) $\delta^{13}C = -16.2$	2890 ± 50
Beta-142229	C (120–133 cm) $\delta^{13}C = -16.6$	3370 ± 60
Beta-142230	$2A_{11}$ horizon (133–158 cm) $\delta^{13}C = -15.7$	2990 ± 80
Beta-142231	$2A_{12}$ horizon (158–171 cm) $\delta^{13}C = -15.8$ 2B (171–240 cm) 2C (240–260 cm)	3110 ± 80

94-2. Located 1.5 km NE of Tlacatecpan (19°40′40.3″N, 98°47′48.6″W), at an elevation of 2318 m. This is a stratified polycyclic profile comprised of 2 weakly developed alluvial soils. Depths indicate short, temporally distant cycles of landscape stability. Beta-73311 compares with Beta-68347 and Beta-68348; see comments on Profile 92-7.

	Ap (0–13 cm)	
Beta-73308	A_1 (13–26 cm)	100.1 ± 0.8% Modern
Beta-73309	A_2 (26–43 cm)	700 ± 60
Beta-73310	C (43–50 cm)	1430 ± 70
Beta-73311 (CAMS-14619)	2C horizon (>50 cm), $\delta^{13}C = -16.5$	7770 ± 60 AMS

94-4. Located 200 m NW of a railroad, approximately 500 m S of the barranca Puente el Muerto (19°41′39.6″N, 98°48′28.2″W), at 2303 m. The profile represents 4 short cycles of soil development, indicated by mineralogical and textural discontinuities.

Beta-73313	Ap (0–30 cm)	490 ± 80
Beta-73314	2AC (30–55 cm)	2650 ± 60
	3C (55–64 cm)	
	4C (>64 cm)	

94-5. Located 50 m N of the barranca Puente el Muerto, 400 m S of Barranca del Estete, 1 km SW of San Pablo Ixquitlan (19°42′15.5″N, 98°48′04.3″W), at 2306 m. This polycyclic profile is comprised of 2 moderately developed soils below the surface horizon, the depths of which suggest formation during cycles of relative landscape stability.

	Ap (0–20)	
Beta-73315	$2Ah_1$ (20–38 cm)	840 ± 80
Beta-73316	$2'Ah_2$ (38–69cm)	3290 ± 80
Beta-73317	2B (69–83 cm)	2030 ± 60
Beta-73318	$3B_1$ (83–118 cm)	1540 ± 70
Beta-73319	$3B_2$ (118–155 cm)	2850 ± 70
Beta-73320	3BC (155–189 cm)	3420 ± 80
Beta-73321	3C horizon (189–240 cm)	3210 ± 60
	4C Tuff (>240 cm)	

99-4. Located 100 m NE of Barranca del Muerto, W of the road between Otumba and San Francisco Tlatica (19°41′33″N, 98°45′46″W), at 2318 m. This polycyclic profile is comprised of 2 soils of alluvial origin with evidence of stratification. The upper soil with a depth of 86 cm is poorly developed and contrasts markedly with the underlying fine-textured soil that shows slightly greater development, characterized by the presence of organic-mineral horizons. The profile was situated adjacent

to archaeological excavations undertaken by Charlton (1979, 1991) in remnants of presumed floodwater irrigation canals and fields. Based on analyses by Pérez (2003:106–7), ceramics associated with the C_1 and C_2 horizons pertain to the Aztec occupation; ceramics associated with the 2 A_{11} horizon correspond to the Mazapa phase (Toltec). No ceramics were recovered from underlying layers. This profile reflects a period of considerable instability following the abandonment of Teotihuacán (also reported in the Texcoco region, south of the Sierra de Patlachique, by Cordoba [1997]).

	Ap (0–55 cm)		
Beta-142221	C_1 horizon, N wall (55–75 cm)	$\delta^{13}C = -17.0$	2980 ± 60
Beta-142225	C_1 horizon, W wall (68–76 cm)	$\delta^{13}C = -18.3$	3340 ± 70
Beta-142222	C_2 horizon, N wall (75–86 cm)	$\delta^{13}C = -18.3$	3540 ± 60
Beta-142223	2 A_{11} horizon, N wall (86–110 cm)	$\delta^{13}C = -17.9$	2890 ± 60
Beta-142227	2 A_{11} horizon, W wall (90–100 cm)	$\delta^{13}C = -19.0$	3350 ± 60
Beta-142224	2 A_{12} horizon, N wall (110–137 cm)	$\delta^{13}C = -19.3$	3080 ± 70
	$2AC_1$ (137–167 cm)		
	$2AC_2$ (167–196 cm)		
	2C (196–222 cm)		

DISCUSSION

The interpretation of ^{14}C dates based on organic materials from soils and paleosols is difficult because these materials reflect an "open system" characterized by intensive exchange of carbon with the atmosphere and biota in the course of soil formation together with possible inputs and losses of organic matter after burial. However, the collection of ^{14}C dates from paleosols in the Teotihuacán Valley can be interpreted to elucidate the major periods of landscape stability (development of continuous soil cover) versus periods of intensification of geomorphologic processes (soil erosion on the slopes and sediment accumulation in the valley bottom) which occurred within the last ~10,000 yr.

Intensive turnover of the organic matter in the soils (SOM) implies the interpretation of its ^{14}C age as mean residence time (MRT) of C in the soil system (Campbell et al. 1967; Geyh et al. 1971). In general, MRT is rather short in most soils, especially in those formed under temperate and tropical climatic conditions with high rates of biological activity and decomposition (Beckmann and Hubble 1974; Herrera and Tamers 1971; Trumbore 2000). In the Teotihuacán Valley, short MRT is evidenced by relatively recent ^{14}C ages in the majority of contemporary surface A horizons (0–30 cm), in the range of 100–300 yr (profiles 92-6 and 92-7 from the upland zone; profiles 92-14, 94-6, 94-2 from the alluvial plain). This implies that in buried paleosols the ^{14}C age of humus gives the "minimum age" of pedogenesis, corresponding to the final stages of soil formation, close to the time of the burial event (Matthews 1985). This mode of interpretation is mostly valid for the studied paleosols, being more reliable for mature upland buried Luvisols and Cambisols (which probably have reached the steady state of organic matter, as defined by Wang et al. [1996]) and somewhat limited for the buried underdeveloped Fluvisols of the alluvial plain, which are not likely to reach a steady state.

Furthermore, the paleosols of each geomorphologic zone reflect specific processes of pedogenesis and diagenesis, which also complicates the interpretation of the ^{14}C dates. In most of the profiles of the upland zone, the buried paleosols are very shallow: nearly all dated horizons are located within 2 m of the present-day land surface, and in some profiles the depth is less than 1 m. In many cases, paleosols are not separated from the modern soil profile by a true C horizon (without signs of modern pedogenesis); thus, they constitute pedocomplexes. In such an environment, rejuvenation of ^{14}C by means of contamination from younger organic carbon from the contemporary soil system is pos-

sible through input from the biomass of roots and microorganisms and vertical migration of organic components due to bioturbation and infiltration.

This dilution by recent organic components can be further incremented by partial uncompensated decomposition of the paleosol humus after burial. This diagenetic loss of humus is likely to cause only a minor change of ^{14}C age *per se* (Matthews 1985). However, it could influence the measurement indirectly in the case of contamination, by increasing the ratio of contaminants with respect to the original organic components of the paleosol.

In case studies of the rejuvenation of organic material in close-to-surface paleosol Ah horizons of Holocene age, the shift of the ^{14}C age was reported to be about 2000 to 3000 yr (Alexandrovskiy and Chichagova 1998; Scharpenseel 1971). A similar shift may apply to the paleosols under consideration, and archaeological evidence in the Teotihuacán Valley partially supports this hypothesis.

Uplands

Assuming that the ^{14}C date represents the minimal age of paleosol formation, close to the moment of soil burial, together with the high probability of rejuvenation, we interpret the ^{14}C age of the upland paleosols as indicative of a time prior to the soil burial, at least for the upper paleosol horizons. In all profiles, with the exception of 92-6, it exceeds 2000 BP. In the profiles 92-1, 92-2, 92-7, 92-11, 94-9 (lower paleosol B-horizon), and 94-10 (upper paleosol Ah horizon), it lies in the range 3000–8000 BP, and in paleosol B horizons of 94-10 it exceeds 10,000 yr.

We argue that the paleosols of the upland zone are the remains of what was formerly a continuous soil cover, locally preserved under tuffs and destroyed elsewhere by erosion. The formation of this soil cover occurred within an extensive period of landscape and vegetation stability which, according to the ^{14}C dates obtained, took place in the Early-Middle Holocene (well before ~3000 BP) and probably extended back to the Late Pleistocene. With respect to the latter assumption, it should be mentioned that well-developed paleosols of Late Pleistocene age, including those formed during the Last Glacial Maximum, are reported from various locations in the central Mexican highlands (Solleiro-Rebolledo et al. 1999; Sedov et al. 2001).

Alluvial Plain

The buried paleosols in the alluvial plain are rather shallow (within 2 m from modern land surface in the majority of profiles), suggesting their susceptibility to contamination by carbon from the modern surface soil. In addition, the paleosols in this zone were formed from fluvial sediments consisting largely of redeposited soil material from different parts of the valley. Thus, they probably contain older allochthonous organic material mixed with in situ humus formed in the course of pedogenesis, and the inherited organic components from the fluvial parent material could make up a considerable part, especially in the B and C horizons.

Rather than corresponding to the minimum soil age/burial event, the ^{14}C dates of the paleosols in the alluvial plain suggest that they are older and closer to (but still younger than) the erosion/sedimentation phase during which the parent material was formed. This inheritance hypothesis enables us to explain various inversions (older ^{14}C ages in the upper horizons) found in many profiles of the alluvial plain and rarely observed in the profiles of the upland zone. This phenomenon seems to depend upon the relation between allochthonous redeposited and in situ pedogenic humus in different parts of the profile and takes place when the upper horizon contains a higher proportion of the allochthonous humus component.

Most of the alluvial paleosol sequences in the Teotihuacán Valley fall between 4000–1000 BP. We interpret these dates as indicative of the period of intensive soil erosion in the upper parts of the valley and pedosediment deposition in its bottom, which occurred during the Late Holocene (probably after 5000 BP). In the very bottom of some alluvial sequences, ^{14}C determinations were considerably older than 5000 ^{14}C BP. These older ages may be indicative of a phase of pedogenesis prior to the period of intensive geomorphologic processes. Judging from their ^{14}C ages, these horizons seem to correspond to the same period of pedogenesis as the paleosols of the upland zone. If this interpretation is correct, then these horizons can be correlated stratigraphically with the upland paleosols and represent the same paleosol cover.

Thus, the interpretation of the ^{14}C data set from the paleosols of the slopes and terraces of the upland zone (representing an Early-Middle Holocene period of landscape stability and continuous pedogenesis) and that of alluvial plain (associated with a Late Holocene period of active erosion/sedimentation) are concordant and complementary.

The proposed correlation among soil profiles is shown in Figure 2. The oldest stages of soil formation found in the uplands (94-10, 92-1, thought to be older than 5000 BP) have no analogs in the alluvial plain. Another stage, probably between 4000 and 2000 BP, is recognized in the soils of the alluvial plain and the slopes of Sierra Patlachique. The youngest episode (>500 BP) corresponds to recent historical and present-day processes.

Archaeological Evidence from Soil Profiles

Although little archaeological data is available which specifically indicates the timing of the processes described here, some elements inadvertently contribute to the development of hypotheses that will benefit from future research. Several horizons provided associated ceramics or remains of structures that were clearly identifiable as corresponding to the Classic period occupation of the urban center of Teotihuacán (about AD 100–650). Ceramic evidence from a single dated horizon in profile 99-4 was clearly related to the Mazapan phase (Toltec occupation, about AD 900–1200). Predominantly Aztec ceramics (about AD 1350–1520) were evident in profile 99-4 in horizons overlying those with ^{14}C determinations. These ceramic materials were likely redeposited during an episode of erosion and do not appear to represent in situ activities. In profile 92-14, a carbonized maize fragment dated to the Aztec period was recovered from sediment that was independently dated. These contexts and the associated ^{14}C determinations are indicated in Table 1. In general, considerable divergence is evident between the sediment dates and the chronological time when human groups occupied the area.

As yet, we do not have sufficient data to permit a systematic comparison between soil ^{14}C dates and independently dated associated archaeological materials (cf. Alexandrovskiy and Chichagova 1998). However, based on rough estimates, we observe that the ^{14}C determinations of sediments in the alluvial plain tend to fall within a range of approximately 2200–2500 cal yr older than the associated archaeological materials. Sediments directly beneath archaeological structures or burials are even more variable: ~1300 yr in the case of 92-13 in the alluvial plain, ~2500 yr in 92-2 and ~4500 yr in 92-1 in the upland zone.

CONCLUSION

The study region has witnessed 3 millennia of intense human activity, beginning in the prehispanic period with its settlement by full-time agriculturalists (~1150 BC, Sanders et al. 1979:201), the expansion of agricultural intensification during the period of the Teotihuacán state's dominance (about AD 100–650), and at the height of the Aztec period through the early Colonial occupation (about AD 1400–1550).

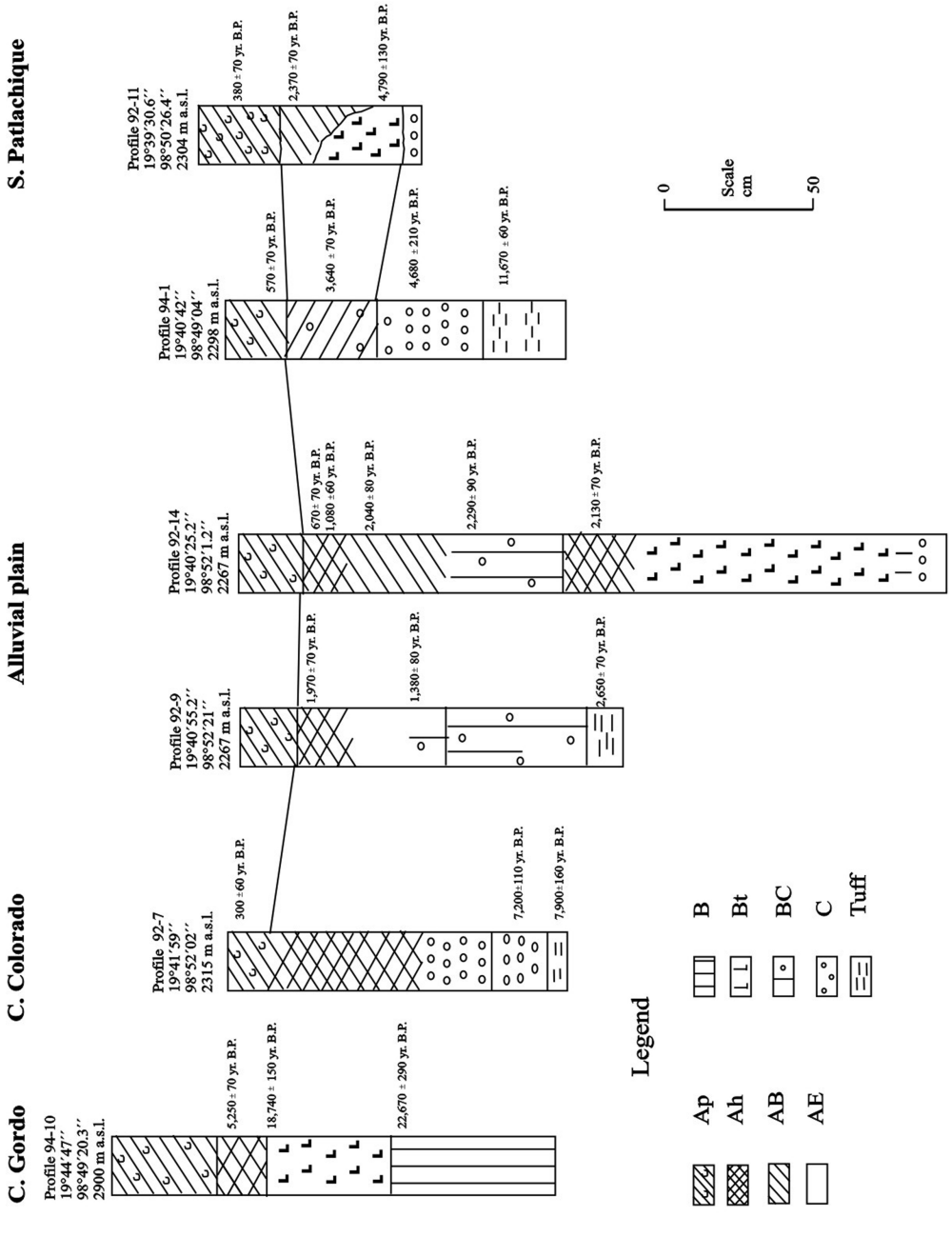

Figure 2 Correlations among horizons from representative profiles in the uplands and alluvial plain of the Teotihuacán Valley, Mexico.

Based on Heine's (1987, 2003) and Cordova's (1997) investigations in the adjacent regions of Puebla-Tlaxcala and Texcoco, respectively, a general model for the Teotihuacán region can be posited as a guide for future research in the area. For example, erosion significantly affects the landscape when population growth and related agricultural activities intensify. Both of these regions were depopulated during the period between AD 100–700 (which parallels increased population in Teotihuacán, cf. Parsons 1968; García Cook 1981), during which time erosion/sedimentation is minimal. After the fall of Teotihuacán, between AD 700 until the Colonial period (about AD 1550), population growth resumes in both Puebla and Tlaxcala, with a corresponding intensification of erosion-sedimentation.

Considering the importance of the prehispanic urban center and its attraction as a pole of population concentration, particularly during the Classic period, we would expect evidence for landscape instability in the Teotihuacán Valley to be associated with periods of increased population as a result of migration to the city, at the same time when adjacent regions are depopulated and relatively stable as their landscapes gradually recover.

Finally, based on the density of human occupation together with intensive agricultural production, we propose the following sequence for the Teotihuacán region:

1. 5000–2000 BP (about 3500–100 BC; relative stability with short, intermittent episodes of erosion; no significant human activity until ~1150 BC);
2. 2000–1500 BP (about 100 BC–AD 650; erosion-sedimentation, deforestation, and intensive agriculture);
3. 1500–1000 BP (about AD 650–1100; relative stability, depopulation, and partial recovery of the landscape followed by gradual resettlement towards the end of the period);
4. 1000–500 BP (about AD 1100–1550; erosion-sedimentation, deforestation, and intensive agriculture).

Ongoing research in the Teotihuacán region is oriented towards the development of a meaningful chronological sequence within which evidence for vegetation change and climatic conditions can be situated in order to better understand how prehispanic inhabitants used, modified, and degraded the landscape.

ACKNOWLEDGMENTS

This research was carried out with support from the Consejo Nacional de Ciencia y Tecnología (CONACYT), Mexico, through grants H9106-0060 and 5412-S9411 to Linda Manzanilla and 25074H to Emily McClung de Tapia, and the Dirección General de Asuntos del Personal Académico of the Universidad Nacional Autónoma de México (PAPIIT/DGAPA-UNAM) through grants IN405997 and IN400403 to Emily McClung de Tapia. Additional logistical support for fieldwork was provided by the Instituto de Investigaciones Antropológicas (UNAM), Instituto de Geografía (UNAM), Instituto de Geología (UNAM), and the Departamento del Hombre y su Ambiente, Universidad Autónoma Metropolitana-Xochimilco. We would like to thank J Cervantes, M Meza, G Alfaro, J Zurita, E Ibarra, J L Villalpando, J García, D Martínez, C Adriano, and J Pérez for their assistance in the field at different stages of the research. We also thank Konstantin Pustovoitov for reviewing the draft. The final version of Figure 1 was prepared by Cesar Fernández Amaro.

REFERENCES

Alexandrovskiy AL, Chichagova OA. 1998. The ^{14}C age of humic substances in paleosols. *Radiocarbon* 40(2): 991–7.

Barba LA. 1995. El impacto humano en la paleogeografía de Teotihuacán [PhD dissertation]. Mexico: Facultad de Filosofía y Letras, Universidad Nacional Autonoma de México.

Beckmann GG, Hubble GD. 1974. The significance of radiocarbon measurements of humus from Krasnozems (Ferralsols) in subtropical Australia. *Transactions of the 10th International Congress on Soil Science* 6: 362–71.

Caballero M, Lozano S, Ortega B, Urrutia J, Macías JL. 1999. Environmental characteristics of Lake Tecocomulco, northern Basin of Mexico, for the last 50,000 years. *Journal of Paleolimnology* 22:399–411.

Campbell CA, Paul EA, Rennie DA, McCallum KJ. 1967. Factors affecting the accuracy of the carbon dating method of analysis to soil humus studies. *Soil Science* 104:81–4.

Cabrera-Castro R. 2002. Nuevas evidencias arqueológicas del manejo de agua en Teotihuacán. El campo y la ciudad. Paper presented at the III Mesa Redonda de Teotihuacán, Centro de Estudios Teotihuacános, Zona Arqueológica de Teotihuacán, Mexico.

Charlton TH. 1979. Investigaciones arqueológicas en el municipio de Otumba, temporada de 1978, 5ª parte: el riego y el intercambio: la expansión de Tula [unpublished report submitted to the Consejo de Arqueología]. Iowa City: University of Iowa.

Charlton TH. 1990. Operation 12, Field 20, irrigation system excavations. Preliminary report on recent research in the Otumba City State. In: Charlton TH, Nichols DL, editors. *Mesoamerican Research Report 3*. Iowa City: University of Iowa. p 210–2.

Cid JR. 1998. Diacronía y sincronía en el sector oeste de la antigua ciudad de Teotihuacán. In: Brambila R, Cabrera R, coordinators. *Los Ritmos de Cambio en Teotihuacán: Reflexiones y Discusiones de su Cronología*. Mexico: Instituto Nacional de Antropología e Historia. p 317–22.

Cordova C. 1997. Landscape transformation in Aztec and Spanish colonial Texcoco, Mexico [PhD dissertation]. Austin: University of Texas at Austin.

García Cook A. 1981. The historical importance of Tlaxcala in the cultural development of the central highlands. In: Sabloff JA, editor. *Supplement to the Handbook of Middle American Indians, V. I. Archaeology.* Austin: University of Texas Press. p 244–76.

Geyh MA, Benzler JH, Roeschman G. 1971. Problems of dating Pleistocene and Holocene soils by radiometric methods. In: Yaalon DH, editor. *Paleopedology: Origin, Nature and Dating of Paleosols*. Jerusalem: International Society of Soil Science and Israel Universities Press. p 63–75.

Heine K. 1987. Anthropogenic sedimentological changes during the Holocene in Mexico and Central America. *Striae* 26:51–63.

Heine K. 2003. Paleopedological evidence of human-induced environmental change in the Puebla-Talxcala area (Mexico) during the last 3500 years. *Revista Mexicana de Ciencias Geológicas* 20(3):235–44.

Herrera R, Tamers MA. 1971. Radiocarbon dating of tropical soil associations in Venezuela. In: Yaalon DH, editor. *Paleopedology: Origin, Nature and Dating of Paleosols*. Jerusalem: International Society of Soil Science and Israel Universities Press. p 109–15.

Hidalgo C. 1996. Étude d'horizons indurés à comportement de fragipan, appelés tepetates, dans les sols volcaniques de la vallée de México. Contribución à la connaissance de leurs caractères et de leur formation [PhD dissertation]. Paris: Université Henri Poincaré, Nancy I, Thèses et documents microfichés nr 146. Orstom éditions.

INEGI. 1983. Texcoco, E14B21 (Topografía), 1:50,000 [map]. Mexico: Instituto Nacional de Estadística, Geografia e Informática.

Kovar A. 1970. The physical and biological environment of the Basin of México. The natural environment, contemporary occupations and 16th-century population of the valley. In: Sanders W, Kovar A, Charlton T, Diehl R. The Teotihuacán Valley Project. V. I. *Occasional Papers in Anthropology nr 10.* University Park: Pennsylvania State University. p 13–67.

Lozano-García MS, Ortega-Guerrero B. 1998. Late Quaternary environmental changes of the central part of the Basin of México; correlation between Texcoco and Chalco basins. *Review of Palaeobotany and Palynology* 99:77–93.

Lozano-García MS, Ortega-Guerrero B, Caballero-Miranda M, Urrutia-Fucugauchi J. 1993. Late Pleistocene and Holocene paleoenvironments of Chalco Lake, central México. *Quaternary Research* 40:332–42.

Matthews J. 1985. Radiocarbon dating of surface and buried soils: principles, problems and prospects. In: Richards K, Arlett R, Ellis S, editors. *Geomorphology and Soils*. London: Allen and Unwin. p 271–88.

McClung de Tapia E. 2000. Prehispanic agricultural systems in the Basin of Mexico. In: Lentz D, editor. *Imperfect Balance. Landscape Transformations in the Pre-Columbian Americas*. New York: Columbia University Press. p 121–46.

McClung de Tapia E, Solleiro-Rebolledo E, Gama-Castro J, Villalpando JL, Sedov S. 2003. Paleosols in the Teotihuacán Valley, Mexico: evidence for paleoenvironment and human impact. *Revista Mexicana de Ciencias Geológicas* 20(3):270–82.

Miehlich G. 1991. Chronosequences of volcanic ash soils. *Hamburger Bodenkündliche Arbeiten* 15. Hamburg.

Millon R, Drewitt B, Cowgill G. 1973. *Urbanization at*

Teotihuacán V. I. The Teotihuacán Map. Part 2. Austin: University of Texas Press.

Mooser F. 1968. Geología, naturaleza y desarrollo del Valle de Teotihuacán. In: Lorenzo JL, editor. *Materiales par el Estudio de Teotihuacán*. Mexico: Instituto Nacional de Antropología e Historia. p 31–38.

Nichols DL. 1988. Infrared aerial photography and prehispanic irrigation at Teotihuacán: the Tlajinga canals. *Journal of Field Archaeology* 15:17–27.

Nichols DL, Frederick C. 1993. Irrigation canals and *chinampas*. Recent research in the northern Basin of Mexico. *Research in Economic Anthropology* (Supplement) 7:123–50.

Nichols DL, Spence M, Borland M. 1991. Watering the fields of Teotihuacán. Early irrigation at the ancient city. *Ancient Mesoamerica* 2:119–29.

Parsons JR. 1968. Teotihuacán, Mexico, and its impact on regional demography. *Science* 162:872–7.

Peña D, Zebrowski C. 1992. *Estudio de los suelos volcánicos endurecidos (tepetates) de las cuencas de México y Tlaxcala (México). Informe del mapa morfopedológico de la vertiente occidental de la Sierra Nevada*. ORSTOM-Paris/Justus Liebig Universität-Giessen/Colegio de Postgraduados-Montecillo/Universidad Autónoma de Tlaxcala. Comisión des Communautés Européenes. Contrat CCE/ORSTOM nr T52-0212.

Pérez J. 2003. La agricultura en Teotihuacán. Una forma de modificación al paisaje [Master's thesis]. Mexico: Facultad de Filosofía y Letras, Universidad Nacional Autónoma de México.

Quantin P. 1992. Etude des sol volcaniques indurés (tepetates) des bassins de México et Tlaxcala (Mexique). Rapport scientifique final. Commission des Communautés Européenes, Contrat CEE/ORSTOM no. TS2-0212.

Sanders W, Parsons J, Santley R. 1979. *The Basin of Mexico: Ecological Processes in the Evolution of a Civilization*. New York: Academic Press.

Scharpenseel HW. 1971. Radiocarbon dating of soils: problems, troubles, hopes. In: Yaalon DH, editor. *Paleopedology: Origin, Nature and Dating of Paleosols*. Jerusalem: International Society of Soil Science and Israel Universities Press. p 77–88.

Sedov S, Solleiro-Rebolledo E, Gama-Castro JE, Vallejo-Gómez E, González-Velázquez A. 2001. Buried palaeosols of the Nevado de Toluca: an alternative record of Late Quaternary environmental change in central Mexico. *Journal of Quaternary Science* 16(4): 375–89.

Solleiro-Rebolledo E, Gama-Castro E, Palacios-Mayorga S, Shoba SA, Sedov SN. 1999. Late Pleistocene paleosols of central Mexico: genesis and paleoenvironmental interpretation. *Eurasian Soil Science* 32(10):1077–84.

Stuiver M, Reimer PJ. 1993. Extended ^{14}C database and revised CALIB 3.0 ^{14}C age calibration program. In: Stuiver M, Long A, Kra RS, editors. Calibration 1993. *Radiocarbon* 35(1):215–30.

Trumbore S. 2000. Age of soil organic matter and soil respiration: radiocarbon constraints on belowground C dynamics. *Ecological Applications* 10(2):399–411.

Wang Y, Amundson R, Trumbore S. 1996. Radiocarbon dating of soil organic matter. *Quaternary Research* 45: 282–8.

RADIOCARBON, Vol 47, Nr 1, 2005, p 177–178

IMPROVED TUBE CRACKER FOR OPENING VACUUM-SEALED GLASS TUBES

Glenn A Norton

Center for Sustainable Environmental Technologies, Iowa State University, 276 Metals Development Building, Ames, Iowa 50011, USA. Email: norton@ameslab.gov.

ABSTRACT. A variety of analytical procedures involve breaking open a glass or quartz vessel containing a gaseous sample, and then quantitatively collecting the sample gases for analysis. In order to do this, a variety of "tube crackers" have been used. This paper discusses an alternate tube cracker that offers numerous advantages over those that have been discussed previously in the literature.

PREVIOUS TECHNIQUES

In one previous approach, a tube cracker is used to break pieces of standard quartz or glass tubing which has been sealed on both ends and contains the sample gases of interest (DesMarais and Hayes 1976). This was offered as a preferred alternative to conventional glass breakseals. The tube cracker uses standard Cajon Ultra Torr™ fittings, along with commercially available corrugated, flexible stainless steel tubing. In that approach, the sample tube is scored, inserted into the tube cracker, and then broken (where the tube was scored) by bending the corrugated steel tubing. It is necessary to fabricate 2 steel cones that serve as liners, which are inserted into the Ultra Torr fittings. The scoring on the tube needs to be situated so it is in between the tips of the 2 steel cones, which ensures that the break occurs in the intended location. We have successfully used this type of tube cracker in our laboratories; however, a number of disadvantages to that approach were noted. For example, difficulties were encountered in positioning the sample tube at the precise location needed for a clean break. This was largely due to the fact that it was impossible to view the tube inside the tube cracker, since it was positioned inside the corrugated steel tubing. The matter is made even worse by the fact that the length of the corrugated tubing can change after bending it a number of times. It can always be collapsed back to its original length, but maintaining a constant length is very difficult due to the corrugated nature of the tubing. Because the length of the corrugated tubing is not constant, this complicates correct positioning of the sample tube in the tube cracker. We view the "blind" cracking of the sample tube as being a major disadvantage of this approach. Other researchers have also reported that the correct positioning of the tubing inside the cracker is difficult because the tubing cannot be seen (Kennedy and Kennedy 1994). In that work, the authors also note that the large surface area of the corrugated tubing can extend the retention time of the gases inside the tube cracker. In addition, glass shards can be trapped between the corrugations in the flexible tubing, which can eventually lead to leaks in the tubing.

In an alternate tube-cracking approach, a sealed sample tube (which tapers to a point on one end) is placed inside a Pyrex™ tube that is closed at the bottom (Kennedy and Kennedy 1994). The Pyrex tube has the barrel of a stopcock sealed into the side wall (located on the upper third of the tube). The sample tube is broken by closing the tap onto the tapered end of the sealed sample tube. A possible drawback to this method is that the fine, tapered tips on the sample tubes are extremely fragile. This increases the chances of accidental breakage and loss of the sample. This is of particular concern in applications where a sample is sealed within a quartz vessel and then combusted at high temperatures, which can result in considerable pressures inside the sample vessel.

Other researchers have also reported the use of a stopcock-type design for breaking sample tubes housed in a glass holder. In one paper, the barrel of a greaseless stopcock was mounted into the wall of the tubing on a standard ball joint, which was closed on the end opposite of the ball joint (Caldwell et al. 1983). Sample tubes are broken by turning the threaded cap on the stopcock and driving the piston in the stopcock against the sample tube.

In yet another study, a greased ball joint was used to break glass tubes (Coleman 1981). The socket end of the ball joint had an adapter on the opposite end to accept glass tubes of the desired diameter. The scored glass tube to be broken is then slid into the adapter and through the ball and socket junction of the greased ball joint. The tube is subsequently broken by slightly flexing the adapter (which has the socket portion of the ball joint) that connects to the ball portion of the joint.

THE IMPROVED TECHNIQUE

In our work, we routinely use a tube cracker similar to that reported by DesMarais and Hayes (DesMarais and Hayes 1976). However, a number of modifications were made to greatly improve performance and ease of use. In our design, the corrugated steel tubing is replaced by a 6″ length of smooth 3/8″ OD × 5/16″ ID (9.6 mm × 8.0 mm) PFA tubing having a 1/32″ (0.8 mm) wall. The 6″ length provides more than adequate tubing flexibility for the break to be easily made. One end of the PFA tubing is connected to a manifold by using a standard Swagelok™ fitting. The other end of the tubing is fitted with a Cajun Ultra Torr 3/8″ × 1/4″ reducing union that has been bored through to enable 1/4″ glass tubing to slide all the way through the fitting. Quartz sample bulbs that have 1/4″ OD stems at the top are used whereby the 1/4″ OD quartz tubing is scored and inserted into the Ultra Torr fitting at the bottom of the tube breaker until the scoring on the tube is in the center 2″ of the PFA tubing. Depending on the application, the diameter of the quartz or glass tubing can be increased after making appropriate modifications to the tube cracker (provided that suitable fittings are available for that size of tubing). Because there is a lot of leeway on how far the 1/4″ glass tubing slides into the PFA tubing, the operator has a great deal of flexibility regarding the length of the tube to be broken and where the break occurs along the length of that tube.

While using this simplified tube cracker in our laboratories, it has performed easily and flawlessly. In addition, it has exhibited superior performance relative to the tube cracker that employs the flexible corrugated steel tubing. Unlike the latter approach, our method uses only commercially available components (i.e. no steel cones need to be manufactured). Since the tubing is translucent, the operator can see everything in the tube cracker, including the exact location and orientation of the scoring. This facilitates making clean breaks and is one of the major advantages of our approach. In addition, because the operator can see everything in the tube breaker, the insertion depth of the glass tube into the tube breaker does not have to be precisely measured and controlled (as it does with the corrugated steel tubing) in order to get a clean break. Unlike some of the other tube crackers, our design does not contain any fragile (e.g. glass housings) or greased components. Because the tubing is smooth rather than corrugated, it is easy to clean (although it is probably best to simply replace the tubing since a new piece costs less than $2), and there are no "pockets" where shards of glass can accumulate. For most applications, this type of tube breaker should be considered as an alternative to other types of tube crackers discussed in the literature.

ACKNOWLEDGMENTS

This work was supported by the US Department of Agriculture's Office of Energy Policy and New Uses through a cooperative agreement with Iowa State University.

REFERENCES

Caldwell WE, Odom JD, Williams DF. 1983. Glass-sample-tube breaker. *Analytical Chemistry* 55:1175–6.

Coleman DD. 1981. Tube cracker for opening samples sealed in glass tubing. *Analytical Chemistry* 53:1963–5.

DesMarais DJ, Hayes JM. 1976. Tube cracker for opening glass-sealed ampoules under vacuum. *Analytical Chemistry* 48(11):1651–2.

Kennedy H, Kennedy DP. 1994. Simplified tube cracker for opening samples sealed in glass tubes while under vacuum. *Analytical Proceedings Including Analytical Communications* 31:299–300.

RADIOCARBON UPDATES

Software Updates

With the recent publication of the IntCal04 special issue (Vol 46, nr 3, 2004), the new CaliBomb software and new versions of the calibration software Calib, BCal, OxCal, and WinCal25, are now available via links on the *Radiocarbon* Web site, http://www.radiocarbon.org/Info/index.html#programs.

Upcoming Conferences

AMS 10th Annual Conference Circular

The 10th International Conference on Accelerator Mass Spectrometry (AMS-10) is being hosted by the Lawrence Livermore National Laboratory's Center for Accelerator Mass Spectrometry. The conference will take place from September 5th through 10th on the campus of the University of California at Berkeley. The purpose of the conference is to provide a forum for scientists to present and discuss recent developments in AMS technology and applications. The first circular is available on our Web site, http://www.radiocarbon.org/Announcements/AMS-10.pdf.

A special session on the "Reservoir Ages of the World Ocean: Progress and Prospect" has been proposed to coincide with the AMS-10 Conference in Berkeley. The proposed session would include presentations of the recent advances in the study of reservoir age corrections worldwide, both from pre-bomb known-age samples and reconstructions of past reservoir ages from a variety of methods (paired marine/terrestrial samples from middens or sediment cores, tree-ring vs. varve comparisons, U/Th-dated corals, sclerochronologically-dated marine corals and molluscs, etc.). Statistical considerations for ΔR values and uncertainties in ^{14}C calibration would also be of interest.

If you are interested in participating, please contact Yaroslav V. Kuzmin (ykuzmin@tig.dvo.ru) or Paula J. Reimer (p.j.reimer@qub.ac.uk) with your possible topic of presentation as soon as possible, so they can put together an outline for the AMS Conference organizers.

LSC 2005 Conference: Advances in Liquid Scintillation Spectrometry

The Central Mining Institute will host the LSC 2005 Conference, and *Radiocarbon* will be publishing the proceedings of the conference. The conference will be held in Katowice, the capital city of Upper Silesia, Poland, from October 17–21, 2005. The organizers welcome you to present your achievements, to learn the latest developments of your colleagues, and to enjoy the traditional hospitality of the Polish people.

The main goal of the conference is to provide a forum for all scientists working in areas related to liquid scintillation counting and spectrometry (LSC). One of the objectives of the conference is to enable and promote the exchange of information, develop future directions in LSC, and give the opportunity to meet old and new friends. The conference organizers would like to pay particular emphasis to environmental studies and applications. Participation of young scientists and students is highly encouraged.

Please check the conference Web site (http://krzew.gig.katowice.pl/gig/lsc.php) for news and updates. Please email conference chairman Stanisław Chałupnik (lsc@gig.katowice.pl) for any further information.

Australasian Archaeometry Conference 2005

The conference will be held at the Australian National University, Canberra, 12–15 December 2005, hosted by the Department of Archaeology and Natural History, RSPAS, and the Centre for Archaeological Research. The organizing committee invite sessions covering all aspects of scientific applications (biological, physical, and chemical sciences) in archaeology. Papers will be accepted until the end of February 2005. Proposals for technical workshops are also being sought and should include details of technical/space requirements. The organizing committee will consider theoretical and interpretative sessions as well as those discussing archaeometrical techniques. Sessions and papers usually focus on Australasia and the broader Asia-Pacific region, but sessions/papers by researchers working in other geographical areas will also be considered, especially if they have some relevance to work within the region (e.g. help to build up technical competency, etc.). Details will be regularly posted on the conference Web site: http://car.anu.edu.au/Archaeometry/archaeometry_conference.html.

19th International Radiocarbon Conference

Conference organizers Christopher Bronk Ramsey and Tom Higham would like to announce dates for the 19th International Radiocarbon Conference which will be held in Oxford, at Keble College, from April 3–7, 2006. Further announcements about the conference will be sent out by email and posted on the conference Web site, http://www.rlaha.ox.ac.uk/orau/conference.html, and the *Radiocarbon* Web site.

RADIOCARBON, Vol 47, Nr 1, 2005, p 1–9

COMPARATIVE RADIOCARBON DATING OF LIGNITE, POTTERY, AND CHARCOAL SAMPLES FROM BABELDAOB ISLAND, REPUBLIC OF PALAU

Atholl Anderson[1] • John Chappell • Geoffrey Clark • Sarah Phear

Centre for Archaeological Research, Australian National University, Canberra ACT 0200, Australia.

ABSTRACT. It is difficult to construct archaeological chronologies for Babeldaob, the main island of Palau (western Micronesia), because the saprolitic clays of the dominant terraced-hill sites and associated ceramic sherds often contain old carbon that originated in lignites. This has implications, as well, for chronologies of sedimentary sequences. Comparative analysis of the dating problem using lignite, pottery, and charcoal samples indicates that, in fact, there are both old and young sources of potential contamination. It is concluded that radiocarbon samples from Babeldaob need to be tested for appropriate carbon content rather than relying solely upon material identification.

INTRODUCTION

The chronology of prehistoric colonization in the west Micronesian archipelago of Palau remains uncertain (Wickler 2001a). In part, at least, this has arisen from variation in research strategies. Palau is divided into two geographical provinces: the northern basalt island of Babeldaob and the southern limestone "rock islands." Archaeological research has tended to focus upon one or the other, and to sample, consequently, different site types, preservation environments, and stratigraphic situations. Working mainly on the rock islands, Masse (1990) estimated the age of initial colonization as about 2000 BP, while the extensive Compact Road project on Babeldaob (Wickler et al. 1997; Wickler 1998; Liston et al. 1998; Liston 1999; Welch 2001) has produced possible archaeological data extending to about 3400 BP, closer to the conclusions of Osborne (1979). In addition, the analysis of sedimentary cores from taro pondfields suggests that some markers of human occupation on Babeldaob might extend to the 6th millennium BP (Athens and Ward 1999, 2001; Welch 2001, 2002). The most recent radiocarbon results and their review show that people had colonized the rock islands, as well as Babeldaob, by earlier than 3000 BP (Clark and Wright 2003; Fitzpatrick 2002, 2003; Phear et al. 2003).

In beginning our archaeological research on Palau in 2000, we were aware that our initial focus upon the large structural features—comprising terraces, ditches, and crowns that are interpreted variously as defensive, domestic, and agricultural complexes (Wickler 2001a, 2002)—entailed grappling with the most difficult of dating problems in Palauan archaeology. Existing ^{14}C ages for these prominent features of the Palauan landscape were particularly diverse, even within the same structural element. While the inception of terracing and related hill-slope constructions was put generally at "the first century AD or perhaps a bit earlier" (Welch 2001:182), the associated ^{14}C ages ranged from about 3400 BP up to about 800 BP, with clusters of dates in the ranges 1600–1500 BP and 1200–800 BP (Phear et al. 2003). Consequently, we sought to investigate potential sources of variation in ^{14}C ages.

As the structural sites were constructed in damp saprolitic clays, almost no bone or midden shell has survived, and that which does is highly degraded. Most ^{14}C samples were, or appeared to be, of charcoal. However, charcoal in these sites is dispersed and generally comminuted, and it can be confused with fragments of a common pottery fabric. This "thin blackware" has yet to be described in detail and its age is known only approximately, from several associated dates on charcoal, as about 2800–1500 BP (Welch 2001:180; 2002:166). It is a thin (2–7 mm thick), grog-tempered ware with a black core which is often heavily eroded. It is encountered commonly in the damp terrace clays as small pieces or grains of a soft, black substance, which in hand specimen is easily confused

[1]Corresponding author. Email: aja@coombs.anu.edu.au.

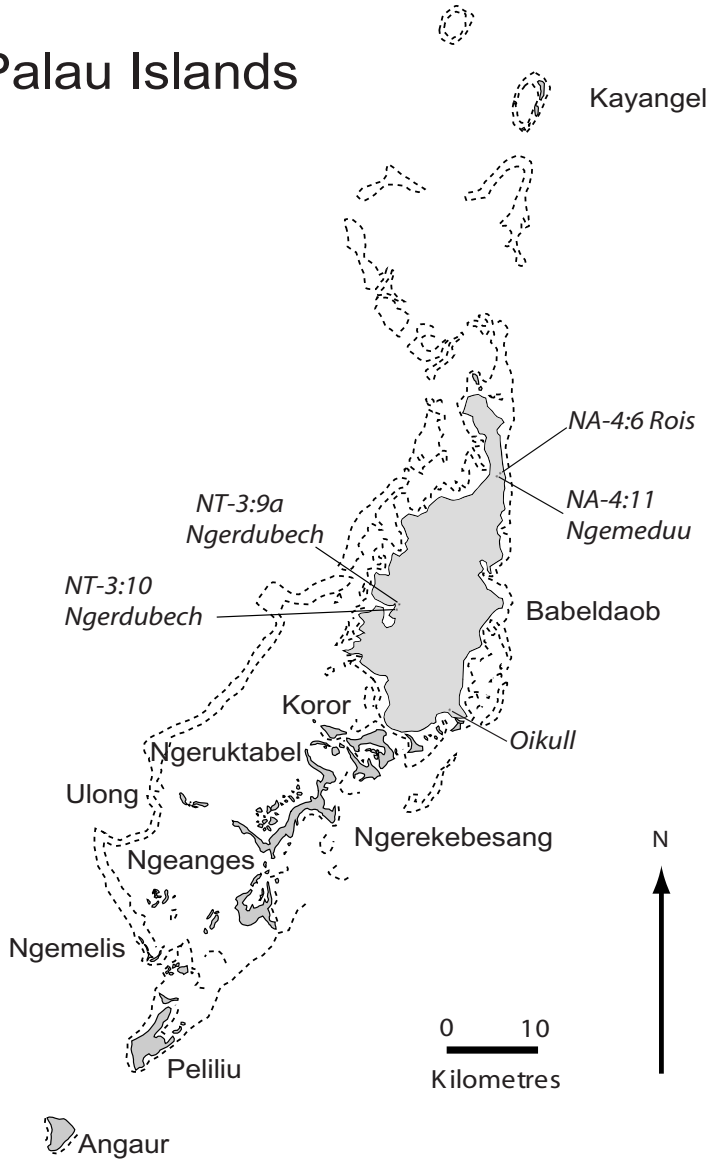

Figure 1 Palau, showing location of sites mentioned in the text

with wood charcoal. Many pieces bear a striking resemblance to the charred endocarp of coconut (*Cocos nucifera*). One matter to investigate, then, was whether some variation in the corpus of Palauan ^{14}C dates could have arisen from the inadvertent use of pottery samples.

The results of deliberate pottery dating show that use of this sample type is fraught with difficulties, as demonstrated by Kolic (1995) (see also Bollong et al. 1993), and has little to recommend it where more suitable materials are available. Pottery has been ^{14}C dated on several occasions in western Micronesia, initially by Taylor and Berger (1968) on sherds from Guam, later by Osborne (1979: 234–41) on sherds from Babeldaob and the rock island Aulong (Ulong) in Palau, and most recently

by Beardsley and Basilius (2002) on charcoal extracted from the fabric of a painted bowl found in a burial cave in Palau.

Some of the results are plausible, but given that human settlement in Micronesia generally was not thought to extend beyond the late Holocene, Osborne (1979:234) concluded that his "sherd dates are all shockingly old, ranging from 8150 to 3320 radiocarbon years." He suggested that this might have arisen from ancient carbon in the clays used for pottery manufacture, and a modern sample of Palauan clay was then dated at 1900 ± 400 BP, with which figure Osborne sought to calibrate his results. This approach is problematic, as Masse (1989) observed, but it highlighted the issue of what was producing anomalous ages in pottery and whether it or other sources of contamination were confined necessarily to that sample material, or indeed to archaeological contexts.

A particular source of potential contamination by old carbon occurs locally in the Babeldaob landscape in the form of soft lignite and dark gray organic clay within the kaolinitic Airai clay formation of upper Tertiary age, overlying the volcanic bedrock and saprolite. Indeed, kaolinitic Airai clay seen at three fairly extensive exposures (Nerassa, Oikull, Ulimang) was found to be flecked, commonly with black organic material, and to grade into dark gray organic clay overlying or underlying lignitic beds. The Airai clay is very suitable for pottery and is said to have been used in traditional Palauan manufacture near Oikull (Vince Blaiyok, personal communication). This is supported by Instrumental Neutron Activation Analysis (INAA) which identified Oikull and Ngimis as likely sources of clay used for making prehistoric pottery (Pavlish et al. 1986). Tiles were made from the Nerassa Island deposit of Airai clay by occupying Japanese during WWII. Considering that much of the clay is carbonaceous, it seems likely that ancient carbon could be retained in low-temperature pottery made from it.

Old-carbon contamination of archaeological materials could occur also if they had been infused by groundwater which was carrying organic compounds derived from the lignite, or if a site was built up of materials that included the lignite. In contrast, mobilization of organic compounds derived from today's soil could lead to young-carbon contamination. Contamination by both old and young carbon, either from lignitic sources or from soil charcoals of unknown age and derivation, could also occur, of course, through erosion and runoff into sedimentary basins. Athens and Ward (1998, 2001) noted this potential difficulty in the dating of sedimentary sequences used to reconstruct patterns of landscape and vegetational change on Palau.

Since lignite deposits and dispersed fragments in saprolites could be mistaken for charcoal incorporated in pottery or deposited in sedimentary basins, there is a significant possibility of confusion in Palauan ^{14}C dating. This paper describes our initial investigation of the problem and the implications of our results. We use pottery and charcoal samples from selected terrace sites to investigate the comparability of ^{14}C dating results and the sources of carbon contamination.

METHODS

Sample Collection

Excavations were renewed at several terrace sites already dated on multiple samples of charcoal. These were NT-3:9a, Japanese pits 1 and 2, and NT-3:10 (details of fieldwork in Wickler 2001b). There were also initial excavations on the crown of the Ngemeduu terrace site and at the Rois terraces (Phear 2004). All of the sites are remote from, or stand much higher in the landscape than, areas of lignite. The sites therefore are expected to have been uncontaminated by groundwater carrying dissolved old-carbon compounds. A carbon-bearing manganese nodule was collected from

an exposure at Ngemeduu and specimens of lignite and organic clay were collected from the Airai clay deposits at Oikull and Ulimang.

Ngerdubech NT-3:9a. Research at this traditional stonework village had produced 13 ^{14}C dates (Liston et al. 1998:Table 61), most of them to the late 2nd millennium AD, as expected from the nature of the site. However, the village had been built partially on earlier cut-and-fill constructed terraces. Two defensive pits had been excavated by Japanese troops during WWII into the riser of one of those terraces. Trenches were excavated further into the terrace from both pits in 1997 (Wickler et al. 1997; Liston et al. 1998). Terrace fill layers were recorded and dated using material identified as coconut (*Cocos nucifera*) nutshell. Excavation trench TR-9 in Pit 1 dated to the 2nd millennium AD (Wk-5901, 280 ± 100 BP; Wk-5898, 570 ± 80 BP), while excavation trench TR-8 in Pit 2 produced similar dates for fill on the southern face of the trench (Wk-5902, 444 ± 72 BP; Wk-5903, 621 ± 72 BP), and on the eastern face of the Japanese pit (Beta-100016, 910 ± 70 BP). However, on the northern face of TR8, the base of the fill was dated as 2994 ± 79 BP (Wk-5904) according to Liston et al. (1998:Table 61).

In 2000, we re-faced the excavation trenches and cut test sections through the stratigraphy as 0.5-m^2 columns. In our view, the various fill layers recognized in earlier work can be regarded as a single stratigraphic unit of terrace fill deposits overlying undisturbed saprolitic clay (Wickler 2001b). We would expect that the terrace construction was of relatively limited duration and therefore that reliable ^{14}C dates would cluster together. We chose ^{14}C samples as noted in Table 1. In TR-9, our samples ANU-11405 (black pottery) and ANU-11391 (charcoal) came from points immediately adjacent to the sampling points for Wk-5901 and Wk-5898, respectively. ANU-11406 (black pottery) is from 0.2 m beneath the location of Wk-5901, and ANU-11855 (charcoal) is 0.4 m above the location of Wk-5898. In TR-8, ANU-11407 (black pottery) was located 0.3 m above the location of Wk-5904.

Ngerdubech NT-3:10. About 35 m northeast of NT-3:9a, TR-1 was excavated on a higher terrace and crown construction, designated NT-3:10 (Liston et al. 1998). TR-1 was 2.2 m deep and 3 dates were produced. From near the base of cultural deposits came Wk-5926 (2809 ± 72 BP) on charcoal that may be from the secondary forest tree, *Macaranga caroliensis*. From 1.65 m came Wk-6469 (2334 ± 60 BP) on charcoal from palm and unidentified taxa, and from 0.9 m came Wk-6468 (2717 ± 58) on unidentified charcoal (Liston 1999). We re-excavated TR-1 in 2000 and took samples from as low as material could be obtained, 1.6 to 1.7 m (ANU-11408, black pottery, and ANU-11837, charcoal). These are adjacent to the location for Wk-6469. ANU-11782 was collected from a road cutting exposure 20 m south of the site and 1 m below the surface.

Rois NA-4.6. Excavation in 2001 of a terrace site at the Rois burial complex (NA-4.6) by Phear (2004) produced some additional samples of black pottery. A 3.2 × 0.5-m trench was excavated on a lower terrace in the complex (TR-4). Black pottery samples were collected at 0.8–0.9 m, Layer V (ANU-11582A, ANU-11583A) within terrace fill material. Results on these cannot be compared directly with charcoal dates from the same excavation, but elsewhere in the constructed features of the same terrace complex, there are dates of 2015 ± 68 BP (Wk-5920) on a sample of ironwood (*Casuarina litorea*) charcoal; 1772 ± 67 BP (Wk-5922) on a charcoal sample, possibly of mangrove (*Rhizophora* sp.); and 1723 ± 68 BP (Wk-5889) on charred grasses (Liston 1999).

Ngemeduu NA-4:11. This crown and terrace complex, also excavated by Phear (2004), disclosed a cultural stratigraphy extending over 4 m deep (Phear 2003). ANU-11658 is a charcoal sample from 4 m deep in the lowest cultural level (Layer VIII) in trench TR1a, which was excavated on the crown. ANU-11659 is a charcoal sample from a posthole at 1.3 to 1.7 m at the base of the cultural stratigraphy in trench TR1i, which was located on the terrace that encircles the crown. Black pottery sample ANU-11783 is also from this trench, at 0.6 m depth.

Non-archaeological samples. ANU-11780 is a sample of lignitic Airai clay from Oikull, taken at 1 m deep in a roadside exposure at lat 7°22.459′N, long 134°35.001′E. ANU-11781 is a soft manganese nodule from the Ngemeduu excavation, at 0.6 m depth.

Sample Treatment

Samples were identified at, and pretreated in, the Australian National University Radiocarbon Laboratory (Canberra) in 3 ways for ^{14}C determination: i) as bulk samples (water-washed and dried), ii) as alkali-soluble extracts (2N NaOH), and iii) as ABA (acid-base-acid) residues. The NaOH extracts were intended to isolate soluble organic compounds that had entered a sample from groundwater. The ABA treatment usually (but not always) removes many such compounds, and the residual carbon in these preparations was expected to be dominantly that which was present when the sample was formed (in the case of charcoal) or manufactured (in the case of pottery).

According to the amount of carbon in a preparation, the ^{14}C content was measured either by liquid scintillation radiometry (typically samples with >0.2 g C) or, when carbon yield was very small, by accelerator mass spectrometry (AMS). The percentage of primary carbon present in the original specimen also was estimated by dividing the weight of carbon present after ABA treatment by the original sample dry weight.

RESULTS

Results are listed in Table 1. It is apparent that while our charcoal samples were not identified to taxa, they produced results which are very comparable with those obtained by earlier researchers on the specific sites, and on terrace sites in general: compare ANU-11855 and ANU-11391 with Wk-5901 and Wk-5898 (Liston et al. 1998:Table 61); also ANU 11837 with Wk-6469 (Liston 1999). There are several potential anomalies, noted below, but with those exceptions it can be said that the charcoal dates on Palauan terraces provide a quite consistent chronology against which to measure dates on pottery fabric. Here, the differences are very marked indeed, as we expected, and they exist both between the black pottery and charcoal samples and within the group of black pottery samples. What causes these effects?

In terms of primary carbon content, the archaeological samples divide into 2 groups: charcoal, with relatively high primary carbon (ANU-11658, ANU-11659), and black pottery, with a low percentage of primary carbon. The dated clay sample from Oikull and the manganese nodule from Ngemeduu also had low percentages of carbon. In terms of apparent ^{14}C ages, the results show a more complex distribution, but the data set indicates that at least 2 sources of contamination potentially may have affected any given sample, one being ancient carbon and the other being relatively young carbon.

Evidence for an ancient carbon source is most apparent in the ABA preparations of black pottery samples, several of which are between 10,000 and 15,000 BP, far exceeding all estimates of the earliest date of occupation of Palau. If accurate, they would be amongst the earliest dates for pottery anywhere in the world. The result of 29,090 BP (ANU-11780) from the putative pottery clay source at Oikull suggests that the ancient source was carbon in the original clay from which the pottery was made. Evidence for a source of young, mobile carbon is seen in the result of 1390 BP (ANU-11781) from the NaOH extract from the manganese nodule, which itself would have contained no primary carbon. Evidence that samples may contain mixtures of these 2 sources is revealed by the difference between NaOH extracts and ABA residues from black pottery: the NaOH extract, which is expected to carry the younger contaminant, gives a lesser age than the ABA residue in each case where the 2

Table 1 ^{14}C ages and contextual data for samples in the comparative dating project, Palau. ANU-11391 B1 is an older sample that was not tested for carbon content.

Lab nr	Provenance	Material	Yr BP	$\delta^{13}C$	Fraction	% C at ABA
Ngerdubech	NT-3:9a Pit 1	TR-9				
ANU-11391 B-1	70–80 cm	Charcoal	600 ± 60	–26.0 ± 2.0	Insoluble	n.d.
ANU-11391 B-2	70–80 cm	Charcoal	570 ± 40	–24.0 ± 2.0	Soluble	—
ANU-11405 B-1	70–80 cm	Black pottery	2880 ± 130	–25.9 ± 0.2	Insoluble	1.5
ANU-11405 B-2	70–80 cm	Black pottery	1230 ± 160	–25.9 ± 0.2	Soluble	—
ANU-11406 B-1	80–90 cm	Black pottery	5120 ± 140	–26.0 ± 0.2	Insoluble	1.5
ANU-11406 B-2	80–90 cm	Black pottery	3610 ± 160	–26.0 ± 0.2	Soluble	—
ANU-11855	70–80 cm	Charcoal	Modern	–24.0 ± 2.0	Whole	—
Ngerdubech	NT-3:9a Pit 2	TR-8				
ANU-11407 B-1	60–70 cm	Black pottery	9630 ± 260	–26.9 ± 0.2	Insoluble	0.6
ANU-11407 B-2	60–70 cm	Black pottery	6230 ± 160	–26.9 ± 0.2	Soluble	—
Ngerdubech	NT-3:10	TR-1				
ANU-11408 B-1	160–170 cm	Black pottery	10,870 ± 190	–26.5 ± 0.2	Insoluble	1.2
ANU-11408 B-2	160–170 cm	Black pottery	7450 ± 180	–26.5 ± 0.2	Whole	—
ANU-11782	100 cm	Black pottery	7880 ± 160	–25.4 ± 0.2	Whole	1.3
ANU-11837	160–170 cm	Charcoal	2060 ± 210	–17.6 ± 2.0	Whole	—
Rois Terrace	NA-4:6	TR-4				
ANU-11582 A	80 cm	Black pottery	13,260 ± 190	–26.4 ± 0.2	Whole	3.9
ANU-11583 A	90 cm	Black pottery	15,240 ± 290	–27.1 ± 0.1	Whole	4.4
Ngemeduu	NA-4:11					
ANU-11658	400 cm	Charcoal	1510 ± 200	–25.4 ± 0.2	Whole	15
ANU-11659	130–170 cm	Charcoal	2140 ± 220	–25.4 ± 0.2	Whole	39
ANU-11783	60 cm	Black pottery	10,580 ± 130	–26.1 ± 0.1	Whole	0.9
Non-archaeological samples						
ANU-11780	100 cm	Lignitic clay	29,090 ± 520	–27.0 ± 0.1	Whole	0.3
ANU-11781	60 cm	Mn nodule	1390 ± 200	–27.8 ± 0.1	Soluble	0.1

fractions were prepared (ANU-11405, ANU-11406, ANU-11407). A similar difference is seen in ANU-11408, where the bulk sample gave a lesser age than the ABA preparation.

The results also indicate that ABA pretreatment fails to remove all the contaminant that enters as mobile carbon. If, at the time of firing, the pottery contained only Tertiary-age carbon from the Airai clay, then all ABA preparations should give "infinite" (or "greater than") ^{14}C ages (*sensu* Stuiver and Polach 1977). In fact, all the black pottery ABA preparations gave finite ages, the lowest being only 2880 BP (ANU-11405); indeed, the ABA preparation from Airai clay gave a finite age of 29,090 BP (ANU-11780). In terms of two-component mixing, the apparent age depends not only on the amount of ancient contaminant retained in the pottery, but also on the age-distortion from residual younger contaminant that has resisted extraction in the ABA pretreatment.

It seems likely that neither of these preparations can be measured because the amount of ancient carbon in the Airai clay is highly variable, the proportion that survives firing has yet to be determined, the efficacy of ABA with these materials has yet to be determined, and the age and quantity of residual contaminants will remain unknown. The possibility that carbon entered at the time of firing or when a pot was in use only confounds the issue further.

DISCUSSION AND CONCLUSIONS

The question confronting field scientists after receiving a set of conflicting ^{14}C determinations is which, if any, of the results represent accurate dates. The answer must be discovered from the logic of data from the field, the laboratory, and from the samples themselves. In the present case, none of

the black pottery results can be regarded as indicating the age of a specimen or its time of burial. Pottery, being derived from clay, contains carbon only as a contaminant. Where ancient carbon within the clay itself survives firing, which on the evidence is the case here, and where young carbon taken up by the pottery has not been fully removed in pretreatment, which again evidently has happened here, then to attempt to infer any chronological meaning is all but futile.

Having eliminated the black pottery, it remains to ask whether charcoal dates are reliable in a context where residues of once-mobile carbon are not fully removed in ABA pretreatment. The carbon content of the specimen is a useful guide to reliability. This can be measured using EDXA; Clark (2004) found that elemental analysis of Palauan archaeological pottery and charcoal produced very similar carbon measurements to those reported here on samples of pottery and charcoal. But it is probably easier to measure carbon content during the ^{14}C dating process, as here. Whereas the black pottery samples contain only a percent or two of carbon, for the charcoal samples the carbon remaining at ABA ranges from 10 to 40% (this is the range for all macroscopic charcoal samples from Palau dated at ANU, of which only two are listed in Table 1). Experiments on carbon from charcoal, using more aggressive oxidative pretreatment (ABOX: Bird et al. 2000; see also Gillespie et al. 1992), show that the ABA fraction is dominantly comprised of original carbon, and that age distortion arising from the failure of ABA to remove young contaminants from it is very difficult to detect in charcoal that is only a few thousand years old. In short, ABA charcoal ages from Palau are expected to be reliable. On that basis, we conclude provisionally that a critical assessment of ^{14}C determinations (Phear et al. 2003) indicates that monumental earthworks cluster in the Palauan sequence in the period 1600–800 cal BP.

There remains the problem of sample identification. Black pottery fragments excavated from Palau often resemble charcoal fragments: both can be soft, rounded, and black, and the smaller the fragment the more readily may one be taken for the other. Thus, to minimize the likelihood of error, in addition to the usual tests of stratigraphic consistency and age reproducibility, the carbon content should be measured at the time of dating and, where the content is low, the ^{14}C result must be taken as something other than sample age. Carbon content may be a more useful measure of origin than attempted wood identification for very small samples, although microscopic, including SEM, examination could be equally useful, if a more elaborate approach. Carbon content analysis ought perhaps to be adopted, retrospectively, for those samples that, although regarded as charcoal, produced quite anomalous ages. Such examples of relevance to the present cases would be Wk-5904 (above) and Wk-5900 (9240 ± 68 BP), also from site NT-3:9a, for which Liston et al. (1998) suggested the possibility of lignite contamination.

A further implication of this issue lies in the dating of horizons of significant change in cores from sedimentary basins. The potential problems arising from carbon contamination, due to lignite, have been canvassed by Athens and Ward (1998, 1999). Welch (2002:170) suggests that at least some apparent charcoal in core samples might actually be lignite and notes that tests to distinguish between these materials when they are fine-grained (using sulphur content, Athens and Ward 1999: 102) have proven, so far, inconclusive. One important instance in which the possibility of carbon contamination is worth further consideration is the Ngerchau core (Athens and Ward 2001) in which 8 grains of pollen from a probable introduced cultigen, the giant swamp taro *Cytopsperma chamissonis*, were dated to the 5th to 6th millennia BP and held as "evidence [which] appears to be the 'smoking gun' establishing human agency at a very early time" (Athens and Ward 2001:172).

There are questions about the contextual evidence, such as the absence of any rise in charcoal or disturbed ground indicators associated with the lowest occurrence of *Cytosperma* pollen (Athens and

Ward 1999:102), and also about the ^{14}C dating. The top sections of this core date to less than 3000 BP and the *Cytosperma* pollen is in the lower sections, for which 5 ^{14}C dates, all on unidentified peat and wood samples, are virtually indistinguishable from the top (3840 ± 90 BP, Beta-127286, at 2.0 m depth) to the bottom (4008 ± 57 BP, Wk-6721, at 5.4 m depth). Athens and Ward (2001) argue that the sequence represents very rapid early accumulation, followed by a sedimentary unconformity, but the same pattern could be produced by carbon contamination, especially of the samples near the top of the peat, where a 6th date was anomalously old (5203 ± 62 BP, Wk-6414, at 2.45 m). The matter must remain in doubt until the carbon content of the samples has been measured. The Ngerchau core is now being re-examined in a joint project between the International Archaeological Research Institute Inc. (IARII) and the Australian National University.

At present, there is a significant discrepancy between a paleoenvironmental inference of settlement in western Micronesia by about 4800–4500 BP (Wickler 2001a) and archaeological results that do not extend currently beyond about 3500–3000 cal BP (Clark 2004). The magnitude of the discrepancy, and the potential for dating materials in both Palauan contexts to be contaminated by environmental sources of carbon, requires further systematic investigation of the kind advocated here before either "long" or "short" prehistoric occupation chronologies can be accepted with confidence.

ACKNOWLEDGMENTS

We thank Stephen Athens, Stephen Wickler (University of Tromsø), Jolie Liston (IARII), and Vince Blaiyok (IARII) for their guidance in the Palauan fieldwork, Vicky Kanai, Rita Olsudong, and the Governor of Ngaraard for governmental support. The community *bai* in Ngeklau were generous in providing accommodation, and the Research School of Pacific and Asian Studies (ANU) likewise in funding the project.

REFERENCES

Athens JS, Ward JV. 1998. The Holocene paleoenvironment of Palau. In: *Intensive Archaeological Survey for the Palau Compact Road, Babeldaob Island, Palau. Historic Preservation Investigations, Phase II. Volume IV.* Honolulu: International Archaeological Research Institute, Inc.

Athens JS, Ward JV. 1999. *Archaeological Data Recovery for the Compact Road, Babeldaob Island, Republic of Palau. Volume IV, The Holocene Paleoenvironment of Palau*. Honolulu: International Archaeological Research Institute, Inc.

Athens JS, Ward JV. 2001. Palaeoenvironmental evidence for early human settlement in Palau: the Ngerchau core. In: Stevenson CM, Lee G, Morin FJ, editors. *Pacific 2000. Proceedings of the Fifth International Conference on Easter Island and the Pacific*. Los Osos, California: Easter Island Foundation. p 164–77.

Beardsley FR, Basilius U. 2002. Sengall Ridge, Belau: burials, spirit walks and painted pottery. *Indo-Pacific Prehistory Association Bulletin: Melaka Papers* 6: 147–51.

Bird MI, Turney CSM, Fifield LK. 2003. Radiocarbon dating of organic- and carbonate-carbon in Genyornis and Dromaius eggshell using stepped combustion and stepped acidification. *Quaternary Science Reviews* 22:1805–12.

Bollong CA, Vogel JC, Jacobson L, van der Westhuizen WA, Sampson CG. 1993. Direct dating and identity of fibre temper in pre-contact Bushman (Basarwa) pottery. *Journal of Archaeological Science* 20:41–55.

Clark G. 2004. Radiocarbon dates from the Ulong site in Palau and implications for western Micronesian prehistory. *Archaeology in Oceania* 39:26–33.

Clark G, Wright D. 2003. The colonisation of Palau: preliminary results from Angaur and Ulong. In: Sand C. editor. *Pacific Archaeology: Assessments and Prospects*. Les Cahiers de l'Archéologie en Nouvelle-Calédonie. Number 5. Nouméa: Museum of New Caledonia. p 85–94.

Fitzpatrick SM. 2002. AMS dating of human bone from Palau: new evidence for a pre-2000 BP settlement. *Radiocarbon* 44(1):217–21.

Fitzpatrick SM. 2003. Early human burials in the western Pacific: evidence for a c. 3000 year old occupation on Palau. *Antiquity* 77:719–31.

Gillespie R, Prosser IP, Dlugokencky E, Sparks RJ, Wallace G, Chappell JMA. 1992. AMS dating of alluvial sediments on the southern tablelands of New South Wales, Australia. *Radiocarbon* 34(1):29–36.

Kolic ED. 1995. Direct radiocarbon dating of pottery: selective heat treatment to retrieve smoke-derived carbon. *Radiocarbon* 37(2):275–84.

Liston J. 1999. *Archaeological Data Recovery for the Compact Road, Babeldaob Island, Republic of Palau. Historic Preservation Investigations, Phase II. Volume V: Lab Analyses, Syntheses and Recommendations*. Honolulu: International Archaeological Research Institute, Inc.

Liston J, Mangieri TM, Grant D, Kaschko MW, Tuggle, HD. 1998. *Archaeological Data Recovery for the Compact Road, Babeldaob Island, Republic of Palau. Historic Preservation Investigations, Phase II. Volume II: Fieldwork Reports*. Honolulu: International Archaeology Research Institute, Inc.

Masse WB. 1989. *The Archaeology and Ecology of Fishing in the Belau Islands, Micronesia*. Part 1 and Part 2. University Microfilms International. Ann Arbor: Michigan.

Masse WB. 1990. Radiocarbon dating, sea-level change and the peopling of Belau. *Micronesica Supplement* 2: 213–30.

Osborne D. 1979. Archaeological test excavations in the Palau Islands 1968–1969. *Micronesica* Supplement 1.

Pavlish LA, Hancock RG, Snyder D, Lucking L. 1986. INAA study of pottery from Palau. In: Olin J, Blackman MJ, editors. *Proceedings of the 24th International Archaeometry Symposium.* Washington DC: Smithsonian Institution Press. p 383–7.

Phear S. 2003. Painted pottery in Palau: new evidence challenges past interpretations. *Antiquity* 77(296): http://antiquity.ac.uk/ProjGall/phear/phear.html.

Phear S. 2004. The monumental earthworks of Palau [PhD dissertation]. Canberra: Australian National University.

Phear S, Clark G, Anderson A. 2003. A radiocarbon chronology for Palau. In: Sand C, editor. *Pacific Archaeology: Assessments and Prospects.* Les Cahiers de l'Archéologie en Nouvelle-Calédonie Number 15. Nouméa: Museum of New Caledonia. p 241–9.

Stuiver M, Polach HA. 1977. Discussion: reporting of ^{14}C data. *Radiocarbon* 19(3):355–63.

Taylor RE, Berger R. 1968. Radiocarbon dating of the organic portion of ceramic and wattle-and-daub house construction materials of low organic content. *American Antiquity* 53:363–6.

Welch DJ. 2001. Early upland expansion of Palauan settlement. In: Stevenson CM, Lee G, Morin FJ, editors. *Pacific 2000. Proceedings of the Fifth International Conference on Easter Island and the Pacific*. Los Osos, California: Easter Island Foundation. p 164–77.

Welch DJ. 2002. Archaeological and palaeoenvironmental evidence of early settlement in Palau. *Bulletin of the Indo-Pacific Prehistory Association* 22:161–73.

Wickler S. 1998. Research summary. In: Wickler S, Welch DJ, Tomonari-Tuggle MJ, Liston J, Tuggle HD, editors. *Intensive Archaeological Survey for the Palau Compact Road, Babeldoab Island, Palau. Historic Preservation Investigations, Phase I. Volume 1: Scope, Background, Results, Evaluation and Recommendations*. Honolulu: International Archaeological Research Institute, Inc.

Wickler S. 2001a. The colonization of western Micronesia and early settlement of Palau. In: Stevenson CM, Lee G, Morin FJ, editors. *Pacific 2000. Proceedings of the Fifth International Conference on Easter Island and the Pacific*. Los Osos, California: Easter Island Foundation. p 185–96.

Wickler S. 2001b. Preliminary field report for the ANU-Tromsø Museum Palau 2000 Project, Babeldaob, Republic of Palau, August–September 2000. Tromsø University Museum.

Wickler S. 2002. Terraces and villages: transformations of the cultural landscape in Palau. In: Ladefoged TN, Graves MW, editors. *Pacific Landscapes: Archaeological Approaches*. Honolulu: Easter Island Foundation. p 63–96.

Wickler S, Addison DJ, Kashko MW, Dye TS. 1997. *Intensive Archaeological Survey for the Palau Compact Road, Babeldoab Island, Palau. Volume II: Area Survey Reports.* Honolulu: International Archaeological Research Institute, Inc.

RADIOCARBON, Vol 47, Nr 1, 2005, p 21–25

AMS RADIOCARBON DATING OF BONE SAMPLES FROM THE XINZHAI SITE IN CHINA

Kexin Liu[1,2] • Baoxi Han[1] • Zhiyu Guo[1] • Xiaohong Wu[3] • Sixun Yuan[3] • Walter Kutschera[4] • Hongji Ma[1] • Alfred Priller[4] • Peter Steier[4] • Eva Maria Wild[4] • Chunqing Zhao[3]

ABSTRACT. Xinzhai is an important archaeological site discovered 40 yr ago and recently re-excavated in the Henan Province, China. It is believed that the cultural characteristics of the Xinzhai site correspond to the Xia dynasty, the first ancient dynasty of China. Radiocarbon measurements on bone samples from this site were performed at the Peking University AMS facility (PKU-AMS) and the Vienna University AMS facility (VERA). Calibrated ages were obtained with the computer program OxCal. The results of these measurements are presented and the related chronology is discussed.

INTRODUCTION

It is well known that Xia was the first ancient dynasty of China. This was recorded in the famous ancient book *Shiji* and in other literature, but there was no exact chronology given in those books and the authors gave different estimations of the chronology. Therefore, radiocarbon measurements and calibrations of samples from related sites become more important for investigating the chronological frame of the Xia dynasty.

From 1999 to 2000, the Xinzhai site in Henan Province, China, was excavated by the College of Archaeology and Museology, Peking University, and the Henan Archaeology Institute. The cultural remains of this site are plentiful and very significant for studying the cultural characteristics of the Xia dynasty. Serial bone samples have been collected from this site for ^{14}C analysis. ^{14}C measurements were performed at the Peking University AMS facility (PKU-AMS) and the Vienna University AMS facility (VERA). This paper describes the importance of the Xinzhai site, its ^{14}C sample measurements and age calibration, and subsequent discussions regarding the Xia chronology.

XINZHAI SITE

The Xinzhai site encompasses a total area of about 700,000 m^2 and is located near Xinmi City in Henan Province, China. It was discovered in the 1960s and a systematic excavation was carried out until 1999. More than 100 hoards, ash pits, and tombs have been discovered and about 300 pottery wares have been unearthed and restored. Many bone samples have also been collected for ^{14}C analysis.

Excavation of the Xinzhai site is very important for archaeological research of the Xia dynasty. Before the excavation of the Xinzhai site, several sites related to the Xia dynasty were excavated and the remains from those sites were identified according to 2 cultural types: Erlitou culture and Longshan culture. The Erlitou site, located near Yanshi City in Henan Province, is a typical Erlitou culture site, and the Wangchenggang site, near Dengfen City, also in Henan Province, is exemplary of the Longshan culture. Archaeological research and ^{14}C analyses showed that the Longshan culture preceded the Erlitou culture and the transition between these 2 cultures was not continuous. Many archaeologists believe that the transition is evident in the remains found at the Xinzhai site and thus can be named the Xinzhai culture (Zhao and Li 2003).

[1]Institute of Heavy Ion Physics, Peking University and Key Laboratory of Heavy Ion Physics, Ministry of Education, Beijing 100871, China.
[2]Corresponding author. Email: kxliu@pku.edu.cn.
[3]School of Archaeology and Museology, Peking University, Beijing 100871, China.
[4]Vienna Environmental Research Accelerator (VERA), Institut für Isotopenforschung und Kernphysik, Universitat Wien, A-1090 Wien, Austria.

In addition to the phase belonging to the Xinzhai culture, remains belonging to the late Longshan and early Erlitou cultures were also found in the Xinzhai site. According to the analysis of the unearthed pottery ware characteristics, the Xinzhai culture can be subdivided into 2 phases: Early Xinzhai and Late Xinzhai. Therefore, the cultural remains of the Xinzhai site can be divided into 4 phases: Late Longshan, Early Xinzhai, Late Xinzhai, and Early Erlitou (Zhao and Li 2003).

SAMPLE PREPARATION AND MEASUREMENT

Contamination was very carefully avoided during sample collection and transportation. All samples selected for ^{14}C measurements are well-preserved bone samples and constitute a series that covers the archaeological phases of the Late Longshan, Early Xinzhai, and Late Xinzhai. Due to the lack of suitable dating material, samples from the Early Erlitou phase do not exist. Serial samples collected from the Erlitou site have been measured previously (Qui and Cai 2001).

Reliable dating results are obtainable when extracted gelatin is used as the dating material (Hedges et al. 1992; Wu et al. 2000). Following a standard method of sample pretreatment and preparation developed in the School of Archaeology and Museology of Peking University, the gelatin contained in the bone samples was extracted and combusted to CO_2. The CO_2 was then reduced to graphite (Wu et al. 2000).

The samples were measured at the upgraded PKU-AMS facility (Liu et al. 2000). The precision and accuracy of ^{14}C measurement for most samples is better than 0.5%. For the purpose of quality control, most samples were measured twice, provided that there were enough dating materials. Sample pretreatment and preparation were also performed twice for the different AMS measurements of one sample. Five samples were measured at the Vienna University AMS facility (VERA) (Priller et al. 2000). For the comparison of the sample pretreatments between the 2 laboratories, gelatin extracted at Peking University and original bone materials of the same samples were sent to the Vienna University AMS laboratory.

CALIBRATION

Since the samples collected from the Xinzhai site have a good stratigraphic sequence, the Bayesian method was applied to the calibration to reduce the calendar age intervals. The program used for the calibration of ^{14}C ages was OxCal 3.9, with the calibration curve IntCal98. Samples were organized into 3 phases according to the pottery sequence. Boundaries were used at the terminals of the sequence and between the phases. If one sample had two or more ^{14}C ages, they were combined to a unique age by using the code command "combine" of OxCal 3.9.

RESULTS AND DISCUSSION

The measured ^{14}C ages and calibrated calendar ages of the samples from the Xinzhai site are shown in Table 1, and Figure 1 is the plot of the OxCal calibration. The ^{14}C ages are all in good agreement between the 2 AMS laboratories and between the 2 measurements by the PKU-AMS facility. Age differences for samples measured at VERA were pretreated separately at Vienna University and Peking University and are also within 1 σ.

Table 1 ^{14}C and calibrated ages of Xinzhai site samples.

Phase	Field nr	Lab code and nr	^{14}C age	Calendar age (BC)
Upper boundary				2170–2040
Late Longshan	T1H123	SA00002	3700 ± 65	2110–1950
	T1H126	SA00014	3675 ± 35	2085–2035
		SA00014-1	3740 ± 30	
		VERA-1430 (gelatin)	3760 ± 45	
		VERA-1429a (bone)	3695 ± 35	
	T1H122	SA00008	3570 ± 35	1960–1875
	T1H120	SA00007	3590 ± 30	2010–1880
	T1H119	SA00001	3485 ± 30	1880–1840
		SA00001-1	3490 ± 35	
1–2 boundary				1850–1780
Early Xinzhai	T1(6)C	SA00006	3535 ± 35	1820–1770
		SA00006-1	3470 ± 35	
	T1H116	SA00012	3480 ± 35	1820–1765
		VERA-1432 (gelatin)	3500 ± 45	
		VERA-1431 (bone)	3490 ± 35	
	T1H112	SA00005	3465 ± 35	1820–1755
	T1H115	SA00019	3530 ± 35	1820–1770
		SA00019-1	3500 ± 35	
	T4H61(6)	SA00028	3500 ± 35	1815–1770
2–3 boundary				1780–1745
Late Xinzhai	T1H40	SA00018	3500 ± 30	1770–1740
		SA00018-1	3470 ± 35	
	T1H26	SA00017	3395 ± 40	1750–1700
		SA00017-1	3455 ± 30	
	T1H76	SA00009	3415 ± 35	1745–1605
	T1H48	VERA-1435 (gelatin)	3460 ± 50	1755–1695
		VERA-1434 (bone)	3425 ± 35	
	T1H45	SA00013	3430 ± 55	1740–1710
		SA00013-1	3390 ± 35	
		VERA-1437 (gelatin)	3450 ± 50	
		VERA-1436 (bone)	3380 ± 35	
	T1H29(1)	SA00016	3410 ± 50	1745–1710
		VERA-1439 (gelatin)	3430 ± 50	
		VERA-1438 (bone)	3390 ± 35	
	T4H66	SA00021	3425 ± 30	1745–1705
	T4H30	SA00020	3490 ± 30	1775–1700
Lower boundary				1730–1675

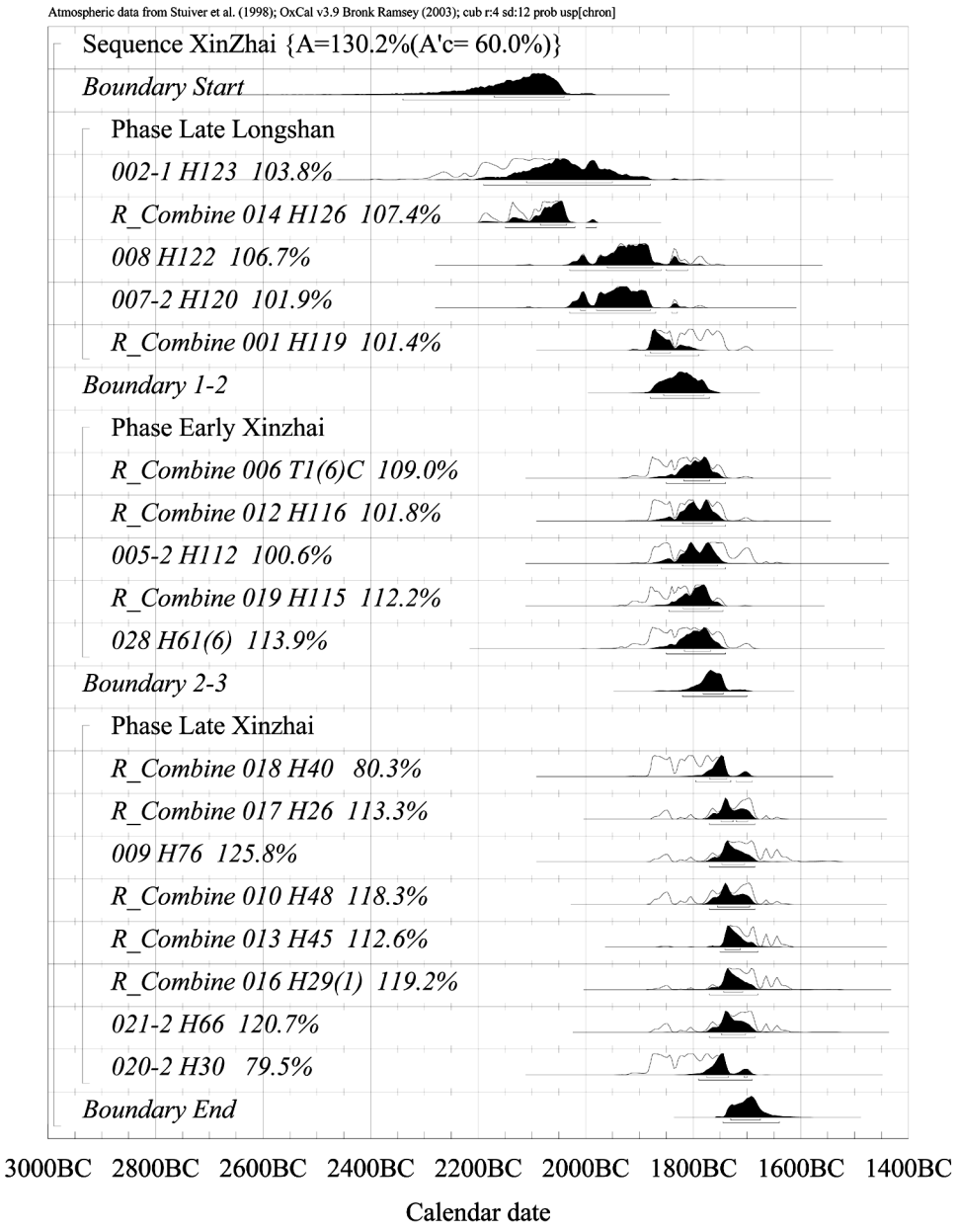

Figure 1 OxCal calibration plot of the Xinzhai site samples

^{14}C measurements of the Xinzhai site serial samples reveal preliminary chronological information about the Xinzhai culture, late Longshan culture, and early Erlitou culture, all of which are related to the Xia dynasty. According to the ages listed in Table 1, the estimated age for the transition from the Longshan culture to the Xinzhai culture is about 1840–1820 BC, and the end age of the Xinzhai culture is about 1720 BC. The Xinzhai merges with the beginning age of the Erlitou culture, which is estimated by the ^{14}C measurement of the Erlitou site serial samples. Twenty samples from the Erlitou site were collected and measured by liquid scintillation counting (LSC) at the Institute of

Archaeology, Academy of Social Science of China—10 of them were bone and 10 were charcoal. Samples were organized into 5 phases for the calibration of ^{14}C ages and the result shows that the upper limit of the Erlitou culture is about 1780–1730 BC (Qui and Cai 2001). More samples from the Erlitou site will be measured by AMS. Given the analysis above, the Xinzhai culture should last about 120 yr.

Chinese archaeologists generally recognize that the early Erlitou culture belongs to the Xia culture. However, there are different opinions regarding the Longshan culture. Some archaeologists believe that the early Xia culture should be found in the late Longshan culture, while others claim that the Longshan culture has no relation to the Xia culture. The recent excavation and archaeological research of the Xinzhai site shows that the Xinzhai culture should belong to the Xia culture (Zhao and Li 2003) and that it is the transition culture between the Longshan and Erlitou cultures. The results of ^{14}C analysis of the Xinzhai site provide a preliminary calendar age for the Xinzhai culture that chronologically predates the Erlitou culture. These findings are important for studies regarding the origin of the Xia dynasty.

ACKNOWLEDGMENTS

We thank professor Boqian Li of the School of Archaeology and Museology, Peking University, for his helpful discussions. This work is supported by the Xia-Shang-Zhou Chronology Project.

REFERENCES

Hedges REM, van Klinken GJ. 1992. A review of current approaches in the pretreatment of bone for radiocarbon dating by AMS. *Radiocarbon* 34(3):279–91.

Liu K, Guo Z, Lu X, Ma H, Li B, Wang J, Zhou G, Yuan J, Ren X, Zhao Q, Zhang Z, Zhang G, Yuan S, Wu X, Li K, Chen C-E. 2000. Improvements of PKU-AMS for precision ^{14}C analysis of the Project of Xia-Shang-Zhou Chronology. *Nuclear Instruments and Methods in Physics Research B* 172:70–4

Priller A, Brandl T, Golser R, Kutschera W, Puchegger S, Rom W, Steier P, Vockenhuber C, Wallner A, Wild E. 2000. Extension of the measuring capabilities at VERA. *Nuclear Instruments and Methods in Physics Research B* 172:100–6

Qiu S, Cai L. 2001. ^{14}C chronological framework in the Xia-Shang-Zhou Chronology Project. *Kaogu (Archaeology)* 1:90–100. In Chinese.

Wu X, Yuan S, Wang J, Guo Z, Liu K, Lu X, Ma H, Li K, Yuan J, Cai L. 2000. AMS radiocarbon dating of a cemetery of Jin marquises in China. *Nuclear Instruments and Methods in Physics Research B* 172:732–5.

Zhao Q, Li B. 2003. The study of Xinzhai site. Inner research report of the Xia-Shang-Zhou Chronology Project. In Chinese.

RADIOCARBON, Vol 47, Nr 1, 2005, p 27–30

NEW BOMB PULSE RADIOCARBON RECORDS FROM ANNUAL TREE RINGS IN THE NORTHERN HEMISPHERE TEMPERATE REGION

G Quarta[1] • M D'Elia • D Valzano • L Calcagnile

Dipartimento di Ingegneria dell'Innovazione, Università di Lecce, via Arnesano, 73100 Lecce, Italy.

ABSTRACT. The "bomb" radiocarbon spike induced by atmospheric nuclear detonations has been reconstructed at a latitude of 40°N by measuring the ^{14}C content in annual rings of a living pine (*Pinus pinea*) at the Accelerator Mass Spectrometry facility of the University of Lecce. We report how the samples were taken, selected, prepared for analysis, and measured. The results are in good agreement with other data sets available for the Northern Hemisphere temperate regions, showing that a curve for the calibration of ^{14}C dates, valid for the whole Northern Hemisphere, can be established for the second half of the 20th century.

INTRODUCTION

The concentration of $^{14}CO_2$ in the atmosphere is a result of natural events, e.g., the production of radioactive carbon dioxide in the stratosphere due to cosmic rays, the stratosphere-troposphere mixing, lateral mixing in the stratosphere, ocean upwelling, exchanges with the terrestrial biosphere, and the radioactive decay of radiocarbon, as well as anthropogenic events like the combustion of fossil fuel and nuclear weapons explosions. For this reason, fluctuations in ^{14}C concentrations in the atmosphere can be used as a tracer for human activity on a local as well as on a global scale. The ^{14}C concentration in tree-ring samples from southern Italy has been measured in order to determine the ^{14}C excess resulting from the nuclear detonations carried out in the atmosphere after World War II. The first aim of the present work was to construct a local calibration curve to be used as a reference for high-resolution ^{14}C dating of recent samples. A comparison of the new data with other data sets already published is intended to make a contribution to the question of whether a bomb peak calibration curve, valid for the whole Northern Hemisphere, can be established.

METHODS: SAMPLE PREPARATION AND AMS MEASUREMENTS

A medium-sized pine tree (*Pinus pinea*) grown in an open field in a suburban area surrounding Brindisi in southern Italy (lat 40°65′N) was chosen for the analysis. The sampling location was chosen in an agricultural area where, in the studied time range, no human activities occurred that could influence the ^{14}C concentration in the air.

The samples were taken from the tree using an increment borer of the type normally used in dendrochronological studies, with an outer diameter of 4 mm and a length of 500 mm. The dendrochronological dating of the rings was accurate because of the clear ring structure of the tree and was verified by ring-width measurements and by comparison with other living pines grown in the same region.

Eighteen samples were selected and prepared for accelerator mass spectrometry (AMS) analysis, with an annual resolution in the peak area between 1959 and 1967. The earlywood of each ring was isolated, split, and then crushed to pieces of about 1-mm length in order to increase the effectiveness of the preparation process. Depending of the ring width, between 20 and 120 mg of sample material was prepared using the common acid-alkali-acid method:

1. Acid attack with HCl (10 mL, 1 M) for 10 hr at room temperature;
2. Rinsing with deionized water to pH = 5;

[1]Corresponding author. Email: gianluca.quarta@unile.it.

3. Alkali attack with NaOH (10 mL, 1M) at 60 °C;
4. Rinsing with deionized water to pH = 7;
5. Acid attack (10 mL, 1 M) for 10 hr;
6. Rinsing with deionized water.

Since the sample preparation procedure used (AAA) allows the removal only of the soluble fraction of the wood structure but not the separation of the lignin part, which should be more susceptible to contamination than cellulose (Hoper et al. 1998), for some rings the cellulose component was also extracted (Hua et al. 2000) and dated. Since no significant differences were found when comparing the ^{14}C concentration of the insoluble fraction and of the cellulose of the same ring, we think that, at least for the studied samples, the contamination induced in the lignin component is negligible.

The obtained purified material (insoluble fraction) was then dried for 3 days at 60 °C. Approximately 8 mg of pretreated material per sample was selected for combustion to CO_2 at 900 °C in a sealed quartz tube together with CuO and silver wool. The CO_2 sample thus obtained was purified and cryogenically transferred to graphitization cells, where it was reduced to graphite using H_2 as the reducing agent and iron powder as the catalyst (D'Elia et al. 2003). Each sample produced enough graphite, 1 mg on average, to allow precise measurements in the accelerator.

The AMS measurements were carried out at the AMS facility of the University of Lecce (Calcagnile et al. 2003) using IAEA C6 (sucrose) standards as a reference and the NIST Oxalic Acid II standard for quality and accuracy control. The $^{14}C/^{12}C$ ratios were corrected for sample preparation and accelerator background and normalized for mass fractionation to –25‰ by using the ^{13}C value measured directly with the accelerator (Calcagnile et al., forthcoming). The $\Delta^{14}C$ value was obtained from the $^{14}C/^{12}C$ ratio, after correcting it for the radioactive decay of both the standard and the sample from 1950 and from the year of growth, respectively (Stuiver and Polach 1977; Hajdas 1993).

RESULTS AND DISCUSSION

The measured $\Delta^{14}C$ and $\delta^{13}C$ terms are listed in Table 1. Figure 1 shows the $\Delta^{14}C$ values measured for the pine and, for comparison, the tree-ring records from 2 other sites in the Northern Hemisphere: Acacia, Hungary (47°35′N) (Hertelendi et al. 1982), and Arizona, USA (32°N) (Goodsite et al. 2001). Comparison of the plotted curves shows that the tree-ring records obtained for southern Italy follow the general trend observed for the other sites in the temperate Northern Hemisphere, in particular the highest $\Delta^{14}C$ value as observed in 1964 (Hua et al. 2000) and a small drop in the ^{14}C concentration seen in 1960–1961, which can be explained as the result of a temporary halt to nuclear detonations in that period due to the "Geneva Convention of Experts for the Discontinuance of Nuclear Weapons." Some significant differences in the maximum value of the ^{14}C concentration occur in the time range between 1963 and 1965. In particular, the data obtained for southern Italy fit surprisingly well with the data from Arizona, while the peak value for Hungary is significantly higher. To explain this, the atmospheric circulation has to be taken into account. In particular, several authors (Dai and Fan 1986; Dai et al. 1992; Levin et al. 1985) have tried to explain this effect as a result of a latitudinal gradient in the $^{14}CO_2$ concentration generated by the injection of ^{14}C-enriched air into the troposphere from the stratosphere during the tree growing season (from spring to early summer). If this is the case, the ^{14}C concentration in the tree rings should be higher when compared with the annual averaged atmospheric value. In order to check this, we compared our data with the "atmospheric" calibration curve averaged over the whole year (solid line in Figure 1) and that one averaged over the tree growing season (dashed line in Figure 1) as reported by Goodsite et al. (2001).

Table 1 Measured $\Delta^{14}C$ and $\delta^{13}C$ values for the pine (suburban area).

	Pine (suburban area)	
Ring (year AD)	$\Delta^{14}C$ (‰)	$\delta^{13}C$ (‰)
1955	37.8 ± 8.1	–24.6 ± 0.3
1959	271.0 ± 8.5	–25.0 ± 0.3
1960	213.7 ± 10.0	–24.7 ± 0.3
1961	246.8 ± 10.0	–22.2 ± 0.2
1962	367.3 ± 10.0	–22.8 ± 0.2
1963	587.2 ± 6.6	–24.6 ± 0.1
1964	821.2 ± 11.3	–24.8 ± 0.1
1965	743.9 ± 11.8	–24.8 ± 0.2
1966	689.1 ± 15.2	–30.5 ± 0.5
1967	619.6 ± 10.7	–24.2 ± 0.1
1971	504.4 ± 9.7	–22.5 ± 0.2
1975	403.0 ± 8.8	–23.2 ± 0.4
1979	295.3 ± 9.0	–24.8 ± 0.1
1983	236.0 ± 9.0	–23.5 ± 0.1
1987	194.4 ± 8.7	–27.5 ± 0.2
1991	158.6 ± 8.3	–27.4 ± 0.3
1995	128.4 ± 8.5	–23.6 ± 0.3

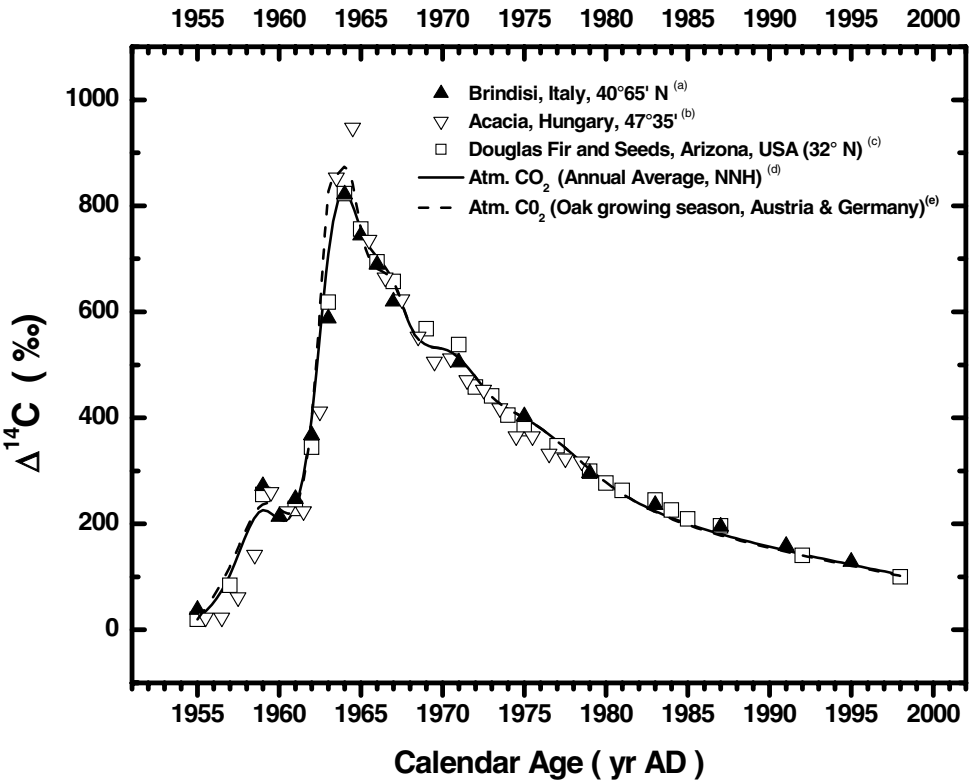

Figure 1 ^{14}C concentration in tree rings versus the calendar age: a) tree-ring data (insoluble fraction) from a living pine (*Pinus pinea*) in Brindisi (Italy), 40°N (see Table 1); b) tree-ring data from Acacia, Hungary (Hertelendi et al. 1982); c) tree-ring and seeds (Douglas fir and cotton) data from Arizona (USA), 32°N (Goodsite et al. 2001); d) annual averaged $^{14}CO_2$ curve for the 30–90° latitude band (Goodsite et al. 2001); e) atmospheric $^{14}CO_2$ from Austria and Germany (48°N) (Levin et al. 1997; Goodsite et al. 2001) averaged only for the oak growing season (April to August).

From Figure 1, it is clear that our data follow the annual averaged "atmospheric" curve very well, and no higher values are observed in the ^{14}C concentration in the tree rings. For this reason, although a latitude dependence is present, these data seem to point towards the absence of seasonal variations related to the injection of air from the stratosphere in the tree growing season at least at the studied latitude. In order to confirm this still preliminary conclusion, other investigations are being carried out by comparing the ^{14}C concentration in the earlywood and latewood portions of the same ring (Olsson and Possnert 1992).

CONCLUSIONS

A new bomb pulse record has been obtained for southern Italy at a latitude of 40°N by measuring the ^{14}C concentration in the rings of a living pine tree (*Pinus pinea*). The results, which are in good agreement with the data sets already available for other tree-ring records, are intended to contribute to the studies of the atmospheric circulation, of the global carbon cycle, and of the atmosphere-oceans interactions. A calibration curve valid for the ^{14}C dates has been also established. As already done by others (Goodsite et al. 2001), it needs to be emphasized that the calibrated ages obtained with the present data sets and those obtained with any of the others already available for the Northern Hemisphere are in good agreement (within 1–2 yr).

ACKNOWLEDGMENTS

We wish to thank Mr Umberto Toma and Mr Lucio Maruccio for their help during sampling and Prof Livio Ruggiero for the helpful discussions about dendrochronological methods.

REFERENCES

Calcagnile L, Quarta G, D'Elia M, Rizzo A, Gottdang A, Klein M, Mous DJW. Forthcoming. A new accelerator mass spectrometry facility in Lecce, Italy. In: Proceedings of the 9th AMS Conference, Nagoya, Japan, 2003. *Nuclear Instruments and Methods in Physics Research B*.

Calcagnile L, Quarta G, D'Elia M, Gottdang A, Klein M, Mous DJW. Forthcoming. Radiocarbon precision tests at the Lecce AMS facility using a sequential injection system. *Nuclear Instruments and Methods in Physics Research B*.

Day KM, Fan CY. 1986. Bomb-produced ^{14}C content in tree rings grown at different latitudes. *Radiocarbon* 28(2A):346–9.

Day KM, Quian Y, Fan CY. 1992. Bomb-produced ^{14}C in tree rings. *Radiocarbon* 34(3):753–6.

D'Elia M, Calcagnile L, Quarta G, Sanapo C, Laudisa M, Toma U, Rizzo A. Forthcoming. Progress at the sample preparation laboratory of the Lecce AMS facility. In: Proceedings of the 9th AMS Conference, Nagoya, Japan, 2003. *Nuclear Instruments and Methods in Physics Research B*.

Goodsite ME, Rom W, Heinemeier J, Lange T, Ooi S, Appleby PG, Shotyk W, van der Knaap WO, Lohse C, Hansen TS. 2001. High-resolution AMS ^{14}C dating of post-bomb peat archives of atmospheric pollutants. *Radiocarbon* 43(2B)495–515.

Hajdas I. 1993. Extension of the radiocarbon calibration curve by AMS dating of laminated sediments of Lake Soppensee and Lake Holzmar [PhD dissertation]. Zürich: Eidgenössische Technische Hochschule.

Hertelendi E, Csongor E. 1982. Anthropogenic ^{14}C excess in the troposphere between 1951 and 1978 measured in tree rings. *Radiochemical and Radioanalytical Letters* 56:103–10.

Hoper ST, McCormac FG, Hogg AG, Higham TFG, Head MJ. 1998. Evaluation of wood pretreatments on oak and cedar. *Radiocarbon* 40(1):45–50.

Hua Q, Barbetti M, Jacobsen GE, Zoppi U, Lawson EM. 2000. Bomb radiocarbon in annual tree rings from Thailand and Tasmania. *Nuclear Instruments and Methods in Physics Research B* 172:359–65.

Levin I, Kromer B, Schoch-Fisher H, Bruns M, Münich M, Berdau D, Vogel JC, Münich KO. 1985. 25 years of tropospheric ^{14}C observations in central Europe. *Radiocarbon* 27(1):1–19.

Olsson IU, Possnert G. 1992. ^{14}C activity in different sections and chemical fractions of oak tree rings, AD 1938–1981. *Radiocarbon* 34(3):757–67.

Stuiver M, Polach HA. 1977. Discussion: reporting of ^{14}C data. *Radiocarbon* 19(3):355–63.

RADIOCARBON, Vol 47, Nr 1, 2005, p 31–37

RECONSTRUCTION OF THE ^{14}C PRODUCTION RATE FROM MEASURED RELATIVE ABUNDANCE

Ilya G Usoskin

Sodankylä Geophysical Observatory (Oulu unit), P.O. Box 3000, FIN-90014 University of Oulu, Finland.
Email: Ilya.Usoskin@oulu.fi.

Bernd Kromer

Heidelberger Akademie der Wissenschaften, Institut für Umweltphysik, INF 229, D-69120 Heidelberg, Germany.
Email: Bernd.Kromer@iup.uni-heidelberg.de.

ABSTRACT. A new method is presented for the reconstruction of the radiocarbon production rate from the measured relative abundance of $\Delta^{14}C$. The method treats the carbon cycle as a linear Fourier filter and thus allows for the correct and unambiguous inversion of the carbon cycle. The ^{14}C production rate, as reconstructed by the Fourier filter method, agrees with the results obtained by the traditional iteration method. Since the 2 methods use completely different approaches, this verifies the validity of the reconstruction. The composite series is presented, based on both methods and their systematic uncertainties.

INTRODUCTION

Information on the cosmic ray flux in the past is of great importance for solar and heliospheric physics as well as for the study of solar-terrestrial relations on long time scales (e.g. Stuiver et al. 1991; Bond et al. 2001). For the time before the era of direct observations of sunspots and related phenomena like aurorae, only cosmogenic isotopes such as ^{14}C, ^{10}Be, and ^{36}Cl can provide a quantitative reconstruction of the cosmic ray flux. Although the radiocarbon production rate is directly proportional to the flux of cosmic rays with energy around a few GeV/nucleon impinging on Earth (Castagnoli and Lal 1980; Alanko et al. 2003), the direct comparison of the relative ^{14}C abundance in tree rings ($\Delta^{14}C$) with the cosmic ray flux is not straightforward. Several processes disturb the cosmic ray signal in the relative ^{14}C concentration in natural archives. One process is related to the long-term changes of the geomagnetic field which shields Earth from low-energy cosmic rays. Using independent paleomagnetic data, one can take this effect into account. The most important process distorting the cosmic signal in $\Delta^{14}C$ is the complex carbon cycle, which effectively leads to attenuation and variable time delay of the cosmic ray signal. While the carbon cycle has been successfully modeled and the measured $\Delta^{14}C$ series can be precisely calculated if the ^{14}C production rate is known from other sources (Siegenthaler et al. 1980; Bard et al. 1997), an inversion of this process (i.e. reconstruction of the production rate from the measured concentration) is not straightforward. Some attempts have been made to solve this problem. For example, Stuiver and Quay (1980) made an assumption on the ^{14}C production rate and then fitted the calculated $\Delta^{14}C$ variations to the actual measurements. Kocharov et al. (1977) suggested to extract a few basic periodicities from the original signal and to treat them separately, but they did not reconstruct the production rate. Kocharov et al. (1983) solved, under simplifying assumptions, a system of linear differential equations describing a 5-reservoir carbon cycle model to determine the ^{14}C production rate. However, their results appeared to be dependent on the assumption of the cosmic ray spectrum. In this paper, we suggest a new method to reconstruct the ^{14}C production rate from the measured $\Delta^{14}C$ which treats the carbon cycle as a Fourier filter, and compare it to the earlier method based upon an iteration approach using the carbon cycle model.

CARBON CYCLE AND THE OESCHGER-SIEGENTHALER BOX MODEL

The carbon cycle in the interrelated system atmosphere-biosphere-ocean is usually described using a box model where the carbon cycle is represented by fluxes between different carbon reservoirs and mixing within the ocean reservoir(s). For the purpose of studying ^{14}C, production and radioactive decay are also included in box models. Free parameters in the Oeschger-Siegenthaler type box model (Oeschger et al. 1974; Siegenthaler et al. 1980) are the ^{14}C production rate Q, the air-sea exchange rate (expressed as turnover rate k), and the vertical eddy diffusion coefficient K, which combines ocean ventilation into a single parameter. Starting from the original representation (Oeschger et al. 1974), a variety of box models have been developed which take into account subdivisions of the ocean reservoir and direct exchange between the deep ocean and the atmosphere at high latitudes. These models have been run in prognostic mode for which the time series of parameter variations are prescribed, such as a reduction in ocean ventilation or sea-ice cover, and the response of the atmospheric $\Delta^{14}C$ level is obtained as output of the model. Obviously, box models of higher complexity allow more realistic scenarios to be tested, but they require a prescription of a larger number of model parameters. However, for the inversion of the model, i.e. to evaluate the ^{14}C production rate Q from the variations of $\Delta^{14}C$ to first order, only the production rate is considered variable, while the gas-exchange rate and ocean mixing are kept constant. Hence, any subdivision of reservoirs or processes would not make sense and the simplest version of a carbon box model is sufficient for this goal. In order to reconstruct the ^{14}C production rate, we ran a version of the Oeschger-Siegenthaler box model (Born 1994) using the pre-industrial steady-state values (K = 4200 m^2yr^{-1}, k = 1/6.9 yr) and a steady-state ocean-depth profile of ^{14}C based on $\Delta^{14}C$ = 135‰ in the top ocean box at the time of the start of the run (11.445 BP). The ^{14}C production rate has been calculated iteratively in each time step (0.01 yr) as the difference between the observed $\Delta^{14}C$ measured in absolutely dated tree rings (interpolated from the decadal data of IntCal98, Stuiver et al. 1998) and the model-calculated $\Delta^{14}C$. The production rate is obtained relative to the modern production rate of 2.2 atoms $cm^{-2}s^{-1}$, although this value may be higher than the steady-state production calculated from the ^{14}C inventory in the model reservoirs (see, e.g., Goslar 2001 and references therein).

CARBON CYCLE AS A FOURIER FILTER

All carbon cycle models consist of a system of linear differential equations describing the carbon exchange between several reservoirs. Consequently, such a process works as a linear Fourier filter—i.e. it does not change the shape of a propagating harmonic signal so that a sine wave is amplified/attenuated and phase-shifted, but its frequency remains the same when propagating through this process either in forward or in backward direction. In such circumstances, the carbon cycle can be considered as a Fourier filter process *G*. Let us denote the functions describing the ^{14}C production rate as Q and q and those for the $\Delta^{14}C$ abundance as D and d, where capital and small letters denote the functions in the time (t) and frequency (f) domains, respectively. We denote the direct and backward Fourier transform operations as F and F^{-1} so that

$$q(f) = F[Q(t)] \equiv \int_{-\infty}^{\infty} Q(t) e^{2\pi i f t} dt \tag{1}$$

$$Q(t) = F^{-1}[q(f)] \equiv \int_{-\infty}^{\infty} q(f) e^{-2\pi i f t} df$$

Using this formalism, the carbon cycle can be formally presented as follows:

$$Q(t) \xrightarrow{F} q(f) \xrightarrow{G} d(f) \xrightarrow{F^{-1}} D(t) \tag{2}$$

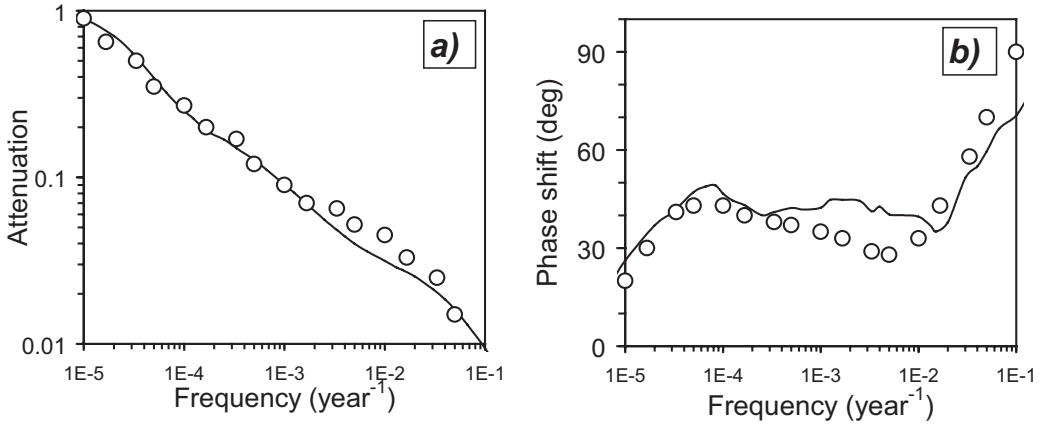

Figure 1 The frequency characteristics of the attenuation and phase-shift coefficients in the carbon atmospheric transport model: line - according to the Oeschger-Siegenthaler box model (Born 1994) used here, and open dots - according to the PANDORA model (e.g. Bard et al. 1997).

First, the original signal (the production rate, *Q[t]*) is transformed to the Fourier series *q(f)*, then the filter *G* describing the carbon transport model is applied to obtain the Fourier representation *d(f)* of the $\Delta^{14}C$ series. Finally, *d(f)* is transformed back to the time series *D(t)* of $\Delta^{14}C$. Since the filter *G* is linear in the frequency domain, the chain (2) can be unambiguously inverted,

$$Q(t) \xrightarrow{F^{-1}} q(f) \xrightarrow{G^{-1}} d(f) \xrightarrow{F} D(t) \tag{3}$$

so that by decomposing the measured $\Delta^{14}C$ series, passing it through the (inverted) filter and composing it again, one can obtain the time series of the ^{14}C production rate. Based upon the general approach described above, we now consider the details of the ^{14}C production rate reconstruction. In our calculations, we use the FFT method, substituting the integrals in Equation 1 by a finite sum,

$$Q_k = Q(k\Delta t) = \sum_{m=-N/2}^{N/(2-1)} q_m e^{(2\pi imt)/(N\Delta t)} \tag{4}$$

$$q_k = \sum_{m=-N/2}^{N/(2-1)} Q_m e^{[(-2)\pi imk]/N}$$

where Δt is the sampling rate and N is the number of the points in the series. The frequency domain representation is $q_k \equiv R(q_k) \exp[i\phi(q_k)]$, where $R(q_k)$ and $\phi(q_k)$ are the amplitude and phase of q_k, respectively. The frequency characteristics of amplification/attenuation and phase-shift coefficients, also called Bode plots (Bode 1945), completely define a process (Jenkins and Watts 1969). The Bode plots of the filter *G* corresponding to the Oeschger-Siegenthaler box model (Born 1994) are shown in Figure 1 together with the frequency characteristics of the 12-box PANDORA model (e.g. Bard et al. 1997). Applying this filter *G* to the series q_k, one can obtain the series $d_k = G(q_k)$ as follows:

$$R(d_k) = A_k \times R(q_k),\ \phi(d_k) = \phi(q_k) + \phi_k \tag{5}$$

where A_k and ϕ_k are the attenuation coefficient and the phase shift for the k^{th} frequency, respectively (see Figure 1). Inverting the filter, one can obtain the Fourier series $q_k = G^{-1}(d_k)$ from d_k:

$$R(q_k) = R(d_k) / A_k,\ \phi(q_k) = \phi(d_k) - \phi_k \quad (6)$$

The representations of the series *q(f)* and *d(f)* in the frequency domain are shown in Figure 2. By applying the inverse Fourier transform, we obtain the ^{14}C production rate *Q(t)* from *q(f)*.

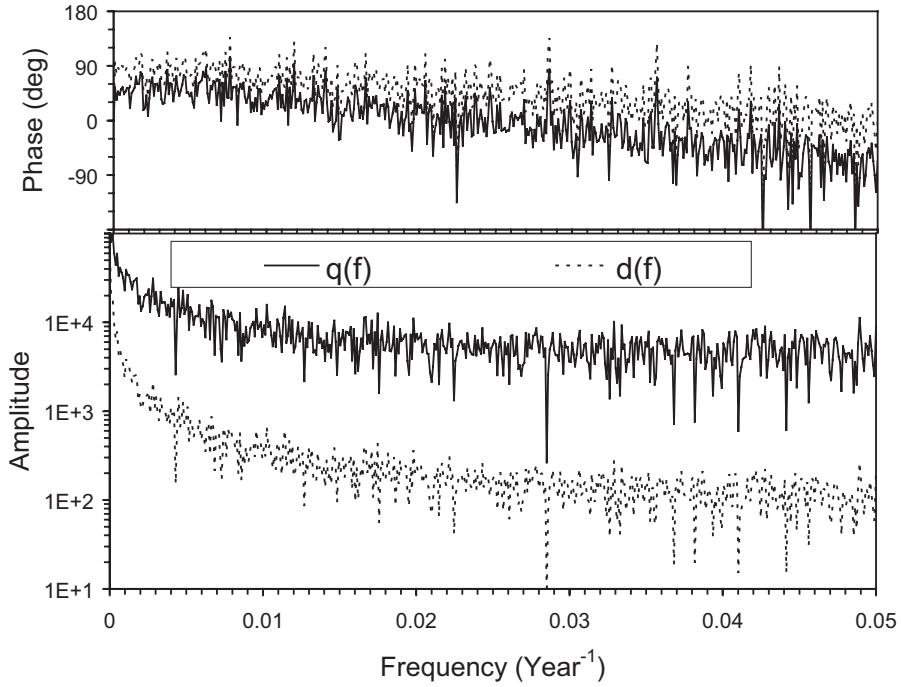

Figure 2 The representations of the production rate *q(f)* (solid line) and the Δ^{14}C series *d(f)* (dotted line) in the frequency domain. The top and bottom panels depict the phase and amplitude, respectively.

The Fourier filter approach provides a useful tool to study cosmic ray flux in the past using the ^{14}C data. Once the frequency characteristics (amplification and phase-shift coefficients) of the carbon transport model are calculated, the method can be readily applied. However, this approach has some shortcomings. Its application is hardly possible for frequencies higher than 0.1 yr^{-1} since the very strong attenuation coefficient in the high-frequency range results in amplification of the noise that is always present in the measured data due to, e.g., local fluctuations of the carbon deposition or due to measurement errors. Accordingly, the high-frequency part of the reconstructed series is dominated by the amplified noise. Another limitation of the method for high frequency is that it substitutes the real-time delay, τ_k, in the carbon cycle for a frequency f_k (corresponding to period T_k) with a phase shift $\phi_k = 2\pi\tau_k/T_k$. This is possible only if the time delay is shorter than half of the period in the signal ($\tau_k < T_k/2$), which is not correct for the high-frequency part of the model and leads to the saturation of the phase shift at 90° ($\pi/2$) for periods shorter than 10 yr (see Figure 1). Therefore, this method cannot reconstruct annual data but requires sampling or low-pass smoothing of the data series with the frequency lower than 0.1 yr^{-1}. Also, the reconstructed data become uncertain near the beginning of the time series because the effective phase shift refers to the unavailable earlier data. This is equivalent to the uncertainties of the initial conditions in the iteration method.

RESULTS

We have presented a reconstruction of the ^{14}C production rate from the relative abundance $\Delta^{14}C$ measured in tree rings, with decadal resolution (Stuiver et al. 1998), using the 2 different approaches described above. Both methods yield similar results. An example of the 2 reconstructions of Q is shown in Figure 3 for the last 2 millennia together with the measured $\Delta^{14}C$. The 2 reconstructed series of the production rate nearly coincide with each other during this as well as during the entire 11,400-yr time intervals (Figure 4). Taking into account that the 2 reconstructions have been performed using very different methods—the iteration fitting procedure and the Fourier filter approach, both based upon the same description of the carbon cycle (Born 1994)—the present result verifies both methods for reconstruction of the ^{14}C production rate. We note that using the frequency characteristics of another carbon cycle model, the 12-box PANDORA model (Bard et al. 1997), leads to the very similar results. However, we would like to stress that both methods assume steady-state conditions at the beginning of the reconstruction and the subsequent $\Delta^{14}C$ in the atmosphere defined solely by changes in the production rate. While variability in the carbon cycle is believed to be rather small during the Holocene and production changes are considered to dominate the decadal- to century-scale $\Delta^{14}C$ fluctuations, the assumption of the steady-state initial condition is possibly invalid for the first few millennia following deglaciation.

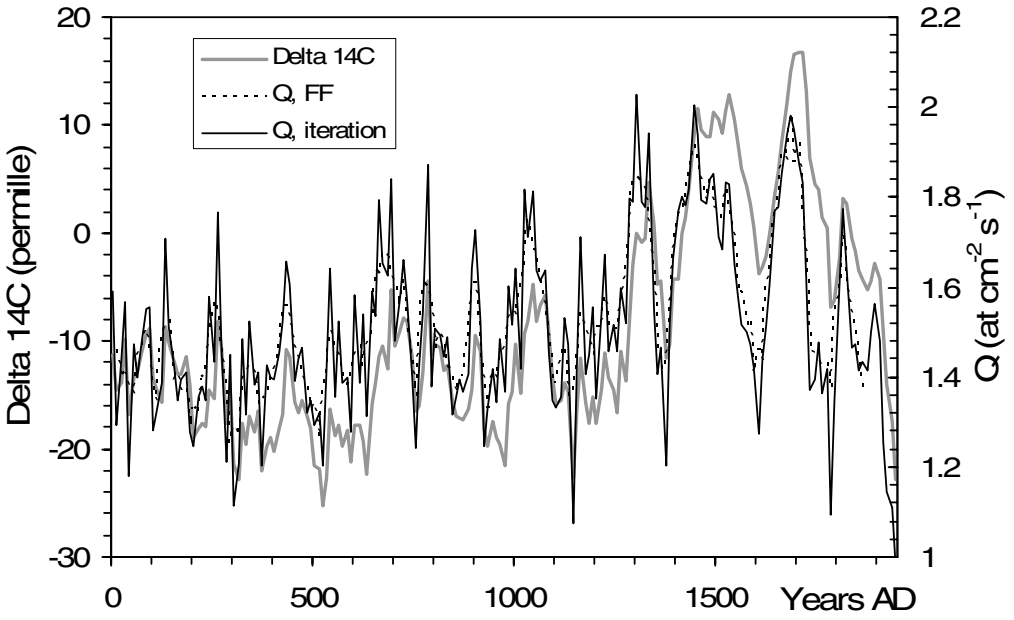

Figure 3 The ^{14}C profiles for the last 2 millennia. The measured decadal $\Delta^{14}C$ (Stuiver and Braziunas 1993) is shown by the gray curve (left axis). The reconstructed ^{14}C production rate Q (right axis) is shown for the iteration method (solid bold curve) and for the Fourier filter (dashed curve) approach.

A composite ^{14}C production rate series, which is the average of the 2 reconstructed series, is given in the upper panel of Figure 5, while the lower panel shows the deviations between the individual and the average series, which serves as a measure of the model uncertainty. The standard deviation is 0.04 (atoms $cm^{-2}s^{-1}$). The mean deviation is zero, and only beyond 11,000 BP do the 2 series start diverging due to the uncertainties near the beginning of the series. Accordingly, our reconstructed ^{14}C production rate series is verified by the 2 very different techniques.

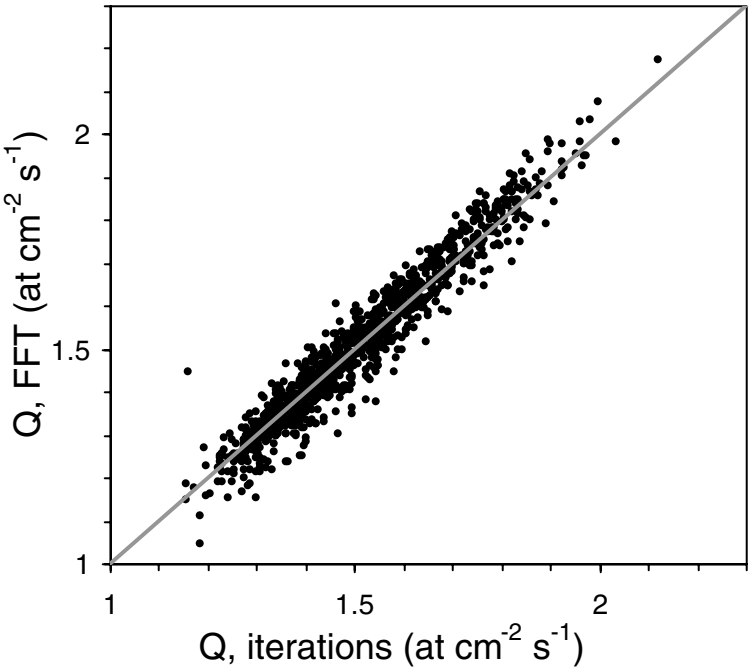

Figure 4 Scatter plot of the ^{14}C production rate Q reconstructed since 11,400 BP by the 2 different approaches: the iteration method and the Fourier filter.

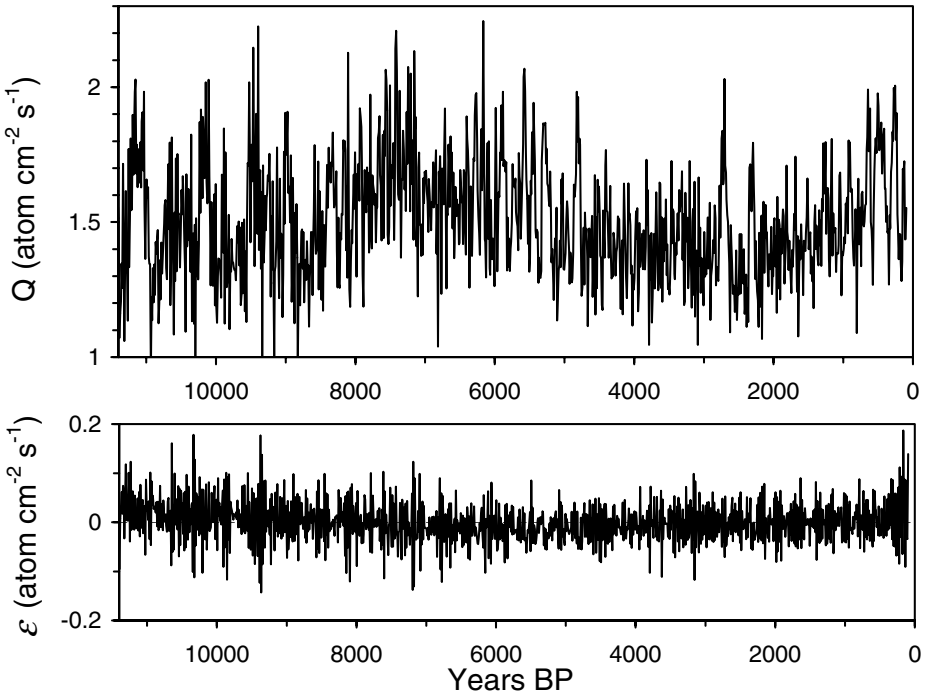

Figure 5 The ^{14}C production rate Q composed as the average of the 2 reconstructions (upper panel) and the systematic errors of the production rate due to the difference in reconstruction methods (bottom panel).

CONCLUSION

The composite series presented here of the ^{14}C production rate on the multi-millennium time scale has important implications for the long-term studies of cosmic rays, solar and heliosphere physics, solar-terrestrial relations, climate, etc. For example, it is common to check the consistency of the ^{10}Be and ^{14}C cosmogenic isotope data by assuming that the ^{14}C production rate is proportional to the ^{10}Be concentration in polar ice, calculating the expected $\Delta^{14}C$ employing a direct carbon cycle model and comparing it to the measured $\Delta^{14}C$ (e.g. Bard et al. 1997). The approach suggested here permits for a direct comparison of the ^{14}C production rate to ^{10}Be data and to study their common features and discrepancies.

ACKNOWLEDGMENTS

We thank Jürg Beer, Gennady Kovaltsov, Manfred Schüssler, and Sami Solanki for stimulating discussions and comments on the manuscript.

REFERENCES

Alanko K, Usoskin IG, Mursula K, Kovaltsov GA. 2003. Effective energy of Neutron Monitor. *Proceedings of the 28th International Cosmic Ray Conference*. Tokyo: Universal Academy Press. p 3901–4.

Bard E, Raisbek GM, Yiou F, Jouzel J. 1997. Solar modulation of cosmogenic nuclide production over the last millennium: comparison between ^{14}C and ^{10}Be records. *Earth and Planetary Science Letters* 150: 453–62.

Bode HW. 1945. *Network Analysis and Feedback Amplifier Design*. New York: Van Nostrand. 577 p.

Bond G, Kromer B, Beer J, Muscheler R, Evans M, Showers W, Hofmann S, Lotti-Bond R, Hajdas I, Bonani G. 2001. Persistent solar influence on North Atlantic surface circulation during the Holocene. *Science* 294:2130–6.

Born M. 1994. Optimierung eines Messsystems zur ^{14}C-Aktivitätsbestimmung mit Proportionalzählrohren [PhD dissertation]. Heidelberg: University of Heidelberg. 81 p.

Castagnoli G, Lal D. 1980. Solar modulation effects in terrestrial production of carbon-14. *Radiocarbon* 22(2):133–58.

Goslar T. 2001. Absolute production of radiocarbon and the long-term trend of atmospheric radiocarbon. *Radiocarbon* 43(2B):743–9.

Jenkins GM, Watts DG. 1969. *Spectral Analysis and Its Applications*. London: Holden-Day. 525 p.

Kocharov GE, Arslanov KA, Dergachev VA, Tleugaliev SK, Chernov SB. 1977. Cyclic activity of the sun and the radiocarbon content in tree rings. *Soviet Astronomical Letters* 3(5):257–8.

Kocharov GE, Vasilev VA, Dergachjev VA, Ostryakov VM. 1983. An 8000-year sequence of galactic cosmic-ray fluctuations. *Soviet Astronomical Letters* 9(2): 110–2.

Oeschger H, Siegenthaler U, Schotterer U, Gugelmann A. 1974. A box diffusion model to study the carbon dioxide exchange in nature. *Tellus* 27(2):168–92.

Siegenthaler U, Heimann M, Oeschger H. 1980. ^{14}C variations caused by changes in the global carbon cycle. *Radiocarbon* 22(2):177–91.

Stuiver M, Braziunas TF, Becker B, Kromer B. 1991. Climatic, solar, oceanic, and geomagnetic influences on Late Glacial and Holocene atmospheric $^{14}C/^{12}C$ change. *Quaternary Research* 35:1–24.

Stuiver M, Quay P. 1980. Patterns of atmospheric ^{14}C changes. *Radiocarbon* 22(2):166–76.

Stuiver M, Reimer PJ, Bard E, Burr GS, Hughen KA, Kromer B, McCormac G, van der Plicht J, Spurk M. 1998. IntCal98 radiocarbon age calibration, 24,000–0 cal BP. *Radiocarbon* 40(3):1041–83.

Suess HE. 1955. Radiocarbon content in modern wood. *Science* 122:415–7.

RADIOCARBON UPDATES

Rodger Sparks Retires

After serving many years as the leader of the Rafter Radiocarbon Laboratory in Lower Hutt, New Zealand, Dr. Rodger Sparks recently announced his retirement. Dr. Christine Prior is taking over leadership of the lab. The radiocarbon community is indebted to Rodger's achievements in ^{14}C dating, and we wish him the best for a happy and well-deserved retirement. We would also like to welcome to the *Radiocarbon* editorial board Nancy Beavan Athfield, who is replacing Rodger Sparks.

VIRI Results Needed

Dr. Marian Scott asks that all labs who have not yet done so, please email their VIRI results as soon as possible to marian@stats.gla.ac.uk.

Upcoming Conferences

AMS 10th Annual Conference Circular

The 10th International Conference on Accelerator Mass Spectrometry (AMS-10) will be hosted by Lawrence Livermore National Laboratory's Center for Accelerator Mass Spectrometry. The conference will take place September 5–10 on the campus of the University of California, Berkeley. The purpose of the conference is to provide a forum for scientists to present and discuss recent developments in AMS technology and applications. The conference Web site is http://ams10.ucdavis.edu/.

LSC 2005 Conference: Advances in Liquid Scintillation Spectrometry

The Central Mining Institute will host the LSC 2005 Conference, and *Radiocarbon* will publish the proceedings of the conference. The conference will be held in Katowice, the capital city of Upper Silesia, Poland, from October 17–21, 2005. The organizers welcome you to present your achievements, to learn the latest developments of your colleagues, and to enjoy the traditional hospitality of the Polish people.

The main goal of the conference is to provide a forum for all scientists working in areas related to liquid scintillation counting and spectrometry. The conference will enable and promote the exchange of information, the development of future directions in LSC, and the opportunity to meet old and new friends. The conference organizers would like to pay particular emphasis to environmental studies and applications. Participation of young scientists and students is highly encouraged.

Please check the conference Web site (http://www.gig.katowice.pl/gig/lsc.php) for news and updates or email conference chairman Stanisław Chałupnik (lsc@gig.katowice.pl) for further information.

19th International Radiocarbon Conference

The 19th International Radiocarbon Conference will be held in Oxford, at Keble College, from April 3–7, 2006. Further announcements about the conference will be sent out via email and posted on the conference Web site, http://www.rlaha.ox.ac.uk/orau/conference.html, and the *Radiocarbon* Web site.

RADIOCARBON, Vol 47, Nr 1, 2005, p 39–55

DATING THE IRON AGE I/II TRANSITION IN ISRAEL: FIRST INTERCOMPARISON RESULTS

Elisabetta Boaretto[1] • A J Timothy Jull[2] • Ayelet Gilboa[3] • Ilan Sharon[4]

ABSTRACT. Nearly a decade ago, a different chronology than the conventional absolute chronology for the early Iron Age in Israel was suggested. The new, lower chronology "transfers" Iron Age I and Iron Age IIA contexts in Israel, traditionally dated to the 11th and 10th centuries BCE, to the 10th and 9th centuries, respectively. Thus, it places the Iron I|IIA transition at about 920–900 BCE. This alternative chronology carries important implications for Israelite history, historiography, and Bible research, as well as for the chronologies of other regions around the Mediterranean. Relevant radiocarbon data sets published to date, which were measured at different sites by different laboratories, were claimed to be incompatible. Therefore, the question of agreement between laboratories and dating methods needs to be addressed at the outset of any study attempting to resolve such a tight chronological dilemma. This paper addresses results pertaining to this issue as part of a comprehensive attempt to date the early Iron Age in Israel based on many sites, employing different measuring techniques in 2 laboratories. The intercomparison results demonstrate that: a) the agreement between the 2 laboratories is well within the standard in the ^{14}C community and that no bias can be detected in either laboratory; and b) calculating the Iron I|IIa transition in 3 different ways (twice independently by the measurements obtained at the 2 labs and then by combining the dates of both) indicates that the lower chronology is the preferable one.

INTRODUCTION

Since 1996, when Finkelstein (1996) first published his suggestion to lower the beginning of Iron Age IIA in Israel from the 10th century BCE (conventional, High Chronology [HC]) to the 9th century BCE (Low Chronology [LC]), the question has not been resolved. Due to the scarcity of stratified artifacts datable on their own merit to the 11th–9th BCE range, the discussion has relied mainly on correlations of Iron Age strata with historical scenarios, based mainly on differing interpretations of the biblical text.

Regions such as Cyprus and Greece, which lack substantial anchors of absolute chronology in the early Iron ages, are directly affected by the Levantine dates. Indeed, the relevance of this dating question for diverse cultural issues regarding the Mediterranean "Dark Ages" and their aftermath has been noted by various authors (e.g. Fantalkin 2001; Gilboa and Sharon 2001, 2003; Kopcke 2002; Coldstream and Mazar 2003; Coldstream 2003; Mazar 2004). Recently, one of the main protagonists of the HC, A Mazar, conceded that Iron IIA indeed encompasses the 9th century, as suggested by the LC (e.g. Mazar 2004:30–31). Thus, the debate now concerns the beginning of Iron IIA—whether or not it should it be placed at about 1000–980 BCE, as maintained by HC adherents, or about 920 BCE, as claimed by LC adherents. This difference of approximately 60 yr is very close to the radiocarbon precision limit. Can ^{14}C dating be solicited to decide this chronological dilemma?

THE TWO PREVIOUSLY PUBLISHED RADIOCARBON DATA SETS

Tel Dor

Gilboa and Sharon (2001) published a series of 22 radiometric dates from an early Iron Age stratified sequence at the coastal site of Tel Dor (Gilboa and Sharon 2001; Sharon 2001). These samples were measured by the Weizmann Institute of Science Radiocarbon Laboratory ("Rehovot")

[1]Radiocarbon Dating Laboratory, Weizmann Institute of Science, Rehovot, Israel 76100.
Corresponding author. Email: Elisabetta.Boaretto@weizmann.ac.il.
[2]NSF-Arizona AMS Laboratory, University of Arizona, Tucson, Arizona 85721, USA.
[3]Zinman Institute of Archaeology, University of Haifa, Mt. Carmel, Haifa, Israel 31905.
[4]Institute of Archaeology, Hebrew University, Jerusalem, Israel 91905.

employing liquid scintillation counting (LSC) and one measurement was done by Beta Analytic, Inc. using accelerator mass spectrometry (AMS). The transitions between the various early Iron Age phases at Tel Dor were calculated then using an algorithm ("transition dating") developed by Sharon (2001). The Iron I|IIA transition at Dor was determined to have occurred well within the 9th century, at around 880–850 BCE. Calculating the same transitions using the OxCal software produced consistent results with the Sharon algorithm (Gilboa and Sharon 2003: Figure 21). These results are thus compatible with the Low Chronology.

Tel Rehov

Bruins et al. (2003) published 34 ^{14}C measurements from 4 consecutive early Iron Age strata at the site of Tel Rehov in the Jordan Valley. These were analyzed by AMS and gas proportional counting (GPC) at the Center for Isotope Research at Groningen. The authors concluded that the transition between Iron Age I and IIA at Tel Rehov (between strata VII and VI) dates to ~980 BCE, about a hundred years earlier than the transition date calculated at Dor. This discrepancy was brushed away on the grounds that the Dor dates were "inconsistent" (Bruins et al. 2003:316), that the stratigraphic sequence at Dor is "complicated" (Coldstream and Mazar 2003), and/or that the dates produced at the Rehovot laboratory, at least in the 1990s, were consistently ~100 yr too low (Mazar 2004:31–34). In a later publication, Mazar presented 3 more dates from the same sequence at Rehov, also measured at Groningen (GrN-26119, GrA-12889, GrA-16848 in Table 1 of Mazar 2003), which were not included in the previous publication.

We calculated the boundaries between the dates of the Rehov strata using OxCal 3.5, considering all the Rehov (single) dates measured at Groningen. One date, GrN-26112 from L1802, was not used because its stratigraphical association is not secure enough—it cannot be assigned unambiguously to either Stratum V or VI. Initially, it was judged to belong to local Phase D-3 (Stratum VII, Iron Age I or I/II transition), and then moved to D-2 (Stratum V/VI, Iron Age IIA; Mazar, personal communication). This date is used (below) only for the purpose of intercomparison, where its exact context is unimportant. Note also that we followed Bruins et al. (2003: Table S1) in assigning locus 2425 to Stratum V. The local phasing of this silo, which produced quite a few dates analyzed in several laboratories (see below), is C-1b/a?—where C-1a is Stratum IV. As our interest is in pinpointing the date of the boundary between strata VII and VI, the distinction between strata V and IV is of lesser importance.

Running this model produces 3 measurements that display poor agreement with the rest of the sequence (misfits): GrN-26119, GrA-16848, GrN-26116. Figure 1 shows the transition between Iron Age I and IIA (the strata VII/VI boundary) after omitting these outliers. While the date proposed by Mazar et al. (980 BCE) is possible at the 68% confidence level, the distribution as a whole is much more compatible with the Low Chronology of 925 BCE. In Sharon et al. (forthcoming), we also calculated the same transition, taking into consideration Rehov dates produced at other ^{14}C laboratories (Rehovot and Tucson), with similar results. This analysis of the Rehov dates is in no way comprehensive. The point is that the Tel Rehov sequence is not nearly as unambiguous nor as decisive as has been suggested (e.g. Holden 2003).

Nevertheless, the Dor and Rehov data sets are not easily reconciled. Especially, dates from Iron Age IIA strata VI and V at Rehov (Bruins et al. 2003: Figure 2, Table S1) have significant 10th-century distributions, while at Dor this century lies well within Iron Age I.

This discrepancy could be accounted for in various ways: 1) the cultural (i.e. in this case, ceramic) horizon traditionally termed Iron IIA starts at Tel Rehov about 80 yr earlier than at Tel Dor (the sites

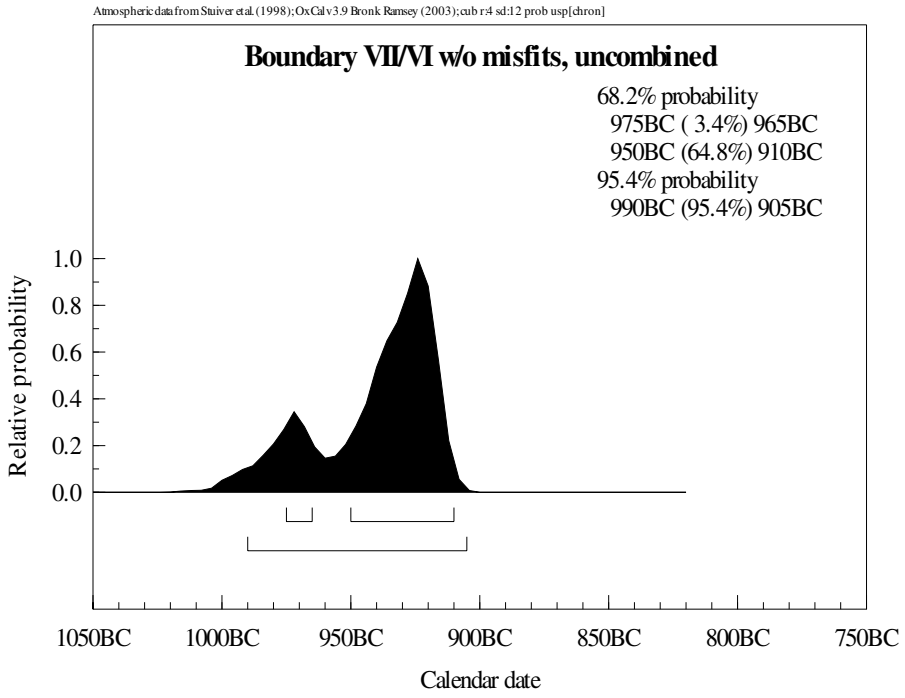

Figure 1 The Iron I/II transition at Tel Rehov based on all published Groningen dates, excluding misfits.

are about 100 km apart); 2) the terminological confusion regarding the ceramic characterization of the horizons (i.e. what the archaeologist at one site defines as Iron IIA differs from what is subsumed under this designation elsewhere); 3) the ceramic assemblages at the 2 respective sites are of very local nature and difficult to compare (this might account for either [1] and/or [2]); 4) the problem may also lie in the archaeological context from which the samples were taken (e.g. redepositions; see, e.g., Finkelstein and Piasetzky 2003); lastly, 5) the possibility of measurement bias between laboratories and/or dating methods (Mazar 2004:31–34).

Some of the archaeological questions have already been discussed (Gilboa and Sharon 2003, where the ceramic sequence of Dor is outlined). A major drawback here is that the Tel Rehov ceramic sequence has not been presented yet. In particular, the nature of the ceramic composition of the crucial Phase D-3 (= Stratum VII) is unclear. In Table S1 and the text of Bruins et al. (2003:317), it is defined as the Iron I/II transition, while in Mazar (1999:15–16) it is defined as Late Iron I. Even at this stage, however, there are enough clues to overcome these obstacles. Particularly, according to Mazar, Cypriot black-on-red and other contemporaneous Cypriot wares are evident at Tel Rehov at least as from Stratum V = Iron IIA, and possibly already in Stratum VI—the 10th century according to the Rehov team, or the last part of that century according to our calculations. At Dor, the same Cypriot wares first appear in the horizon termed there "Ir2a." Thus, these 2 horizons must be at least partially contemporary (and it is hardly conceivable that the occupations bearing these imports at inland Tel Rehov are earlier than the levels bearing the same imports at coastal Dor). However, the Ir2a horizon at Dor was ^{14}C dated to the 9th century BCE.

MATERIALS AND METHODS

Therefore, the purpose of this paper is to address the last possibility mentioned above—whether or not the problem may be found in a specific laboratory/method, and concurrently, whether ^{14}C analyses are accurate and precise enough to resolve the chronological question at hand.

With the current ^{14}C analytical precision (±30–35 yr), even ignoring additional uncertainties introduced by the calibration, differentiating between chronological hypotheses separated by less than a century is a challenge. Clearly, one needs to study as many sites as possible, using as many samples as possible. The samples must have a well-defined context and should ideally originate in occupations dating to immediately before and after the sought-for transition. It is also essential to know the precision and accuracy of the ^{14}C analyses themselves, which reflect sample preparation protocols as well as analytical procedures. It also has to be determined whether or not these factors vary during the duration of the study at any one laboratory, and most importantly, whether the accuracy of one lab is the same as that of another. Here, we address these issues as part of a larger study involving over 400 analyses from about 20 Iron Age sites in Israel. The results presented here are only those of samples that were measured by more than one laboratory or technique. The samples chosen for this intercomparison originate in archaeological contexts, the relative attribution of which, to either Iron Age I or II, are not in dispute (for most of them, see Tables 6–7 and pages 301, 372–373 of Mazar [1990]).

Laboratory Procedures

Since we were aiming for a higher resolution than ever attempted before in an archaeological project in the Levant, we imposed higher quality controls on our research than the current standard, including several methods specifically developed for this project.

To counter the effects of possible interlaboratory or intermethod bias, an elaborate protocol of replications was devised. ^{14}C analyses were performed in 2 laboratories, in Rehovot and at the University of Arizona ("Tucson"). In samples from which over 1 g of pure carbon could be obtained, decay counting (using LSC in Rehovot) was performed. AMS measurement was performed on all the samples in Tucson, and in almost all cases (except for extremely small samples) on triple targets. Some specimens were cleaned and pretreated in Rehovot and then analyzed in Tucson, and some were both prepared and analyzed in Tucson. For the latter, wood charcoal was homogenized in Rehovot before it was sent to Tucson, while charred seeds were sent intact.

Chemical pretreatment consisted of crushing the seeds to allow the solutions to interact with the material inside them, and charred wood was crushed and homogenized. The acid-base-acid procedure was applied in the following steps: 1 hr at 80 °C 1N HCl, 1–0.5%; NaOH as many times as required until the solution became clear; and 1 hr at 80 °C 1N HCl.

As an additional measure of control over the LSC measurements, part of the CO_2 produced for decay counting was converted to graphite and measured by AMS. Lastly, where possible, a portion of the original material from the samples was kept in the lab, so that if anomalies should be observed (in any one of the procedures), the entire experiment could be repeated.

Note that nearly all the samples were replicated in one form or another, some as many as 10 times or more. The average number of replications per sample was four.

Statistical Modeling

The first issues that need to be addressed are repeatability, reproducibility, and bias. Following Scott et al. (2003:219), we define *repeatability* as the degree of agreement between measurements on the same sample, made under identical conditions in one laboratory. *Reproducibility* refers to the degree of agreement between measurements of the same sample with different methods, under different conditions, or in different laboratories. Together, the repeatability and reproducibility constitute the precision of measurement. By *bias* (or inaccuracy), we refer to consistent differences between different methods, protocols, or laboratories. Within these issues, we need to consider the treatment of obviously aberrant results, as well as smaller deviations that may cause the actual spread of replicated results to be wider than the distribution expected under the quoted measurement error.

The Fourth International Radiocarbon Intercomparison (FIRI; Scott et al. 2003, see especially pages 213–218, 252–260, and Figures 7.1–7.7) demonstrates that while little or no bias can usually be detected between laboratories, ^{14}C measurements generally do not conform to the "ideal" standard distribution. The actual distribution under extensive replication is wider than the quoted errors. This effect is more noticeable in LSC than in AMS; it is also not related to sample age. Even after the exclusion of the more-obvious outliers and the recalculation of central moments, the observed distributions are wider than the theoretical expectation. Indeed, the case could hardly be different, for the quoted error denotes, at best, the variability within the same measurement run. Additional sources of error—such as variability due to different machines, different measurement protocols, different chemical cleaning and pretreatment, and even differences in storage conditions and length of storage prior to measurement—would all inevitably lead to a wider distribution than indicated by the individual measurement error.

Once outliers—or distributions in excess of the expected statistical errors—have been identified, the problem of how to treat them remains. The dilemma here is that, on the one hand, basing conclusions on data known to be partially faulty would not be prudent. On the other hand, the greatest danger in this sort of study is selectivity (explicitly or implicitly removing data that are not consistent with preconceived interpretations).

The experimental design we devised allows us to distinguish several types of outliers:

a) Intra-lab errors. A divergent result within a series of measurements, made under identical conditions in one laboratory. The probable source of error is the measurement itself.
b) Inter-lab inconsistencies. Divergent results between measurement methods or laboratories. The probable source of error here are laboratory procedures. In the case of decay-counting, differentiating between type (a) and type (b) is usually not possible because there rarely is enough raw material for replication.
c) Archaeological errors. Results which replicate well but radically deviate from their supposed archaeological placement, i.e. diverge significantly from other measurements of the same typo-stratigraphic horizon, or absolutely do not fit the typo-stratigraphic sequence. The probable source of error is archaeological.

Different strategies of dealing with divergent data are found in the literature. The strategy used in the current study is as follows.

First, suspect measurements were rechecked to see if some independent cause for the aberrant reading (physical or archaeological) could be located. If so, all the measurements in which the same problem was found were eliminated, whether or not they agreed with other results.

Visual and microscopic examination of some of the graphite targets that were used in the accelerator and gave divergent results had indeed shown an anomalous behavior of the graphite in the cathode during the sputtering process. The possible reason for this phenomenon is improper pressing of the graphite. All these targets were excluded from the study.

The samples that were excluded on archaeological grounds were, e.g., the Hazor XII/XI samples (RTT 3700, 3701, 3702, 3703, 3704), which produced dates in the early 2nd millennium. (But the Hazor dates are still useful for the purpose of intercomparison, residuality notwithstanding.)

As already noted above, one method used to cross-check the samples prepared for LSC in Rehovot was to extract a small amount of CO_2 during sample preparation and measure it with AMS. It turned out that these samples fluctuated widely and without any correlation with the date obtained for the same sample by AMS or LSC. We do not yet know the exact reason for this. Since this exercise is not part of the normal operational run in the laboratory, it was decided to defer investigation of this phenomenon and to simply not use results obtained this way.

An interesting and fairly consistent offset was noted on some samples prepared and dated in the Tucson laboratory, labeled "b." These samples were run differently than the rest of the Tucson targets (labeled "a" and "aa"). Before graphitization, the CO_2 from these "b" samples was run through a mass spectrometer to measure the $\delta^{13}C$. We suspect that the sample gas might have been mixed with the reference gas before the recollection for the graphitization. We have investigated this problem further and identified possible differences in procedure used by mass spectrometer operators, which might account for such differences. All the "b" targets were excluded from the analysis.

In a few cases, we noted that a single AMS batch had several outliers. This raised the possibility of either instability in the accelerator during that run or problems with the measurement of the standards. In these cases, we prepared and re-ran several of the samples included in these batches (from the material left at Rehovot). These suspicions were unfounded, and most of the re-runs faithfully replicated the previous results. Indeed, the fact that independently pretreated samples run after a 2-yr interval gave very similar results greatly enhances our confidence in the stability of the system and the AMS measurements. Such re-runs account for samples with many replications (typically 3 measurements in Tucson and 6 in Rehovot).

If, even after all these steps, a replicated series did not pass the χ^2 test, we left the potentially outlying measurements in, but used the sampled standard deviation instead of the combined error term whenever dates were combined (Bevington and Robinson 1992).

The next step of analysis is to construct a model for the collation of all of the dates together with the order of the contexts from which they were collected (as determined by stratigraphic and typological analyses). In the present study, we employ the standard Bayesian inference approach (Bronk Ramsey 1994, 1995).

THE ASSESSMENT OF BIAS

The following analyses were carried out:

1. Measurements intended to assess the effect of pretreatments: intercomparison of AMS dates of samples prepared in Rehovot and prepared in Tucson, both analyzed in Tucson.

Twenty-two samples were split between Rehovot and Tucson, pretreated in these 2 labs, and measured by AMS in Tucson, producing 90 individual measurements (Table 1). This exercise was carried out during a 3-yr interval, using different machines during normal operation time. Table 1 includes all outliers except ones that may be omitted due to some procedural error as explained above.

Table 1 Single measurements of the 22 samples divided between Tucson and Rehovot.

				Tucson		Rehovot	
Material	Site	Strata	Period	AA/T sample #[a]	^{14}C age ±1 σ (BP)	RTT sample#[b]	^{14}C age ±1 σ (BP)
Charcoal	Hazor	XII/XI	Iron I	AA40992	2945 ± 50	3700*	2975 ± 35
Charcoal	Hazor	XII/XI	Iron I	AA40993	2965 ± 50	3701*	2940 ± 30
Olive pits	Hazor	XII/XI	Iron I	AA40994	3060 ± 50	3702*	3060 ± 30
Charcoal	Hazor	XII/XI	Iron I	AA40995	3650 ± 50	3703*	3570 ± 53
Charcoal	Hazor	XII/XI	Iron I	AA40996	3370 ± 60	3704*	3375 ± 30
Olive pits	Yoqne‘am	XVII (b?)	Late Iron I	T18150a	2778 ± 42	3778.3	2781 ± 45
				T18150aa		3778.4	2866 ± 45
				—	—	3778.5	2802 ± 46
				Average	2818 ± 29	*Average*	2817 ± 26
Charcoal	Yoqne‘am	XIVb	Early Iron IIA	T18151a	2739 ± 35	3780.3	2635 ± 45
				T18151Aaa	2726 ± 43	3780.4	2657 ± 55
				—	—	3780.5	2663 ± 69
				Average	2739 ± 35	*Average*	2649 ± 31
Charcoal	Hazor	Xa	Iron IIA	T18152a	2731 ± 37	3783.3	2680 ± 48
				T18152aa	2674 ± 35	3783.4	2822 ± 40
				—	—	3783.5	2795 ± 38
				Average	2700 ± 27	*Average*	2777 ± 24
Olive pits	Hazor	IXa	Late IIA	T18153a	2693 ± 35	3785.4	2675 ± 48
				T18153aa	2705 ± 52	3785.5	2707 ± 46
				—	—	3785.6	2683 ± 46
				Average	2697 ± 24	*Average*	2689 ± 27
Olive pits	Hazor	Xb	Early Iron IIA	T18154a	2576 ± 66	3786.3	2615 ± 81
				T18154aa	2656 ± 35	3786.4	2448 ± 48
				—	—	3786.5	2695 ± 47
				Average	2639 ± 31	*Average*	2585 ± 126
Seeds	H. Rosh Zayit	IIa	Iron IIA	T18155a	2687 ± 35	3798.3	2763 ± 37
				T18155aa	2693 ± 47	3798.4	2753 ± 37
				—	—	3798.5	2749 ± 38
				Average	2689 ± 28	*Average*	2755 ± 22
Seeds	H. Rosh Zayit	IIa	Iron IIA	T18156a	2683 ± 35	3799.3	2729 ± 37
				T18156aa	2728 ± 68	—	—
				Average	2692 ± 31	*Average*	2729 ± 37
Charcoal	Tell Keisan	9a	Late Iron I	T18157a	2938 ± 35	3803.3	2817 ± 48
				T18157aa	2862 ± 65	3803.4	2940 ± 50
				—	—	3803.5	2997 ± 35
				—	—	3803.6	2871 ± 42
				—	—	3803.7	2798 ± 36
				—	—	3803.8	2799 ± 36
				Average	2921 ± 31	*Average*	2870 ± 82
Charcoal	Tell Keisan	13	LB | Iron I	T18158a	3022 ± 47	3804.3	2960 ± 35
				T18158aa	2985 ± 36	3804.4	2997 ± 35
				—	—	3804.5	2996 ± 35
				Average	2999 ± 29	*Average*	2984 ± 20
Olive pits	Tel Rehov	E-1b(=V)	Iron IIA	T18159a	2671 ± 35	3808.3	2693 ± 35
				T18159aa	2700 ± 37	3808.4	2671 ± 35
				—	—	3808.5	2669 ± 35
				Average	2685 ± 25	*Average*	2678 ± 20

Table 1 Single measurements of the 22 samples divided between Tucson and Rehovot. *(Continued)*

				Tucson		Rehovot	
Material	Site	Strata	Period	AA/T sample #[a]	^{14}C age ±1 σ (BP)	RTT sample #[b]	^{14}C age ±1 σ (BP)
Olive pits	Tel Rehov	D-4 (=VII)	Late? Iron I	T18150a	2889 ± 35	3809.4	2830 ± 34
				T18150aa	2952 ± 44	3809.5	2861 ± 36
				Average	2913 ± 27	*Average*	2845 ± 25
Seeds	Tell Qasile	X	Late Iron I	T18161a	2780 ± 35	3932.3	2746 ± 50
				T18161aa	2862 ± 38	3932.4	2763 ± 76
				—	—	3932.5	2683 ± 49
				—	—	3932.6	2651 ± 37
				Average	2818 ± 26	*Average*	2692 ± 24
Seeds	Megiddo	K4=VIA	Late Iron I	T18163a	2864 ± 40	3944.3	2974 ± 63
				—	—	3944.4	2982 ± 47
				—	—	3944.5	2904 ± 58
				Average	2864 ± 40	*Average*	2957 ± 31
Seeds	Megiddo	H5	Early Iron IIA	T18167a	2788 ± 38	3949.3	2821 ± 47
				T18167aa	2807 ± 42	3949.4	2899 ± 48
				Average	2796 ± 28	*Average*	2859 ± 34
Olive pits	Tel Miqne-'Ekron	IV	Late Iron I	T18168a	2872 ± 36	4282.3	2894 ± 53
				T18168a	2895 ± 38	4282.4	2837 ± 42
				—	—	4282.5	2899 ± 47
				Average	2883 ± 26	*Average*	2872 ± 27
Olive pits	Megiddo	K6 (=VIIA?)	LB | Iron I	T18169a	2907 ± 37	4499.3–1.1	2884 ± 37
				T18169aa	2876 ± 40	4499.3–1.2	2866 ± 43
				—	—	4499.3–1.3	2927 ± 39
				Average	2893 ± 27	*Average*	2894 ± 23
Olive pits	Megiddo	K6 (=VIIA?)	LB | Iron I	T18170a	3018 ± 56	4500.3.1–1	2940 ± 38
				T18170aa	2947 ± 36	4500.3.1–2	2906 ± 37
				—	—	4500.3.1–3	2909 ± 37
				Average	2968 ± 30	*Average*	2918 ± 22

[a]AA or T = pretreated and measured in Tucson by AMS.

[b]RTT = pretreated and prepared as graphite in Rehovot and measured by AMS in Tucson; * = the average of 3 measurements.

To exclude the possibility of a meaningful difference between the 2 laboratories, a Bland-Altman plot (Bland and Altman 1986) of the data from Table 1 is shown in Figure 2. In Figure 3, the same data with the analytical error are compared. In Figure 2, the *x* axis denotes the average of the Tucson and Rehovot (AMS) ^{14}C determinations for the same sample. The *y* axis denotes the difference between the Tucson average and Rehovot (AMS) average for the same sample. The mean difference and standard deviation of the differences between the 2 laboratories is 9.96 ± 57.56 yr. The mean difference value is represented in the plot by the solid line. The dashed lines represent the mean difference ±1.96*1 σ, which is indicated in the plot with the dashed line at +123 yr and –103 yr. All the points are included in the region between the 2 lines. The paired Student's *t* test provided a *t* value of 0.81 and a *p* value of 0.43. Thus, the null assumption of no difference between the labs cannot be negated at a reasonable statistical confidence level. In Figure 3, the *y* axis denotes the average of the multiple measurements of the sample prepared in Rehovot, in ^{14}C BP; the error bars are ±1 standard deviation. The *x* axis denotes the same for samples prepared in Tucson. The line of equality, *x* = *y* line, which represents the perfect match, is indicated (dashed). Approximately the same number of points fall on either side of this line, meaning that in about half of the cases, Rehovot produced higher dates than Tucson and vice versa. Also shown is the best-fit regression line, which is conditioned to pass through the origin of the axes, and its correlation coefficient. Likewise, the δ^{13}C was found to be in good agreement between the 2 laboratories.

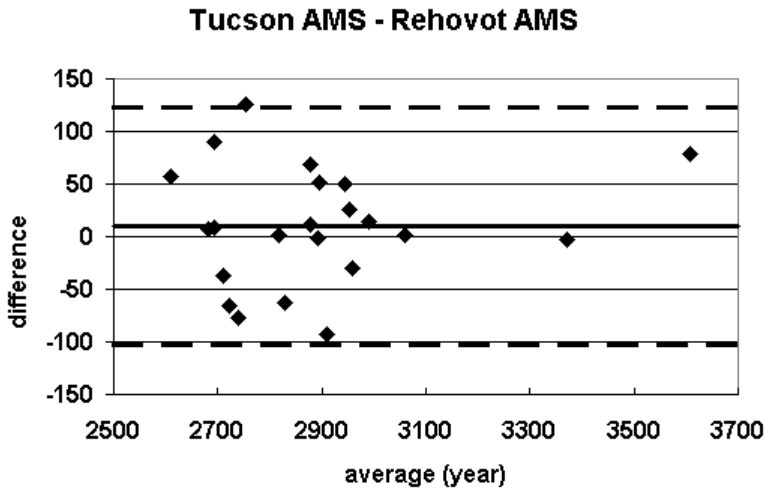

Figure 2 Tucson AMS/Rehovot AMS pretreatment intercomparison results. The *x* axis represents the average of the measurements for the sample prepared and measured in Tucson and for the sample prepared in Rehovot and measured in Tucson; the *y* axis represents the difference of the samples prepared and measured in Tucson and the samples prepared in Rehovot and measured in Tucson. The $y = 9.96$ line (solid) and the $1.96*(\pm 57.56)$ lines (dashed) are indicated.

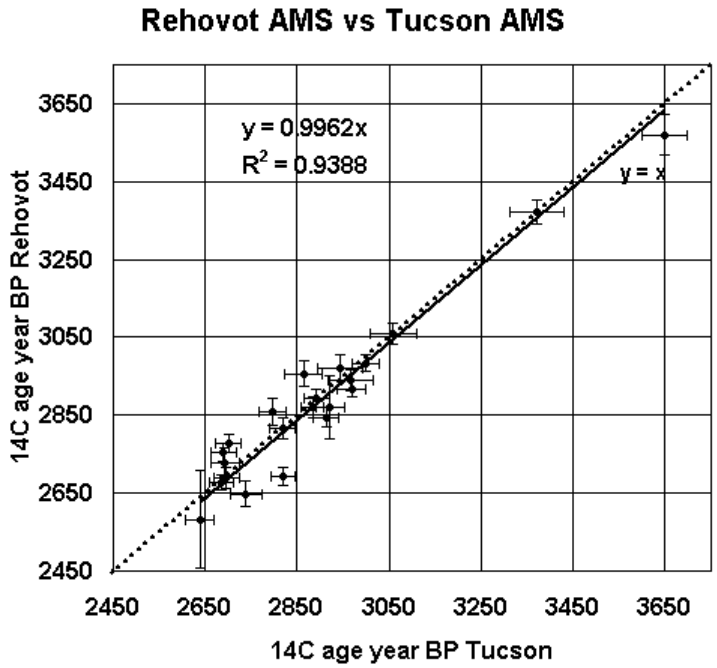

Figure 3 Tucson/Rehovot pretreatment intercomparison results. The *x* axis represents the samples prepared and measured in Tucson; the *y* axis represents the samples prepared in Rehovot and measured in Tucson. The $y = x$ line (dashed) and the best-fit line (solid) for the set of points are indicated.

2. Measurements intended to compare AMS and LSC dates: same pretreatment and different measurement methods.

This exercise is intended to assess the effects of dating techniques. It includes 14 samples pretreated at Rehovot and measured by LSC in Rehovot and by AMS in Tucson. Of these, 5 samples underwent 3 different procedures: LSC (pretreated and measured in Rehovot), AMS prepared at Rehovot and measured in Tucson, AMS prepared and measured in Tucson.

Table 2 LSC and AMS results for sample measurements from Rehovot and Tucson.

Material	Site	Stratum	Period	LSC sample #	LSC[a] ^{14}C age ±1 σ (BP)	RTT sample #	AMS[b] ^{14}C age ±1 σ (BP)	Tucson sample #	AMS[c] ^{14}C age ±1 σ (BP)
Olive pits	Yoqne'am	XVII (b?)	Late Iron I	—	—	3777.3	2830 ± 60	—	—
				—	—	3777.4	2910 ± 45	—	—
				—	—	3777.5	2790 ± 80	—	—
				3777.1	2866 ± 25	—	2866 ± 33*	—	—
Olive pits	Yoqne'am	XVII (b?)	Late Iron I	—	—	3778.3	2781 ± 45	T18150a	2778 ± 42
				—	—	3778.4	2866 ± 45	T18150aa	2853 ± 39
				—	—	3778.5	2802 ± 46	—	—
				3778.1	2776 ± 25	—	2817 ± 26*	—	2818 ± 29*
Charcoal	Yoqne'am	XVIIa	Late Iron I	—	—	3779.3	2815 ± 45	—	—
				—	—	3779.4	2870 ± 60	—	—
				—	—	3779.5	2800 ± 55	—	—
				3779.1	2926 ± 30	—	2824 ± 30*	—	—
Charcoal	Yoqne'am	XIVb	Early Iron IIA	—	—	3780.3	2635 ± 45	T18151a	2739 ± 35
				—	—	3780.4	2657 ± 55	T18151aa	2726 ± 43
				—	—	3780.5	2663 ± 69	—	—
				3780.1	2725 ± 25	—	2649 ± 31*	—	2739 ± 35*
Seeds	H. Rosh Zayit	IIa	Iron IIA	—	—	3798.3	2763 ± 37	T18155a	2687 ± 35
				—	—	3798.4	2753 ± 37	T18155aaA	2693 ± 47
				—	—	3798.5	2749 ± 38	—	—
				3798.1	2745 ± 30	—	2755 ± 23*	—	2689 ± 27*
Seeds	H. Rosh Zayit	IIa	Iron IIA	—	—	3799.3	2729 ± 37	T158156a	2683 ± 35
				—	—	—	—	T18156aa	2728 ± 68
				3799.1	2745 ± 30	—	2729 ± 37*	—	2692 ± 31*
Charcoal	Tell Keisan	9a-b	Late Iron I	—	—	3802.3	2820 ± 50	—	—
				—	—	3802.4	2820 ± 50	—	—
				—	—	3802.5	2885 ± 50	—	—
				3802.1	2870 ± 35	—	2842 ± 29*	—	—
Charcoal	Tell Keisan	9a	Late Iron I	—	—	3803.3	2817 ± 48	T18157a	2938 ± 35
				—	—	3803.4	2940 ± 50	T18157aa	2862 ± 65
				—	—	3803.5	2997 ± 35	—	—
				—	—	3803.6	2871 ± 42	—	—
				—	—	3803.7	2798 ± 36	—	—
				—	—	3803.8	2799 ± 36	—	—
				3803.1	2893 ± 50	—	2870 ± 82*	—	2921 ± 31*
Olive pits	Tel Rehov	D-3? D-2?	Iron IIA	—	—	3807.3	2763 ± 35	—	—
				—	—	3807.4	2716 ± 35	—	—
				—	—	3807.5	2757 ± 20*	—	—
				3807.1	2760 ± 40	—	—	—	—
Seeds	Tell Qasile	X	Late Iron I	—	—	3931.3	2820 ± 55	—	—
				—	—	3931.4	2935 ± 41	—	—
				—	—	3931.5	2936 ± 41	—	—
				3931.1	2853 ± 25	—	2911 ± 26*	—	—

Table 2 LSC and AMS results for sample measurements from Rehovot and Tucson. *(Continued)*

Material	Site	Stratum	Period	LSC sample #	LSC[a] ^{14}C age ±1 σ (BP)	RTT sample #	AMS[b] ^{14}C age ±1 σ (BP)	Tucson sample #	AMS[c] ^{14}C age ±1 σ (BP)
Seeds	Bet Shemesh	3	Iron IIB	—	—	3937.3	2524 ± 36	—	—
				—	—	3937.4	2427 ± 35	—	—
				—	—	3937.5	2478 ± 34	—	—
				3937.1	2500 ± 40	—	2475 ± 20*	—	—
Charcoal	Bet Shemesh	Early 3	Iron II A/B	—	—	3987.3	2844 ± 34	—	—
				—	—	3987.4	2889 ± 35	—	—
				—	—	3987.5	2952 ± 51	—	—
				3987.1	2879 ± 40	—	2882 ± 22*	—	—
Charcoal	Tel Hevron	VII	Iron I	—	—	4148.3	3013 ± 36	—	—
				—	—	4148.4	2909 ± 53	—	—
				—	—	4148.5	3025 ± 37	—	—
				4148.1	3010 ± 35	—	2998 ± 23*	—	—
Seeds	Bethsaida	VI	Iron I or II	—	—	4281.3	2775 ± 50	—	—
				—	—	4281.4	2800 ± 40	—	—
				—	—	4281.5	2780 ± 40	—	—
				4281.1	2820 ± 35	—	2786 ± 25*	—	—

[a]Samples pretreated and measured by LSC in Rehovot.
[b]Samples pretreated at Rehovot and measured by AMS in Tucson; average measurements denoted by *.
[c]Samples pretreated and measured by AMS in Tucson; average measurements denoted by *.

The LSC/AMS results are shown in Table 2 and are represented in Figures 4 and 5 (as Bland-Altman plots) and in Figure 6. Figure 4 is the Bland-Altman plot for the LSC Rehovot and AMS Rehovot results. In Figure 4, the *x* axis denotes the average of Rehovot LSC and AMS ^{14}C determinations for the same sample. The *y* axis denotes the difference between the Rehovot LSC and Rehovot (AMS) average for the same sample. The mean difference and standard deviation of the differences between the 2 methods is 15.9 ± 39.0 yr. The mean difference value is represented in the plot by the solid line; the dashed lines represent the mean average ±1.96*1 σ (indicated in the plot with the dashed line at +92.4 yr and –60.6 yr). In Figure 5, the *x* axis denotes the average of Rehovot LSC and Tucson ^{14}C determinations for the same 5 samples. The *y* axis denotes the difference between the Rehovot LSC and Tucson average for the same sample. The mean difference and standard deviation of the differences between the 2 laboratories is –5.0 ± 46.0 yr. The mean difference value is represented in the plot by the solid line. The dashed lines represent the mean average ±1.96*1 σ (indicated in the plot with the dashed line at +85.7 yr and –95.7 yr).

In Figure 6, the *y* axis for each point denotes the average of the multiple AMS measurements for samples prepared in Rehovot and measured in Tucson, in ^{14}C BP; the error bars are ±1 standard deviation. The *x* axis denotes the ^{14}C age for the same samples measured by LSC in Rehovot. The line of equality, $x = y$ line, is indicated. Also shown is the best-fit regression line, which is conditioned to pass through the origin of the axes, and its correlation coefficient. With a mean average of the differences between the 2 laboratories of 15.9 yr, the paired Student's *t* test provided a *t* value of 1.45 and a *p* value of 0.17. Thus, the null assumption of no difference between the labs cannot be negated at a reasonable statistical confidence level.

Figure 6 also presents the 5 samples for which all 3 procedures were performed (the samples prepared at Tucson are identified by a cross symbol, while the same samples prepared in Rehovot are designated by a diamond). In these cases as well, it is impossible to detect a systematic difference between the laboratories that is larger than the errors quoted by them.

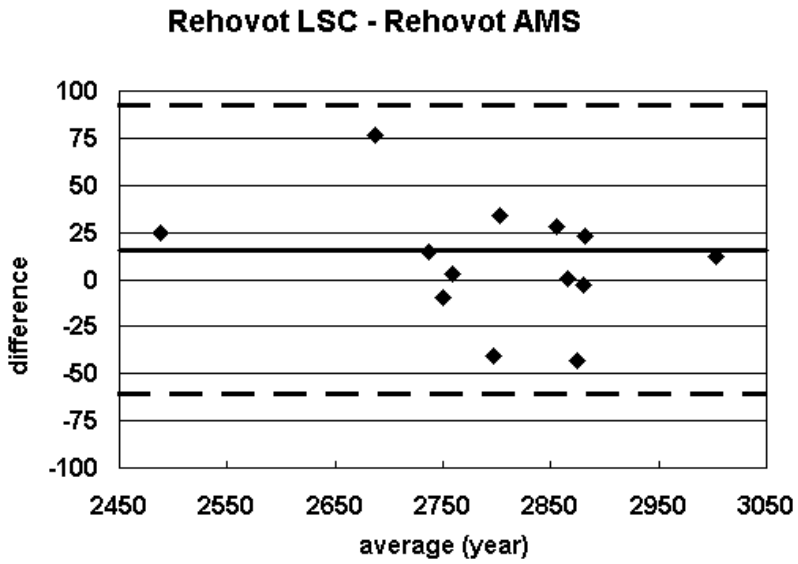

Figure 4 Rehovot LSC/AMS Rehovot intercomparison results. The *x* axis represents the average of the measurements for the sample prepared and measured in Rehovot by LSC and for the sample prepared in Rehovot and measured in Tucson by AMS; the *y* axis represents the difference of the samples prepared and measured in Rehovot by LSC and the samples prepared in Rehovot and measured in Tucson. The $y = 15.9$ yr line (solid) and the 1.96*(±39.0) lines (dashed) are indicated.

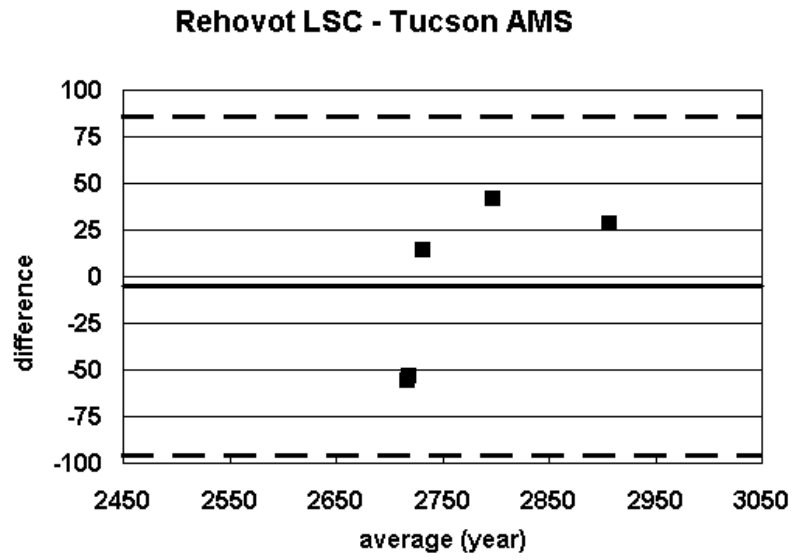

Figure 5 Rehovot LSC/AMS Tucson intercomparison results. The *x* axis represents the average of the measurements for the sample prepared and measured in Rehovot by LSC and for the sample prepared and measured in Tucson by AMS; the *y* axis represents the difference of the samples prepared and measured in Rehovot by LSC and the samples prepared and measured in Tucson. The $y = -5.0$ yr line (solid) and the 1.96*(±46.0) lines (dashed) are indicated.

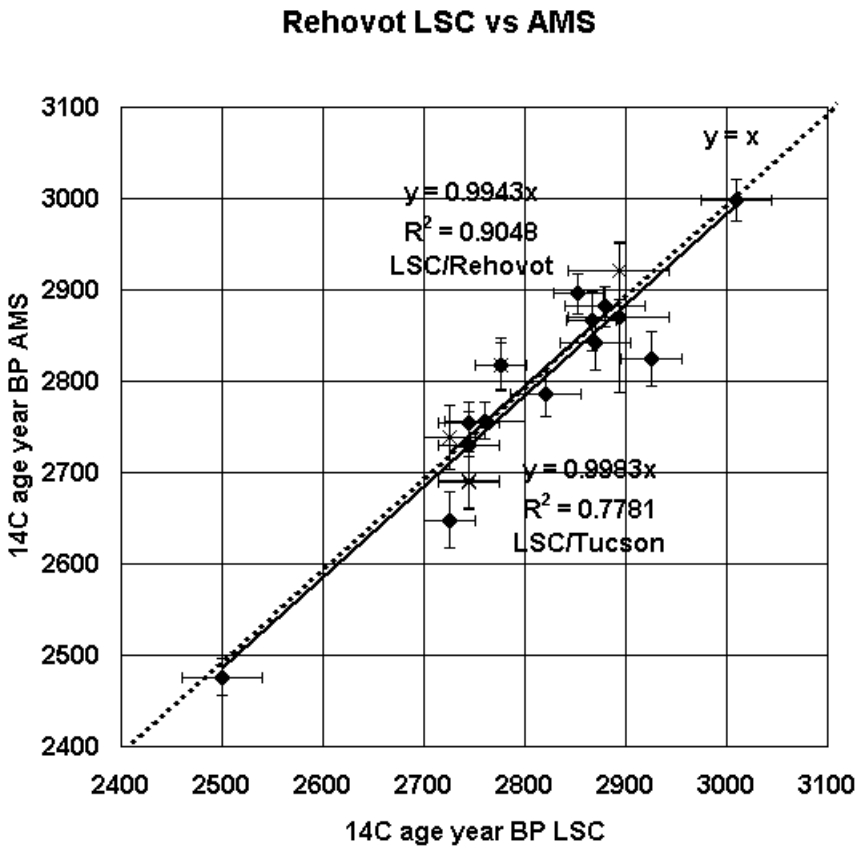

Figure 6 Rehovot LSC/Rehovot AMS/Tucson AMS intercomparison results. The *x* axis represents the samples prepared and measured at Rehovot by LSC; the *y* axis diamond symbols represent samples prepared in Rehovot and measured in Tucson by AMS; the *y* axis cross symbols are samples prepared and measured at Tucson by AMS. The $y = x$ line (dashed) and the best-fit (continuous) line are indicated.

3. Intercomparison with Tel Rehov published dates measured at Groningen.

In 3 cases, dates from Tel Rehov, produced at Rehovot and/or Tucson, may be compared with dates produced from the same contexts at Groningen (published in Bruins et al. 2003; Mazar 2004). However, it must be emphasized that contrary to the results presented in the previous paragraphs, the comparison here is of more indirect nature. In each case, the material analyzed in the different laboratories is from the same locus but might not be exactly the same (a similar exercise was presented in Mazar 2004: Tables 1–2).

In averaging the different ^{14}C dates from the same locus, all sets pass the χ^2 test, even the set related to L2862, where the 2 Groningen measurements differ considerably. This indicates that, in general, there is good agreement between the laboratories. Averaging the sets of data separately for each laboratory, only in one case out of three (in the sample from Locus 1802) are the Rehovot averages separated by more than 3 σ from the Groningen (single) measurement. In the other 2 cases, the averages are the same, based on the quoted errors. The restricted number of measurements does not permit a more detailed analysis, but they definitely are in agreement and no bias can be detected.

Table 3 Groningen, Rehovot, and Tucson data for Tel Rehov samples taken from the same loci.[a]

			Groningen		Rehovot		Tucson	
Material	Area-phase (stratum)	Locus	Sample #	^{14}C age ±1 σ (BP)	Sample #	^{14}C age ±1 σ (BP)	Sample #	^{14}C age ±1 σ (BP)
Olive pits	D-3	2862	GrA-19033[b]	2835 ± 45	RTT-3805	2775 ± 35	—	—
		—	GrN-26119[c]	2720 ± 30	—	2810 ± 35	—	—
		—	—	—	—	2815 ± 35[d]	—	—
Olive pits	D-2 (V)	1802	GrN-26112	2805 ± 15	RTT-3807	2765 ± 35	—	—
		—	—	—	—	2715 ± 35	—	—
		—	—	—	RT-3807	2795 ± 40	—	—
		—	—	—	—	2760 ± 40	—	—
		—	—	—	—	2785 ± 35	—	—
Olive pits	D-4 (VII)	1836	GrN-26121	2890 ± 30	RTT-3809	2830 ± 35	T18150A	2890 ± 35
		—	GrA-18825	2870 ± 50	—	2860 ± 35	—	2950 ± 45

[a]GrN = Groningen decay counting; GrA = Groningen AMS; RTT = Rehovot AMS; RT = Rehovot LSC; T = Tucson AMS.
[b]In Table 1 of Mazar (2004), this sample is attributed to L2862, and in Bruins et al. (2003) to L4815, both of Phase D-3.
[c]From Table 1 of Mazar (2004). The obviously outlying result may have been due to the fact that the sample was small and was diluted to produce enough material for GPC (van der Plicht, personal communication).
[d]Cited erroneously as 2785 ± 25 in Mazar (2004). In the errata addendum to the paper, it is corrected to 2800 ± 20, which is the average of these 3 measurements.

THE IRON I/IIA TRANSITION DATE USING THE INTERCOMPARISON EXERCISE DATA

The archaeological contexts which yielded the samples presented here were grouped into 2 broad archaeological horizons for the purposes of this exercise—those originating from Iron Age I contexts and those of Iron Age IIA (see Table 1). The simplest model, | Iron Age I | Iron Age IIA |, was used with the "|" standing for a "boundary" term, and the object-of-interest being the temporal distribution of the middle boundary (Bronk Ramsey 2000). This has the effect of reducing the archaeological variables in the system, *inter alia*, meaning that the intermediate horizon, which we termed "Ir1|2" (Gilboa and Sharon 2003: Table 21), is not represented in this paper. This omission, or possible gap, does not affect the results of intercomparison, but needs be taken into account when interpreting the results of the models. Within this general model, several different sub-models were tested:

a) Individual measurements from each laboratory, and both laboratories together, no combination.
b) As above, but results which were flagged as being in "poor agreement," with the model being removed stepwise, starting with the poorest, until the general agreement index becomes acceptable (over 60%).
c) Results from each laboratory separately, each replicated set combined (whether or not they pass the χ^2 test), and the two laboratories together, all results of the same replication (within- and between-laboratories) combined.
d) As above, but outliers (i.e. individual measurements that cause the replicated set to fail the χ^2 test) removed. Although one replicated set was consistently flagged as having a poor fit with the rest of the sequence (T18167 = RT3949; a seeds sample from Megiddo H5 [=VB – IVA]) was retained since the overall agreement of the model is acceptable.

All the models gave broadly similar results, with the peaks of the boundary distribution varying in the order of magnitude of 20–25 yr between the different model runs, and the limits of the 68% and 95% highest-density regions slightly more (Table 4).

Table 4 Iron I|IIA transition calculated in different ways.[a]

	Tucson	Rehovot	Rehovot and Tucson
Not combined with misfits	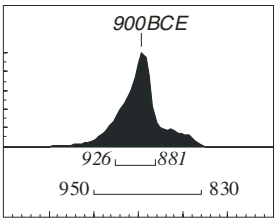	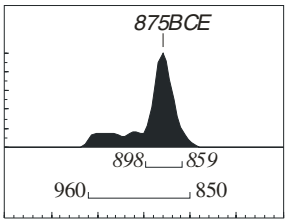	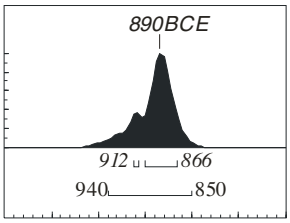
	3 misfits: T18154a, T18154aa, T18167aa	6 misfits: 3932.5–6, 3786.4, 3783.4, 3949.3–4	7 misfits: 3932.5–6, 3786.4, 3783.4, T18167aa, 3949.3–4
Not combined after the removal of misfits until the overall agreement is >60%	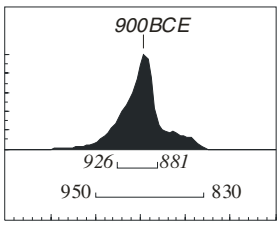	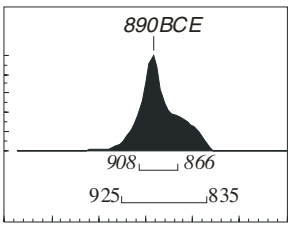	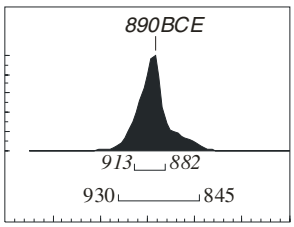
	3 misfits: T18154a, T18154aa, T18167aa	3 misfits left: 3932.5, 3783.5, 3949.3	5 misfits left: 3932.5, 3783.4–5, T18167aa, 3949.3
Combined with outliers	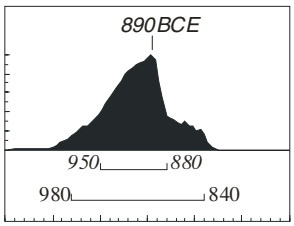	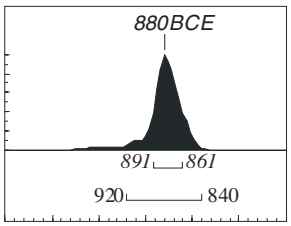	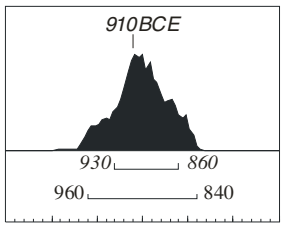
	No outliers 1 misfit: T18167	2 outliers: 3803.5, 3786.4 1 misfit: 3949	4 outliers: T18161aa, 3803.5, 3786.4, 3783.4 1 misfit: T18167 = 3949
Combined after the removal of outliers	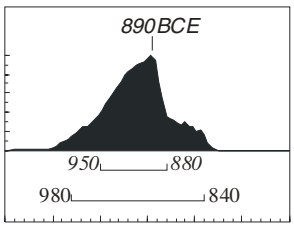	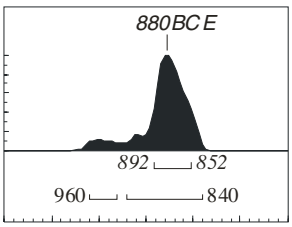	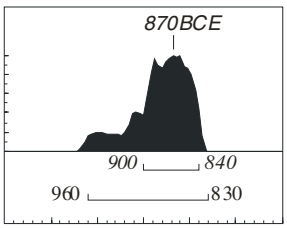
	1 misfit: T18167	1 misfit: 3949	1 misfit: T18167 = 3949

[a]The dates in italicized numerals at the top of each plot are the maximum likelihood estimate; the dates in the smaller range immediately below the plot are the 68% highest-density interval, and dates in non-italicized numerals in the bottom range are the 95% highest-density interval.

CONCLUSIONS

The ^{14}C intercomparison exercise presented here is one of the most comprehensive to have been run between laboratories on a substantial number of real archaeological samples. Its implications must be assessed at different levels.

Bias or No Bias?

The reproducibility between the Tucson and Rehovot laboratories as presented here is as close as one could expect, and certainly well within the standards of the FIRI exercise. No bias can be detected either between the laboratories, between different pretreatment procedures, or between measuring techniques. Given enough measurements (see below), the outcome regarding the object of inquiry here, the Iron I|II transition, would have, *grosso modo*, been the same had we confined ourselves to one lab/method only. This is a prerequisite in the framework of our more comprehensive research, which, as mentioned, involves 400 or so measurements. For the time being, many measurements are made by one method/laboratory only, though we are currently expanding the intercomparison program to include not only more samples and other laboratories, but also more detailed characterization of the materials used for ^{14}C analysis. A detailed study of different preparation procedures used in different laboratories may shed light on the reasons for the still existing outliers.

Can ^{14}C Dating Resolve the Levantine Iron Age Dilemma?

The obvious answer here is yes, provided that enough measurements are available. Given the current state-of-the-art technology in archaeological seriation, ^{14}C accuracy and precision, and statistical modeling, the investigation of the chronology of the eastern Mediterranean in this period will have to be based on numerous, replicated dates, taken from different sites and measured by different procedures. A large, replicated data set is the only way to overcome the inevitable noise in the model.

The Iron I|II transition dates as calculated here range between 910–875 BCE, diverging only by 10–25 yr between the 2 labs. They are about 30 yr higher than the transition dates calculated based on the Dor dates alone (880–850, e.g. Gilboa and Sharon 2003: Table 21)—another issue awaiting investigation. However, they provide further empirical support for a lower chronology.

We must stress again that we do not consider the transition dates presented here as the final conclusion of our research for 3 main reasons: a) they were calculated using only the measurements participating in the intercomparison exercise—a small fraction of the forthcoming ~400 dates we have measured; b) clustering the dates into (only) 2 very broad archaeological horizons (Iron I and Iron II), as was done here, is not sufficient for the typological resolution this problem requires; c) the data set presented in this paper lacks dates from the horizon that we termed "Iron I|II." This, and a much more detailed, relative placement of all the dates in the Iron I–II continuum will be considered when all of our results are taken into account.

ACKNOWLEDGMENTS

This research was carried with the support of the Israel Science Foundation (Grant No. 778/00), the Kimmel Center of Archaeological Sciences at the Weizmann Institute of Science, the Research Authority at the Hebrew University, the Research Authority at the University of Haifa, and the US National Science Foundation (Grant EAR01–15488).

REFERENCES

Bevington PR, Robinson DK. 1992. *Data Reduction and Error Analysis for the Physical Sciences*. Boston: WCB/McGraw-Hill.

Bland JM, Altman DG. 1986. Statistical method for assessing agreement between two methods of clinical measurement. *The Lancet* 1:307–10.

Bronk Ramsey C. 1994. Analysis of chronological information and radiocarbon calibration, the program OxCal. *Archaeological Computing Newsletter* 41:11–6.

Bronk Ramsey C. 1995. Radiocarbon calibration and the analysis of stratigraphy, the OxCal program. *Radiocarbon* 37(2):425–30.

Bronk Ramsey C. 2000. Comment on "The use of Bayesian statistics for ^{14}C dates of chronologically ordered samples: a critical analysis." *Radiocarbon* 42(2):199–202.

Bruins H, van der Plicht J, Mazar A. 2003. Response to comment on "^{14}C dates from Tel Rehov: Iron-Age chronology, pharaohs and Hebrew kings." *Science* 302:568c.

Coldstream JN. 2003. Some Aegean reactions to the chronological debate in the southern Levant. *Tel Aviv* 30:247–58.

Coldstream JN, Mazar A. 2003. Greek pottery from Tel Rehov and Iron Age chronology. *Israel Exploration Journal* 53:29–48.

Fantalkin A. 2001. Low Chronology and the Greek protogeometric and geometric pottery in the southern Levant. *Levant* 33:117–25.

Finkelstein I. 1996. The archaeology of the United Monarchy: an alternative view. *Levant* 27:177–87.

Finkelstein I, Piasetzky E. 2003. Wrong and right; high and low: ^{14}C dates from Tel Rehov and Iron Age chronology. *Tel Aviv* 30:283–95.

Gilboa A, Sharon I. 2001. Early Iron Age radiometric dates from Tel Dor: preliminary implications for Phoenicia, and beyond. *Radiocarbon* 43(3):1343–51.

Gilboa A, Sharon I. 2003. An archaeological contribution to the early Iron Age chronological debate: alternative chronologies for Phoenicia and their effects on the Levant, Cyprus and Greece. *Bulletin of the American Schools of Oriental Research* 332:7–80.

Holden C. 2003. Dates boost conventional wisdom about Solomon's splendor. *Science* 300:229–31.

Kopcke G. 2002. 1000 BCE? 900 BCE? A Greek vase from Lake Galilee. In: Ehrenberg E, editor. *Leaving No Stones Unturned: Essays on the Ancient Near East and Egypt in Honor of Donald P Hansen*. Winona Lake: Eisenbrauns. p 109–17.

Mazar A. 2004. Greek and Levantine Iron Age chronology: a rejoinder. *Israel Exploration Journal* 54:24–36.

Scott EM. 2003. The Fourth International Radiocarbon Intercomparison (FIRI). *Radiocarbon* 45(2):35–150.

Sharon I. 2001. "Transition dating"—a heuristic mathematical approach to the collation of ^{14}C dates from stratified sequences. *Radiocarbon* 43(3):345–54.

Sharon I, Gilboa A, Boaretto E. Forthcoming. ^{14}C and the early Iron Age of Israel—Where are we really at? A commentary on the Tel Rehov radiometric dates. *Proceedings of the 2nd EuroConference SCIEM 2000.* Vienna: Austrian Academy of Sciences.

RADIOCARBON, Vol 47, Nr 1, 2005, p 57–65

PRE-BOMB $\Delta^{14}C$ VARIABILITY AND THE SUESS EFFECT IN CARIACO BASIN SURFACE WATERS AS RECORDED IN HERMATYPIC CORALS

Thomas P Guilderson[1,2] • Julia E Cole[3] • John R Southon[1,4]

ABSTRACT. The $\Delta^{14}C$ content of surface waters in and around the Cariaco Basin was reconstructed from radiocarbon measurements on sub-annually sampled coral skeletal material. During the late 1930s to early 1940s, surface waters within and outside of the Cariaco Basin were similar. Within the Cariaco Basin at Islas Tortugas, coral $\Delta^{14}C$ averages –51.9 ± 3.3‰. Corals collected outside of the basin at Boca de Medio and Los Testigos have $\Delta^{14}C$ values of –53.4 ± 3.3‰ and –54.3 ± 2.6, respectively. Additional ^{14}C analyses on the Isla Tortugas coral document an ~11‰ decrease between ~1905 (–40.9 ± 4.5‰) and ~1940. The implied Suess effect trend (–3‰/decade) is nearly as large as that observed in the atmosphere over the same time period. If we assume that there is little to no fossil fuel $^{14}CO_2$ signature in Cariaco surface waters in ~1905, the waters have an equivalent reservoir age of ~312 yr.

INTRODUCTION

The Cariaco Basin is a small, shallow silled (~140 m) basin located on the northwest Venezuelan margin. Detailed records of past climate variability spanning nearly 600,000 yr are preserved in the basin's rapidly accumulating sediments (Peterson et al. 2000). The sedimentary record is comparably undisturbed by bioturbation due to anoxic conditions at depth. The combination of a lack of bioturbation and seasonally distinct sedimentary input components (terrigenous versus biogenic) conspire to provide an environment that promotes the formation and preservation of distinct annual laminae or varves. Variations in biogeochemical, geochemical, and sedimentological proxies in these sediments have been interpreted to reflect variations in regional sediment discharge, the strength of the tradewinds, and the position of the Intertropical Convergence Zone (e.g. Black et al. 1999; Hughen et al. 1998, 2000; Peterson et al. 1991, 2000).

Although numerous paleoceanographic studies have taken advantage of the unique records preserved in the marine sediments, including detailed radiocarbon-calendar calibrations (e.g. Hughen et al. 2000), a detailed assessment of the natural-^{14}C or pre-bomb variability has not previously been made. We use annually banded corals from several sites within and around the basin to determine the seasonal variability in pre-bomb $\Delta^{14}C$ as it relates to air-sea exchange, surface water dynamics, and the potential influence of the Orinoco River and local fluvial input.

General Oceanography

Sea surface temperatures in the Cariaco Basin vary in response to both radiative forcing and ocean dynamics. The sea surface temperature minimum in the Cariaco Basin follows the local upwelling regime, with lowest temperatures occurring in April/May. Upwelling in the basin occurs in response to both direct or local wind forcing in relation to the seasonal migration of the Intertropical Convergence Zone (ITCZ) and the replacement of warm, less saline surface waters with subsurface cooler, salty waters through lateral advection and mesocale eddies (Astor et al. 2003). The seasonal sea surface temperature maximum occurs during late boreal summer and early fall during the time of minimum wind speed. Salinity varies seasonally in direct response to the passage of the ITCZ and

[1]Center for Accelerator Mass Spectrometry, Lawrence Livermore National Laboratory, Livermore, California 94551, USA.
[2]Corresponding author. Email: tguilderson@llnl.gov. Also at Department of Ocean Sciences, University of California-Santa Cruz, Santa Cruz, California 94056, USA.
[3]Department of Geosciences, University of Arizona, Tucson, Arizona 85721, USA.
[4]Now at Department of Earth System Science, University of California-Irvine, Irvine, California 92697, USA.

regional fluvial input from the Río Unare and Río Tuy. The salinity minimum occurs during the August-October rainy season.

The shallow sill inhibits advection of interior waters; thus, the characteristics of the surface waters are primarily controlled by surface waters of the Caribbean and subtropical underwater. Waters shallower than the sill depth interact with surface waters from the outside of the basin. Vertical mixing between upper, well-ventilated waters and those at depth is inhibited by the presence of a strong pycnocline. The boundary between oxic and anoxic waters varies in conjunction with the strength and duration of the upwelling season. This boundary averaged 280 ± 40 m between 1996 and 1998 (Astor et al. 2003; Muller-Karger et al. 2001).

METHODS

Several cores from long-lived coral colonies were collected in 1996 and 1998 using diver-operated hydraulic drilling gear. For this study, 3 cores were utilized. A *Siderastrea siderea* was cored in March 1996 from the Los Testigos archipelago (11°23′N, 63°08′W) to the northeast of the Cariaco Basin (Figure 1). Also in March of 1996, a *Montastrea annularis* was drilled on the southwestern side of the Isla Tortuga (10°54′N, 65°14′W) opening on the Cariaco Basin. The final specimen that we have worked on is a *Montastrea annularis* drilled in July 1998 from Boca de Medio (11°55′N, 66°36′W) in the Los Roques archipelago. The Los Roques archipelago is outside of the Cariaco Basin proper and should represent a well-mixed non-upwelling site. The Los Testigos site is also outside of the Cariaco proper but is influenced by the same water masses in conjunction with coastal upwelling. In addition, Los Testigos undergoes a pronounced seasonal cycle in salinity as a consequence of Orinoco River discharge.

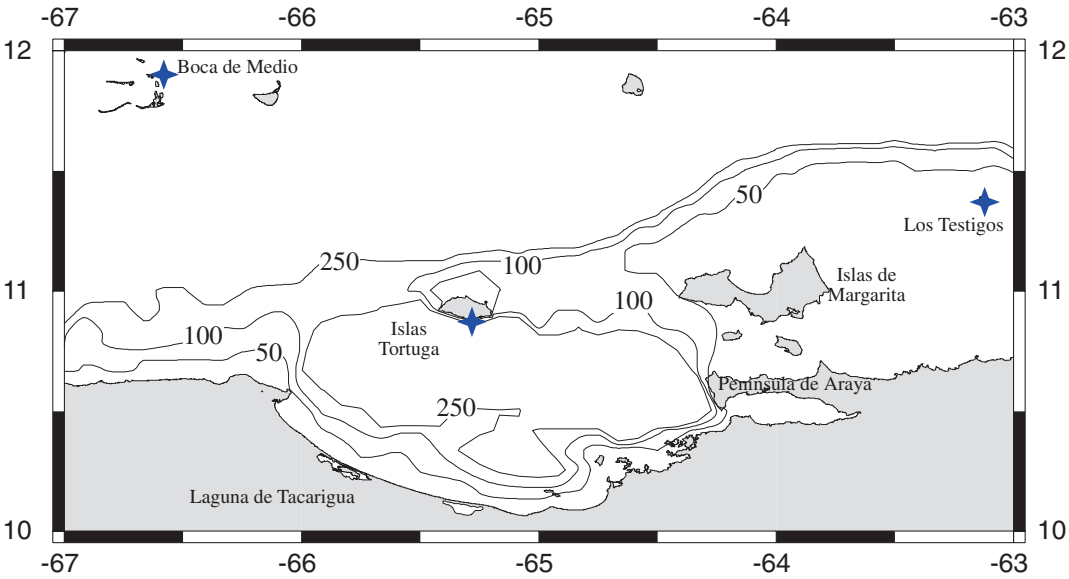

Figure 1 Map of the Cariaco Basin and locations (crosses) of the coral samples discussed. Contours are depths (meters) along the main Venezuelan continental margin.

The cores (9 cm diameter) were cut into ~5-mm slabs, ultrasonically cleaned in distilled water, and air-dried. None of the sampled regions were infiltrated with boring filamentous algae or other organisms. After identifying the major vertical growth axis, pre-bomb levels were identified using density

banding, and the coral was sequentially sampled at 1-mm increments in the time period of interest with a low-speed drill. The coral age-models were derived using a combination of sclerochronology (e.g. Dodge and Vaisnys 1980) and the seasonal cycle recorded in the carbon and oxygen isotopic composition of the coral skeleton (Cole et al. 1993; Guilderson and Schrag 1999; among others). For the Boca de Medio and Testigos samples, ages were assigned using annual density bands and counting back from the top of the coral core. We assumed, based on published literature (e.g. Fairbanks and Dodge 1979), that dense bands formed in the warmest season and assigned the month of September to the samples that coincided with dense bands. Years were determined by counting bands back from the known date of collection. In these samples, density banding was reasonably clear and we assume no more than a 1-yr possible age error. Our isotopic results from the intervals sampled confirm the annual nature of these bands. In the Tortuga sample, density banding was less clear, particularly in the oldest regions. We analyzed stable oxygen and carbon isotopes at 1-mm resolution throughout the core and developed an age model using the seasonal cycle of $\delta^{18}O$. We assumed that the most positive values of $\delta^{18}O$ correspond with the coolest month and assigned seasonal positive extremes to March of each year (the coolest month, on average, in the COADS SST data from 11°N, 64°W). Linear interpolation between annual tie points provide the subannual chronology. We assume a slightly larger age uncertainty in the Tortuga core, on the order of ±1–2 yr at the base.

All drilled samples were analyzed for $\delta^{18}O$ and $\delta^{13}C$ at the University of Arizona, using a Micromass Optima™ stable isotope ratio mass spectrometer with an Isocarb™ (common acid bath) automated preparation device. Analytical error, based on replicate analyses of an in-house standard, is approximately ±0.07‰ for $\delta^{18}O$ and ±0.04‰ for $\delta^{13}C$. Values are presented relative to PDB.

^{14}C sampling focused on samples spanning the late 1930s and 1940s. In specimens that had a faster growth rate (*M. annularis* from Tortuga and Boca de Medio), we analyzed every other 1-mm increment, whereas every sample from the slower growing colony (*S. siderea* from Testigos) was analyzed. Individual samples (8–10 mg) were placed in individual vacutainers, evacuated, heated, and then acidified with orthophosphoric acid at 90 °C. The evolved CO_2 was purified, trapped, and converted to graphite in the presence of an iron catalyst in individual reactors similar to the method described by Vogel et al. (1987). Graphite targets were measured at the Center for Accelerator Mass Spectrometry, Lawrence Livermore National Laboratory (Davis et al. 1990). ^{14}C results are reported as age-corrected $\Delta^{14}C$ (‰) as defined by Stuiver and Polach (1977) and include a background subtraction and the $\delta^{13}C$ correction obtained from the stable isotope results. Analytical precision and accuracy of the ^{14}C measurements is ±3.5‰ (1 σ) as monitored with an in-house homogenized coral standard and officially distributed secondary and tertiary ^{14}C standards.

RESULTS

Over the time frame of overlap (late 1930s through early 1940s), $\Delta^{14}C$ values at all 3 locations are very similar (Table 1). The mean Isla Tortuga $\Delta^{14}C$ is –51.9‰ (n = 40), the Boca de Medio $\Delta^{14}C$ averages –53.4‰ (n = 42), and the Los Testigos sample mean is –54.4‰ (n = 53). All 3 locations experience similar range in $\Delta^{14}C$. $\Delta^{14}C$ is not very well correlated with $\delta^{18}O$ (Figure 2) in the sense that there is not a consistent or strong seasonal cycle (in $\Delta^{14}C$). Between 1905 and 1908, $\Delta^{14}C$ values as recorded in the Islas Tortugas coral average –40.9‰ (n = 41; Figure 3). When compared to the Northern Hemisphere atmosphere in 1905 (–4.2‰), these results yield an equivalent reservoir age of 312 yr. The equivalent rate of change between ~1906 to ~1940 is –3‰ per decade.

Table 1 Weighted average of the absolute fraction modern and age-corrected $\Delta^{14}C$ (Stuiver and Polach 1977) from corals in the Cariaco region for 4 time windows.

Site		Abs Fm	$\Delta^{14}C$	±	*n*
Isla Tortugas					
1937.68	1943.29	0.9481	–51.9	3.3	40
1905.07	1907.71	0.9591	–40.9	4.5	41
Boca de Medio					
1942.48	1948.33	0.94660	–53.4	3.3	42
Los Testigos					
1934.21	1946.21	0.9457	–54.3	2.6	53

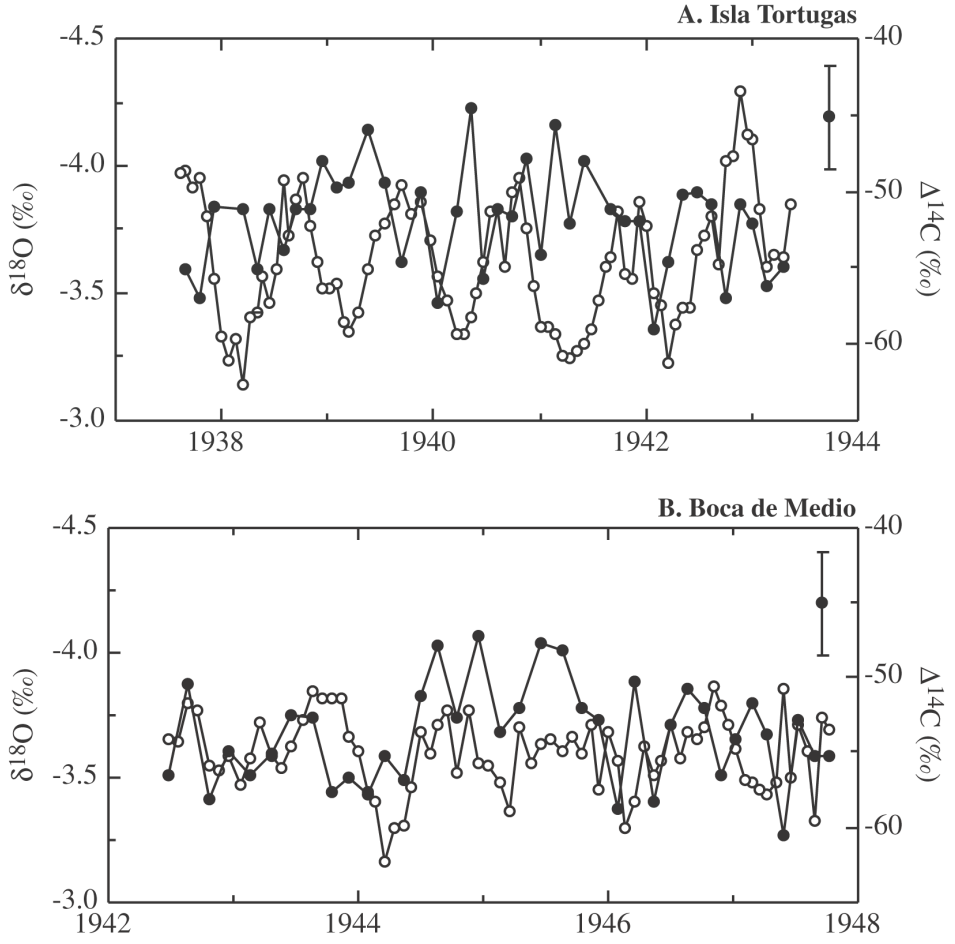

Figure 2 Coral $\Delta^{14}C$ (solid symbol) and $\delta^{18}O$ (open symbol) from a) Islas Tortugas, b) Boca de Medio, and c) Los Testigos. Data are plotted such that warmer sea surface temperatures (more negative $\delta^{18}O$) are upward. For clarity, we have plotted a representative 1-σ $\Delta^{14}C$ error bar to the right of each panel; d) the 3 coral-based ^{14}C time-series on a common time frame: Los Testigos (star), Boca de Medio (open symbol), and Islas Tortugas (closed symbol).

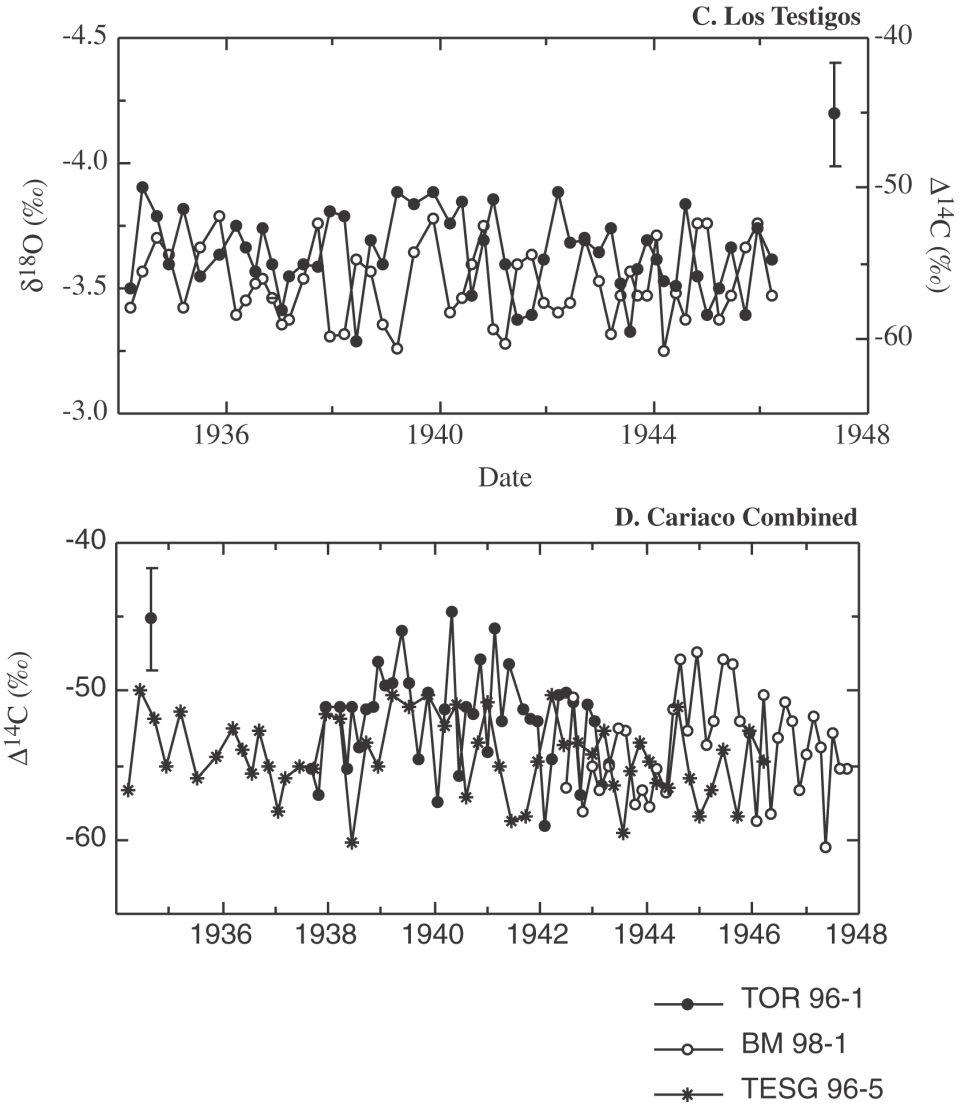

Figure 2 *(Continued)* Coral $\Delta^{14}C$ (solid symbol) and $\delta^{18}O$ (open symbol) from a) Islas Tortugas, b) Boca de Medio, and c) Los Testigos. Data are plotted such that warmer sea surface temperatures (more negative $\delta^{18}O$) are upward. For clarity, we have plotted a representative 1-σ $\Delta^{14}C$ error bar within each panel; d) The 3 coral-based ^{14}C time-series on a common time frame: Los Testigos (star), Boca de Medio (open symbol), and Islas Tortugas (closed symbol).

DISCUSSION

In the late 1930s to early 1940s, the 3 locations have similar absolute fraction modern or age-corrected $\Delta^{14}C$. No strong correlation between upwelling season and $\Delta^{14}C$ is observed. Over the respective sampling intervals, a z-score normalization (in which the mean is subtracted from the data and the result is divided by the standard deviation) of the individual $\delta^{18}O$ and $\Delta^{14}C$ shows no correlation (Figure 4). This is not surprising given the relatively shallow water that is the source for upwelling in the Cariaco Basin and along the Venezuelan Margin. In general, upwelling in this

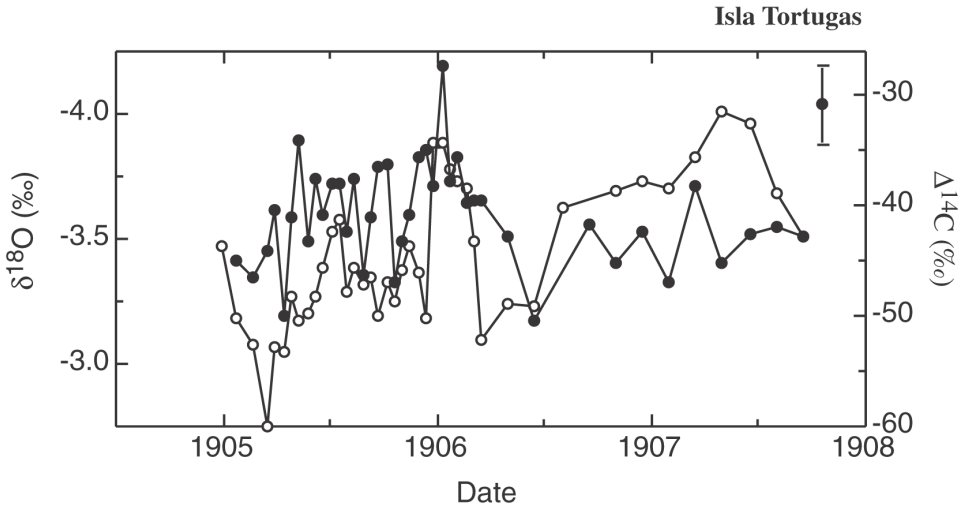

Figure 3 Turn-of-the-century coral $\Delta^{14}C$ at Isla Tortugas (solid symbols) and $\delta^{18}O$ (open symbols). Note the slightly different scales relative to Figure 2.

region taps subtropical underwater, a recently ventilated water mass that during formation undergoes significant air-sea exchange. Thus, in contrast to the conventional view of the influence of upwelling on $\Delta^{14}C$, very little depletion occurs. This indicates that there is very little difference in the ^{14}C character of the upwelled water and surface waters of the Caribbean, in stark contrast to the observations provided by nutrients (Astor et al. 2003; Thunell, personal communication). This observation reinforces the concept that ^{14}C in DIC is primarily a water-mass tracer, whereas nutrient content is a combination of pre-formed nutrient concentration (if applicable) and remineralization of recently exported particulates.

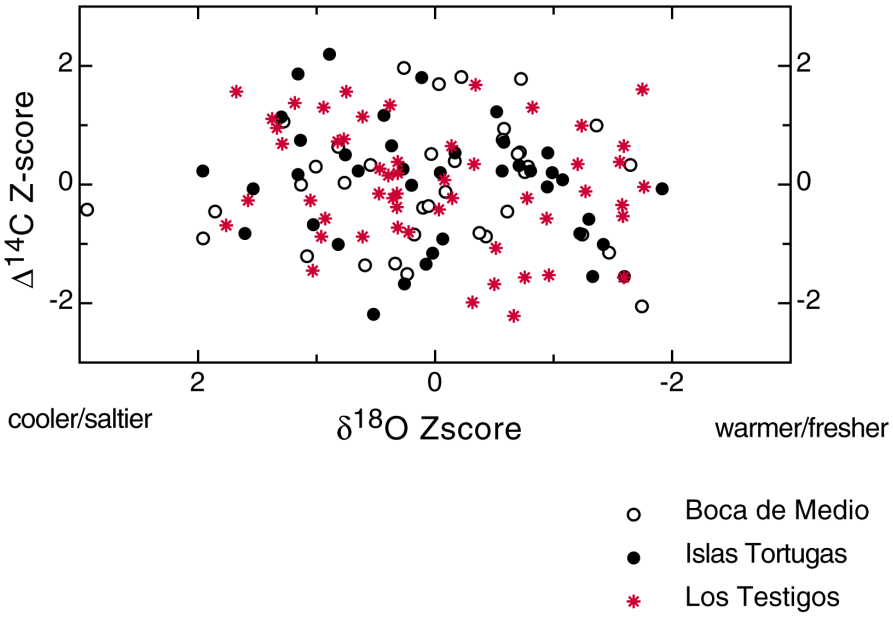

Figure 4 *Z*-score normalized $\delta^{18}O$ versus $\Delta^{14}C$ for the respective time-windows. Symbols as in Figure 2d.

It is instructive to assess the effect of ^{14}C-barren fossil fuel burning on atmospheric CO_2 and the subsequent effect observed in the ocean. The $\Delta^{14}C$ of ocean DIC oceanic response integrates air-sea CO_2 exchange and ocean dynamics. Over the length of the post-industrial period, atmospheric $^{14}CO_2$ has decreased from ~ –4‰ in 1880 (pentad centered on 1880) with similar values in 1900 (~ –3‰) to ~ –25‰ in 1950 prior to the advent of atmospheric nuclear weapons testing, yielding a rate of about –3‰ per decade. The Cariaco Basin's decrease in $\Delta^{14}C$ (Suess effect) is also about 3‰/decade determined between ~1905 and ~1940 and is similar to that predicted in a simple 1-D diffusion model (Table 2). Although it is possible that the observed decrease in $\Delta^{14}C$ observed at Cariaco is the result of ocean dynamics (e.g. changes in the water mass feeding the upwelling), the interpretation of least astonishment is that the decrease is a consequence of air-sea exchange and the carbon isotopic signature of fossil fuel CO_2 entering the surface ocean.

Table 2 Suess effect depletion of age-corrected $\Delta^{14}C$ recorded in circum-Atlantic surface water time-series. For comparison, we also present the synthetic marine response in a 1-D advection-diffusion model, and as recorded in the atmosphere (Stuiver et al. 1998). Coral and model data were averaged on the pentad centered on 1905 and 1940. (— means no Suess effect within uncertainty of measurements.)

Site, date	$\Delta^{14}C$ (‰)	Suess ^{14}C %/decade
North Rock Bermuda (Druffel 1997)		
1905	–46	—
1940	–44	
Honduras (Druffel 1980)		
1905	–47	–2.0
1940	–54	
Pickles Reef, Florida (Druffel 1997)		
1905	–49	—
1940	–48	
Plantation Key, Florida (Druffel 1982)		
1905	–49	—
1940	–52	
Islas Tortugas, this study		
1905	–42	–3.0
1940	–52	
1-D model (Stuiver et al. 1998)		–1.5
Atmosphere		–3.8

Our value is in general agreement with that determined by Druffel (1980) on a coral from Belize/Honduras, but not in exact agreement with the coral-based records from the Florida Keys (Druffel 1982; Druffel 1997) and Bermuda (Druffel 1997). Over the respective overlapping post-industrial period (~1880–1940), there is no significant linear trend in $\Delta^{14}C$ in the Bermuda and Florida Keys records, nor over the interval of common overlap (Figure 5). The Florida Keys records exhibit a

strong $\Delta^{14}C$ decrease between ~1940 and the mid-1950s, whereas the Bermuda record exhibits no decrease in $\Delta^{14}C$ over the length of the Suess interval. The subtle differences in the timing and amplitude of the Suess effect between the various records reinforces the potentially competing influences of air-sea exchange and ocean dynamics on the ^{14}C isotopic signature of surface waters.

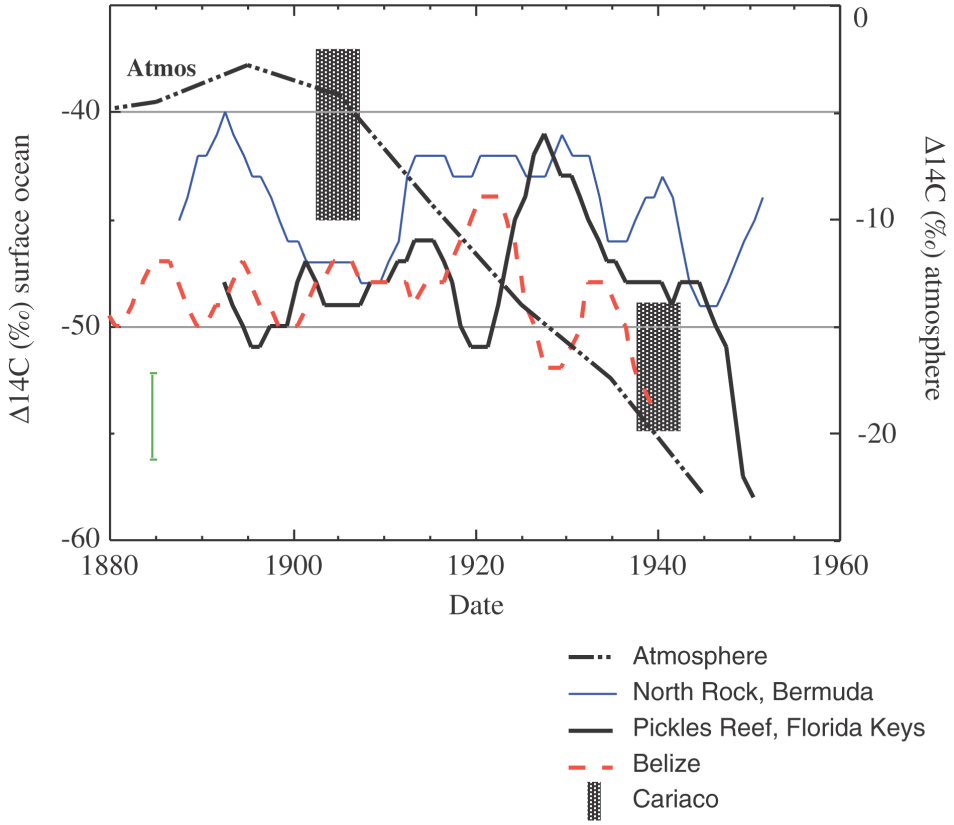

Figure 5 $\Delta^{14}C$ time histories (AD 1880–1950) of the atmosphere and the surface ocean as recorded in circum-Caribbean/Atlantic corals. Atmosphere data (dash dot) from Stuiver et al. (1998). Coral data are presented from Bermuda (thin solid line; Druffel 1997), Florida Keys (thick solid line; Druffel 1997), Belize (dashed; Druffel 1980), and Cariaco Basin (hatched boxes, this study). Coral data from Druffel are presented as pentad averages derived from annual linear interpolations to the original annual and biannual data. Representative 1-σ error bar for the Druffel data is in the lower left corner of the figure. Note that left and right vertical axes correspond to surface water (coral) and atmosphere data, respectively.

CONCLUSION

We have reconstructed the $\Delta^{14}C$ of late-1930s and early-1940s surface waters in and around the Cariaco Basin from hermatypic corals. We do not see a significant difference in values from within (Isla Tortugas, –51.9 ± 3.3‰) and outside (Boca de Medio, –53.4 ± 3.3‰; Los Testigos, –54.3 ± 2.6) of the basin. These values are similar to those of subtropical surface waters and indicate a shallow, well-ventilated source that feeds upwelling in the basin.

Samples from Isla Tortugas demark an ~11‰ decrease between ~1905 and ~1940. The implied Suess effect trend (–3‰/decade between 1905 and 1940) is nearly as large as that observed in the atmosphere (–4‰/decade) and larger than that estimated from other circum-Atlantic corals spanning the same time range.

If we assume that there is little to no fossil fuel $^{14}CO_2$ signature in Cariaco surface waters in ~1905, the waters have an equivalent reservoir age of ~312 yr. This is slightly younger than the ~420 yr reservoir age derived from measurements on mid-19th century planktonic foraminifera recovered from sediment cores (Black et al. 1999). The difference reflects natural variability related to stratification and the extent of air-sea isotopic equilibration in the basin and the formation regions of the subtropical underwaters.

ACKNOWLEDGMENTS

Collection of the coral cores supported by the NSF (OCE-9510062) to J E C and ^{14}C analyses by the UCDRD and LLNL/LDRD program to T G and J S. Comments and criticisms of this manuscript were provided by P Reimer and K Hughen. Preparation of graphite targets was performed by T G. We thank J Westbrook and P Zermeño for pressing the vast majority of graphite samples into targets, and H Barnett for help in sampling and processing cores. ^{14}C analyses were performed under the auspices of the US Department of Energy by the University of California Lawrence Livermore National Laboratory (contract W-7405-Eng-48). Data will be digitally archived at NOAA's World Data Center-A (Boulder, Colorado, USA).

REFERENCES

Astor Y, Muller-Karger F, Scranton MI. 2003. Seasonal and interannual variation in the hydrography of the Cariaco Basin: implications for basin ventilation. *Continental Shelf Research* 23:125–44.

Black DE, Peterson LC, Overpeck JT, Kaplan A, Evans MN, Kashgarian M. 1999. Eight centuries of North Atlantic Ocean atmosphere variability. *Science* 286: 1709–13.

Cole JE, Fairbanks RG, Shen GT. 1993. Recent variability in the Southern Oscillation: isotopic results from a Tarawa atoll coral. *Science* 260:1790–3.

Davis JC, Proctor ID, Southon JR, Caffee MW, Heikkinen DW, Roberts ML, Moore TL, Turteltaub KW, Nelson DE, Loyd DH, Vogel JS. 1990. LLNL/UC AMS facility and research program. *Nuclear Instruments and Methods in Physics Research B* 52:269–72.

Dodge RE, Vaisnys JR. 1980. Skeletal growth chronologies of recent and fossil corals. In: Rhoads DC, Lutz RA, editors. *Skeletal Growth of Aquatic Organisms, Top. Geobiology Volume 1*. New York: Plenum. p 493–517.

Druffel EM. 1980. Radiocarbon in annual coral rings of the Pacific and Atlantic oceans [PhD dissertation]. San Diego: University of California, San Diego. 213 p.

Druffel EM. 1982. Banded corals—changes in oceanic C-14 during the little ice age. *Science* 218:13–9.

Druffel ERM. 1997. Pulses of rapid ventilation in the North Atlantic surface ocean during the past century. *Science* 275:1454–7.

Druffel ERM. 1996. Post-bomb radiocarbon records of surface corals from the tropical Atlantic Ocean. *Radiocarbon* 38(3):563–72.

Guilderson TP, Schrag DP. 1999. Reliability of coral records from the western Pacific warm pool: a comparison using age-optimized records. *Paleoceanography* 14:457–64.

Hughen KA, Overpeck JT, Lehman SJ, Kashgarian M, Southon J, Peterson LC, Alley R, Sigman DM. 1998. Deglacial changes in ocean circulation from an extended radiocarbon calibration. *Nature* 391:65–8.

Hughen KA, Southon JR, Lehman SJ, Overpeck JT. 2000. Synchronous radiocarbon and climate shifts during the last deglaciation. *Science* 290:1951–4.

Muller-Karger F, Varela R, Thunell R, Scranton M, Bohrer R, Taylor G, Capelo J, Astor Y, Tappa E, Tung-Yuan H, Walsh JJ. 2001. Annual cycle of primary production in the Cariaco Basin: response to upwelling and implications for vertical export. *Journal of Geophysical Research* 106:4527–42.

Peterson LC, Haug GH, Hughen KA, Rohl U. 2000. Rapid changes in the hydrologic cycle of the tropical Atlantic during the last glacial. *Science* 290:1947–51.

Peterson LC, Overpeck JT, Kipp NG, Imbrie J. 1991. A high-resolution late-Quaternary upwelling record from the anoxic Cariaco Basin, Venezuela. *Paleoceanography* 6:99–119.

Stuiver M, Polach H. 1977. Discussion: reporting of ^{14}C data. *Radiocarbon* 19(3):355–63.

Stuiver M, Reimer PJ, Braziunas TF. 1998. High-precision radiocarbon age calibration for terrestrial and marine samples. *Radiocarbon* 40(3):1127–51.

Vogel JS, Southon JR, Nelson DE. 1987. Catalyst and binder effects in the use of filamentous graphite for AMS. *Nuclear Instruments and Methods in Physics Research B* 29:50–6.

RADIOCARBON, Vol 47, Nr 1, 2005, p 75–87

BLANK CORRECTION FOR $\Delta^{14}C$ MEASUREMENTS IN ORGANIC COMPOUND CLASSES OF OCEANIC PARTICULATE MATTER

Jeomshik Hwang[1] • Ellen R M Druffel

Department of Earth System Science, University of California-Irvine, Irvine, California 92697, USA.

ABSTRACT. Contaminant carbon (blank carbon) was studied for its impact on the carbon isotope measurements ($\Delta^{14}C$ and $\delta^{13}C$) of 3 organic compound classes of oceanic particulate organic matter. Two methods of blank correction and associated uncertainties were studied. First, the carbon blanks were quantified manometrically and the isotope ratios of the blank carbon were measured directly. Second, the isotope ratios of the blank carbon were estimated using the standard dilution method from the difference in $\Delta^{14}C$ values between unprocessed and processed standards. The 2 methods agreed within the uncertainties. The standard deviations of numerous $\Delta^{14}C$ measurements made on processed standard compounds were comparable to those of real samples. Blank correction using the standard dilution method is much less sensitive to the error in determination of blank carbon mass than is correction using the directly measured mass and $\Delta^{14}C$ values of the blank carbon. The standard dilution method is recommended for correcting $\Delta^{14}C$ analyses of small samples that involve incorporation of a significant amount of blank carbon.

INTRODUCTION

The advent of accelerator mass spectrometry (AMS) has made radiocarbon isotope measurements possible on very small samples. As sample size decreases, the importance of extraneous carbon, or the procedural blank, increases. If the sample size is sufficiently large, the effect of the blank is minimized. However, frequently it is not possible to obtain large samples of environmental materials. Blank corrections for isotope ratio measurements are different from those for quantitative analyses because the isotopic signature of the blank must be considered as well as its mass. In the unique case where the isotopic signature of the blank is the same as that of the sample, there is no need to correct the sample results.

Assuming that blank carbon has constant mass and isotopic signatures in all samples, the ^{14}C measurement can be easily blank-corrected. However, since blank correction requires information on the mass and the isotopic signature of the blank, the uncertainty in either or both of these terms may require processing of as many blanks and standards as samples.

An important additional issue in blank correction is the assignment of uncertainties to blank-corrected results. Although a measurement uncertainty is reported with the $\Delta^{14}C$ result by AMS laboratories, the total uncertainty is larger if sample preparation incorporates a significant amount of blank carbon. Total uncertainties should include the uncertainties of the mass and isotopic signature of the blank carbon.

In a previous study, we separated several organic compound classes from oceanic particulate organic matter (POM) and reported their carbon isotope ratios (Hwang and Druffel 2003). Because of extensive sample handling and chemical treatments, incorporation of blank carbon was inevitable. For example, extraneous carbon may have been introduced as a result of incomplete removal of organic solvents, presence of carbon-containing impurities in reagents, bleeding of organic carbon from ion-exchange resins, vaporization of vacuum grease, incorporation of dust, and leakage of CO_2 into the vacuum manifold. We studied the cumulative effect of these sources on the carbon isotope ratio measurements and compared different methods of blank correction. We report an example of blank correction based on our $\Delta^{14}C$ measurements of organic compound classes of oceanic POM. Hereafter, "samples" refer to the organic fraction samples in our previous work (Hwang and Druffel 2003).

[1]Corresponding author. Email: jeomshik@uci.edu.

PROCESSING OF SAMPLES, BLANKS, AND STANDARDS

In previous work, we separated 3 organic compound classes: lipids, total hydrolyzable amino acids (THAA), total hydrolyzable neutral carbohydrates (TCHO), as well as the acid-insoluble fraction from sinking POM. These 4 organic fractions comprised about 82 (±5)% of the total organic matter, with the rest lost during processing. Carbon isotope ratios of the organic fractions as well as total organic matter were measured.

A detailed description of the isolation method can be found in Wang et al. (1998). Briefly, lipids were extracted first using a 2:1 volume:volume mixture of methylene chloride:methanol. One half of the remaining sample was hydrolyzed with 6N HCl for 19 hr at 100 °C under N_2 gas. The hydrolyzate was neutralized with 1.5N NH_4OH, then eluted through a cation-exchange resin column to isolate THAA. The other half of the sample was hydrolyzed for 2 hr in 72% H_2SO_4 at room temperature, then for 3 hr in 1.2N H_2SO_4 at 100 °C. The hydrolyzate was neutralized with $Ba(OH)_2$ powder and NH_4OH, then eluted through an anion and cation mixed-resin column to isolate TCHO. Any organic carbon that remained after HCl-hydrolysis was defined as the acid-insoluble fraction. Separated organic fractions were transferred to quartz tubes (Vycor™), acidified with 1 mL of 3% phosphoric acid overnight, dried, evacuated under vacuum with CuO and silver foil, and flame-sealed, then combusted at 850 °C for 2 hr. Volume of the cryogenically purified CO_2 gas was measured manometrically. The last digit of the pressure gauge reading (0.01) was equivalent to 2 μg C. A split of the resultant CO_2 was graphitized on a Co catalyst under H_2 gas at 580 °C for 8 hr. The $\Delta^{14}C$ and $\delta^{13}C$ values were measured at the National Ocean Sciences AMS Facility, Woods Hole Oceanographic Institution, USA (NOSAMS); the Center for AMS Research, Lawrence Livermore National Laboratory, USA (LLNL); and the Keck Carbon Cycle AMS Laboratory, University of California, Irvine, USA (KCCAMS). The internal precision for the $\Delta^{14}C$ and $\delta^{13}C$ measurements was 5‰ and 0.1‰, respectively.

For the purpose of blank correction, we ran zero-material blanks by processing initially empty reaction vessels in a manner identical to the processing of a sample. Therefore, "blank carbon" in this paper is extraneous carbon introduced during the processing for separation of each organic fraction and combustion of extracted samples to CO_2 gas, which are the main processes for contamination. Contaminant carbon introduced during further processing—including splitting CO_2 gas for $\Delta^{14}C$ and reducing it to graphite—is not counted in the blank correction in this paper.

We also analyzed cod liver oil (SQUIBB), an amino acid standard solution (SIGMA AA-S-18, 18 amino acids), and anhydrous D-glucose powder (Fisher, certified grade) as standards for lipid, THAA, and TCHO fractions, respectively, in a manner identical to the processing of a sample. Two sizes of each standard were processed. One size was close to the range of sizes typically obtained for organic fractions of sinking POM (0.5 to 0.9 mg C) and the other was larger (2 to 4 mg C). The presumed "true" $\Delta^{14}C$ and $\delta^{13}C$ values of the standards were obtained by combustion of large (2.8 to 11 mg C) unprocessed material to minimize the blank effect from the combustion process.

RESULTS AND DISCUSSION

Direct Measurements of Masses and Isotopic Signatures of Blank Carbon

The average masses of blank carbon were 0.025 ± 0.017, 0.042 ± 0.038, and 0.053 ± 0.029 mg C for lipids, THAA, and TCHO, respectively. These are 3, 6, and 7% of the average masses of the lipid, THAA, and TCHO samples that were previously obtained for POM, respectively. The blank carbon would cause significant differences in the $\Delta^{14}C$ results if the $\Delta^{14}C$ values of blank carbon were different from those of the samples. The mass of the blank carbon for the acid-insoluble fraction was

0.006 ± 0.002 mg C, or 0.4% of the average sample size. In the worst-case scenario, blank carbon ($\Delta^{14}C = -1000‰$) would change the $\Delta^{14}C$ value of a sample ($\Delta^{14}C = 0‰$) by 4‰ according to a simple mass balance calculation, which is small compared to the uncertainty of the $\Delta^{14}C$ measurement.

Masses of blank carbon for each organic fraction do not show a statistical distribution around a mean, likely because of the small number of repetitions. Therefore, we assigned 1 standard deviation for each sample type as the uncertainty in the mass of the blank. However, it should be noted that 1 standard deviation in this case provides a smaller confidence level than in the case of a normal distribution (68%).

For the $\Delta^{14}C$ measurements, material from 5 to 6 runs was combined to obtain enough CO_2. Because of this pooling, information regarding the variability of the individual isotope ratios of blank carbon was lost. The $\Delta^{14}C$ values of blank carbon measured from the combined blanks were –800, –313, and –171‰ for lipids, THAA, and TCHO, respectively (Table 1).

Table 1 Measured and estimated values of masses and isotopic signatures of the blank for each organic fraction.

Type	Blank mass (m_b) measured[1] (mg C ± 1 SD)	Blank mass (m_b) estimated[2] (mg C)	$\Delta^{14}C$ (Δ_b) measured[3] (‰)	$\Delta^{14}C$ (Δ_b) estimated[4] (‰)	$\Delta^{14}C$ (Δ_b) estimated[2] (‰)
Lipids	0.025 ± 0.017 (6)	—	–800 ± 5	–600 ± 470	—
THAA	0.042 ± 0.038 (6)	0.023 ± 0.028	–313 ± 5	–630 ± 420	–950 ± 1300
TCHO	0.053 ± 0.029 (6)	—	–171 ± 5	–400 ± 300	—
Acid insoluble	0.006 ± 0.002 (5)	—	—	—	—

[1]Measured mass of blank carbon (m_b). The uncertainties are 1 standard deviations of the masses of blank of individual processing. In parentheses is the number of analyses.

[2]Estimated mass and the $\Delta^{14}C$ value of blank carbon for THAA using 2 standards: an AA standard solution and glutamic acid. The standard dilution method was used for calculation (see text). The uncertainties are propagated errors of the standard errors for slopes of the linear regression lines.

[3]Measured $\Delta^{14}C$ values of the accumulated blanks. The uncertainty reported by CAMS, LLNL is reported.

[4]The $\Delta^{14}C$ values calculated from the measured m_b and the results of the processed and the unprocessed standards. Each set (m_{s+b}, Δ_{s+b}) of standards was used with average Δ_s and m_b to calculate Δ_b using equation (1). The average of the calculated Δ_b values for each type is reported here. The uncertainties are the largest value among the calculated uncertainties using each set (m_{s+b}, Δ_{s+b}) of standards, and the standard deviation of calculated Δ_b values.

Estimation of Isotopic Signatures of Blank Carbon Using Standards

If incorporation of blank carbon has a significant effect on the $\Delta^{14}C$ measurement of samples, an effect will be observed when chemical standards are processed in the same way as the sample. Therefore, the change in $\Delta^{14}C$ of a standard by processing can be used to estimate the mass and $\Delta^{14}C$ value of the blank carbon (Pearson et al. 1998; McNichol et al. 2000).

The $\Delta^{14}C$ and $\delta^{13}C$ values and the sizes of the processed standards are listed in Table 2. The $\Delta^{14}C$ values of the smaller-sized standards after processing were lower than the true values by 17‰, 38‰, and 49‰ for lipids, THAA, and TCHO standards, respectively (Table 2). These changes are larger than measurement uncertainties reported by AMS laboratories (3–8‰), clearly showing the need for blank corrections.

The variability of $\Delta^{14}C$ values for the processed standards provides an estimate of the uncertainty expected for real samples, provided their sizes and $\Delta^{14}C$ values are similar to the samples. The standard deviations for $\Delta^{14}C$ values of standards of similar size (0.5–0.9 mg C) to our samples were ±14, ±10, and ±15‰ for lipids, THAA, and TCHO standards, respectively (Table 2).

Table 2 The masses, $\Delta^{14}C$, $\delta^{13}C$ values and the average values (±SD) of the unprocessed and processed standards.

Standard		Size (mg C)	$\Delta^{14}C$ (‰)	Average	$\delta^{13}C$ (‰)	Average
Cod liver oil	unprocessed (Δ_{std})	2.98	47		–25.5	
		11.69	44		–25.5	
		9.83	46		–25.4	
		11.31	37		–25.4	
		0.58	38	43 ± 5	–25.4	–25.4 ± 0.1
		1.48	45		–25.4	
		2.22	44		–25.3	
		7.21	43		–25.4	
	processed (Δ_{std+b})	3.32	39	36 ± 5	–25.4	–25.4 ± 0.1
		3.53	37		–25.4	
		0.85	11		–25.7	
		0.92	34	26 ± 14	–25.5	–25.6 ± 0.1
		0.67	34		–25.5	
AA standard solution	unprocessed (Δ_{std})	3.60	–166		–19.9	
		3.19	–189	–176 ± 12	–19.9	–19.9 ± 0.1
		1.69	–173			
	processed (Δ_{std+b})	2.49	–192		–20.2	
		0.74	–226		–20.9	
		0.77	–222		–20.7	
		0.74	–211	–214 ± 10	–20.7	–20.7 ± 0.1
		0.73	–211		–20.6	
		0.65	–200		–20.7	
D-glucose	unprocessed (Δ_{std})	8.08	107		–10.2	
		8.63	88		–10.2	
		7.65	96		–10.0	
		8.20	101		–10.0	
		7.14	95	98 ± 6	–9.9	–10.0 ± 0.1
		0.67	106		–10.0	
		0.93	94		–10.0	
		1.81			–10.0	
		5.10	95		–10.0	
	processed (Δ_{std+b})	1.823	89	84 ± 5	–10.5	–10.6 ± 0.1
		1.810	80		–10.8	
		0.578	45		–10.5	
		0.558	67	49 ± 15	–10.7	–10.6 ± 0.1
		0.520	54			
		0.560	32		–10.7	

As a test for consistency of blanks (i.e. constant mass and isotopic signatures of blank carbon from run to run), the true isotopic signatures of the standards were estimated from those of the processed standards using the standard dilution method. If isotope ratios of at least 2 different-sized standards are measured, the true value of the standard can be estimated from a mass balance equation (Hayes 2002):

$$\Delta_{s+b} m_{s+b} = \Delta_b m_b + \Delta_s m_s = \Delta_b m_b + \Delta_s (m_{s+b} - m_b) \quad (1)$$

where Δ is $\Delta^{14}C$, m is mass of carbon, and subscripts $_b$ and $_s$ are blank and standard, respectively. Fractional abundance of ^{14}C must be rigorously used for the mass balance calculation. For environmental samples, however, using $\Delta^{14}C$ instead of fractional abundance will cause a negligible error compared to the measurement uncertainty of $\Delta^{14}C$ (see John Hayes' excellent lecture notes: Hayes 2002). Assuming that Δ_b and m_b are constant, equation (1) can be expressed as a linear equation with $1/m_{s+b}$ as the x variable and Δ_{s+b} as the y variable:

$$\Delta_{s+b} = \Delta_s + (\Delta_b - \Delta_s)m_b \times \frac{1}{m_{s+b}} \quad (2)$$

The true $\Delta^{14}C$ (or $\delta^{13}C$) of the standard (Δ_s) is the y intercept of the linear regression line. The $\Delta^{14}C$ values of the standards for several different sizes that have undergone the same separation processes as the samples were used to calculate Δ_s (Figure 1a–c). The y intercepts (Δ_s) calculated by linear regression of the data were 40 ± 11‰, –190 ± 16‰, and 99 ± 14‰ (the uncertainties are standard errors) for cod liver oil, AA standard solution, and D-glucose, respectively. These were within the uncertainties of the true $\Delta^{14}C$ values of the unprocessed standards (thick lines on the y axes of each graph: 43 ± 5, –176 ± 12, and 98 ± 6 for cod liver oil, AA standard solution, and D-glucose, respectively). Since the true $\Delta^{14}C$ values of the standards could indeed be estimated from those of the processed standards, this indicates that the masses and the isotopic signatures of blank carbon were consistent from run to run within the error range of our true values (Figure 1).

Theoretically, both the mass and isotopic signature of the blank carbon can be calculated using the standard dilution method if two or more kinds of standards are used. Two different values for the slope in equation (2), $(\Delta_b - \Delta_s)m_b$, from 2 different standards, enable calculation of both Δ_b and m_b, when Δ_s is known. However, only 1 standard was used for each organic fraction in previously reported work. Therefore, only 1 mass balance equation was available for 2 variables, requiring one of them to be determined by an independent method. Once m_b or Δ_b is determined, the other can be calculated using the mass balance equation (1). For example, $\Delta^{14}C$ of blank carbon (Δ_b) for a lipid standard (measured mass of the standard, m_{s+b} = 0.92 mg C; Δ_{s+b} = 34‰) can be calculated from the $\Delta^{14}C$ value of the unprocessed standard (Δ_s = 43‰) and mass of blank carbon (m_b = 0.025 mg C) using equation (1); $34‰ \times 0.92 = \Delta_b \times 0.025 + 43‰ \times (0.92–0.025)$, Δ_b = –288‰. Averages of the estimated Δ_b values from results of the processed standard for each organic fraction in this way are –600 ± 470‰, –630 ± 420‰, and –400 ± 300‰ for lipids, THAA, and TCHO fractions, respectively (Table 1). The estimated $\Delta^{14}C$ values have large uncertainties; therefore, they are not different from the measured values. The large uncertainties are mainly caused by the uncertainties in m_b measurements.

For the THAA fraction, glutamic acid was also used as a standard later in the laboratory. We used the results of glutamic acid, in addition to those of the AA standard solution, to calculate Δ_b and m_b using the standard dilution method. Both Δ_b and m_b were calculated using the values of the 2 linear regression lines (Figure 2 and Table 1). Unfortunately, the uncertainties for Δ_b and m_b were large, mainly because the slopes were similar to each other (–17.6 and –24.4). Subtraction of 2 similar values with large uncertainties resulted in a large total uncertainty. Therefore, for the effective use of the standard dilution method, it is crucial to choose standards that have considerably different $\Delta^{14}C$ values to obtain a small total uncertainty.

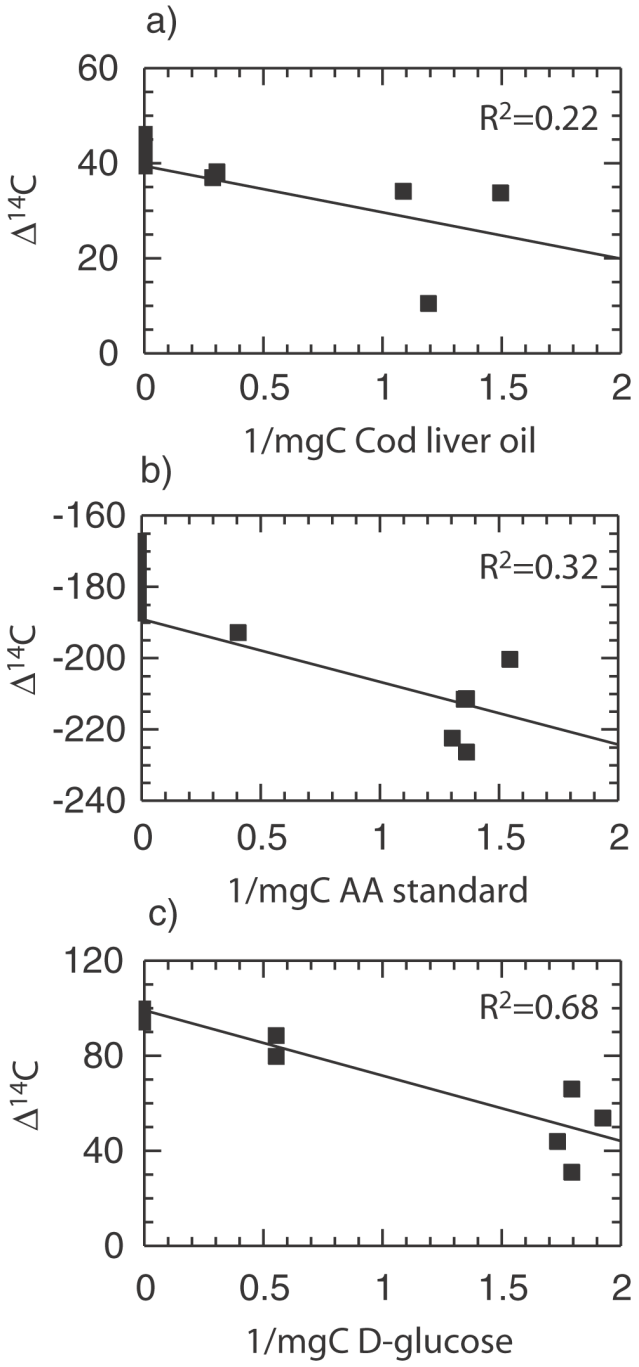

Figure 1 Estimation of true $\Delta^{14}C$ values of the standards from those of the processed standards for a) cod liver oil, b) AA standard solution, and c) D-glucose by the standard addition method. The thick line on the left *y* axis of each graph indicates the true values determined by combustion of large unprocessed standards, with 1 standard deviation of individual standards (Table 2).

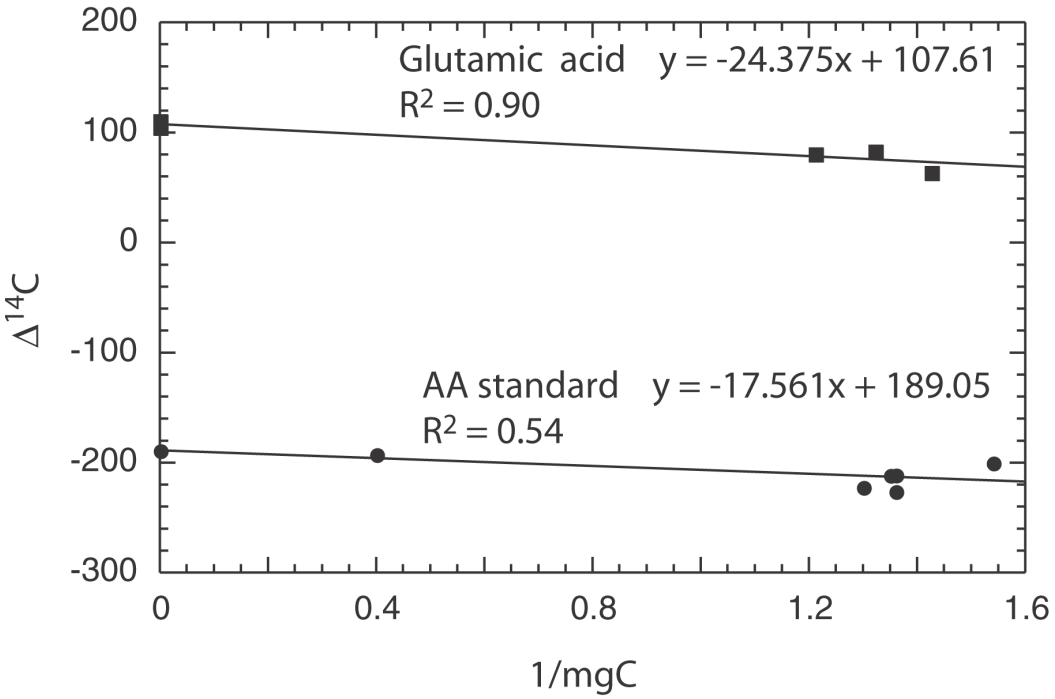

Figure 2 The standard dilution method was used to calculate the mass and $\Delta^{14}C$ value of blank carbon for the THAA fraction from the results of an AA standard solution and glutamic acid (see text).

Blank Correction and Associated Uncertainties

Blank correction can be performed using the mass balance equation:

$$\Delta_{smp} = \frac{\Delta_{smp+b} \times m_{smp+b} - \Delta_b \times m_b}{m_{smp+b} - m_b} \quad (3)$$

where subscript $_{smp}$ is sample, and $_b$ is blank. Equation 3 can be used when Δ_b, m_b, and their uncertainties can be directly determined. However, the uncertainty of Δ_b could not be determined because the mass of blank carbon from individual processing was too small for $\Delta^{14}C$ measurement.

However, mathematically more robust calculations for both blank correction and uncertainty determination can be used when one or more of these numbers is not measured directly. Equation (3) is modified in equation (4), so that $\Delta_b \times m_b$ can be determined indirectly from the processed (Δ_{std+b}) and unprocessed (Δ_{std}) standards:

$$\Delta_{smp} = \frac{\Delta_{smp+b} \times m_{smp+b} - [\Delta_{std+b} \times m_{std+b} - \Delta_{std} \times (m_{std+b} - m_b)]}{m_{smp+b} - m_b} \quad (4)$$

where subscript $_{std}$ is standard.

The total uncertainties can be determined mathematically in equation (4) because the uncertainties for all variables are available. (Detailed equations for the total uncertainty calculation appear in the Appendix.) The blank-corrected $\Delta^{14}C$ value of a sample (Δ_{smp}) is calculated from one sample result (Δ_{smp+b}, m_{smp+b}) using the results of a processed standard (Δ_{std+b}, m_{std+b}). Table 3 shows an example

of blank correction for a lipid $\Delta^{14}C$ measurement (Δ_{smp+b} = –36‰, m_{smp+b} = 0.79) using 3 sets of standard results (Δ_{std+b} = 34‰, 34‰, 11‰ when m_{std+b} = 0.92, 0.67, and 0.85 mg C, respectively). The average value (–21‰) of the 3 results of Δ_{smp} is reported as the blank-corrected $\Delta^{14}C$ value. The total uncertainty for each standard result ($\sigma\Delta_{smp}$ in each row in Table 3) is calculated using equation (A1). The larger of the average of the total uncertainties ($\sigma\Delta_{smp}$) and the standard deviation of the 3 blank-corrected $\Delta^{14}C$ values (Δ_{smp}) is reported as the final uncertainty (in this case, 15‰).

Table 3 An example of blank correction. A measured $\Delta^{14}C$ value (Δ_{smp+b}) is blank corrected using equation (4). The total uncertainties are calculated using equation (A1). Three sets of standard results (Δ_{std+b}, m_{std+b}) are used to correct the sample result. The average value (–21‰) of the calculated Δ_{smp} (–27.8, –30.7, and –3.0‰) is taken as the blank-corrected value. The larger of the average (9.5‰) of the total uncertainties ($\sigma\Delta_{smp}$, 10.0, 8.2, and 10.2‰) and the standard deviation (15‰) of the blank-corrected values (Δ_{smp}, –27.8, –30.7, and –3.0‰) is taken as the final uncertainty. Therefore, the blank-corrected result in this example is –21 ± 15‰. (The lower set of rows is a continuation of the upper set.)

Standards	Δ_{smp+b}[1] ‰	$\sigma\Delta_{smp+b}$[2] ‰	Δ_{std+b}[3] ‰	$\sigma\Delta_{std+b}$[2] ‰	Δ_{std}[4] ‰	$\sigma\Delta_{std}$[4] ‰	m_{smp+b}[5] mg	σm_{smp+b}[6] mg	m_{std+b}[3] mg	σm_{std+b}[6] mg
Lipids	–36	5	34	5	43	5	0.79	0.04	0.92	0.092
	–36	5	34	5	43	5	0.79	0.04	0.67	0.067
	–36	5	11	5	43	5	0.79	0.04	0.85	0.085

m_b[7] mg	σm_b[7] mg	$\frac{\partial\Delta_{smp}}{\partial\Delta_{smp+b}}$	$\frac{\partial\Delta_{smp}}{\partial\Delta_{std+b}}$	$\frac{\partial\Delta_{smp}}{\partial\Delta_{std}}$	$\frac{\partial\Delta_{smp}}{\partial m_{smp+b}}$	$\frac{\partial\Delta_{smp}}{\partial m_{std+b}}$	$\frac{\partial\Delta_{smp}}{\partial m_b}$	Δ_{smp}[8] ‰	$(\sigma\Delta_{smp})^2$	$\sigma\Delta_{smp}$[9] ‰
0.025	0.017	1.0	–1.2	1.2	–10.8	11.8	–92.5	–27.8	100.9	10.0
0.025	0.017	1.0	–0.9	0.8	–6.9	11.8	–96.3	–30.7	67.0	8.2
0.025	0.017	1.0	–1.1	1.1	–43.1	41.8	–60.2	–3.0 Avg = –21 SD = 15	103.2	10.2

[1]Measured $\Delta^{14}C$ value of a lipid fraction.
[2]The internal precision (the measurement uncertainty only) is given as the uncertainty of any measured $\Delta^{14}C$ values.
[3]$\Delta^{14}C$ values and mass of the processed standards. Three sets of $\Delta^{14}C$ value and mass of the processed cod liver oil were used for blank correction of 1 sample $\Delta^{14}C$ value.
[4]Average $\Delta^{14}C$ value of the unprocessed cod liver oil and 1 standard deviation as the uncertainty.
[5]Mass of lipid fraction measured manometrically.
[6]5% of the measured value was assigned as an uncertainty for any measured mass.
[7]Measured mass of blank carbon. One standard deviation was assigned as the uncertainty.
[8]Blank-corrected values.
[9]The total uncertainties of the blank-corrected result.

An example of a lipid $\Delta^{14}C$ measurement (first row in Table 3, Δ_{smp+b} = –36‰, Δ_{std+b} = 34‰, Δ_{std} = 43‰, m_{smp+b} = 0.79, m_{std+b} = 0.92; second row, m_b = 0.025) was used as a model case to study the dependence of the total uncertainty on m_b and m_{std+b} in the following discussion. Equation (4) is especially useful when direct measurements of m_b and Δ_b are subject to large uncertainties. The uncertainty ($\sigma\Delta_{smp}$) of the blank-corrected result is not heavily dependent on m_b, as explained by the small values of $\partial\Delta_{smp}/\partial m_b$ ($\partial\Delta_{smp}/\partial m_b$ = –93, meaning a –93‰ change in Δ_{smp} per 1 mg error in determination of the mass of the blank. See the first row of Table 3 and the Appendix for the calculation of $\partial\Delta_{smp}/\partial m_b$. An error of ±0.017 mg C (σm_b), associated with determination of m_b, is equivalent to ±1.6‰ in the final result. Figure 3 shows that when equation (4) is used (solid line),

the blank-corrected $\Delta^{14}C$ value does not change much depending on m_b. However, if the directly measured values (Equation 3) are used, the blank-corrected $\Delta^{14}C$ value changes much more than the $\Delta^{14}C$ value determined by the standard dilution method (Equation 4). For example, $\partial\Delta_{smp}/\partial\, m_b = [m_{smp+b} \times (\Delta_{smp+b}-\Delta_b)]/(m_{smp+b}-m_b)^2 = 789‰/\text{mg C}$ when the same values are used.

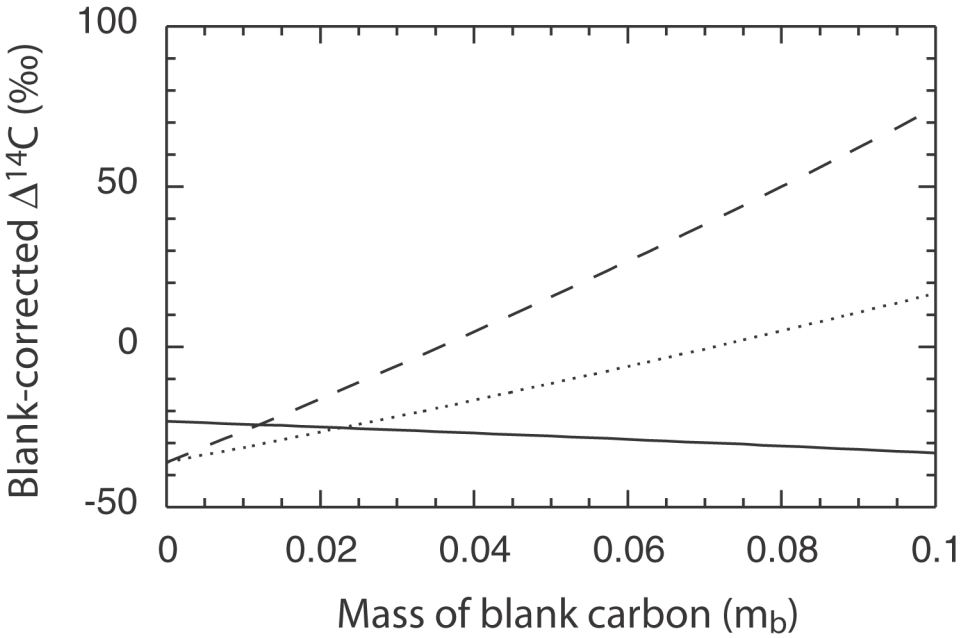

Figure 3 A model case showing the dependence of blank-corrected $\Delta^{14}C$ results on the mass of blank carbon (m_b). All other parameters were fixed in the model case and m_b was varied to simulate an error in its determination. Blank-corrected results were much less sensitive when equation (4) was used (standard dilution method, solid line) than when equation (3) was used (direct measurements). The dotted and dashed are when the blank $\Delta^{14}C$ value was –400‰ and –800‰, respectively.

Low sensitivity to the uncertainty in m_b is important because the direct measurements of m_b can be erroneous. The incorporation of blank carbon during the simulated processing of a sample may not adequately mimic the incorporation of extraneous carbon when a sample is present. This may be caused by differences in the physical environment, such as the surface of the sample, existence of mineral in the real sample to enhance the sorption of blank carbon, or other factors. Manometric determination of CO_2 also can be erroneous. During the cryogenic purification of CO_2, other vapors (such as N_2O, NO, HCl, and H_2O) can escape a dry ice/isopropyl alcohol trap and be collected in the liquid nitrogen trap with the CO_2 gas (Pearson et al. 1998; Currie at al. 2000). For the absolute determination of CO_2 gas, other analytical methods (such as gas chromatography and mass spectrometry) are necessary (Pearson et al. 1998).

It is important to use a small standard when employing the standard dilution method for blank correction because the total uncertainty of the blank-corrected value increases as m_{std+b} increases (Figure 4). This is because the effect of blank becomes less significant as the size of a standard increases. The total uncertainty was calculated as a function of the size of a standard, using our model case in Table 3 to demonstrate this. When the size of the standard exceeds 1 mg C, total uncertainty exceeds 10‰. Although 2 sizes of standards were processed, the larger standards resulted in over ±20‰ total uncertainties.

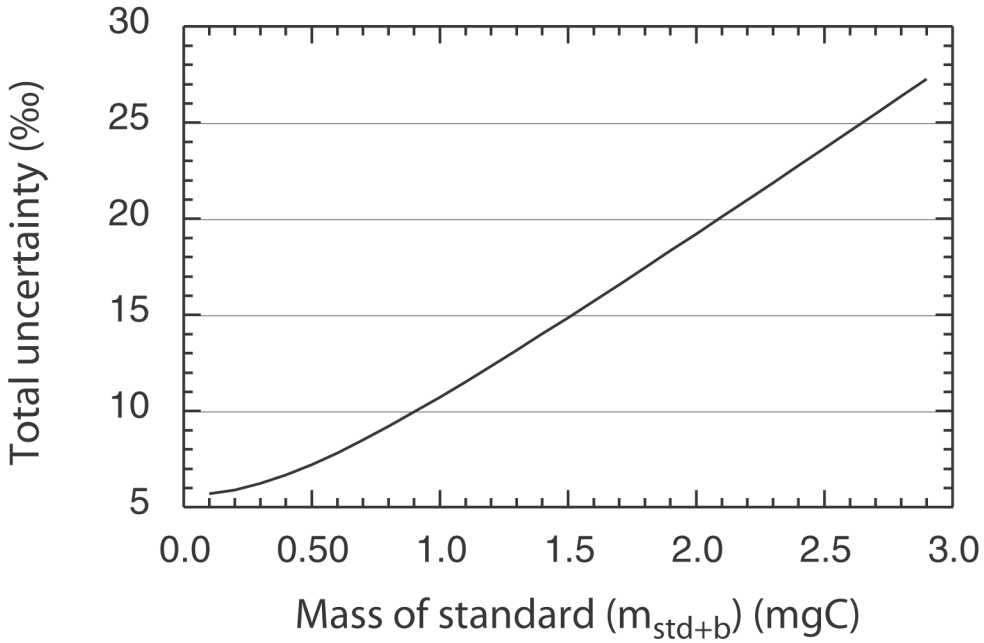

Figure 4 A model case showing the dependence of total uncertainty of a blank-corrected $\Delta^{14}C$ value of a sample on the mass of standard when the standard dilution method was used. The total uncertainty was calculated using equation (A1), varying m_{std+b} and consequently Δ_{std+b}, but with the other parameters fixed. As the mass of a standard increases, total uncertainty increases as well. The plot shows that the mass of the standard should be smaller than 1 mg C to obtain a total uncertainty smaller than 10‰.

The total uncertainties of $\Delta^{14}C$, when equation (4) was used for blank correction of samples in previous work, were 15‰ for lipids (Table 3) and 13 and 21‰ for THAA, and TCHO, respectively (not shown). These values are comparable to the standard deviations of the processed standards of similar size discussed previously in the section "Estimation of Isotopic Signatures of Blank Carbon Using Standards" (Table 2). The fact that the uncertainties determined by the 2 methods are comparable makes the assigned total uncertainties meaningful. Furthermore, it implies that if a proper standard is used, the uncertainty obtained from the processed standard can be justifiably assigned for a sample.

Verification of Blank-Corrected Values

The $\Delta^{14}C$ value of a total organic matter sample can be calculated using a mass balance equation from the percentages of the 4 organic fractions extracted from the sample and their $\Delta^{14}C$ values. Although not perfect (because the recovered fractions comprise only about 82% of the bulk samples), the $\Delta^{14}C$ values calculated in this way can be compared to those measured independently by combustion of total organic matter samples. When the initial results of the organic fractions were used without blank correction, the calculated $\Delta^{14}C$ values of the total organic matter samples (open squares in Figure 5) were lower than the measured values by an average of 16 (±10)‰. This is consistent with the existence of a blank carbon with a $\Delta^{14}C$ value lower than that of the sample. After blank correction using the standard dilution method (solid squares in Figure 5), the average difference between the calculated and measured $\Delta^{14}C$ values was 1 ± 10‰.

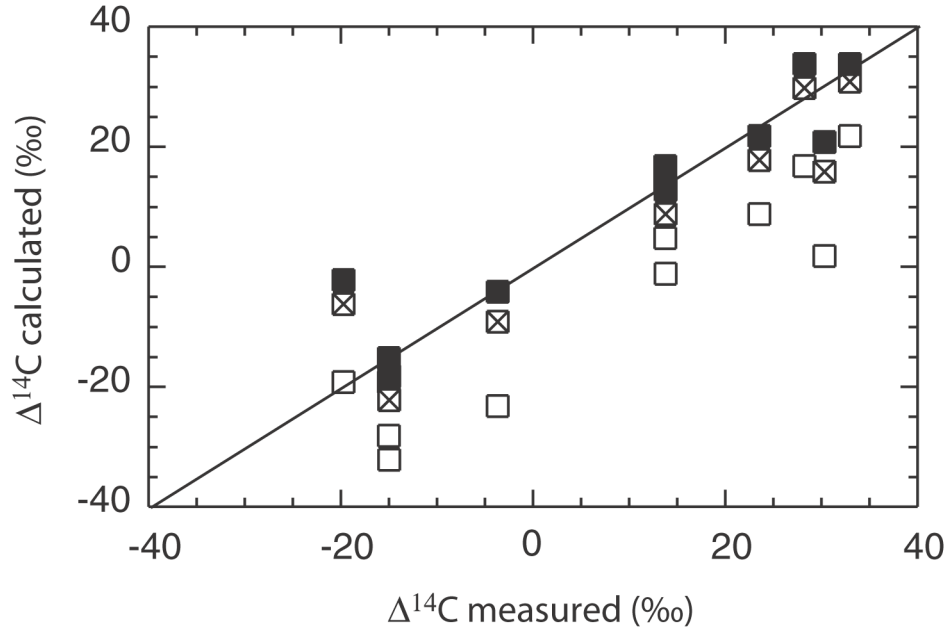

Figure 5 Independently measured $\Delta^{14}C$ values of the total organic matter were compared to the calculated values from the 4 organic fractions using a mass balance equation. Open squares are the results when raw $\Delta^{14}C$ values of the organic fractions were used for a mass balance calculation. Solid squares and open squares with diagonal crosses are the results when $\Delta^{14}C$ values of the organic fractions were blank-corrected using measured m_b and estimated Δ_b (standard dilution method) and measured m_b and Δ_b (direct measurements), respectively. The calculated $\Delta^{14}C$ values using blank-corrected values of the organic fractions were close to the $\Delta^{14}C$ values of total organic matter.

CONCLUSION

It has been shown that the incorporation of contaminant carbon during processing can change the $\Delta^{14}C$ values of small organic samples beyond the uncertainties inherent in the $\Delta^{14}C$ measurements themselves. Two methods of blank correction were compared. For direct measurements, repetition of processing is necessary to obtain enough CO_2 for the $\Delta^{14}C$ measurements. The uncertainty in the $\Delta^{14}C$ determination of individual blanks cannot be obtained by this method. The total uncertainty by this method heavily depends on the uncertainty in determination of the mass of blank carbon, the measurement of which may be erroneous (i.e. contaminating gases). Furthermore, handling of small-volume samples on a vacuum line to combine the individual blanks is subject to more contamination.

The standard dilution method is recommended for blank correction, though it is time consuming and requires numerous $\Delta^{14}C$ measurements of standards. Processing of two or more types of standards is the best method to obtain both the mass and $\Delta^{14}C$ values of blank carbon. However, it must be noted that the standards should have a wide range of $\Delta^{14}C$ values in order to obtain small total uncertainties.

When only one kind of standard is used, the mass of blank carbon needs to be determined by an independent method. However, blank correction using this method is not very sensitive to the error in determination of the mass of blank carbon. Another advantage of the standard dilution method is that the standard can be chosen or made to simulate samples closely. For example, an amino acid

mixed with carbon-free minerals can be used as a standard for THAA of POM or sediment. The results of standards can provide a realistic estimate of the actual total uncertainty for isotopic measurements of samples. This is useful especially when multiple analyses of one sample are not possible due to size limitations.

ACKNOWLEDGMENTS

We thank Sheila Griffin for guidance in the laboratory; John Southon, Guaciara dos Santos, and Xiaomei Xu at the Keck Carbon Cycle AMS Laboratory at UC Irvine; Ann McNichol, Al Gagnon, and John Hayes at NOSAMS, WHOI; John Southon and colleagues at CAMS, LLNL for $\Delta^{14}C$ and $\delta^{13}C$ measurements; Sue Trumbore and Shuhui Zheng for shared resources; and John Southon and Ann Pearson for valuable and insightful comments on the manuscript. This research was supported by the UCOP Marine Science Fellowship Program (to J H), ACS Petroleum Research Fund, and NSF Chemical Oceanography Program (to E R M D).

REFERENCES

Currie LA, Kessler JD, Marolf JV, McNichol AP, Stuart DR, Donoghue JC, Donahue DJ, Burr GS, Biddulph D. 2000. Low-level (submicromole) environmental ^{14}C metrology. *Nuclear Instruments and Methods in Physics Research B* 172:440–8.

Hayes JM. 2002. Practice and principles of isotopic measurements in organic geochemistry [lecture]. URL: <http://www.nosams.whoi.edu/general/jmh/IsoNotesAug02.pdf>. Accessed 2003 March.

Hwang J, Druffel ERM. 2003. Lipid-like material as the source of the uncharacterized organic carbon in the ocean? *Science* 299:881–4.

McNichol AP, Ertel JR, Eglinton TI. 2000. The radiocarbon content of individual lignin-derived phenols: technique and initial results. *Radiocarbon* 42(2):219–27.

Pearson A, McNichol AP, Schneider RJ, von Reden KF, Zheng Y. 1998. Microscale AMS ^{14}C measurement at NOSAMS. *Radiocarbon* 40(1):61–75.

Wang X-C, Druffel ERM, Griffin S, Lee C, Kashgarian M. 1998. Radiocarbon studies of organic compound classes in plankton and sediment of the northeastern Pacific Ocean. *Geochimica et Cosmochimica Acta* 62: 1365–78.

APPENDIX

Error Analysis

The total uncertainty of the blank-corrected values using equation (4) can be calculated by the following equation:

$$(\partial\Delta_{smp})^2 = \left(\frac{\partial\Delta_{smp}}{\partial\Delta_{smp+b}}\right)^2(\partial\Delta_{smp+b})^2 + \left(\frac{\partial\Delta_{smp}}{\partial\Delta_{std+b}}\right)^2(\partial\Delta_{std+b})^2 + \left(\frac{\partial\Delta_{smp}}{\partial\Delta_{std}}\right)^2(\partial\Delta_{std})^2 \quad \text{(A1)}$$

$$+ \left(\frac{\partial\Delta_{smp}}{\partial m_{smp+b}}\right)^2(\partial m_{smp+b})^2 + \left(\frac{\partial\Delta_{smp}}{\partial m_{std+b}}\right)^2(\partial m_{std+b})^2 + \left(\frac{\partial\Delta_{smp}}{\partial m_b}\right)(\partial m_b)^2$$

where Δ and m are $\Delta^{14}C$ (or $\delta^{13}C$) and mass of blank carbon, respectively, and subscripts $_{smp}$, $_{std}$, and $_b$ are sample, standard, and blank, respectively;

$$\frac{\partial\Delta_{smp}}{\partial\Delta_{smp+b}} = \frac{m_{smp+b}}{m_{smp+b} - m_b}$$

$$\frac{\partial \Delta_{smp}}{\partial \Delta_{std+b}} = \frac{-m_{std+b}}{m_{smp+b} - m_b}$$

$$\frac{\partial \Delta_{smp}}{\partial \Delta_{std}} = \frac{m_{std+b} - m_b}{m_{smp+b} - m_b}$$

$$\frac{\partial \Delta_{smp}}{\partial m_{smp+b}} = \frac{-m_b \times (\Delta_{smp+b} - \Delta_{std}) + m_{std+b} \times (\Delta_{std+b} - \Delta_{std})}{(m_{smp+b} - m_b)^2}$$

$$\frac{\partial \Delta_{smp}}{\partial m_{std+b}} = \frac{-\Delta_{std+b} + \Delta_{std}}{m_{smp+b} - m_b}$$

$$\frac{\partial \Delta_{smp}}{\partial m_b} = \frac{m_{smp+b} \times (\Delta_{smp+b} - \Delta_{std}) - m_{std+b} \times (\Delta_{std+b} - \Delta_{std})}{(m_{smp+b} - m_b)^2} .$$

RADIOCARBON, Vol 47, Nr 1, 2005, p 89–97

A SIMPLE, EXTREMELY STABLE SINGLE-TUBE LIQUID SCINTILLATION SYSTEM FOR RADIOCARBON DATING

Pall Theodórsson

Science Institute, University of Iceland, Dunhaga 3, IS-107 Reykjavík, Iceland. Email: pth@raunvis.hi.is.

ABSTRACT. This paper describes a simple and compact liquid scintillation radiocarbon dating system, ICELS, and demonstrates its long-term stability and reproducibility to a precision level rarely presented before, better than 0.04% (3 ^{14}C yr). Inexpensive systems of this kind may, in the future, help to meet increasing demand for high precision (±16 to ±20 ^{14}C yr) and strict quality control. ICELS comprises a compact detector unit, where a 3-mL dome-shaped vial, with an optimal light reflector, sits on the top of a vertical 30-mm photomultiplier tube. Sample changing is manual. The high voltage is set at the balance point for each sample, securing maximal counting stability. The quench correction method used (spectrum restoration) corrects with 0.04% precision for all parameters that can normally shift the ^{14}C spectrum. For 3 mL of benzene at 71% ^{14}C counting efficiency (recent carbon 23 cpm), the background is 1.72 cpm behind a 5-cm-thick shield of lead (27 kg) and 1.53 cpm behind 10 cm of lead. The background count rate corrected for atmospheric pressure variations was completely stable over 47- and 57-d testing periods for the 2 systems.

INTRODUCTION

Liquid scintillation (LS) counting has been the preferred method of radiometric radiocarbon dating laboratories established during the last 3 decades. The systems used today are nearly all based on the 2-photomultiplier tube (PMT) coincidence technique, and were originally designed for biomedical tracer studies where a variety of radioisotopes of wide energy and quench level range are measured. Since the mid-1980s, low-level systems of similar type but redesigned or modified for low-level counting, have been produced (Kojola et al. 1984; Noakes et al. 1989) and are now preferred in ^{14}C dating despite their higher price.

From the beginning of high-precision (±16 to ±20 ^{14}C yr) LS dating in the 1970s until the early 1990s, high precision was mainly reserved for the establishment of the dendrochronological ^{14}C time scale. Today, this precision, together with strict quality control, is increasingly applied to archaeological studies requiring long counting times, which, for economic reasons, may be difficult to meet. This paper describes a new laboratory-built system, ICELS, which is radically different from modern commercial LS systems, as simplicity, compactness, and ease of use in ^{14}C dating has been emphasized in its design. Systems of this kind may, in the future, help to secure sufficient counting capacity in high-precision dating.

The main aim in designing ICELS has been to use it to solve the dilemma of the earliest Norse settlement in Iceland (Theodórsson 1998). ^{14}C dating strongly indicates that settlement occurred about 150 yr earlier than previously thought. These results have been rejected as archaeologically unacceptable by Icelandic archaeologists and historians. High-precision dating of 50–100 samples can presumably resolve this serious dilemma.

NEW DESIGN PREREQUISITES

ICELS differs from modern commercial LS counting systems in various respects, as the latter have some features that are superfluous in ^{14}C dating. The main features of ICELS and differences from conventional systems are the following:

1. A single 30-mm-diameter PMT replaces the dominating 2-tube (50 mm diameter) coincidence arrangement, resulting in a simple and compact detector unit. This greatly reduces the dimensions and the weight of the system.

2. Replacing the 2 tubes with 1 smaller tube reduces the beta and gamma radiation the vial is exposed to from natural radioactivity in the glass bulb of the PMT, lowering the background.
3. A 3-mL dome-shaped vial with an optimal light reflector, sitting on the top of the vertical PMT, secures high photon collection at the cathode.
4. Modern LS systems have a built-in pulse height analyzer with 2000 channels or more. In ICELS, it is replaced by 4 counting channels, sufficient for high-precision dating, as demonstrated by Pearson (1979, 1983) in his pioneering dendrochronological work.
5. A logarithmic amplifier is advantageous when radioisotopes of wide energy and quench range are measured. In ^{14}C dating, a linear keV calibrated energy scale is more appropriate, with counting window limits given by a basic physical unit (keV) rather than by an instrument-dependent parameter.
6. Benzene dating samples are usually quenched to some degree. The high voltage is set at the balance point of each sample, which secures maximal stability of counting efficiency and minimizes the quench correction needed. In conventional systems, all samples are counted at the same high voltage, irrespective of quench level.
7. The simplicity of the electronic unit enhances reliability and makes maintenance easier.
8. Automatic changing of 200 samples or more, which significantly increases the size and price of conventional systems, is indispensable in tracer work, where a large number of samples are measured. In ^{14}C dating using a stable system, ICELS offers little advantage, as counting periods are generally 2 d or more. Therefore, ICELS has manual sample changing.

Regarding the last point, there is a widespread belief that automatic cyclic measurements of a number of unknown, standard, and background samples, usually extending 2 weeks or more, increases accuracy (Gupta and Polach 1985). G W Pearson, using a late-1960s LS system with 4 fixed counting windows, demonstrated that the count rate of both background and standard samples was, after appropriate corrections, constant for several years (Pearson 1983). Therefore, cyclic counting adds nothing to the precision when the system is operated in a balance counting mode.

THE NEW LS SYSTEM, ICELS

ICELS was designed and built at the Science Institute specifically for ^{14}C dating. It is based on earlier development work in Iceland (Einarsson 1992; Einarsson and Theodórsson 1995). ICELS comprises a shielded detector unit (27 kg with an economical 5-cm-thick shield of lead); a compact, dedicated electronic unit ($32 \times 25 \times 9$ cm^3); and a laptop computer, which controls the counting operations and processes the signals. The simplicity of the electronic unit and the resulting simplicity in data recording have been emphasized.

A specially made dome-shaped 3-mL quartz vial sits on top of a vertical 30-mm-diameter PMT, touching the tube but without optical coupling (Figure 1). The vial is wrapped (a process taking 2 min), except for its bottom, with 2 layers of a thin teflon tape, which provides high light reflection. This simple arrangement results in a closed vial/phototube geometry, with high collection of the scintillation photons at the PMT cathode. The samples are 3 mL of benzene to which 45 mg butyl-PBD is added.

The electronic unit of ICELS is quite simple. It has a dedicated linear amplifier of modest speed, as only moderately sized pulses need to be detected. The PMT can thus be operated at lower voltage than when a conventional LS system is used, where single cathode electron pulses need to be detected. The amplified pulses are sent in parallel to 4 pulse height discriminators, D1 to D4, which are triggered when an input pulse overrides their individually set threshold voltages, DV1 to DV4, produced by a fixed resistor chain. The discriminators are read by the computer, and when one or

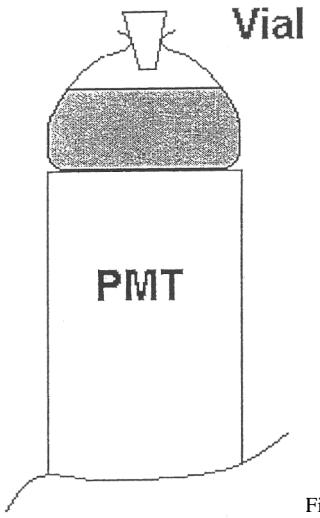

Figure 1 A schematic figure of the detector unit

more have been activated, one count is added in the respective computer internal pulse-summing registers, N1 to N4.

The discriminator voltages DV1 and DV3 define the lower and upper limits of the ^{14}C window. The number of pulses in this window, $N(^{14}C)$, is therefore:

$$N(^{14}C) = N1 - N3 \quad (1)$$

Discriminator voltages of D2 and D4 are set at 0.44 × DV3 and 1.25 × DV3, respectively, and are used to facilitate the setting of the high-voltage balance point, as described below.

DETERMINING ^{14}C BALANCED SETTING

To secure the highest stability of counting efficiency, the system is operated in a balanced counting mode (McCormac 1992; Theodórsson et al. 2003,) where the PMT high voltage is set at a value that gives a maximum count rate in a fixed ^{14}C window for an unquenched sample. The discriminator voltage ratio DV3/DV1 determines explicitly the balanced window limits as well as the counting efficiency, and these will be exactly the same for any similar LS system with the same discriminator voltage ratio and similar light collection. Figure 2 shows the lower and upper limits (keV) of a balanced window as a function of the discriminator voltage ratio DV3/DV1 (Theodórsson et al. 2003).

When selecting a ^{14}C window, its lower energy limit is usually set above the maximum energy of tritium beta particles (18 keV). A discriminator ratio of 5.37 was selected, resulting in a ^{14}C counting window from 25.4 to 136 keV, as the background rises rather steeply below the lower window limit (Figure 3). Figure 4 shows the ^{14}C spectrum at balanced high voltage and the channels corresponding to the 4 discriminators. The detection efficiency in the ^{14}C counting window is 71%.

The balanced PMT high voltage for the selected fixed ^{14}C counting window was determined by measuring an unquenched high-activity ^{14}C benzene sample (about 200 Bq) in steps of increasing PMT high voltage. Figure 5 shows the count rate in the ^{14}C window as a function of high voltage. It goes through a maximum at a voltage value called balance point, denoted by HV_{bal}. Determining the balance point of a single-PMT system is considerably simpler than for conventional 2-PMT systems (McCormac 1992).

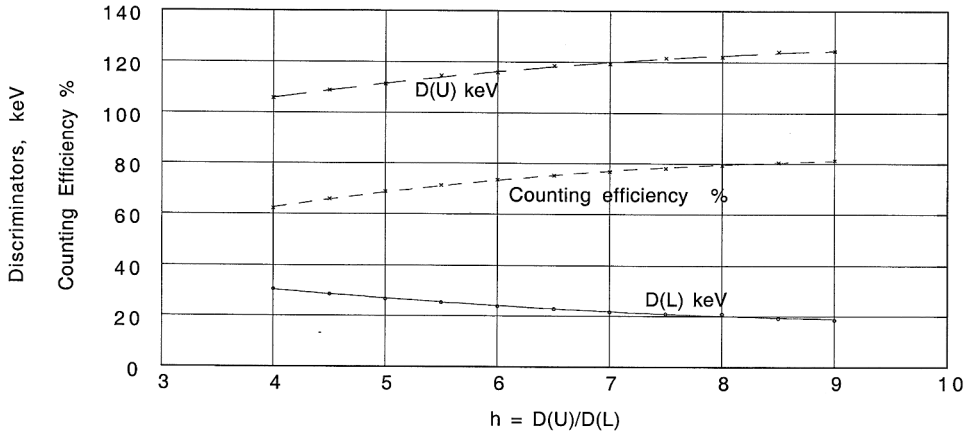

Figure 2 Lower [D(L)] and upper limit [D(U)] (keV) of a balanced window versus ratio of upper and lower discriminator voltage.

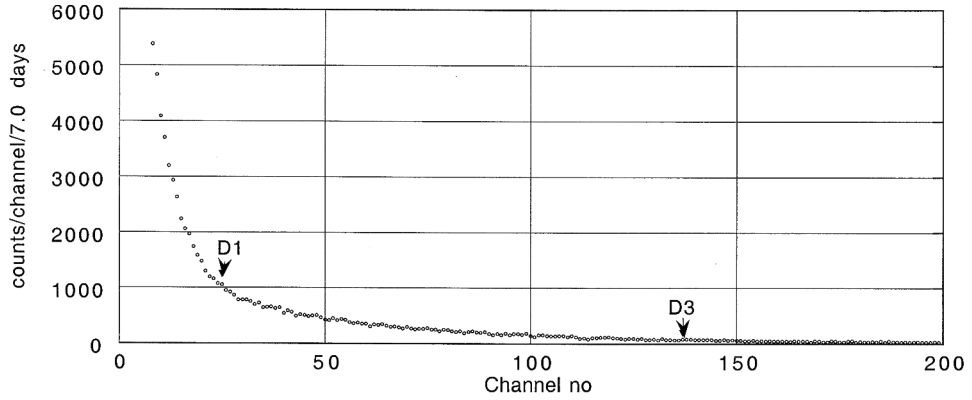

Figure 3 Background pulse height spectrum

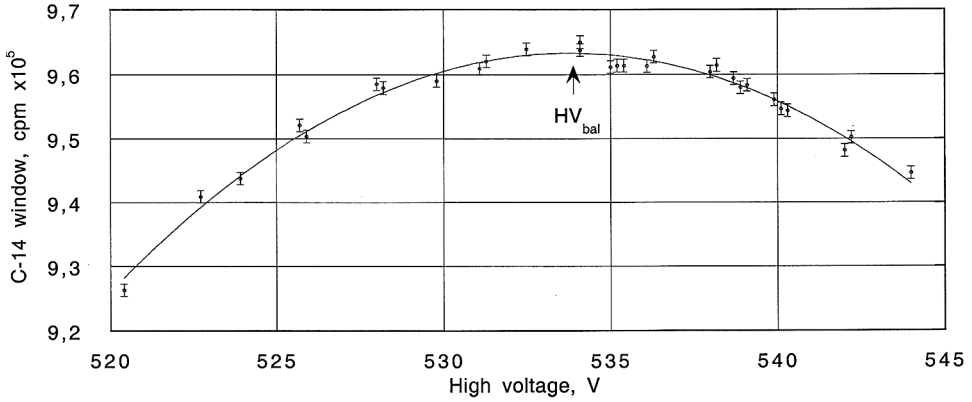

Figure 4 Pulse height spectrum of ^{14}C. Error bars are shown on day 41.

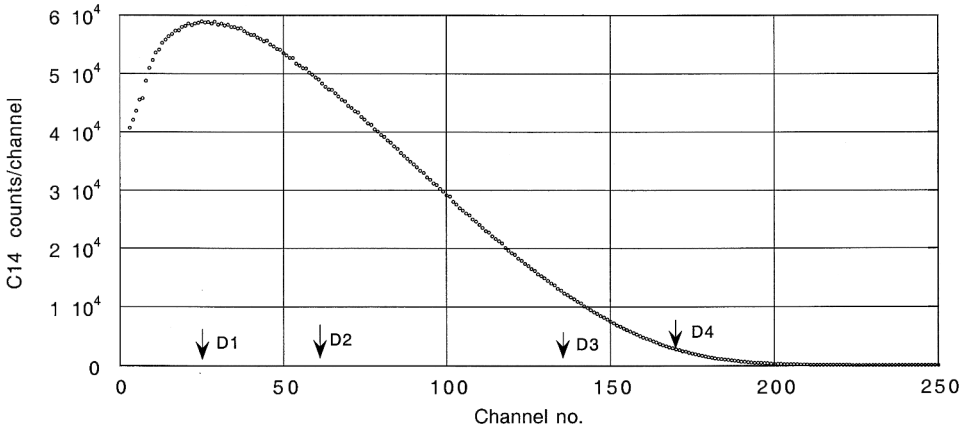

Figure 5 ^{14}C count rate versus high voltage

SETTING BALANCED HV FOR DATING SAMPLES

Small impurities in synthesized benzene dating samples shift the ^{14}C pulse height spectrum to lower pulse size and changes the counting efficiency compared to the unquenched reference sample. A measure of this shift can be determined by the conventional channel ratio method. An ^{241}Am gamma (60 keV) source is inserted close to the vial and counted for about 5 min. The channel ratio *AM* defined by

$$AM = (N2–N3) / (N1–N3) \tag{2}$$

is sensitive to spectrum shift.

^{241}Am has been selected because its gamma energy lies in the energy range of the beta particles of ^{14}C. For ICELS, the reference sample has an *AM* value of 0.49 at the balance point. If *AM* for a sample to be dated deviates from 0.49, the high voltage is adjusted to a value that sets *AM* to this balance value, which restores the spectrum to the same position as that of an unquenched reference sample. A separate quench correction study that will be published in the near future shows that the error due to quench correction can be kept below 4 ^{14}C yr.

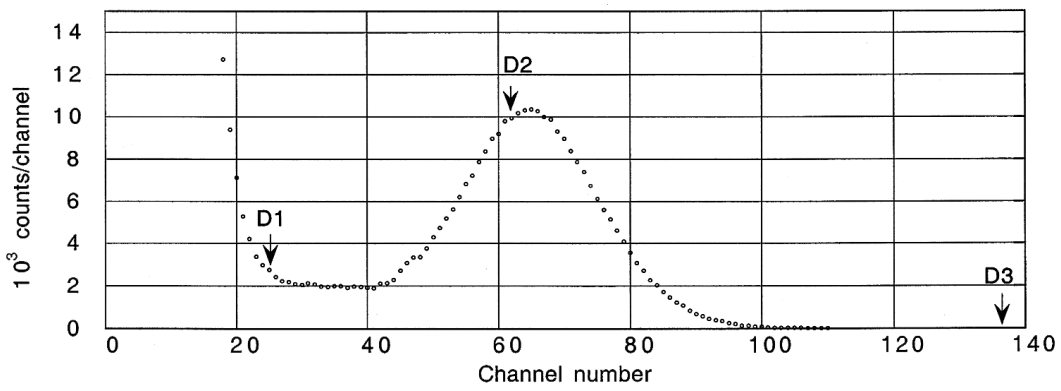

Figure 6 Pulse height spectrum of an external ^{241}Am source

COUNTING STABILITY OF ICELS

The long-term counting stability of ICELS has been studied in detail, as well as the influence of all parameters that affect the counting efficiency.

Influence of Power Line Voltage

Using an external multichannel pulse height analyzer, the channel number of the middle of the 60-keV peak of ^{241}Am was determined at a line voltage of 200, 220, and 240 volts. The peak channel number varied by less than 0.3%, which is similar to the measuring error. Line voltage variations evidently have a negligible effect on the counting efficiency.

Influence of Ambient Temperature

Because of the high internal stability of amplifier gain and high voltage, any likely temperature variations in the electronic unit should have a negligible effect on the ^{14}C spectrum. This was tested as above at varying temperatures of the electronic unit, from 13 °C to 33 °C, measured in 7 approximately equal steps. The channel number of the ^{241}Am 60-keV peak was practically the same at all temperatures, with a 0.3% rms deviation from the mean channel number, similar to the estimated measuring error.

The detector unit is, however, quite sensitive to temperature variations, as the internal gain of the PMT decreases linearly by 0.46% per °C (Theodórsson et al. 2003). When a sample is initially set at its balance point, a drift of 8 °C from the initial temperature will change the counting efficiency by only 0.1%. Therefore, it should not be difficult to keep the error, due to this source, within acceptable limits during the counting period of each sample, generally 1 to 7 d.

Long-Term Stability of Counting Efficiency

In a general stability study of ICELS, extending over 110 d, a high-activity ^{14}C benzene sample (about 170 Bq) was measured periodically for 16 to 24 hr. Between counting periods, the vial was removed from the detector unit and other test measurements were made. Twice the sample was measured, several days unattended, and 24-hr readings recorded. The results of all these measurements (Figure 7) show the system's excellent long-term counting stability and reproducibility in sample changing. The slow, linear decline in the count rate is due to a small, constant evaporation loss, verified by weighing the vial accurately a few times during the testing period. The standard deviation of the measured points from the line is 0.036% (corresponding to 2.9 ^{14}C yr), practically the same as the uncertainty due to counting statistics in individual daily-measured values, 0.034%.

In a later 26-d continuous test, with a higher-activity ^{14}C sample (872 cps) showing no benzene loss, the 24-hr mean values of the count rate gave a standard deviation of 0.013% (corresponding to 1.0 ^{14}C yr). The expected standard deviation due to statistics is practically the same, 0.012%.

Correction for Quenching and Other Parameters That Can Shift the ^{14}C Spectrum

Impurity molecules in synthesized benzene samples absorb light, resulting in fewer photons falling on the cathode of the PMT, thus shifting the ^{14}C spectrum to lower energies. Other parameters can shift the ^{14}C spectrum: variation in sample volume (from 1.0 to 3.0 mL), eccentric positioning of the vial on the PMT, and variation in vials and light reflection. It will be shown in a future paper that a shift in ^{14}C counting efficiency due to variation in all these parameters is corrected for by the quench correction method, described briefly above (spectrum restoration), with an error less than 0.04% (3.2 ^{14}C yr).

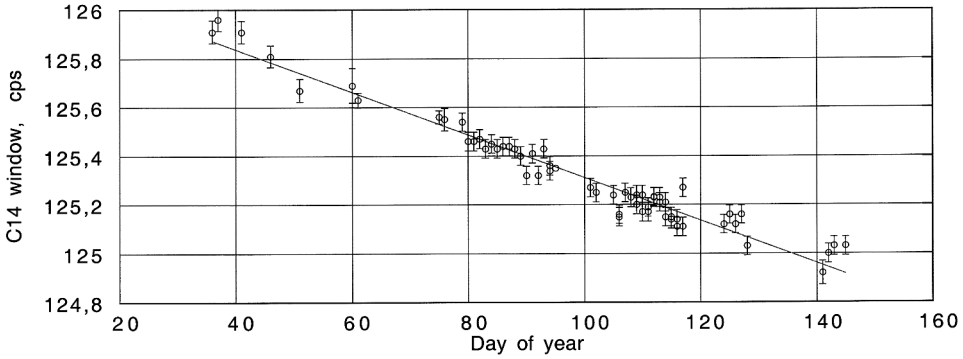

Figure 7 Count rate with 1-σ error bars of a high-activity ^{14}C benzene sample measured periodically for 16 to 24 hr over a period of 110 d.

Replacing PMT

The count rate of a high-activity sample was measured with 3 types of 30-mm-diameter PMTs after the system had been set at the balance point for each tube. Two different tubes were measured for 1 type (D842) and 1 tube was tested twice. The counting time was 24 hr, resulting in a standard statistical deviation of 0.009 cps (0.13%). The rms deviation from the mean of the 6 measurements (Figure 8) is 0.007 cps. Exchanging PMTs, or using another ICELS for that matter, therefore gives no measurable change in counting efficiency—further evidence for the excellent counting efficiency stability. Thus, it is easy to produce systems with exactly the same counting efficiency.

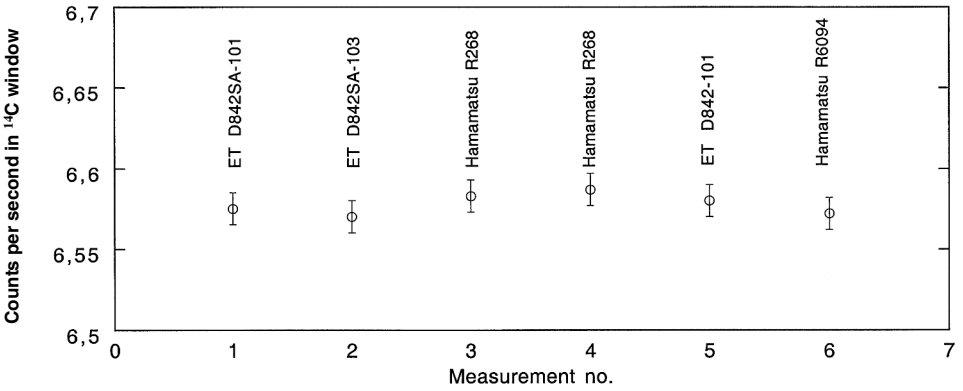

Figure 8 The count rate of a ^{14}C standard for different PMTs

Background Stability

The long-term stability of the background count rate of LS dating systems has generally been tested by measuring the background repeatedly in 100-min periods. This is far from satisfactory, since the background must be measured in periods with similar length as normal counting time of dating samples in order to reveal eventual small but significant fluctuations. Therefore, the background was measured of 2 ICELS systems (Table 1) continuously for 57 d and 47 d, respectively (Figure 9).

PMT D842SA was specially manufactured in 2002 with a bulb of newly developed high-purity glass and D190XSA was manufactured in 1990 from the best available glass at that time. Both types were made specially by Electron Tubes Limited (UK) for this low-level work. The higher background in system Fe is due to a lighter shield and higher K/Th/U concentrations in the glass bulb of the PMT.

Table 1 Systems used for background measurements.

System	Shield	PMT	Production year	Vial nr	Background cpm
Pb	10 cm lead	D842SA	2001	13	1.53
Fe	10 cm iron	D190XSA	1991	12	3.37

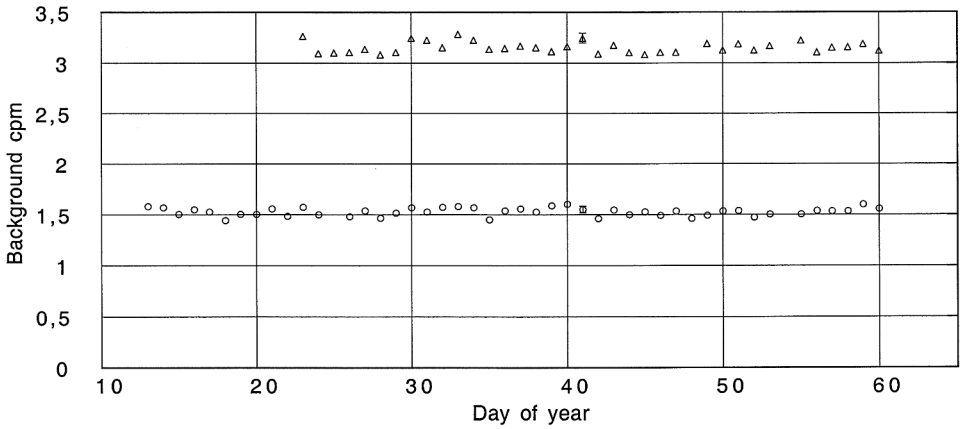

Figure 9 Long-term 24-hr average values of background count rate for 2 ICELS systems (see Table 1). For clarity, the standard error is only shown on 1 point in each series.

From the data (6-hr counting periods), 24-hr and 4-d average background values were calculated. The background depends linearly on atmospheric pressure; an increase in pressure reduces the background. From the daily average values of background and atmospheric pressure, the linear correlation factor $\Delta B/\Delta P$ (cpm/100 mbar) was calculated and used to find the corrected background values, both for the 24-hr and 4-d mean values (Table 2). The root mean square (σ, rms) deviations of the average corrected background values have been calculated as well as the theoretical rms values, based on the statistical nature of the background pulse rate (Table 2).

Table 2 Long-term background measurements, corrected for variations in atmospheric pressure.

System	$\Delta B/\Delta P$ cpm/100 mb	σ 24-hr measured cpm	σ 24-hr expected cpm	σ 4-d measured cpm	σ 4-d expected cpm
Pb	–0.010	0.0042	0.0032	0.0022	0.0016
Fe	–0.012	0.0042	0.0047	0.028	0.024

The result shows that the measured σ for both systems is only slightly larger than the statistically calculated values, even for the 4-d averages. The corrected 4-d background is practically constant over the long testing period.

CONCLUSION

A simple and compact single-PMT liquid scintillation counting system, specifically designed for ^{14}C dating, has been built and tested to higher precision (0.03–0.04%) than that reported for any similar system. Sample changing is manual. The total weight of the instrument is 30 kg. The stability of its counting efficiency, including quench correction and sample changing, is better than 0.04%. The background is 1.53 cpm when the detector unit is shielded by 10 cm of lead, and 1.73 cpm in a 5-cm-thick shield weighing 27 kg. Systems of this type may, in the future, greatly facilitate high-precision dating.

ACKNOWLEDGMENTS

I acknowledge the financial support of the Science Fund of Iceland and I gratefully thank S A Einarsson for putting at my disposal his diaries from the development of Kvartett, the predecessor of ICELS. Finally, I acknowledge the advice given by Ron McAlpine, technical director of Electron Tubes Ltd.

REFERENCES

Einarsson S. 1992. Evaluation of a prototype low-level liquid scintillation multisample counter. *Radiocarbon* 34(3):366–73.

Einarsson S, Theodórsson P. 1995. Stability of a new, multichannel, low-level liquid scintillation counter system, Kvartett. *Radiocarbon* 37(2):727–36.

Gupta SK, Polach HA. 1985. *Radiocarbon Dating Practices at ANU*. Canberra: Australian National University. 94 p.

Kojola H, Polach H, Nurmi J, Oikari T, Soini E. 1984. High-resolution low-level liquid scintillation beta-spectrometer. *International Journal of Applied Radiation and Isotopes* 35(10):949–52.

McCormac FG. 1992. Liquid scintillation counter characterization, optimization and benzene purity correction. *Radiocarbon* 34(1):37–45.

Noakes JE, Valenta RJ. 1989. Low background liquid scintillation counting using an active sample holder and pulse discrimination electronics. *Radiocarbon* 31(3):332–41.

Pearson GW. 1979. Precise ^{14}C measurement by liquid scintillation counting. *Radiocarbon* 21(1):1–21.

Pearson GW. 1983. The development of high-precision ^{14}C measurements and its application to archaeological time scale problems [PhD dissertation]. Belfast: Queen's University Belfast.

Theodórsson P. 1998. Norse settlement of Iceland—close to AD 700? *Norwegian Archaeological Review* 31: 29–38.

Theodórsson P, Ingvarsdottir S, Gudjonsson GI. 2003. Balanced window in ^{14}C liquid scintillation counting. *Radiocarbon* 45(1):113–22.

RADIOCARBON, Vol 47, Nr 1, 2005, p 99–113

ESTIMATING TURNOVER OF SOIL ORGANIC CARBON FRACTIONS BASED ON RADIOCARBON MEASUREMENTS

Sander Bruun[1,2] • Johan Six[3,4] • Lars S Jensen[1] • Keith Paustian[4]

ABSTRACT. In this paper, we examine 3 different models used to estimate turnover of soil organic carbon (SOC) fractions using radiocarbon measurements: one conventional carbon dating model and two bomb ^{14}C models. One of the bomb ^{14}C models uses an atmospheric ^{14}C record for the period 22,050 BC to AD 2003 and is solved by numerical methods, while the other assumes a constant ^{14}C content of the atmosphere and is solved analytically. The estimates of SOC turnover obtained by the conventional ^{14}C dating model differed substantially from those obtained by the bomb ^{14}C models, which we attribute to the simplifying assumption of the conventional ^{14}C model that the whole SOC fraction is of the same age. The assumptions underlying the bomb ^{14}C models are more applicable to SOC fractions; therefore, the calculated turnover times are considered to be more reliable. We used Monte Carlo simulations to estimate the uncertainties of the turnover times calculated with the numerically solved ^{14}C model, accounting not only for measurement errors but also for uncertainties introduced from assumptions of constant input and uncertainties in the ^{14}C content of the CO_2 assimilated by plants. The resulting uncertainties depend on systematic deviations in the atmospheric ^{14}C record for SOC fractions with a fast turnover. Therefore, the use of the bomb ^{14}C models can be problematic when SOC fractions with a fast turnover are analyzed, whereas the relative uncertainty of the turnover estimates turned out to be smaller than 30% when the turnover time of the SOC fractions analyzed was longer than 30 yr, and smaller than 15% when the turnover time was longer than 100 yr.

INTRODUCTION

Two distinct theoretical approaches have been taken in the use of radiocarbon to estimate turnover of soil organic carbon (SOC) fractions, namely, the conventional ^{14}C dating model and the bomb ^{14}C model.

According to Scharpenseel and Schiffmann (1977), Paul et al. (1964) first began using ^{14}C dating as a means to study SOC dynamics. Since then, a number of studies have used ^{14}C dating to estimate the turnover or mean residence time of SOC fractions (Martel and Paul 1974; Jenkinson and Rayner 1977; Gilet-Blein et al. 1980; Anderson and Paul 1984; Bol et al. 1999). However, the determination of the turnover time in these studies relies on the theory developed for age determination of archaeological samples, with the prerequisite that the whole sample is of the same age (Libby 1952). This is probably true for the layers of peat soils (Geyh et al. 1971), but obviously not for SOC fractions in general. Therefore, conventional ^{14}C dating leads to biased turnover estimates of SOC fractions. Some of the above-mentioned authors have therefore introduced the terms "the apparent mean residence time" or "equivalent age" for the values obtained. However, interpretation of these values remains difficult (Perrin and Willis 1964; Geyh et al. 1971).

Another model used to estimate SOC turnover relies on the increased level of atmospheric ^{14}C as a consequence of nuclear bomb activity in the 1950s and 1960s (Balesdent 1987; Harkness et al. 1991; Harrison and Broecker 1993; Hsieh 1996; Trumbore 1993; Trumbore et al. 1996; Bird et al. 2002; Chen et al. 2002; Agnelli et al. 2002). Because of the recent appearance of the bomb peak, this method is used to estimate short-term carbon turnover. However, the method may also be used to estimate turnover of more resistant fractions of SOC by taking advantage of the natural decay of ^{14}C.

[1]Department of Agricultural Sciences, The Royal Veterinary and Agricultural University, Thorvaldsensvej 40, DK-1871 Frederiksberg C, Denmark.
[2]Corresponding author. Email: sab@kvl.dk.
[3]Department of Agronomy and Range Science, University of California-Davis, Davis, California 95616, USA.
[4]Natural Resource Ecology Laboratory, Colorado State University, Fort Collins, Colorado 80523, USA.

We use the term "SOC fractions" for fractions of SOC that can be isolated from the rest of the SOC by physical or chemical fractionation procedures. The SOC fractions can be isolated either from specific horizons or from the whole profile. To be useful in the context of the ^{14}C analyses, the isolated SOC fractions should be as homogeneous as possible with respect to chemical composition and physical protection, and therefore also with respect to turnover (Trumbore and Zheng 1996). Examples of such SOC fractions that have been used in combination with ^{14}C analyses are the hydrolyzable and non-hydrolyzable fractions (e.g. Campbell et al. 1967; Trumbore et al. 1996), different density fractions (e.g. Baisden et al. 2002), and differently sized organomineral fractions (e.g. Anderson and Paul 1984).

The objectives of the current study were to critically analyze the possibilities of estimating turnover of SOC fractions by ^{14}C measurements, and to analyze the uncertainties of the estimates caused by the assumptions underlying the different approaches. We review 3 different theoretical approaches to estimate SOC turnover by ^{14}C-based methods, compare the results, and determine the situations in which they can be used to obtain reliable estimates.

METHODS

The Conventional ^{14}C Dating Model

The theoretical basis for ^{14}C dating is the exponential decay of ^{14}C. In a sample where all the carbon has entered at the same time, the specific activity is described by

$$A(t) = A_I(t)\exp(-\lambda a) \tag{1}$$

where $A(t)$ is the specific activity of the sample corrected for fractionation during photosynthesis by the ^{13}C content (Stuiver and Polach 1977), $A_I(t)$ is the specific activity of the sample when it was formed, λ is the decay rate constant of ^{14}C, and a is the time since the sample was formed (i.e. its age). Therefore, the age of the sample is

$$a = \frac{1}{\lambda}\ln\left(\frac{A_I(t)}{A(t)}\right) \tag{2}$$

In standard ^{14}C dating, A_{abs} is used as the standard ^{14}C content of new material, and the decay rate constant is based on the Libby half-life of ^{14}C (Stuiver and Polach 1977). A_{abs} is defined as 95% of the activity in 1950 of an oxalic acid standard, which is estimated to be equal to the atmospheric steady-state level of pre-bomb atmospheric activity. To correct the ^{14}C age for changes in atmospheric ^{14}C content (and therefore $A_I(t) \neq A_{abs}$), ^{14}C calibrations have been constructed coupling real age with ^{14}C age (Stuiver et al. 1998; Damon and Peristykh 2000).

If it is assumed that the measured SOC fraction is in steady-state between inputs and decay, the turnover time (τ) is equal to the age or the mean residence time of the sample. Therefore, if we assume that the activity of the input is equal to A_{abs} and that all the carbon in a sample entered the soil at the same time, then the turnover time is

$$\tau = \frac{1}{\lambda}\ln\left(\frac{A_{abs}}{A(t)}\right) \tag{3}$$

The Bomb ^{14}C Model

Several models have been formulated that use the peak of ^{14}C to estimate turnover of SOC fractions (Balesdent and Guillet 1982; Balesdent 1987; Harkness et al. 1991; Cherkinsky and Brovkin 1993; Hsieh 1993; Trumbore et al. 1996). All the models are fundamentally similar and make use of the same basic assumptions.

The ^{14}C bomb models assume that the turnover of the analyzed SOC fractions is well described by first-order kinetics. As SOC consists of carbon of very varying degradability, this is not a plausible assumption for total SOC. Therefore, the models are applied to SOC fractions. An important feature of these SOC fractions is that the isolated SOC has to be more homogeneous than the total SOC pool with respect to chemical and physical protection. Other basic assumptions in the model are that the inputs to the SOC fractions are constant and that the soil C level is at equilibrium between input and decay. Furthermore, we need to know the ^{14}C content of the plant material entering the soil. These values are usually calculated from the atmospheric ^{14}C content at the time of plant growth.

The bomb ^{14}C model can be formulated in both continuous and discrete form. As soils receive continuous inputs of organic matter in the form of litter fall and rhizodeposition, we chose to use the continuous form here. We introduce a distribution, $\varphi(a, t)$, of SOC. This distribution is defined such that $\varphi(a, t)da$ is the amount of organic carbon in a given fraction of SOC at time t, which has entered the soil between a and $a + da$. Thus, a can be conceived as the age of the organic carbon and $\varphi(a, t)$ as an age distribution. A cohort of SOC of age a must have formed a years ago, i.e. at time $t - a$. Therefore, an assumption of first-order kinetics means that the age distribution of age a at time t is given by

$$\varphi(a, t) = I(t - a)\exp(-ka) \tag{4}$$

where $I(t) = \varphi(0, t)$ denotes the rate with which new material enters the SOC fraction (the input) at time t, and k is the first-order decay constant for the SOC fraction.

By similar arguments to the above and by considering the exponential decay of ^{14}C, the specific activity $[A(a, t)]$ of a cohort of SOC of age a at time t is given by

$$A(a, t) = A_I(t - a)\exp(-\lambda a) \tag{5}$$

where $A_I(t) = A(0, t)$ is the specific activity of new material at time t, and λ is the decay constant of ^{14}C. This equation assumes that no isotopic fractionation occurs during the decomposition process.

As $\varphi(a, t)da$ is the amount of SOC in the fraction of ages a to $a + da$, $\varphi(a, t)da\,A(a, t)$ is the activity of ^{14}C in the same age interval. Therefore, the specific activity of the whole SOC fraction is given by

$$A(t) = \frac{\int_0^\infty \varphi(a, t)A(a, t)da}{\int_0^\infty \varphi(a, t)da} \tag{6}$$

Insertion of Equation 4 and Equation 5 into Equation 6 leads to

$$A(t) = \frac{\int_0^\infty I(t-a)\exp[-(k+\lambda)a]A_I(t-a)da}{\int_0^\infty I(t-a)\exp(-ka)da} \quad (7)$$

Defining the standardized input history as $i(t) = I(t)/\bar{I}$, where $\bar{I}$ is the average input to the SOC fraction, and inserting this in Equation 7 results in

$$A(t) = \frac{\int_0^\infty i(t-a)\exp[-(k+\lambda)a]A_I(t-a)da}{\int_0^\infty i(t-a)\exp(-ka)da} \quad (8)$$

We see that the specific activity is independent of the mean input, but not the input history (i.e. the variation in inputs that has occurred in the past).

To be able to use Equation 8 to estimate k, we need to know the standardized input history. However, there is no apparent way to estimate the inputs to SOC fractions. Furthermore, measurements of total litter inputs are generally difficult and rarely performed in long-term studies. If we assume that the input to a SOC fraction is constant, $\varphi(0, t) = I$, and that the soil has reached steady-state, then Equation 4 reduces to

$$\varphi(a) = I\exp(-ka) \quad (9)$$

which is the age distribution at steady-state.

To estimate the model parameters k and I, we use the measured amount of carbon in the SOC fraction, C, and the measured specific activity, A. The amount of C can be found by integrating over the age distribution

$$C = \int_0^\infty \varphi(a)da = \int_0^\infty I\exp(-ka)da = \frac{I}{k} \quad (10)$$

whereas the specific activity can be found by insertion into Equation 5

$$A(t) = k\int_0^\infty \exp[-(k+\lambda)a]A_I(t-a)da \quad (11)$$

This is the equation that can be used to estimate the decomposition rate k of SOC fractions by tracking the peak of ^{14}C. We call this equation "the bomb ^{14}C equation," and it can only be solved for k by numerical integration and iteration. The value of k can then be used to derive I from Equation 10 and the amount of carbon in the SOC fraction. If several samples have been taken, either at the same or at different points in time, the value of k can be optimized by defining an optimization criterion.

If we assume that the specific activity of inputs to the SOC fraction is constant (A_I), Equation 5 reduces to

$$A(a) = A_I \exp(-\lambda a) \tag{12}$$

and the specific activity of the SOC fraction can be found by inserting Equation 12 into Equation 11

$$A = kA_I \int_0^\infty \exp[-(k+\lambda)a]da = \frac{A_I k}{k+\lambda} \tag{13}$$

from which k can be isolated

$$k = \frac{A\lambda}{A_I - A} \tag{14}$$

The assumption of first-order kinetics means that the turnover time can be found as $\tau = k^{-1}$; therefore, if the activity of the inputs is assumed to be equal to A_{abs}, then

$$\tau = \frac{A_{abs} - A}{A\lambda} \tag{15}$$

In most applications of bomb ^{14}C models, the ^{14}C is essentially used as a non-radioactive tracer for estimating turnover on relatively short time scales. However, due to the radioactive decay of ^{14}C, these equations can also be used to estimate dynamic parameters of SOC fractions with turnover times that are much longer. However, since the ^{14}C content of the atmosphere has not been constant, the use of the bomb ^{14}C model on SOC fractions of slow turnover requires that the ^{14}C record extends several thousand years back, which is much longer than has usually been used in applications of the bomb ^{14}C model.

Construction of an Atmospheric ^{14}C Record

We used the data of Stuiver et al. (1998) to construct a yearly atmospheric ^{14}C record for the Northern Hemisphere by cubic spline interpolation of $\Delta^{14}C$ values for the period 22,050 BC to AD 1955. For the years between 1955 and 1959, we calculated the average of the values observed for each year in organic materials by Tauber (1967), Vogel (1970), Baxter and Walton (1971), Barrette et al. (1980), Burchuladze et al. (1989), Olsson and Possnert (1992), and Goodsite et al. (2001). For 1959 until 1996, we used the average summer (May to September) atmospheric $\Delta^{14}C$ values observed by Levin et al. (1985) and Levin and Kromer (1997) for central Europe. To extend the record beyond 1996, we extrapolated the $\Delta^{14}C$ observations from 1975 to 1996 by an exponential model [$\Delta^{14}C = 375 \exp(-0.0621Y)$] where Y is years after 1975). The resulting complete ^{14}C record is shown in Figure 1.

Comparison of Turnover Estimates by 3 Different Methods

Thus, there are 3 different methods that can be used to calculate turnover times of SOC fractions based on ^{14}C measurements: 1) the conventional ^{14}C dating model using Equation 3; 2) the numerical solution of the bomb ^{14}C equation, by solving for k in Equation 11; and 3) the analytical solution of the bomb ^{14}C equation, Equation 15.

To compare these different methods, we used all 3 methods to calculate the turnover time corresponding to values of the specific activities of a theoretical sample taken in 2002.

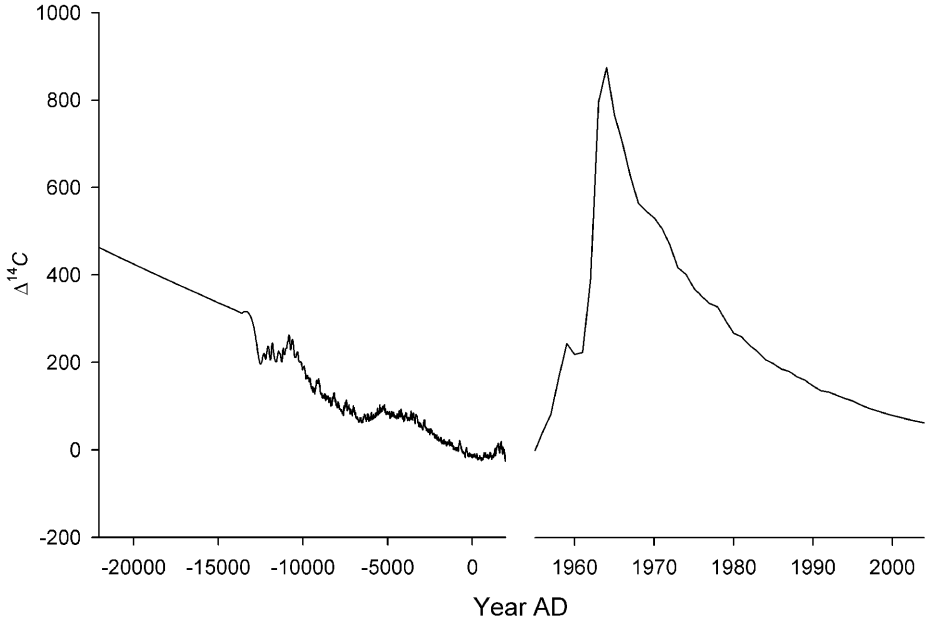

Figure 1 Record of $\Delta^{14}C$ values used in the models to calculate turnover of SOC fractions. See text for details about the construction of the record.

Assessment of the Uncertainties of the Numerical Bomb ^{14}C Model

To determine the uncertainties associated with the assumptions of the numerical solution of the bomb ^{14}C equation (Equation 11), we used Monte Carlo simulations. We tested the uncertainties introduced by the assumption of constant inputs and the use of regional data for the ^{14}C content of the specific activity of the inputs entering the SOC fraction. We used 10 different random input histories generated by drawing random numbers from a distribution with an interannual variation similar to that observed in natural ecosystems.

Knapp and Smith (2001) observed that the coefficient of variation (CV) of the interannual net primary production ranged from 3% to 33% for different natural ecosystems, with a mean value of 20.4%. Thus, the standardized input histories were generated by drawing random numbers from a normal distribution with a mean of 1 and a standard deviation of 0.204.

The uncertainty of the ^{14}C content of the inputs was assessed by compiling data from a range of different sources reporting ^{14}C content of different plant-derived materials of known age (Figure 2a). The atmosphere is not completely mixed, and therefore an offset exists between the 2 hemispheres. Furthermore, low and very high latitudes in the Northern Hemisphere also seem to deviate somewhat from the mid-latitudes (Dai and Fan 1986; Kromer et al. 2001). Thus, only samples from sites between 30°N and 60°N were selected. The values from Baxter and Walton (1971) were originally included in the analysis, but they exhibited considerably more variation than the rest of the data and were therefore excluded.

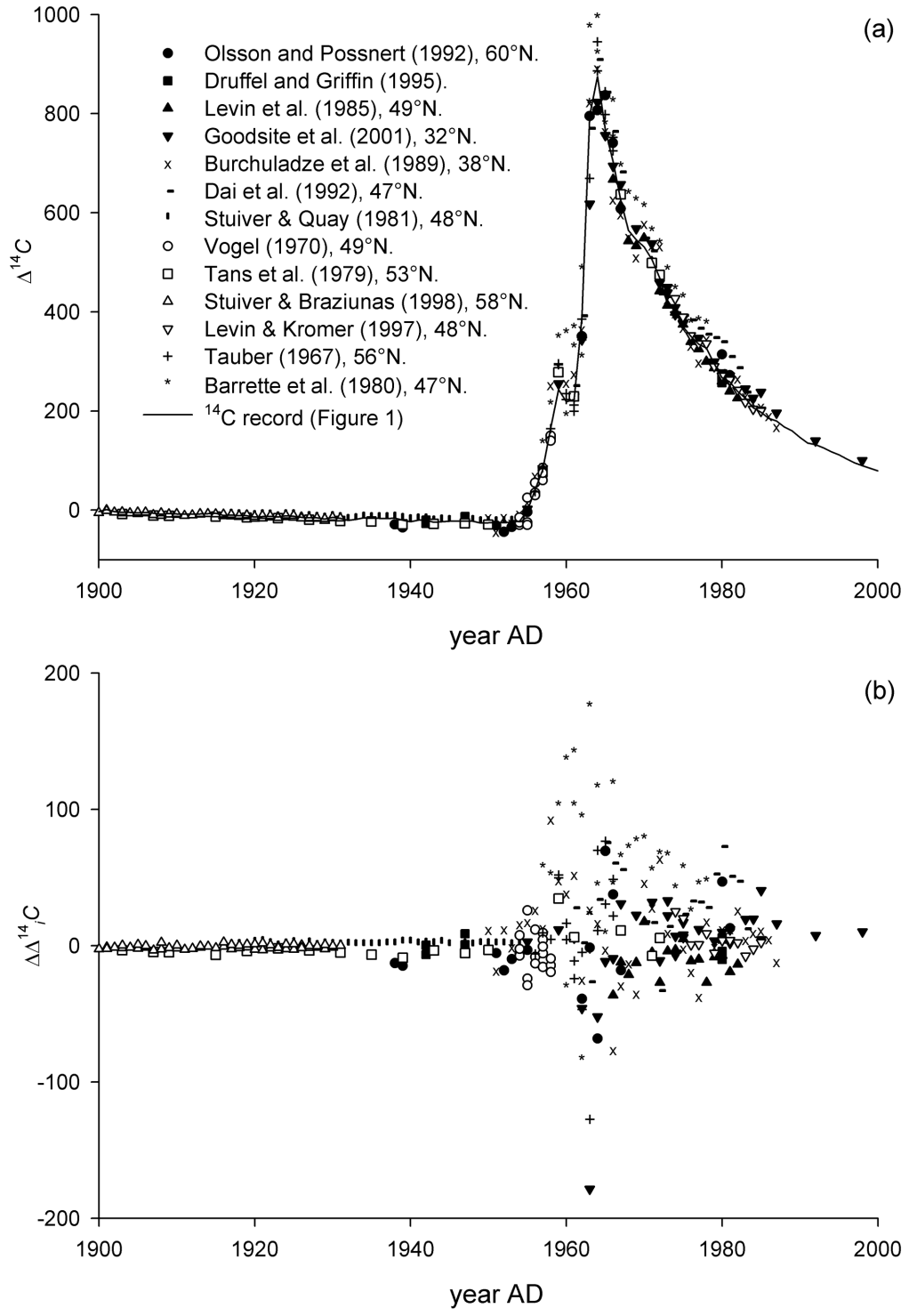

Figure 2 Data used to assess the variation in $\Delta^{14}C$ values from different sites in the latitudinal range from 30°N to 60°N: a) $\Delta^{14}C$ values of different organic materials from published sources, and b) the deviation from the $\Delta^{14}C$ record: $\Delta\Delta_i^{14}C$ = the values observed for the organic materials – the $\Delta^{14}C$ value of the ^{14}C record.

In order to get enough samples to reliably estimate the variation, we calculated the variance in age groups where the variation seemed relatively constant. The standard deviation around the $\Delta^{14}C$ value in the *j*th age group was calculated as

$$\sigma_j = \sqrt{\sum_{i=1}^{n_j} \frac{(\Delta\Delta_i^{14}C)^2}{n_j}} \quad (16)$$

where $\Delta\Delta_i^{14}C$ is the difference between the $\Delta^{14}C$ value of the *i*th sample and the record of the same year and n_j is the number of samples in the *j*th age group. The estimated standard deviation in the different age groups is shown in Table 1.

Table 1 Standard deviation of organic materials (Figure 2) in age groups around the $\Delta^{14}C$ values from the ^{14}C record (Figure 1). The values are calculated for each age group according to Equation 16.

Age group (year AD)	σ_j (‰)
–1949	2.96
1950–1954	8.87
1955–1960	35.5
1961–1962	60.8
1963	106
1964–1965	49.9
1966–1969	46.2
1970–1974	28.6
1975–1979	22.9
1980–1983	21.4
1984–	12.8

The differences between the $\Delta^{14}C$ value of the sample and of the constructed ^{14}C record ($\Delta\Delta_i^{14}C$) are shown in Figure 2b. The variation around the values in the record appears to be random, but it is also evident that the values measured at some sites are systematically higher than at others. This indicates that specific sites may deviate systematically from the ^{14}C record. Based on the estimated variation, we constructed 10 different $\Delta^{14}C$ activity histories in 2 different ways, one representing random deviations and one representing systematic deviations from the ^{14}C record. The random $\Delta^{14}C$ histories were generated by drawing 10 random numbers for each year from a standardized normal distribution (i.e. $\mu = 0$ and $\sigma = 1$). These values were multiplied by the standard deviation, σ_j, in Table 1 to obtain a deviation from the ^{14}C record for the year in question. The obtained deviation was added to the $\Delta^{14}C$ value in the ^{14}C record to obtain a $\Delta^{14}C$ value for the input that year. The systematic $\Delta^{14}C$ histories were generated by drawing 10 random numbers from a standardized normal distribution, one for each activity history. This value was multiplied by the standard deviation, σ_j, in Table 1 and again added to the $\Delta^{14}C$ value in the ^{14}C record to obtain a $\Delta^{14}C$ value for the input of the year in question.

By combining the input histories with the activity histories, we obtained 2 sets of 10 input/activity histories: 1) 10 input/activity histories with random variation in size of the inputs and random variation in the $\Delta^{14}C$ values, and 2) 10 input/activity histories with random variation in the size of the

inputs and systematic variation in the $\Delta^{14}C$ values. Realistic input/activity histories will probably lie somewhere between these two extremes.

The 2 sets of input/activity histories were used to test the variation in turnover estimates by Monte Carlo simulation, using Equation 8 to calculate the decay rate constant, k, for each input/activity history in the 2 sets. This was done for a range of different specific activities of a theoretical SOC fraction in order to determine the relationship between the measured activity of a SOC fraction and the variation in the estimates of k.

RESULTS

Comparison of Different Methods

The results of the comparison of the different methods for estimating the turnover of SOC fractions are shown in Figure 3. Evidently, the invalid assumptions of the conventional ^{14}C method cause it to produce results that do not agree with the other methods. The analytical solution of the bomb ^{14}C is expected to result in better turnover estimates for all values of the specific activity and is just as easy to calculate. As the analytical solution to the bomb ^{14}C equation encompasses one simplifying assumption more than the numerical solution (constant ^{14}C content of inputs), the numerical solution is expected to be better than the analytical solution. However, as seen in Figure 3, the analytical solution produces results that are relatively close to the numerical solution for SOC samples of slow turnover. Because the ^{14}C record long back in time shows $\Delta^{14}C$ values considerably larger than 0‰ (which is the value corresponding to an input with specific activity of A_{abs}), the analytical solution does not approach the numerical when the turnover time becomes very slow. Of course, the analytical method could be improved by using better values than A_{abs} for the pre-bomb atmospheric ^{14}C activity. However, as this value varies in time, these corrections seem too troublesome compared to finding the numerical solution. This means that the analytical solution can be used when the turnover time of the SOC fraction is sufficiently long and the required precision is not very high.

Uncertainties of Estimates by the Bomb ^{14}C Equation

Figure 4 shows the relationship between the turnover time and the specific activity of the theoretical samples of 2002. In each figure, there are 10 lines, each corresponding to a different input/activity history. Each of the 10 lines in the figures can be thought of as a possible outcome within the variation in the size of the input and its ^{14}C content. Evidently, the differences between the activities of SOC fractions of the 10 input/activity histories are much more extensive in the case of systematic variation than in cases with random variation in the ^{14}C content. In addition, as the bomb peak has 2 flanks, certain values of the specific activity can correspond to 2 turnover times.

In Figure 5a, the relationship between the average estimated turnover time and the coefficient of variation (CV) of the estimated turnover time is given for the samples taken in 1964, 1966, 1983, and 2002 for the input/activity histories with random variation in ^{14}C content. The coefficient of variation is less than 16%, which is acceptable compared with the uncertainties arising as a consequence of model assumptions, such as the first-order decay of SOC fractions. The uncertainties are quite small over the whole range of turnover times, but are larger for short turnover times than for long.

The results of the random input histories with systematic variation in $\Delta^{14}C$ values showed much more variability, with CVs larger than 50% for SOC fractions with turnover times smaller than 15 yr (Figure 5b). However, the estimates are quite reliable even in the case of systematic variation in the

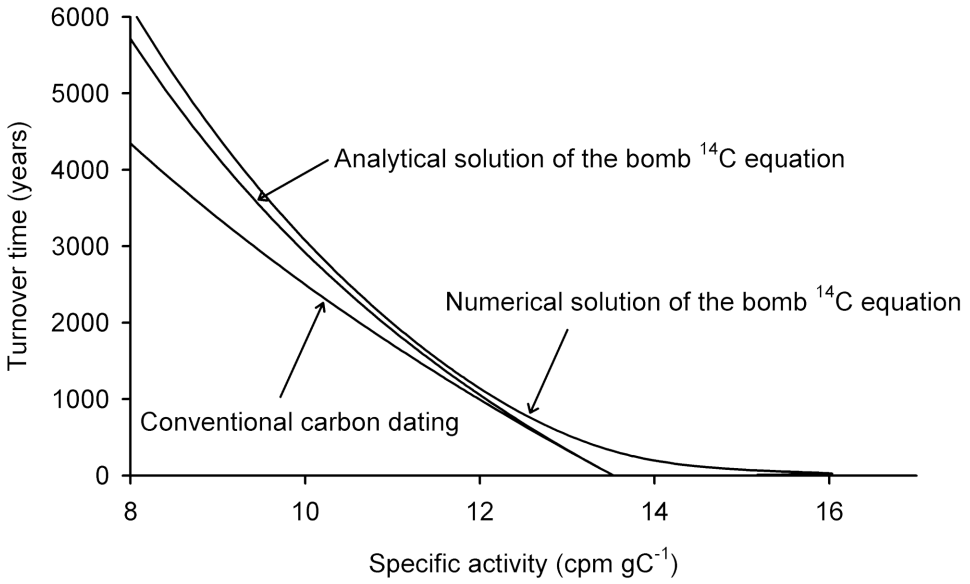

Figure 3 Relationship between the 3 different methods of estimating turnover of SOC fractions: conventional ^{14}C dating (Equation 3), numerical solution of the bomb ^{14}C equation by solving for k in Equation 11, and the analytical solution of the bomb ^{14}C equation (Equation 15).

activity history between the years, as long as the SOC fraction is not turning over too fast. For example, the relative uncertainty is smaller than 30% if the turnover time of the SOC fraction is longer than 30 yr, and smaller than 15% when the turnover time is longer than 100 yr.

DISCUSSION

Our analysis helps to clarify the consequences of the assumptions underlying the different methods used to estimate kinetic parameters of SOC fractions based on ^{14}C measurements. The conventional ^{14}C dating model effectively assumes that all the carbon in the SOC fraction is of the same age. As SOC fractions contain carbon that has entered the soil continuously over a long period, this is a questionable assumption. Therefore, the method should only be used in special situations (e.g. the layers of peat soils).

The bomb ^{14}C equation is based on a number of assumptions. First of all, it is assumed that the soil has reached equilibrium between decomposition and inputs. This means that only soils fairly close to equilibrium can be used. The requirement for long periods without changes in climate and vegetational composition may mean that the analysis can only be carried out for soils with native vegetation. Furthermore, because SOC fractions of slow turnover need a long time to reach equilibrium, very slow or inert fractions may be impossible to analyze. The assumption of equilibrium also requires that the inputs are constant and that the ^{14}C content of the inputs are known. However, we allow variations in inputs and deviations from the ^{14}C record as long as these errors average out and therefore do not significantly influence the estimates. Hsieh (1993) showed that large random variation in the inputs influenced estimates of SOC turnover only marginally. We also found only marginal changes in SOC turnover estimates as a result of the variation of the inputs alone (results not shown here). However, variation in the ^{14}C content had a more critical influence on the estimates. Most applications of bomb ^{14}C models combine Δ^{14}C values from atmospheric measurements and measurements of organic materials to construct a ^{14}C record with supposedly representative values for the hemisphere in question. Our results show that the uncertainties of the estimates are still quite

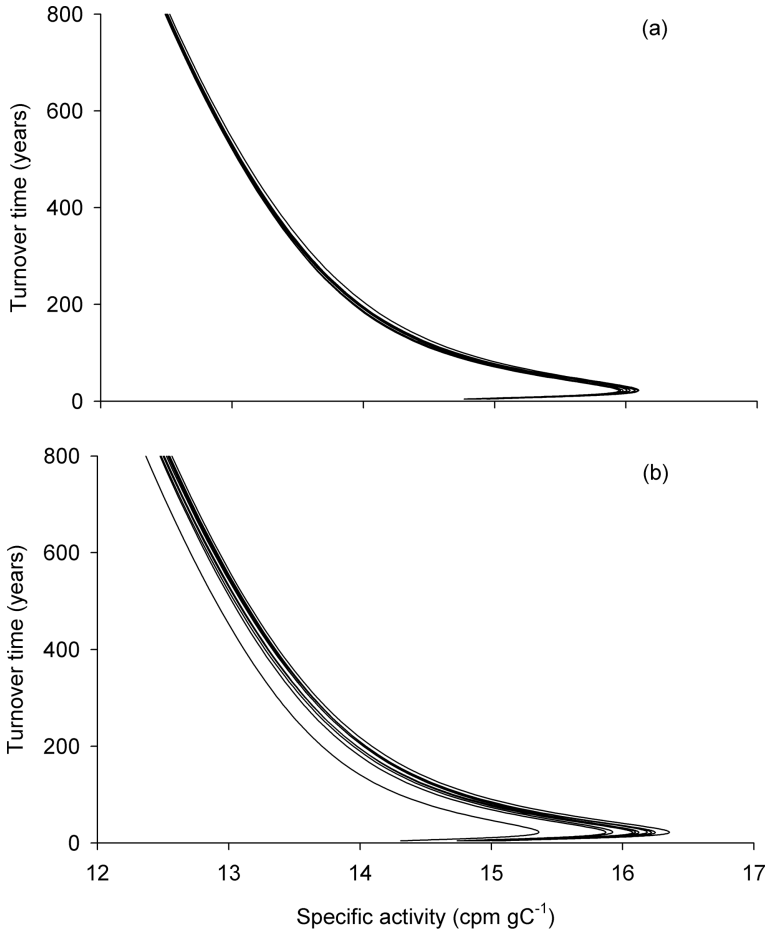

Figure 4 Uncertainties of estimates of the turnover time ($\bar{\tau}$) caused by random variation in the inputs, and a) random variation, and b) systematic variation in ^{14}C content from year to year. See text for details.

small if the variation of ^{14}C content around the value in the record can be assumed to be random. However, as the SOC sample has received inputs from vegetation at the same site all the time, the ^{14}C content is likely to be offset from the record in a systematic way. In our assessment of the variability, we even limited the organic materials to latitudes between 30°N to 60°N. If systematic deviations from the record occur, this could influence the estimates of SOC fraction turnover considerably. Thus, the estimates for fast SOC fractions can be uncertain depending on the reliability of the ^{14}C record. If we wish to estimate turnover of fast SOC fractions, values of ^{14}C content of materials from sites closer to the site of sampling should be sought. Furthermore, the estimates of turnover times based on these methods should always be accompanied by an error estimate made by Monte Carlo simulations, based on the uncertainty of the ^{14}C record for the sampling site.

Most applications of bomb ^{14}C models use a ^{14}C record covering only the bomb ^{14}C pulse and thereby assume the $\Delta^{14}C$ value of the inputs before the pulse is 0‰. However, the record from the ^{14}C calibrations shows that this is invalid. We argue that in order to estimate turnover of SOC fractions of slow turnover, the ^{14}C record has to be extended backwards at least 3 or 4 times longer than

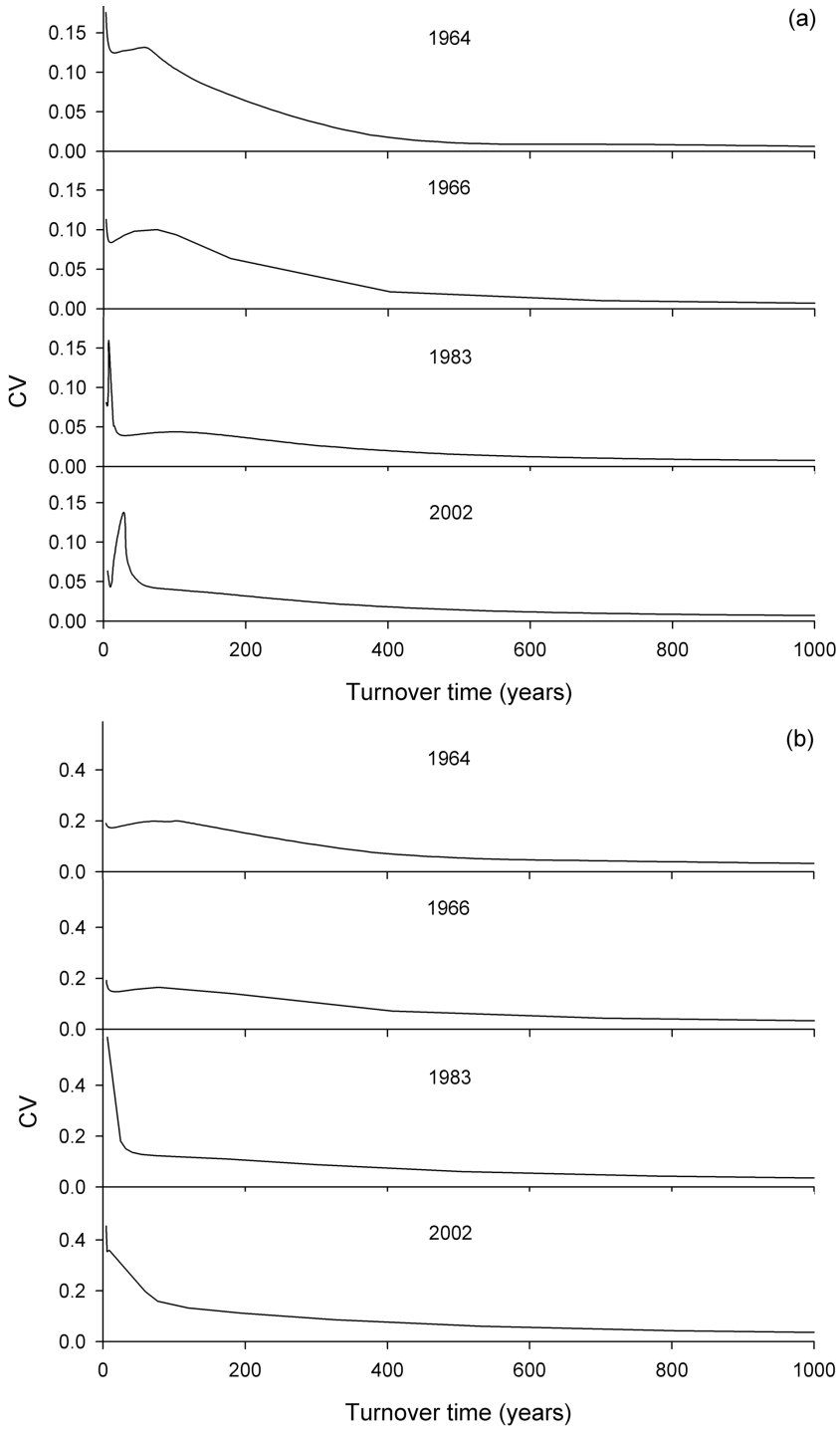

Figure 5 Relationship between average turnover time (τ) and coefficient of variation (CV) of the turnover time of theoretical samples of SOC fractions from 1964, 1966, 1983, and 2002. The turnover time is estimated for 10 input/activity histories with random variation in the inputs and a) random variation, and b) systematic variation in ^{14}C content from year to year. See text for details.

the turnover time to be estimated. Since this extended record is used to estimate SOC fractions of slow turnover where the precision of the method is quite high even in the face of systematic errors, the record from the ^{14}C calibrations can quite safely be used to estimate SOC fractions of slow turnover from everywhere in the world.

Another assumption of the bomb ^{14}C models is that the SOC fractions decay by first-order kinetics. If SOC fractions are uniform with respect to chemical composition and physical protection, they should have a more uniform decomposition rate, which will enable their description by first-order kinetics. Therefore, researchers have endeavored to isolate organic matter pools consisting of relatively homogeneous material (Trumbore and Zheng 1996; Magid et al. 1996; Sohi et al. 2001). Thus, the application of the theory presented here depends on our ability to obtain fractions that are described well by first-order kinetics.

The bomb ^{14}C model also assumes that no isotopic fractionation occurs during the decay of organic matter. This is of concern because SOC gradually becomes enriched with the stable isotope ^{13}C during decomposition (Balesdent et al. 1993; Balesdent and Mariotti 1996). Balesdent and Mariotti (1996) and Ehleringer et al. (2000) reviewed different hypotheses explaining the ^{13}C enrichment during decomposition but were unable to determine their relative importance. As long as the mechanistic basis of the enrichment has not been elucidated, the hypotheses cannot be included in our models. However, the increase in $\delta^{13}C$ values is usually less than 4‰ (Balesdent and Mariotti 1996). If all of this enrichment is ascribed to fractionation, this means an additional fractionation for the heavier ^{14}C isotopes of less than 8‰, which is very small and on the order of the measurement error.

CONCLUSIONS

Compared to the numerical solution of the bomb ^{14}C equation, which is assumed to be the best according to the underlying assumptions, the analytical solution is much easier to apply and can be used to obtain results that are sufficiently close to the numerical solution when the SOC fractions analyzed turn over relatively slowly. The uncertainty of the estimates of the numerical solution of the bomb ^{14}C equation is large for SOC fractions with fast turnover due to the uncertainty of the ^{14}C record of litter input at the sampling site, whereas it appears to be negligible when SOC factions turning over relatively slowly are analyzed. For example, the relative uncertainty is smaller than 30% if the turnover time of the SOC fraction is longer than 30 yr, and smaller than 15% when the turnover time is longer than 100 yr.

REFERENCES

Agnelli A, Trumbore SE, Corti G, Ugolini FC. 2002. The dynamics of organic matter in rock fragments in soil investigated by ^{14}C dating and measurements of ^{13}C. *European Journal of Soil Science* 53(1):147–59.

Anderson DW, Paul EA. 1984. Organo-mineral complexes and their study by radiocarbon dating. *Soil Science Society of America Journal* 48(2):298–301.

Baisden WT, Amundson R, Cook AC, Brenner DL. 2002. Turnover and storage of C and N in five density fractions from California annual grassland surface soils. *Global Biogeochemical Cycles* 16(4):1117.

Balesdent J. 1987. The turnover of soil organic fractions estimated by radiocarbon dating. *The Science of the Total Environment* 62:405–8.

Balesdent J, Girardin C, Mariotti A. 1993. Site-related $\delta^{13}C$ of tree leaves and soil organic matter in a temperate forest. *Ecology* 74(6):1713–21.

Balesdent J, Guillet B. 1982. Les datations par le ^{14}C des metières organiques des sols. *Science du Sol* 2:93–112.

Balesdent J, Mariotti A. 1996. Measurement of soil organic matter turnover using ^{13}C natural abundance. In: Boutton TW, Yamasaki SI, editors. *Mass Spectrometry of Soils.* New York: Marcel Dekker. p 83–111.

Barrette L, Lasalle P, Martel Y, Samson C. 1980. Variations of ^{14}C in oats grown from 1957 to 1978 in Québec. *Radiocarbon* 22(2):410–4.

Baxter MS, Walton A. 1971. Fluctuations of atmospheric carbon-14 concentrations during the past century. *Proceedings of the Royal Society of London, Series A* 321:105–27.

Bird M, Santrùcková H, Lloyd J, Lawson E. 2002. The

isotopic composition of soil organic carbon on a north-south transect in western Canada. *European Journal of Soil Science* 53(3):393–403.

Bol RA, Harkness DD, Huang Y, Howard DM. 1999. The influence of soil processes on carbon isotope distribution and turnover in the British uplands. *European Journal of Soil Science* 50(1):41–51.

Burchuladze AA, Chudy M, Eristavi IV, Pagava SV, Povinec P, Sivo A, Togonidze GI. 1989. Anthropogenic ^{14}C variations in atmospheric CO_2 and wines. *Radiocarbon* 31(3):771–6.

Campbell CA, Paul EA, Rennie DA, McCallum KJ. 1967. Applicability of the carbon-dating method of analysis to soil humus studies. *Soil Science* 104(3): 217–24.

Chen Q, Sun Y, Shen C, Peng S, Yi W, Li Z, Jiang M. 2002. Organic matter turnover rates and CO_2 flux from organic matter decomposition of mountain soil profiles in the subtropical area, south China. *Catena* 49(3):217–29.

Cherkinsky OA, Brovkin VA. 1993. Dynamics of radiocarbon in soils. *Radiocarbon* 35(3):363–7.

Dai K, Fan CY. 1986. Bomb-produced ^{14}C content in tree rings grown at different latitudes. *Radiocarbon* 28(2A):346–9.

Dai K, Qian Y, Fan CY. 1992. Bomb-produced ^{14}C in tree rings. *Radiocarbon* 34(3):753–6.

Damon PE, Peristykh AN. 2000. Radiocarbon calibration and application to geophysics, solar physics, and astrophysics. *Radiocarbon* 42(1):137–50.

Druffel ERM, Griffin S. 1995. Radiocarbon in tropospheric CO_2 and organic materials from selected Northern Hemisphere sites. *Radiocarbon* 37(3):883–8.

Ehleringer JR, Buchmann N, Flanagan LB. 2000. Carbon isotope ratios in belowground carbon cycle processes. *Ecological Applications* 10(2):412–22.

Geyh MA, Benzler JH, Roeschmann G. 1971. Problems of dating Pleistocene and Holocene soils by radiometric methods. In: Yaalon, editor. *Paleopedology.* Jerusalem: Israel University Press. p 63–75.

Gilet-Blein N, Marien G, Evin J. 1980. Unreliability of ^{14}C dates from organic matter of soils. *Radiocarbon* 22(3):919–29.

Goodsite ME, Rom W, Heinemeier J, Lange T, Ooi S, Appleby PG, Shotyk W, van der Knaap WO, Lohse C, Hansen TS. 2001. High-resolution AMS ^{14}C dating of post-bomb peat archives of atmospheric pollutants. *Radiocarbon* 43(2B):495–515.

Harkness DD, Harrison AF, Bacon PJ. 1991. The potential of bomb-^{14}C measurements for estimating soil organic matter turnover. In: Wilson WS, editor. *Advances in Soil Organic Matter Research: The Impact on Agriculture and the Environment*. Colchester: Royal Society of Chemistry. p 239–51.

Harrison K, Broecker W. 1993. A strategy for estimating the impact of CO_2 fertilization on soil carbon storage. *Global Biogeochemical Cycles* 7(1):69–80.

Hsieh YP. 1993. Radiocarbon signatures of turnover rates in active soil organic carbon pools. *Soil Science Society of America Journal* 57(4):1020–2.

Hsieh YP. 1996. Soil organic carbon pools of two tropical soils inferred by carbon signatures. *Soil Science Society of America Journal* 60(4):1117–21.

Jenkinson DS, Rayner JH. 1977. The turnover of soil organic matter in some of the Rothamsted classical experiments. *Soil Science* 123(5):298–305.

Knapp AK, Smith MD. 2001. Variation among biomes in temporal dynamics of aboveground primary production. *Science* 291(5503):481–4.

Kromer B, Manning SW, Kuniholm PI, Newton MW, Spurk M, Levin I. 2001. Regional $^{14}CO_2$ offsets in the troposphere: magnitude, mechanisms, and consequences. *Science* 294(5551):2529–32.

Levin I, Kromer B. 1997. Twenty years of atmospheric $^{14}CO_2$ observations at Schauinsland station, Germany. *Radiocarbon* 39(2):205–18.

Levin I, Kromer B, Schoch-Fisher H, Bruns M, Münnich M, Berdau D, Vogel JC, Münnich KO. 1985. 25 years of tropospheric ^{14}C observations in central Europe. *Radiocarbon* 27(1):1–19. (Data online: http://cdiac.esd.ornl.gov/trends/co2/cent.htm.)

Libby WF. 1952. *Radiocarbon Dating*. Chicago: University of Chicago Press. 124 p.

Magid J, Gorissen A, Giller K. 1996. In search of the elusive "active" fraction of soil organic matter: three size-density fractionation methods for tracing the fate of homogeneously ^{14}C-labeled plant materials. *Soil Biology and Biochemistry* 28(1):89–99.

Martel YA, Paul EA. 1974. The use of radiocarbon dating of organic matter in the study of soil genesis. *Soil Science Society of America Proceedings* 38(3):501–6.

Olsson IU, Possnert G. 1992. ^{14}C activity in different sections and chemical fractions of oak tree rings, AD 1938–1981. *Radiocarbon* 34(3):757–67.

Paul EA, Campbell CA, Rennie DA, McCallum KJ. 1964. Investigations of the dynamics of soil humus utilizing carbon dating techniques. *Proceedings of the 8th International Congress of Soil Science* 3:201–8.

Perrin RMS, Willis EH. 1964. Dating of humus podzols by residual radiocarbon activity. *Nature* 202(4928): 165–6.

Scharpenseel HW, Schiffmann H. 1977. Radiocarbon dating of soils: a review. *Zeitschrift für Pflanzenernährung und Bodenkunde* 140(2):159–74.

Sohi SP, Mahieu N, Arah JRM, Powlson DS, Madari B, Gaunt JL. 2001. A procedure for isolating soil organic matter fractions suitable for modeling. *Soil Science Society of America Journal* 65(4):1121–8.

Stuiver M, Braziunas TF. 1998. Anthropogenic and solar components of hemispheric C-14. *Geophysical Research Letters* 25(3):329–32.

Stuiver M, Polach HA. 1977. Discussion: reporting of ^{14}C data. *Radiocarbon* 19(3):355–63.

Stuiver M, Quay PD. 1981. Atmospheric ^{14}C changes resulting from fossil fuel CO_2 release and cosmic ray flux variability. *Earth and Planetary Science Letters* 53:349–62.

Stuiver M, Reimer PJ, Bard E, Beck JW, Burr GS, Hughen KA, Kromer B, McCormac G, van der Plicht J, Spurk M. 1998. IntCal98 radiocarbon age calibration, 24,000–0 cal BP. *Radiocarbon* 40(3):1041–83. (Data online: http://www.dur.ac.uk/a.r.millard/calibration.html).

Tans PP, de Jong AFM, Mook WG. 1979. Natural atmospheric ^{14}C variation and the Suess effect. *Nature* 280: 826–8.

Tauber H. 1967. Copenhagen radiocarbon measurements VIII. Geographic variation in atmospheric ^{14}C activity. *Radiocarbon* 9:246–56.

Trumbore SE. 1993. Comparison of carbon dynamics in tropical and temperate soils using radiocarbon measurements. *Global Biogeochemical Cycles* 7(2):275–90.

Trumbore SE, Chadwick OA, Amundson R. 1996. Rapid exchange between soil carbon and atmospheric carbon dioxide driven by temperature change. *Science* 272: 393–6.

Trumbore SE, Zheng S. 1996. Comparison of fractionation methods for soil organic matter ^{14}C analysis. *Radiocarbon* 38(2):219–29.

Vogel JC. 1970. Groningen radiocarbon dates IX. *Radiocarbon* 12(2):444–71.

Vol 47, Nr 1 **Radiocarbon** 2005

CONTENTS